

TECHNISCHE UNIVERSITÄT MÜNCHEN
Lehrstuhl für Energiesysteme

Online analysis of the tar content of biomass gasification producer gas

Panagiotis Mitsakis

Vollständiger Abdruck der von der Fakultät für Maschinenwesen der Technischen
Universität München zur Erlangung des akademischen Grades eines

Doktor-Ingenieurs

genehmigten Dissertation.

Vorsitzender: Univ.-Prof. Dr.-Ing. Harald Klein
Prüfer der Dissertation: 1. Univ.-Prof. Dr.-Ing. habil. Hartmut Spliethoff
2. Univ.-Prof. Dr.rer.nat. Frank Behrendt,
Technische Universität Berlin

Die Dissertation wurde am 29.03.2011 bei der Technischen Universität München eingereicht und durch die Fakultät für Maschinenwesen am 21.11.2011 angenommen.

Acknowledgments

The research of the present thesis is carried out at the Institute for Energy Systems of the Technische Universität München.

First of all, I would like to thank the supervisor of this dissertation, Prof. Dr.-Ing. habil. Hartmut Spliethoff, who gave me the opportunity to come to Munich and accomplish my PhD studies.

My most grateful thanks to all of my colleagues for their help and support. Special thanks to Matthias Mayerhofer, Günter Zapf and Matthias Gaderer for the co-operation and their advice during the whole project. Very warm thanks to Theodoros Papadopoulos and Marco Losurdo for their useful help to the computational part of my research.

There were many people who gave interesting feedback and valuable suggestions during my research. One of them I would like to thank especially for is Stelios Arvelakis, who offered me a lot of friendly help and advice. He was always open to discussions and transferred his knowledge and experience to me. Our conversations were scientific but funny as well and have enlightened my way of thinking.

My sincere gratitude to Sotirios Karellas for his earlier work, which was the motivation and start of the research part of this thesis.

I am very happy to acknowledge the help of all my students whom I was privileged to teach and from whom I also learned much. They were all a fun bunch with lots of enthusiasm and ideas who provided me with very useful input.

I also wish to thank Prof. Dr.-Ing. Harald Klein and Prof. Dr.rer.nat. Frank Behrendt for taking part in the examination committee.

Last but by no means least, I would like to express my appreciation to the people from the workshop (Albert Daschner, Martin Haindl, Jürgen Knösch and Robert Riss), who offered their time and help in the constructive part of this research thesis.

Except for the scientific part all these years in Munich, there is always the other side of life. I have been fortunate to come across many good friends with whom I had a great and enjoyable time. Many thanks to all of my friends in Munich and especially to Charalampos Daniilidis, Theodoros Papadopoulos, Kimon Karras, Iason Vittorias, Nana Kouri, Petros Mettas, Marco Losurdo, Tilemachos Matiakis, Prodromos Tsipouridis, Apostolos Gkazepis, Christina Yfanti, Natasa Ananiadi, Sofia Arvaniti and Costas Paggios for the time that we have spent together and the memories which I would cherish for a long time to come.

Finally, I would like to thank the Greek State Scholarship Foundation (I.K.Y.) for the financial support during my PhD studies.

...in memory of my father

*Ζήσε μονάχα τη στιγμή και άσε το μετά,
ένα σωσίβιο η ζωή που ξεφουσκώνει αργά.*

Μάνος Ξυδούς

*Live just for the moment and let the future,
life is a lifejacket that deflates slowly.*

Manos Xydous

Abstract

Biomass is considered to be one of the renewable energy sources with the highest potential to contribute to the energy need through the substitution of fossil fuels. The use of biomass for the production of energy and fuels has gained much attention during the last years. Especially gasification is the most widely used thermochemical process for converting biomass into gaseous and consequently into liquid biofuels.

One of the most important problems during the gasification process is the amount of condensable hydrocarbons (tars) which are produced within the process and create problems in the downstream use of the producer gas (e.g in fuel cells, gas turbines) for heat and power generation.

Except for the conventional measurement techniques for the determination of the tar content in biomass gasification producer gas, innovative optical techniques can also be successfully used. In an effort to improve the already existing tar measurement methods, this scientific work deals with a new online and non-intrusive quantitative and qualitative measurement technique for the analysis of tar compounds. For this purpose, a transportable optical measurement system based on Laser Induced Fluorescence (LIF) spectroscopy is designed and developed in order to provide online analysis of the tar content in different gasification facilities.

The optical facility is calibrated by being coupled to a specially designed tar mixing station, which generates eligible tar concentrations, in order to enable not only the qualification but also the quantification of gas phase tar compounds and to define the concentration of single tar compounds in their mixtures. By exploiting the different spectroscopic behavior of each individual tar compound, it is possible to investigate mixtures of tars according to their specific fluorescence emission.

The performed experiments in two different gasification test rigs have revealed that up to fourteen compounds, which are representative of each tar class, can be analyzed online by means of Laser Induced Fluorescence (LIF) spectroscopy. The online setup evaluates the influence of different gasification parameters such as temperature, pressure, steam to biomass ratio as well as the type of biomass feedstock used, on the tar composition. Moreover, the influence of the reactor configuration and the type of bed material on tar formation can be examined.

The quantitative analysis of aromatic and polycyclic aromatic hydrocarbons (tars) is of high importance in order to verify the suitability of the producer gas for its further downstream use for the production of energy and fuels. The obtained results reveal the possibility of qualifying and quantifying tar mixtures directly downstream from a gasification unit demonstrating that the transportable experimental setup can be used for the continuous monitoring of gasifier tars.

Zusammenfassung

Biomasse gilt als einer der erneuerbaren Energien mit dem größten Potenzial zur Substitution von fossilen Brennstoffen. Die Nutzung von der Biomasse für die Energie- und Brennstoffherzeugung hat in den letzten Jahren mehr Aufmerksamkeit erhalten. Besonders die Vergasung ist der am weitesten verbreitete Prozess für die thermochemische Umwandlung von Biomasse zu gasförmigen und weiter zu flüssigen Biokraftstoffe.

Eines der größten Probleme im Vergasungsprozess ist die Entstehung von kondensierbaren Kohlenwasserstoffen (Teere), die zu Problemen in der Weiternutzung des Produktgases (z.B. in Brennstoffzellen, Gasturbinen), in der Wärme- und Energieerzeugung führen.

Abgesehen von konventionellen Messverfahren zur Bestimmung des Teergehalts im Produktgas aus Biomassevergasung, können auch innovative optische Techniken erfolgreich angewandt werden. Diese wissenschaftliche Arbeit befasst sich mit einem neuen Online- und berührungslosen, sowohl quantitativen als auch qualitativen Messverfahren zur Analyse der Teerkomponenten. Zu diesem Zweck, wird ein transportables optisches Messsystem basierend auf Laser Induzierter Fluoreszenzspektroskopie (LIF) ausgelegt und entwickelt um die Online-Analyse des Teergehalts in verschiedenen Vergasern zu ermöglichen.

Die optische Anlage ist zur Kalibrierung an eine speziell entwickelte Teermischstrecke gekoppelt, die verschiedene Teerkonzentrationen erzeugen kann, um nicht nur die Qualifizierung sondern auch die Quantifizierung der Teerverbindungen zu ermöglichen und die Konzentration der einzelnen Komponenten in Teermischungen zu definieren. Durch die Auswertung der unterschiedlichen spektroskopischen Eigenschaften der einzelnen Teerkomponenten, ist es möglich Teermischungen in Abhängigkeit von ihrer spezifischen Fluoreszenzemission zu untersuchen.

Die durchgeführten Experimente in zwei verschiedenen Vergasungsprüfständen ergaben, dass bis zu vierzehn Komponenten, Vertreter aus jeder Teerklasse, online mittels Laser Induzierter Fluoreszenzspektroskopie (LIF) analysiert werden können. Mit der Anlage wird der Einfluss verschiedener Vergasungsparameter wie Temperatur, Druck, Dampf-Verhältnis sowie die Art der verwendeten Biomassebrennstoffe, auf die Teerzusammensetzung online ausgewertet. Darüber hinaus kann der Einfluss der Reaktorkonfiguration und der Art des Bettmaterials auf die Teerbildung untersucht werden.

Die quantitative Analyse von aromatischen und polyzyklischen aromatischen Kohlenwasserstoffen (Teere) ist von großer Bedeutung, um die Eignung des Produktgases für seine weitere nachgelagerte Verwendung zur Energie- und Brennstoffherzeugung zu kontrollieren. Die Ergebnisse belegen, dass die Qualifizierung und Quantifizierung der Teermischungen direkt hinter einem Vergaser möglich ist, und demonstrieren, dass die transportable Versuchsanlage für die kontinuierliche Überwachung von Teeren aus Vergasung verwendet werden kann.

Contents

1	Introduction	1
1.1	Tar problem	2
1.2	Motivation and outline of the thesis	2
2	Biomass gasification	5
2.1	Decentralized conversion of biomass	5
2.2	Application of biomass gasification for the production of energy and fuels	7
2.3	Gasification technologies	10
2.3.1	Principles of biomass gasification	10
2.3.2	Autothermal and allothermal gasification	13
2.4	Biomass gasification producer gas	21
2.4.1	Quality of the producer gas	21
2.4.2	Tar content in the producer gas	24
3	Biomass gasification tars	31
3.1	Definition of tars and their specific features	31
3.2	Mechanism of tar formation and conversion in the gasification process	32
3.3	Tar cleaning systems	33
3.3.1	Physical removal of tar	34
3.3.2	Chemical removal of tar	36
3.4	Classification of tar compounds	37
3.4.1	Primary, secondary and tertiary tars	39
3.4.2	Five tar classes system	40
3.5	Tar dewpoint	41
3.6	Tar measurement methods	42
3.6.1	Conventional Cold Solvent Trapping (CST)-Tar protocol	42
3.6.2	Petersen column	43
3.6.3	Gas chromatography	44
3.6.4	High Performance Liquid Chromatography (HPLC)	45
3.6.5	Solid Phase Adsorption (SPA)	45
3.6.6	Online tar analyzer	46
3.6.7	Molecular Beam Mass Spectrometry (MBMS)	47

3.6.8	Laser ionization system coupled to a gas chromatograph/ ion trap mass spectrometer	48
3.6.9	Photo Ionization Detector (PID)	49
3.6.10	Raman spectroscopy	49
3.6.11	Overview of tar measurement methods	49
4	Laser Induced Fluorescence spectroscopy	51
4.1	Basic principles of Laser Induced Fluorescence (LIF) spectroscopy	51
4.2	Detection of polycyclic aromatic hydrocarbons by means of LIF spectroscopy	54
5	Experimental setup of the laser measurement technique	57
5.1	Optical facility for the investigation of tars	57
5.1.1	Motivation and background	57
5.1.2	Design and development of the optical facility	57
5.1.3	Design and construction of the transportable optical setup	59
5.1.4	Advantages of the optical setup-Drawbacks of former existing methods	60
5.2	Tar mixing station	61
5.2.1	Design and construction of the tar mixing station	61
5.2.2	Theoretical assessment of the concentration of gas phase tar compounds	62
5.2.3	Validation of the tar concentration from the tar mixing station . . .	70
5.3	Analysis of the optical signals	73
5.3.1	Calibration of the laser system	73
5.3.2	Numerical evaluation of the spectra	78
5.3.3	Measurement of model compounds and their mixtures	79
5.3.4	Qualitative and quantitative measurement of biomass gasification tars	81
5.4	Accuracy of the measurement procedure	82
5.4.1	Measurement error due to numerical approximation	82
5.4.2	Measurement error due to chemical reactions	83
5.4.3	Measurement error due to the parameters of the optical setup . . .	83
6	Experimental results	85
6.1	Experimental facility for biomass gasification	85
6.1.1	The Biomass Heatpipe Reformer-BioHPR (TUM)	85
6.1.2	Atmospheric circulating fluidized bed (TUD)	88
6.2	Test program at the TUM and TUD gasifiers	90
6.2.1	Operational parameters of the pressurized bubbling fluidized bed (BioHPR)	93
6.2.2	Operational parameters of the atmospheric circulating fluidized bed	95

6.3	Online measurement of the tar content with the optical setup	99
6.3.1	Results from TUM gasifier	99
6.3.2	Results from TUD gasifier	103
7	Evaluation of the experimental results	109
7.1	Evaluation of the optical results	109
7.1.1	Results from parallel measurement techniques	109
7.1.2	Comparison between optical and parallel measurement techniques .	116
7.2	Influence of gasification parameters on the tar content	123
7.2.1	Reactor type	123
7.2.2	Biomass feedstock	125
7.2.3	Reactor temperature	127
7.2.4	Reactor pressure	131
7.2.5	Steam to biomass ratio	133
7.2.6	Bed material	137
7.2.7	Overview of the influence of different parameters on the tar content	139
8	Summary	141
A	Appendix	143
A.1	Tar compounds and structures	143
A.2	Parameters for the mass transfer model	145

Notations

Abbreviations

AER	Absorption Enhanced Reforming
BDHS	Biomass District Heating System
BFB	Bubbling Fluidized Bed
BIGCC	Biomass Integrated Gasification Combined Cycle
BioHPR	Biomass Heatpipe Reformer
BTG	Biomass Technology Group
CAS	Chemical Abstract Service
CCD	Charged Coupled Device
CEN	Comité Européen de Normalisation
CFB	Circulating Fluidized Bed
CFBG	Circulating Fluidized Bed Gasifier
CHNS	Carbon Hydrogen Nitrogen Sulphur
CHP	Combined Heat and Power
CH	Hydrocarbons
CST	Cold Solvent Trapping
CUTEC	Clausthaler Umwelttechnik Institut GmbH
DDGS	Distilled Dried Grains with Solubles
DH	District Heating
DME	Dimethylether
DTI	Danish Technological Institute
ECN	Energy research Centre of the Netherlands
EI	Electron Impact
ER	Equivalence Ratio
ESP	Electrostatic Precipitator
FID	Flame Ionization Detector
FT	Fischer Tropsch
GC	Gas Chromatograph
GHG	Greenhouse Gases
HHV	Higher Heating Value
HPLC	High Performance Liquid Chromatography
HT	High Temperature

IC	Ion Chromatography
ICCD	Intensified Charged Coupled Device
ICE	Internal Combustion Engine
ICP-OES	Inductively Coupled Plasma Optical Emission Spectroscopy
IGCC	Integrated Gasification Combined Cycle
IGT	Institute of Gas Technology
KTH	Kungliga Tekniska Högskolan
LAMS	Laser (Ionizations) Mass Spectrometer
LC	Liquid Chromatography
LHC	Light Hydrocarbons
LHV	Low Heating Value
LDA	Laser Doppler Anemometry
LDV	Laser Doppler Velocimetry
LI	Laser Ionization
LIF	Laser Induced Fluorescence
M&L	Medium & Large
MBMS	Molecular Beam Mass Spectrometry
MS	Mass Spectrometer
NREL	National Renewable Energy Laboratory
ORC	Organic Rankine Cycle
PAH	Polycyclic Aromatic Hydrocarbon
PDI	Phase Doppler Interferometry
PID	Photo Ionization Detector
PID	Piping and Instrumentation Diagram
PIV	Particle Image Velocimetry
PLS	Partial Least Squares
PNA	Polynuclear Aromatics
PDU	Process Development Unit
PFB	Pressurized Fluidized Bed
PNL	Pacific Northwest Laboratory
PVC	PolyVinyl Chloride
RET	Resonance Energy Transfer
S&M	Small & Medium
SBR or S/B	Steam to Biomass Ratio
SCW	Supercritical Water
SNG	Synthetic Natural Gas

SPA	Solid Phase Adsorption
SPE	Solid Phase Extraction
TCPDU	Thermochemical Process Development Unit
TD	Thermal Desorption
TMBMS	Transportable Molecular Beam Mass Spectrometer
TPS	Termiska Processer AB, Sweden
TUD	Technische Universiteit Delft
TUM	Technische Universität München
UCG	Ultra Clean Gas
UET	Umwelt-und Energietechnik
UV	Ultraviolet
VTT	Valtion Teknillinen Tutkimuskeskus
XRD	X-Ray Diffraction

Symbols

A	Surface area	$[m^2]$
a	Constant factor	[-]
b	Cell pathlength	$[m]$
C	Concentration	$[g/m^3]$
const.	constant	[-]
D	Diffusion coefficient	$[m^2/s]$
d	day	[-]
E	Energy	[Joule]
F	Volume flow	$[m^3/s]$
F	Profile function	
G	Square difference of measured and approximated profile	
H	Enthalpy	$[kJ/mol]$
I	Signal intensity	[Counts]
K	Mass transfer coefficient	$[m/s]$
k	Film mass transfer coefficient	$[m/s]$
L	Characteristic length	$[m]$
M	Molar mass	$[g/mol]$
P	Pressure	[Pa]
Q	Mass flow	$[kg/s]$
R	General gas constant (8,31441kJ/kmolK)	$[kJ/kmolK]$
S	Saturation level	[-]
T	Temperature	[Kelvin]

t	tons	[-]
V	Volume	[m^3]
Vol	Volume	[m^3]
w	Velocity	[m/s]

Greek symbols

δ	Effective thickness of stagnant-film layer	[m]
ε	Characteristic Lennard-Jones energy	[-]
ε	Molar absorptivity	[counts]
λ	Wavelength	[nm]
μ	Viscosity of compound i	[Pa s]
μ	Dipole momentum	[Debye]
ν	atomic diffusion volume	[cm^3/mol]
ρ	density	[kg/m^3]
σ	binary pair characteristic length	[Angstrom]
Φ	Quantum efficiency	[-]
χ	scalar	[-]
Ω	diffusion collision integral	[-]

Subscripts and Superscripts

A	Nitrogen
B	Tar compound
approx	Approximated
b	Boiling point
c	Critical
D	Diffusion
db	dry base
daf	Dry ash free
ext	External
el	Electronic
F	Fluorescence
i	General index for tar compound
i	General index for profile point
m	General index
meas	Measured
nc	Nitrogen

R	Reaction
rot	Rotation
Sat	Saturation
sys	System
th	Thermal
v	General index
vib	Vibration

1 Introduction

The use of fossil fuels as primary energy source gives rise to an increasing emission of environmentally hazardous species (NO_x , CO_2 , SO_x), which is becoming a growing problem during the last years. As long as the environmental concerns are increasing, a number of environmental-friendly processes are currently under development.

Commensurate with these existing facts, it has become apparent that the continued emissions of greenhouse gases (GHGs) and loss of carbon sinks are influencing the world climate. The main strategy proposed to ameliorate the effects of climate change is to reduce global demand for fossil fuel resources [1]. An old technology that currently seems to be promising in tackling this issue is the gasification of biomass.

Biomass is considered to be one of the renewable energy sources with the highest potential to contribute to the world's energy need. The use of biomass can provide a more positive solution—a renewable source of energy services, including heat, electrical energy, and transportation fuels, which can reduce CO_2 emissions, sulphur and heavy metals in the atmosphere, while potentially improving rural income and energy security through the substitution of coal, oil and natural gas [2].

At present, forestry, agricultural and municipal residues and wastes are the main feedstocks for the generation of electricity and heat from biomass. In addition, a very small share of sugar, grain, and vegetable oil crops are used as feedstocks for the production of liquid biofuels. Today, biomass supplies some 50 EJ¹ globally, representing 10% of the global annual primary energy consumption. This is mostly traditional biomass used for cooking and heating [3].

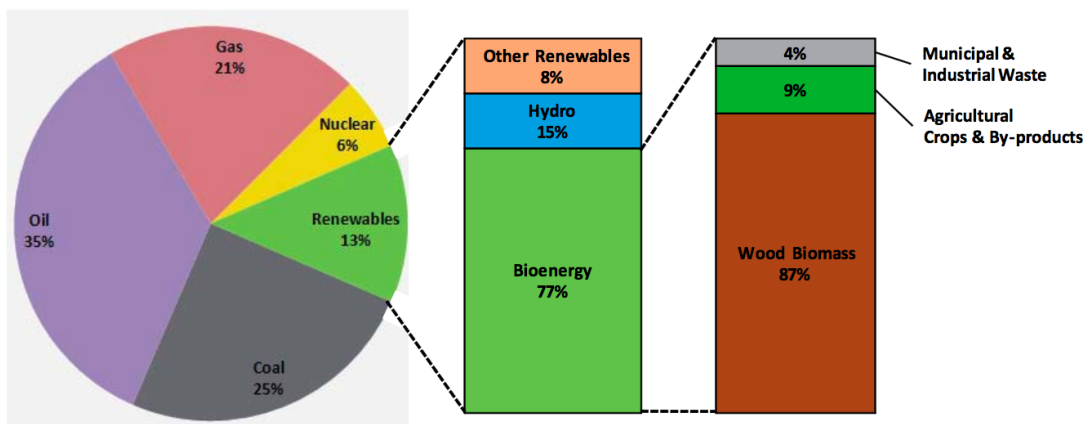


Figure 1.1: Share of bioenergy in the world primary energy mix [4], [5].

¹1 EJ = 1018 Joules (J) = 1015 kilojoules (kJ) = 24 million tonnes of oil equivalent (Mtoe)

To achieve the bioenergy potential targets in the longer term, government policies, and industrial efforts need to be directed at increasing biomass yield levels and modernising agriculture in regions such as Africa, the Far East and Latin America, as well as at directly increasing global food production and thus the resources available for biomass. This can be achieved by technological development, and by the diffusion of best sustainable agricultural practices. The sustainable use of residues and wastes for bioenergy, which present limited or zero environmental risks, needs to be encouraged and promoted globally [3].

1.1 Tar problem

One of the most important and probably the major problem in the use of biomass for the production of biogenous gases through the gasification route is the amount of undesirable tars and particulates within this process.

Historically “tar” is an operationally defined parameter, based largely on organics from gasification that condensed under operating conditions of boilers, transfer lines, and internal combustion engine (ICE) inlet devices. Such a definition requires a more detailed chemical explanation in the light of the greatly expanded uses proposed for both high- and low-energy gas from a variety of biomass and waste materials. At present, the literature contains many data on the “destruction”, “conversion”, “removal”, etc., of “tars”, “condensibles”, “heavy hydrocarbons”, etc., without a consistent definition of these terms and without a description of the sampling and analytical methods used for the organics of interest. Though the data presented are useful in the context of the system being studied, they are limited in their transfer to other systems because they are “apparatus dependent” [1].

Therefore, considering the formation of heavy hydrocarbons (tars) as one of the main problems during the gasification process, the determination of the tar content is of high importance in order to verify the suitability of the producer gas for its further downstream use. Different sampling and analysis methods have been proposed and developed by researchers and manufacturers for solving the tar problem, however no standard or recommended procedure exists except for the Tar Protocol, which specifies a way for tar measurement and has become a pre-standard [6].

1.2 Motivation and outline of the thesis

The motivation of this thesis is to develop a new online and non-intrusive measurement system based on optical techniques, which allows not only the quantification but also the qualification of biomass gasification tars downstream to a gasification reactor. This thesis deals with the design and construction of an experimental transportable facility based on optical measurement techniques, which can be coupled downstream to different

gasification test rigs for determining the amount of tars produced in the gasification process.

Chapter 2 points out the decentralized conversion of biomass as well as its use for the production of energy and fuels. Furthermore, an overview of the gasification technologies is presented while the analysis of the gasification's producer gas regarding its main compounds and its tar content is described as well. Special attention is paid to the influence of the reactor type and the gasification parameters on the tar content.

Chapter 3 outlines the definition of tars as well as the mechanism of tar formation and cracking in the gasification process. Moreover, the different tar cleaning technologies are mentioned while the classification of the tar compounds is described in detail. Finally the different existing methods for the analysis of tars are presented.

Chapter 4 deals with the theoretical background and basic principles of Laser Induced Fluorescence (LIF) spectroscopy, which is the applied optical technique for the detection and measurement of aromatic and polycyclic aromatic hydrocarbons.

The experimental setup of the laser measurement technique is presented in chapter 5. The design and development of the transportable optical facility as well as the tar mixing station, which is used for the calibration of the optical setup, are described in detail. In addition, the calibration of the laser system and the numerical evaluation of the spectra for the qualitative and quantitative measurement of biomass gasification tars are analyzed while the accuracy of the measurement procedure is discussed as well.

Chapter 6 describes the pressurized bubbling fluidized bed reactor of Technical University of Munich and the atmospheric circulating fluidized bed reactor of Delft University of Technology, which are used for the experiments, while it presents the experimental results of the gasification tests conducted in both fluidized bed test rigs.

The evaluation of the experimental results and the comparison between the optical and different parallel measurement techniques takes place in chapter 7, where the influence of the gasification parameters on the concentration of tar compounds is analyzed in detail.

The thesis is concluded in chapter 8 with a summary of the design of the online optical setup as well as its calibration process, the performed experimental results and a discussion about future directions and research.

2 Biomass gasification

2.1 Decentralized conversion of biomass

The predominant use of biomass today consists of fuel wood used in non-commercial applications, in simple inefficient stoves for domestic heating and cooking in developing countries, where biomass contributes some 22% to the total primary energy mix. This traditional use of biomass is expected to grow with increasing world population, but there is significant scope to improve its efficiency and environmental performance, and thereby help to reduce biomass consumption and related impacts [3].

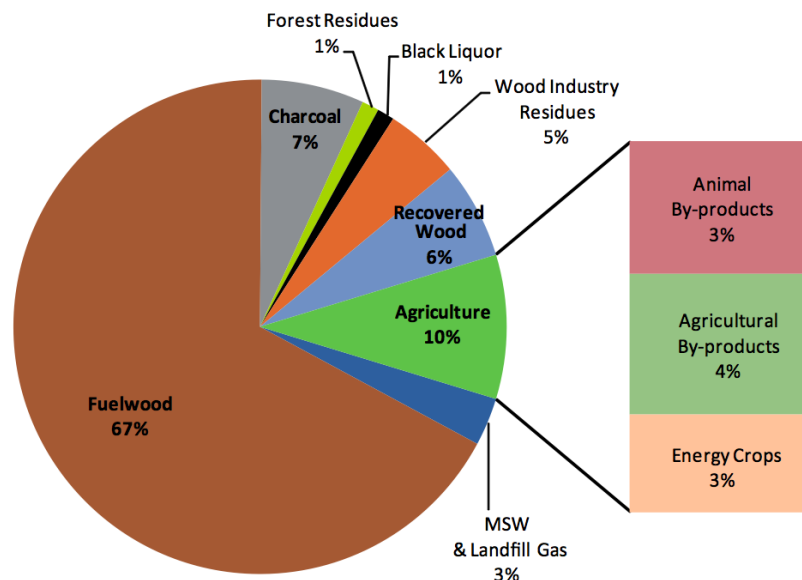


Figure 2.1: Share of the biomass sources in the primary bioenergy mix [5].

In industrialised countries, the total contribution of modern biomass is on average only about 3% of total primary energy, and consists mostly of heat-only and heat and power applications. Many countries have targets to significantly increase biomass use, as it is foreseen as a key contributor to meeting energy and environmental policy objectives. Current markets mostly involve domestic heat supply (e.g. pellet boilers), large-scale industrial and community CHP generation (particularly where low cost feedstocks from forest residues are available), and co-firing in large coal-based power plants. Globally, the use of biomass in heat and industrial energy applications is expected to double by 2050 under business-as-usual scenarios, while electricity generation from biomass is projected to increase, from its current share of 1.3% in total power production to 2.4–3.3% by 2030 corresponding to a 5-6% average annual growth rate [3].

There are many bioenergy routes which can be used to convert raw biomass feedstock into a final energy product (Fig. 2.2). Several conversion technologies have been developed that are adapted to the different physical nature and chemical composition of the feedstock, and to the energy service required (heat, power, transport fuel). Upgrading technologies for biomass feedstocks (e.g. pelletisation, torrefaction and pyrolysis) are being developed to convert bulky raw biomass into denser and more practical energy carriers for more efficient transport, storage and more convenient use in subsequent conversion processes [3].

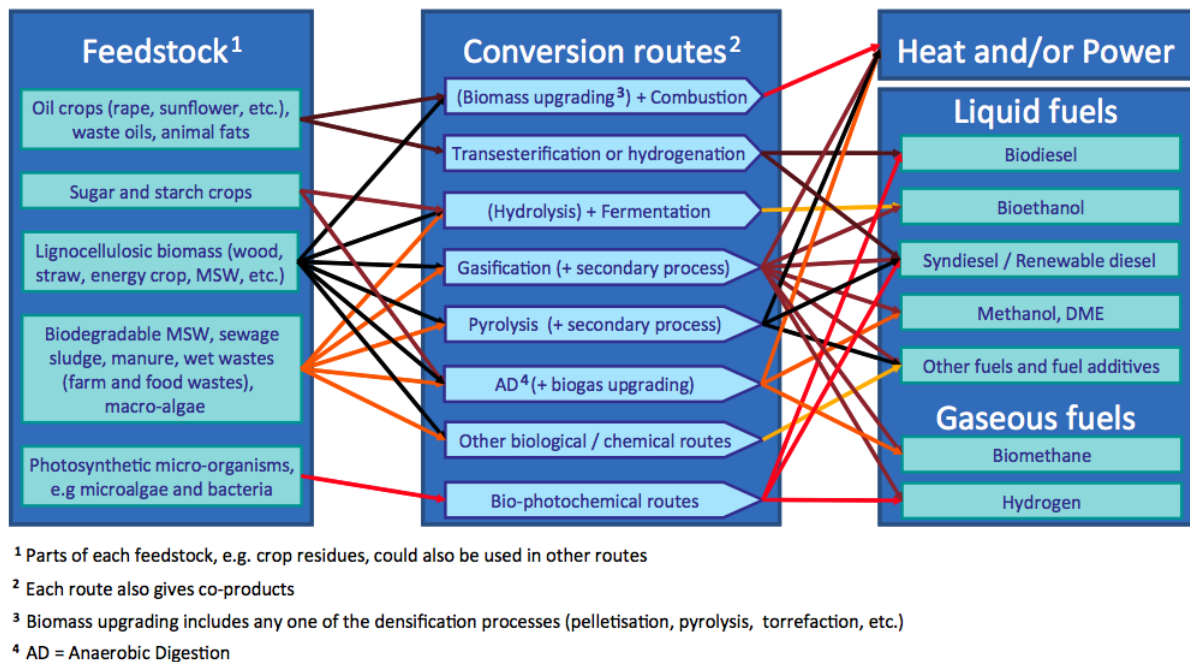


Figure 2.2: Schematic view of bioenergy routes [7].

The production of heat by the direct combustion of biomass is the leading bioenergy application throughout the world, and is often cost-competitive with fossil fuel alternatives. For a more energy efficient use of the biomass resource, modern, large-scale heat applications are often combined with electricity generation in combined heat and power (CHP) systems. In the longer term, if reliable and cost-effective operation can be widely demonstrated, gasification promises greater efficiency, better economics on both small and large-scale as well as lower emissions compared with other biomass-based power generation options. Other technologies (such as Organic Rankine Cycle and Stirling engines), which are currently in the demonstration stage, could prove economically viable in a range of small-scale applications, especially for CHP (Fig. 2.3).

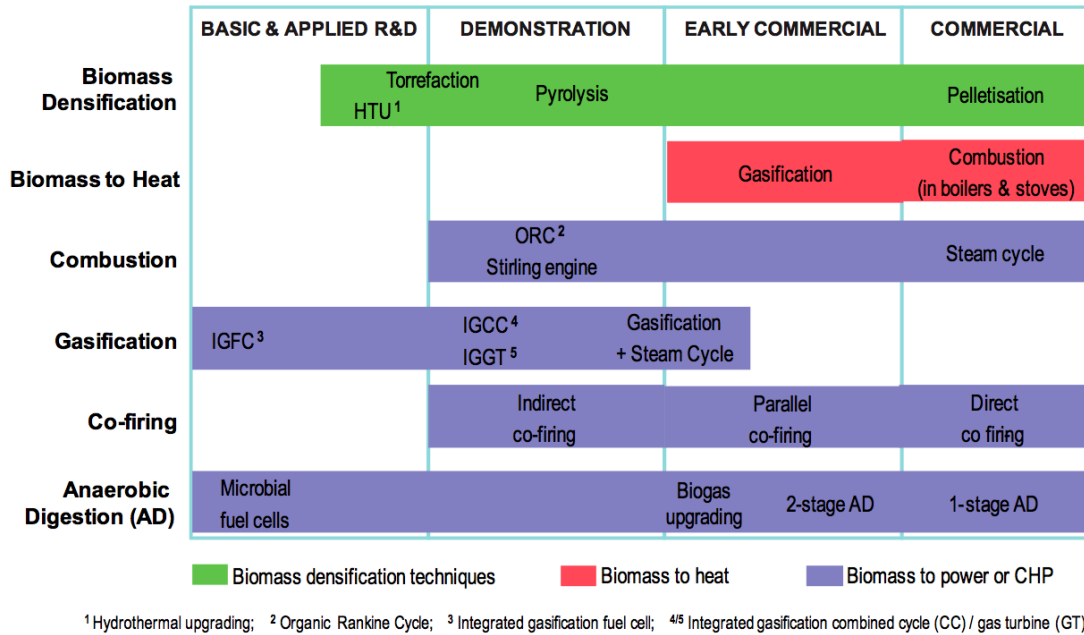


Figure 2.3: Development status of the main technologies to upgrade biomass and/or to convert it into heat and/or power [7].

2.2 Application of biomass gasification for the production of energy and fuels

Gasification is a thermo-chemical process that converts carbonaceous materials (coal, petroleum coke, biomass, etc.) into a combustible gas called producer gas. Biomass is one of the most abundant renewable energy sources on earth and is considered by far the highest quality form of indirect solar energy. Biomass energy is economic to produce and provides more energy than using other renewable energy sources [8].

The gasification of biomass is a thermal treatment, which results in a high production of gaseous products and small quantities of char and ash [9]. Gasification is carried out at high temperatures, where solid biomass undergoes thermal decomposition to form gas-phase products that typically include H_2 , CO , CO_2 , CH_4 , H_2O , larger gaseous hydrocarbons (CHs), tars, char, and ash [10]. This producer gas can be further used (downstream) for heat and power generation as well as for the production of transportation fuels.

Combined Heat and Power (CHP) plants have gained much attention in the last years. The use of the producer gas from biomass gasification directly in gas turbines or high temperature fuel cells generates not only electricity but a considerable amount of heat as well. Biomass gasifier/gas turbines are projected to have bio-electricity efficiencies of 40–45%, or more than double those of Rankine-cycle systems. The heat produced from the electricity generating process is captured and utilized for domestic purposes and can be used in steam turbines to generate additional electricity [11], [12].

Biomass Integrated Gasification Combined Cycle (BIGCC) technology demonstrates efficient, clean and cost-effective power generation from biomass [13]. Several projects have been initiated for IGCC applications over the last decade, however, only two have been implemented, the SYDKRAFT plant at Värnamo based on FOSTER WHEELER technology and the ARBRE plant based on TPS technology [14].

Furthermore, the use of biomass for district heating has been expanding rapidly in many European countries and especially in Austria and Germany [15]. A DH installation consists of network pipelines, which transfer heat to the consumers and then return back to the heat production station. The transportation pipelines are sized for the peak load demand, in order to respond to the worst case scenario. Several approaches have been already investigated for the design of Biomass District Heating Systems (BDHS) combined with biomass gasification and combustion facilities [16].

Another route is the biohydrogen production through the utilization of biomass feedstocks. Compared with traditional hydrogen-production process by physical and chemical methods, microbial conversion of biomass, such as agricultural and industrial wastes and residues, into biohydrogen gas using fermentative bacteria is an environmentally friendly and energy-saving process, and is attracting increasing interest as a useful way of converting biomass into hydrogen [17], [18].

Recently, biomass gasification in supercritical water or with in situ carbon dioxide capture using calcium oxide sorbents is a promising pathway for the renewable and sustainable production of hydrogen. Biomass gasification in supercritical water (SCW) is a promising technology for utilizing high moisture content biomass [19] while the application of CO_2 sequestration technologies could result in the net removal of CO_2 from the atmosphere. A recent review over the existing CO_2 capture and separation processes was published by Florin et al. [20].

Concerning the production of transportation fuels via biomass gasification, a market of bio-automotive fuels supported by governments in many countries already exists. These liquid transportation fuels are based on the use of food crops. From the viewpoint of economics, environment, land use, water use, chemical fertilizer use, etc., however, there is a strong preference for the use of woody, grassy materials as well as agricultural residues, municipal wastes and industrial wastes (e.g. black liquor) as a feedstock. Thus, the production of the synthetic transportation fuels such as biomethanol, bioethanol, DME (dimethyl-ether), FT (Fischer-Tropsch) fuel, SNG (synthetic natural gas) and hydrogen via gasification and synthesis is promising [21].

As shown in figure 2.4, bioethanol from sugar crops, biodiesel from oil crops and biogas from organic wastes are classified as the 1st generation bio-automotive fuels. The various biomass feedstock used for producing bio-automotive fuels can be grouped into two basic categories. The first is the currently available “first-generation” feedstock, which comprises various grain and vegetable crops. These are harvested for their sugar, starch, or oil content and can be converted into liquid fuels using conventional technology. The 2nd

generation of bio-automotive fuel feedstock comprises lignocellulosic biomass mainly from forest and agricultural residues, such as tree barks, tops and branches, demolition wood, tall grasses, and crop residues [21].

First generation (conventional) biofuels			
Biofuel type	Specific names	Biomass feedstock	Production process
Bioethanol	Conventional bioethanol	Sugar beet, grains	Hydrolysis & fermentation
Vegetable oil	Pure plant oil (PPO)	Oil crops (e.g. rape seed)	Cold pressing/extraction
Biodiesel	Biodiesel from energy crops Rape seed methyl ester (RME), fatty acid methyl/ethyl ester (FAME/FAEE)	Oil crops (e.g. rape seed)	Cold pressing/extraction & transesterification
Biodiesel	Biodiesel from waste FAME/FAEE	Waste/cooking/frying oil/animal fat	Transesterification
Biogas	Upgraded biogas	(Wet) biomass	Digestion
Bio-ETBE		Bioethanol	Chemical synthesis
Second generation biofuels			
Biofuel type	Specific names	Biomass feedstock	Production process
Bioethanol	Cellulosic bioethanol	Lignocellulosic material	Advanced hydrolysis & fermentation
Synthetic biofuels	Biomass-to-liquids (BTL): Fischer-Tropsch (FT) diesel Synthetic (bio)diesel Biomethanol Heavier (mixed) alcohols Biodimethylether (Bio-DME)	Lignocellulosic material	Gasification & synthesis
Biodiesel	Hydro-treated biodiesel	Vegetable oils and animal fat	Hydro-treatment
Biogas	SNG (Synthetic Natural Gas)	Lignocellulosic material	Gasification & synthesis
Biohydrogen		Lignocellulosic material	Gasification & synthesis or Biological process

Figure 2.4: Classification of 1st and 2nd generation bio-automotive fuels [22].

The hydrolysis pathway relies on advanced enzymes that can catalyze cellulose and lignocellulose into sugars and then ferment into ethanol. The gasification pathway uses high temperatures, controlled levels of oxygen, and chemical catalysts to convert biomass into synthetic fuels, including FT-diesel, DME, biomethanol, bioethanol, SNG and hydrogen. Another possible pathway to produce 2nd generation bioautomotive fuel is pyrolysis from which a liquid fuel, bio-oil, is obtained. Bio-oil does not appear in the above Fig. 2.4 because of a number of severe problems as an automotive fuel, such as poor volatility, high viscosity, coking, corrosiveness and high water content [21].

An overview of possible products obtained from biomass gasification process is illustrated in figure 2.5.

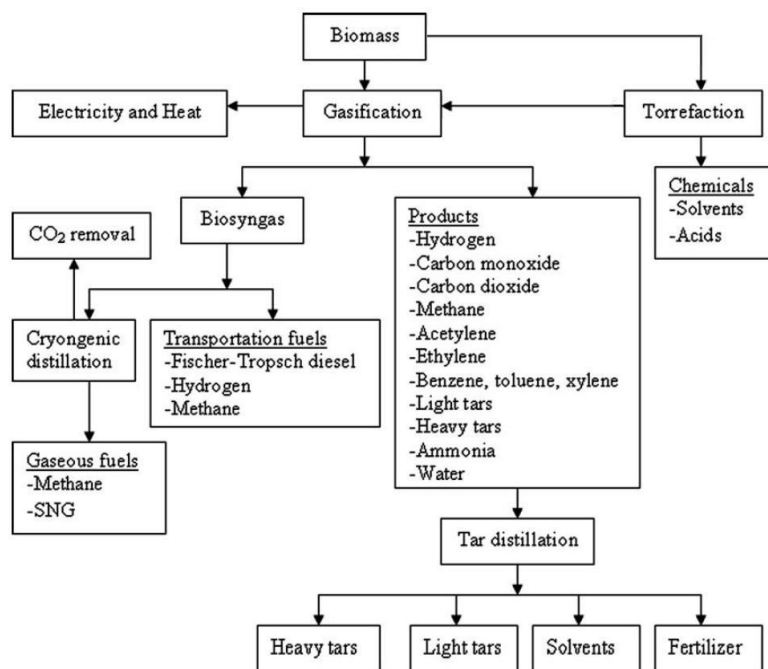


Figure 2.5: Products from biomass gasification process [8].

2.3 Gasification technologies

2.3.1 Principles of biomass gasification

Biomass is a complex mixture of organic compounds and polymers. The major types of compounds are lignin and carbohydrates, such as cellulose and hemicellulose, whose ratios and resulting properties are species dependent. Lignin, the cementing agent for cellulose, is a complex polymer of phenylpropane units. Cellulose is a polymer formed from d(+)-glucose, while the hemicellulose polymer is based on hexose and pentose sugars (Fig. 2.6).

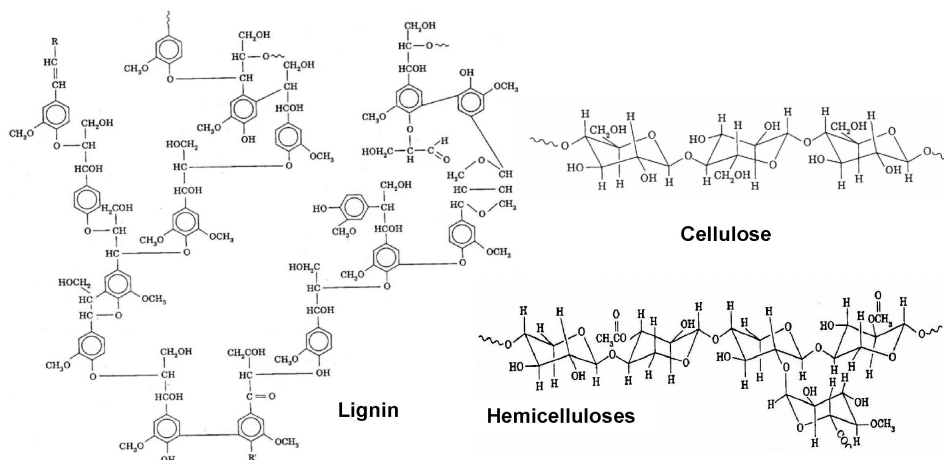


Figure 2.6: Biomass structure [23].

Thermochemical gasification is the conversion by partial oxidation at elevated temperature of a carbonaceous feedstock such as biomass into a gaseous energy carrier. This gas contains carbon monoxide, carbon dioxide, hydrogen, methane, trace amounts of higher hydrocarbons such as ethane and ethene, water, nitrogen (if air is used as the oxidising agent) and various contaminants such as small char particles, ash, tars and oils. The partial oxidation can be carried out using air, oxygen, steam or a mixture of them [24].

Gasification occurs in a number of sequential steps:

- **drying** to evaporate moisture
- **pyrolysis** to give gas, vaporised tars or oils and a solid char residue
- **gasification** or **partial oxidation** of the solid char, pyrolysis tars and pyrolysis gases

When a solid fuel is heated to 300 – 500 °C in the absence of an oxidising agent, it pyrolyses to solid char, condensable hydrocarbons or tar, and gases. The relative yields of gas, liquid and char depend mostly on the rate of heating and the final temperature. Generally in gasification process, pyrolysis proceeds at a much faster rate than gasification and the latter is thus the rate controlling step.

The gas, liquid and solid products of pyrolysis then react at high temperature, where gasification takes place, with the oxidising agent (typically air, steam, nitrogen, carbon dioxide, oxygen or a combination of these) to give permanent gases of CO , CO_2 , H_2 , and small quantities of hydrocarbon gases. Char gasification is the interactive combination of several gas-solid and gas-gas reactions in which solid carbon is oxidised to carbon monoxide and carbon dioxide, and hydrogen is generated through the water-gas shift reaction. The gas-solid reactions of char oxidation are the slowest and limit the overall rate of the gasification process [24].

Biomass gasification process is described by the following heterogeneous and homogeneous reactions (see Tables 2.1, 2.2). In the heterogeneous reactions gaseous molecules react with solid charcoal resulting in gaseous products, while in the homogeneous ones, only reactions between gaseous molecules take place.

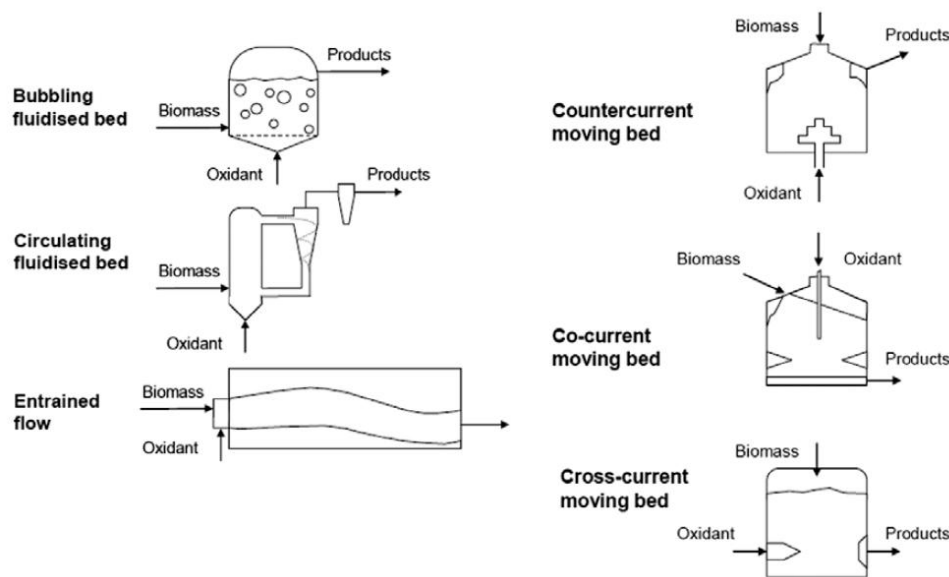
Table 2.1: Heterogeneous reactions.

$C + O_2 \leftrightarrow CO_2$	$\Delta H_R = -406 \text{ kJ/mol}$	Oxidation of carbon
$C + 1/2O_2 \leftrightarrow CO$	$\Delta H_R = -123 \text{ kJ/mol}$	Partial oxidation of carbon
$C + CO_2 \leftrightarrow 2CO$	$\Delta H_R = +172 \text{ kJ/mol}$	Boudouard reaction
$C + 2H_2 \leftrightarrow CH_4$	$\Delta H_R = -74 \text{ kJ/mol}$	Hydrogen gasification
$C + H_2O \leftrightarrow CO + H_2$	$\Delta H_R = +131 \text{ kJ/mol}$	Heterogeneous water-gas reaction

Table 2.2: Homogeneous reactions.

$CH_4 + H_2O \leftrightarrow CO + 3H_2$	$\Delta H_R = +206 \text{ kJ/mol}$	Steam reforming
$CO + H_2O \leftrightarrow CO_2 + H_2$	$\Delta H_R = -42 \text{ kJ/mol}$	Water-gas shift reaction
$CH_4 + 2O_2 \leftrightarrow CO_2 + 2H_2O$	$\Delta H_R = -802 \text{ kJ/mol}$	Methane oxidation
$CO + 1/2O_2 \leftrightarrow CO_2$	$\Delta H_R = -283 \text{ kJ/mol}$	Oxidation of carbon monoxide
$H_2 + 1/2O_2 \leftrightarrow H_2O$	$\Delta H_R = -242 \text{ kJ/mol}$	Oxidation of hydrogen

Several types of gasifiers have been developed, which are divided into three main groups: entrained flow gasifiers, fluidized bed gasifiers (bubbling/circulating) and fixed bed gasifiers, where the last is subdivided into: counter-current (updraft), co-current (downdraft) and cross-current moving bed. The main differences concern how reactants and products are moved around inside the reactor (especially the way in which the solid fuel and the gasification agent are contacted), the different gasification agents applied (air, oxygen and/or steam) and the resulting reaction conditions. The reactors may be operated at atmospheric pressure or at higher pressures, but the latter is only applicable to bubbling or circulating fluidized bed reactors as well as to entrained flow gasifiers. An overview of the different gasifier types is illustrated in the following figure 2.7.

**Figure 2.7:** Overview of different gasifier types [25].

Fixed-bed gasifiers involve reactor vessels in which the biomass material is either packed in or moves slowly as a plug, with gases flowing in between the particles [26]. Fixed-bed gasifiers are usually fed from the top of the reactor and can be designed in either updraft or downdraft configurations. With fixed-bed updraft gasifiers, the air or oxygen

passes upward through a hot reactive zone near the bottom of the gasifier in a direction countercurrent to the flow of solid material [27]. They can be scaled up; however, they produce a product gas with very high tar concentrations. This tar should be removed for the major part from the gas, creating a gas-cleaning problem. Fixed-bed downdraft gasifiers are limited in scale and require a well-defined fuel, making them not fuel-flexible, but they produce lower tar concentrations than the updraft ones [28].

Entrained flow gasifiers need pulverized fuel and are generally more suitable for coal rather than biomass gasification as they operate in temperatures above the ash melting point of biomass fuels. On the other hand, fluidized bed gasifiers are typically operated at 1075–1275K (limited by the melting properties of the bed material) and cannot be applied for the gasification of coal, as due to the lower reactivity of coal compared to biomass, a higher temperature is required ($> 1575\text{K}$) [28]. Fluidized-bed gasifiers take advantage of the excellent mixing characteristics and high reaction rates of gas–solid contacting [29].

The bubbling fluidized bed gasifier tends to produce a gas with tar content between that of the updraft and downdraft gasifiers. Some pyrolysis products are swept out of the fluid bed by gasification products, but are then further converted by thermal cracking in the freeboard region [29]. The circulating fluidized-bed gasifiers employ a system where the bed material circulates between the gasifier and a secondary vessel. The circulating fluidized-bed gasifiers are suitable for fuel capacity higher than 10MW_{th} [30].

2.3.2 Autothermal and allothermal gasification

The two main categories of the thermal gasification of biomass in terms of heat supply to the gasification reactions are the following:

- **Autothermal** (or direct) gasification
- **Allothermal** (or indirect) gasification

In the autothermal process, biomass is gasified directly by steam and oxygen at a temperature between 750 °C and 950 °C. In this case the required heat for the gasification is provided through the exothermic reaction of the partial oxidation of biomass. Autothermal gasifiers with oxygen (or oxygen-enriched air) produce a gas with medium heating value and lower hydrogen concentration compared to the product gas from indirectly heated (allothermal) gasifiers. The inert N_2 concentration is negligible when using oxygen. However, the CO_2 concentration is relatively increased compared to the producer gas from allothermal gasification.

In the allothermal process, the required gasification heat is provided externally through a heat exchanger or the circulation of heat carrying bed material between a gasifier and a combustor. Steam is introduced as gasification agent together with the feedstock in the reactor to promote the gasification reaction and increase the hydrogen yield. Indirectly heated gasifiers are designed to take advantage of the higher reactivity of biomass relative to coal and to produce a gas with higher hydrogen content than autothermal gasifiers.

Some of the advantages and drawbacks of autothermal and allothermal gasification in fluidized bed reactors are presented in the following tables 2.3, 2.4 [21].

Table 2.3: Advantages and drawbacks of autothermal gasification.

Advantages	Drawbacks
<ul style="list-style-type: none"> • Simple reconstruction of gasifier by switching gasification agent from air to oxygen to obtain nitrogen-free syngas • Simple pre-treatment of biomass • Suitable for M&L scale bio-automotive fuel plant over 200 MW • Since most operate at high pressure, product gas compression is not needed for downstream purification and synthesis unit operations 	<ul style="list-style-type: none"> • The erosion of refractory due to circulating hot solids in the gasifier can present some potential operational difficulties • Tars and CH_4 reforming is a challenge • High capital investment • An expensive and energy-consuming oxygen production plant is needed

Table 2.4: Advantages and drawbacks of allothermal gasification.

Advantages	Drawbacks
<ul style="list-style-type: none"> • No oxygen demand to obtain nitrogen-free syngas • Low investment costs • No or simple pre-treatment of biomass • Easy feeding of biomass • Suitable for biomass-based S&M scale bio-automotive fuel plant up to 200 MW • Avoiding problems of S-poisoning of Ni catalyst by bed material circulation between gasifier and combustor • Low temperature operation • Technology has been developed and demonstrated for heat and electricity production 	<ul style="list-style-type: none"> • Since most operate at low pressure, they require product gas compression for downstream purification and synthesis unit operations • The erosion of refractory due to circulating hot solids in the gasifier can also present some potential operational difficulties • Tars and CH_4 reforming needs downstream catalytic upgrading • Syngas cleaning is a big challenge • Steam conversion efficiency is low. The ratio of steam to biomass and energy recovery must be optimized in order to obtain high gasification efficiency

Examples of autothermal gasifiers

An example of autothermal gasification is realized by VTT Technical Research Centre of Finland, which recently started the UCG-programme (Ultra Clean Fuel Gas), in which a 500 kW_{th} pilot plant is constructed [31]. The flowsheet of this plant can be seen in

figure 2.8 and it consists of a pressurized circulating fluidized bed reactor, catalytic reforming, and further cleaning and conditioning. The catalytic reformer is meant to reduce hydrocarbons completely and methane by over 95%.

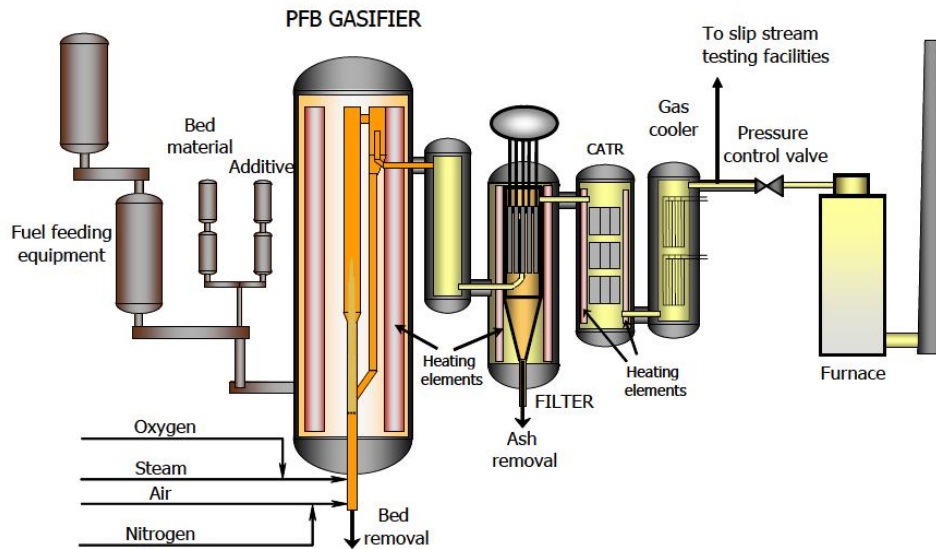


Figure 2.8: VTT's 500 kW PDU (Process Development Unit) for syngas and ultra clean fuel gas [32].

An Integrated Gasification Combined Cycle (IGCC) plant at Värnamo, Sweden based on FOSTER WHEELER technology can be seen in figure 2.9. The plant consists of pressurized steam/oxygen blown gasification, hot gas cleaning as well as reforming and upgrading of the producer gas.

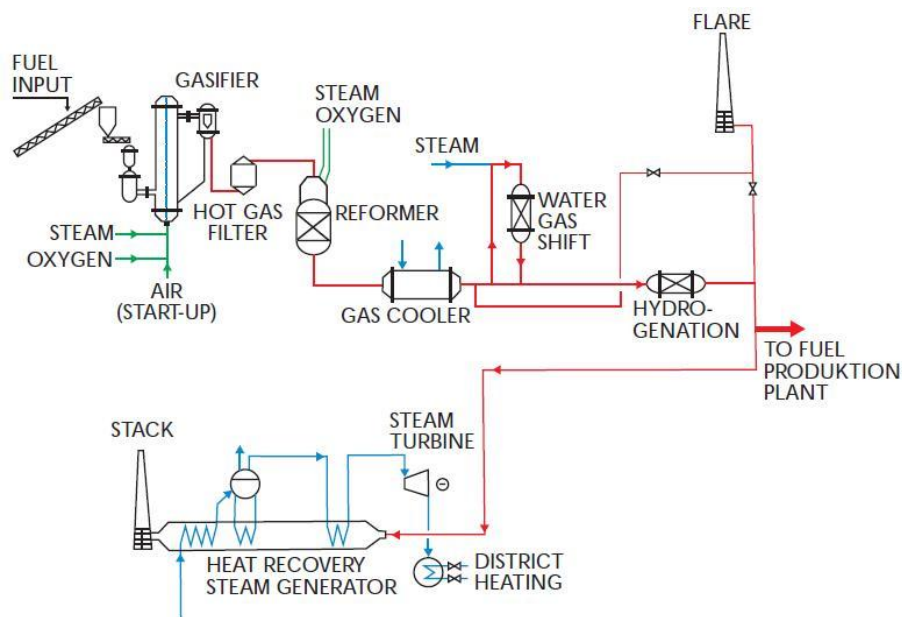


Figure 2.9: Process flow diagram of the Värnamo plant [33].

The plant produces about 6 MW_e electricity to the grid as well as 9 MW_{th} to the district heating system of the city of Värnamo, from a total fuel input equivalent to 18 MW . The accumulated operating experience amounts to about 8500 hours of gasification with more than 3600 hours of IGCC operation [33].

The Carbo-V process (see figure 2.10) is a relatively new development from the Umwelt-und Energietechnik (UET), a company in Freiberg, Germany. The process is described by three steps. In the 1st stage, the dried biomass is carbonized in a specially developed low temperature gasifier (NTV), where it is broken down by partial oxidation (low temperature carbonization) with air or oxygen at temperatures ranging between 400 and 600 °C to form biocoke and low temperature carbonization gas. In the 2nd stage, the low temperature carbonization gas containing tar is hypostoichiometrically burnt with air and/or oxygen in the combustion chamber of the Carbo-V gasifier at temperatures ranging between 1300 °C and 1500 °C. Finally, in the 3rd stage, the biocoke from the low temperature gasifier is blown into the Carbo-V reactor below the combustion chamber and there it reacts with the gas from the combustion chamber [33].

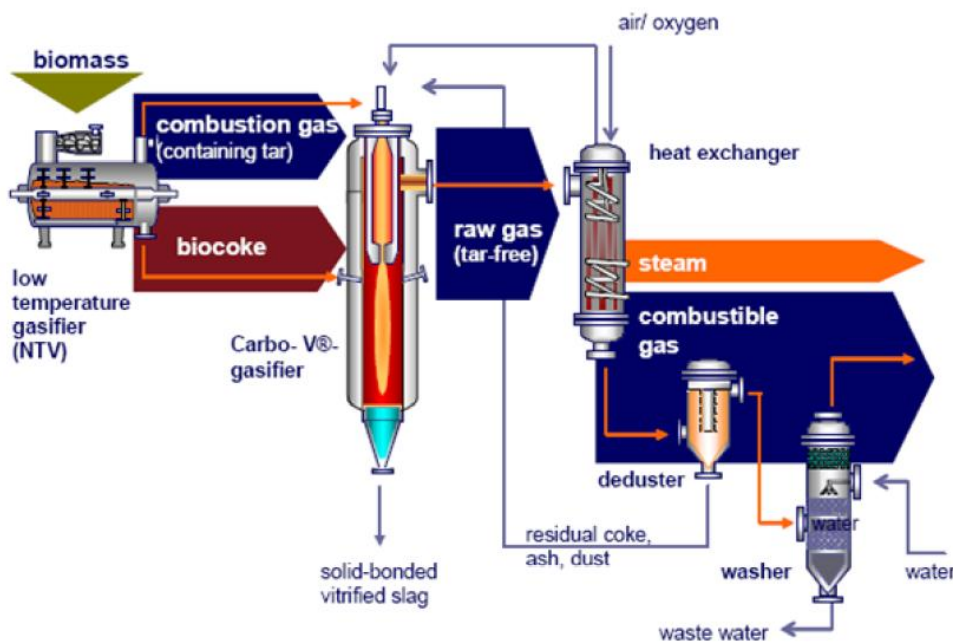


Figure 2.10: Carbo-V Process [33].

The GTI/IGT RENUGAS Process (see Figure 2.11) employs a 20 bar pressurized bubbling fluidized bed process. The process was extensively tested with a variety of biomass materials, including bark-paper, sludge mixtures, bagasse, and pelletized alfalfa stems in a 12 tons/day PDU at IGT test facilities in Chicago, USA. In January 2005, GTI completed the shakedown of a new 24 t/d, adiabatic Flex Fuel Test Facility in Des Plaines, Illinois. This facility is capable of gasifying up to 30 tons/day of biomass and at operating pressures up to 25 bar [34].

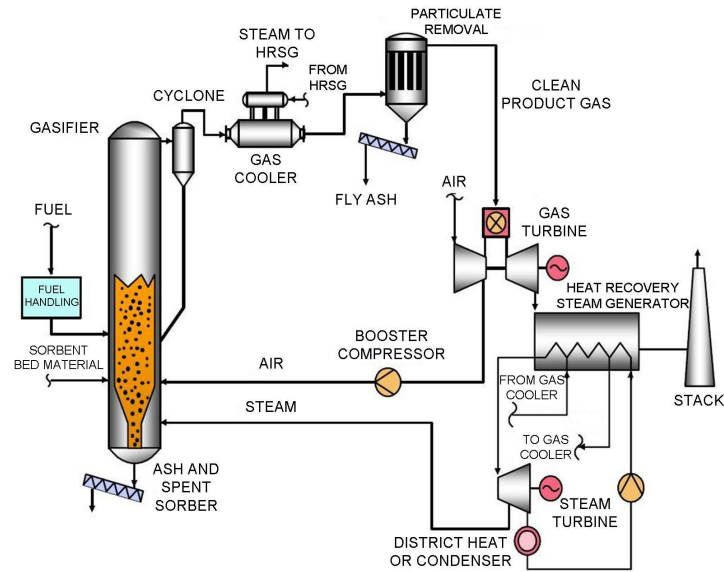


Figure 2.11: RENU GAS Process [35].

Finally, the german institute CUTE C has recently constructed an oxygen-blown 0,4 MW_{th} CFB gasifier connected to a catalytic reformer (see figure 2.12. Part of the gas is compressed and directed to a Fischer–Tropsch synthesis reactor [21].

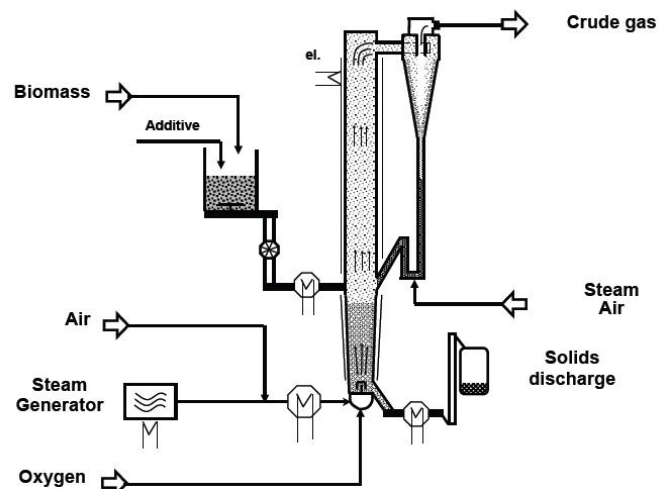


Figure 2.12: CUTE C Gasifier [36].

Examples of allothermal gasifiers

Concerning allothermal gasification, one of the most typical examples of allothermal processes is the Battelle gasification process, which produces a medium-Btu product gas without the need for an oxygen plant. The process (see figure 2.13) consists of two reactors and their integration into the overall gasification process. The two physically separate reactors used are: a **gasification reactor** in which the biomass is converted into

a medium Btu gas and residual char and a **combustion reactor** that burns the residual char to provide heat for gasification. Heat transfer between reactors is accomplished by circulating sand between the gasifier and the combustor [37].

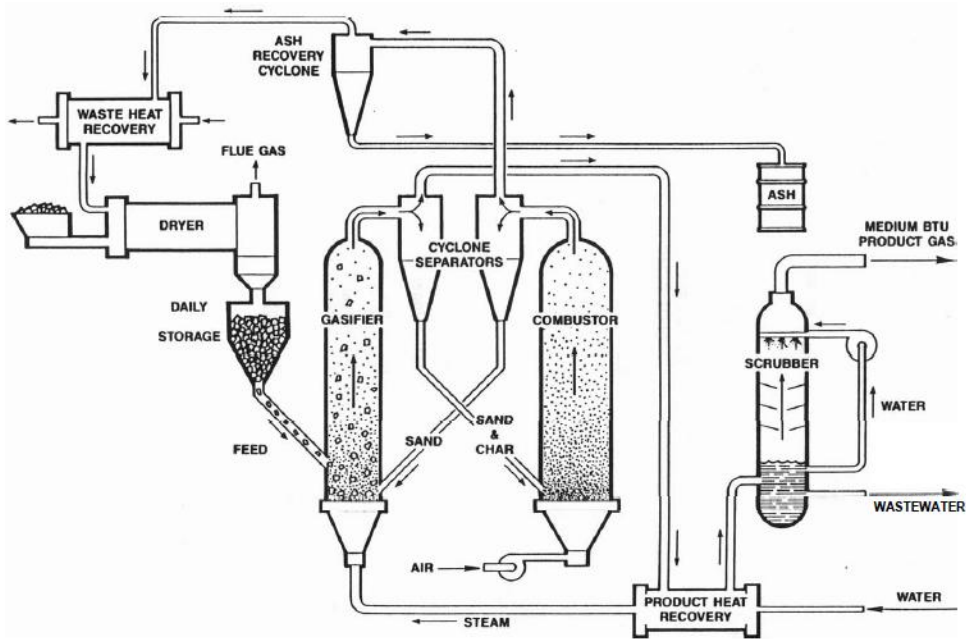


Figure 2.13: The Battelle gasification process [37].

In the Blue Tower (Blauer Turm), regenerative feedstock is used to manufacture a clean, hydrogen-rich product gas (called Blue Gas) via a process of staged reforming. This Blue Gas is used in the climate-friendly production of hydrogen and electricity. The process is illustrated in figure 2.14 and consists of three phases.

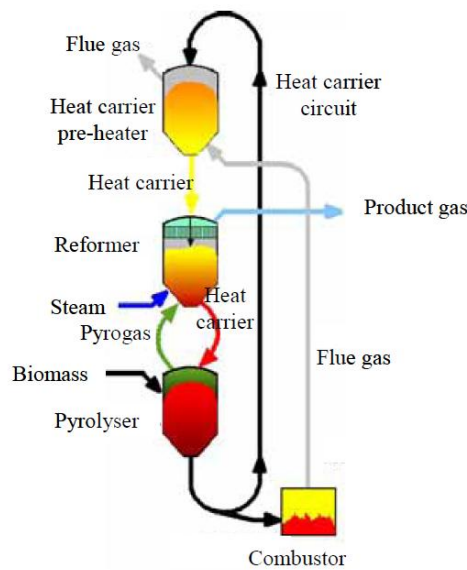


Figure 2.14: The Blue Tower gasification process [38].

Firstly, biomass is fed into the pyrolysis reactor where temperatures of approx. 600 °C lead to thermal decomposition of the feedstock. 80% of this feedstock is converted into a gas while 20% remains as solid material (coke), which is subsequently used to generate the process heat required by the Blue Tower. The produced gas is purified in a second stage (called reforming) by the addition of steam at approximately 950 °C into a clean, CO_2 -neutral product gas. The required heat for thermal decomposition (phase 1) and gas refinement (phase 2) is provided by heated ceramic beads. These ceramic beads move through the process steps from top to bottom in the Blue Tower in a closed cycle, and dissipate their heat step-by-step. The solid material (coke) described above is burned in order to heat up the beads [39].

An innovative process for combined heat and power production based on steam gasification has been demonstrated in Güssing (8 MW_{th} CHP plant). Biomass is gasified in a dual fluidized bed reactor. The producer gas is cooled, cleaned and used in a gas engine (see figure 2.15).

The fluidized bed gasifier consists of two zones, a gasification zone and a combustion zone. The gasification zone is a bubbling bed fluidized with steam, to produce a nitrogen-free producer gas. The combustion zone is a circulating bed fluidized with air which delivers the heat for the gasification process via the circulating bed material. The producer gas is cooled and cleaned by a two stage cleaning system. A heat exchanger reduces the temperature from 850 °C to about 150 °C. The first stage of the cleaning system is a fabric filter to separate particulates, which return back to the combustion zone of the gasifier. In the second stage the gas is scrubbed to remove tar compounds. The dust from the filter, the spent scrubber liquid saturated with tar, and the condensate are thermally decomposed by recycling them to the combustion zone of the gasifier. The clean gas is finally fed into a gas engine to generate electricity and heat [33].

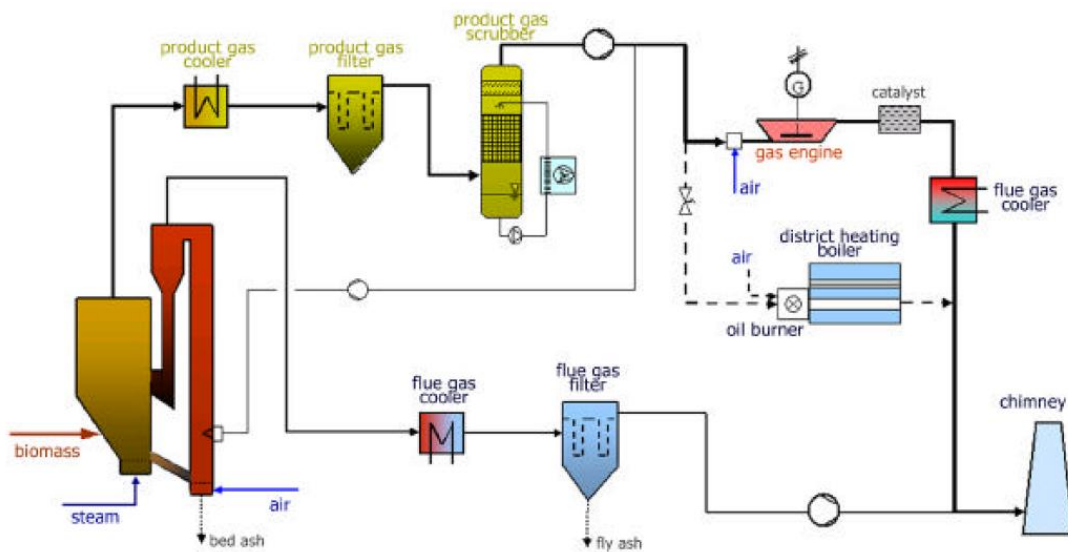


Figure 2.15: Process flow sheet of the Güssing CHP plant [33].

Another allothermal gasification process is developed by the Energy research Centre of the Netherlands (ECN) and is optimized for the production of Substitute Natural Gas (SNG). The Milena gasifier contains separate sections for gasification and combustion. Figure 2.16 shows a simplified scheme of the MILENA process. The gasification section consists of three paths: riser, settling chamber and downcomer. The combustion section contains two parts, the bubbling fluidized bed combustor and the sand transport zone. The arrows in figure 2.16 represent the circulating bed material. The gasifier is now scaled up from lab-scale 30 kW_{th} (in operation since 2004) to 800 kW_{th} . The construction of the Milena pilot plant is finished in 2008 for SNG production [40].

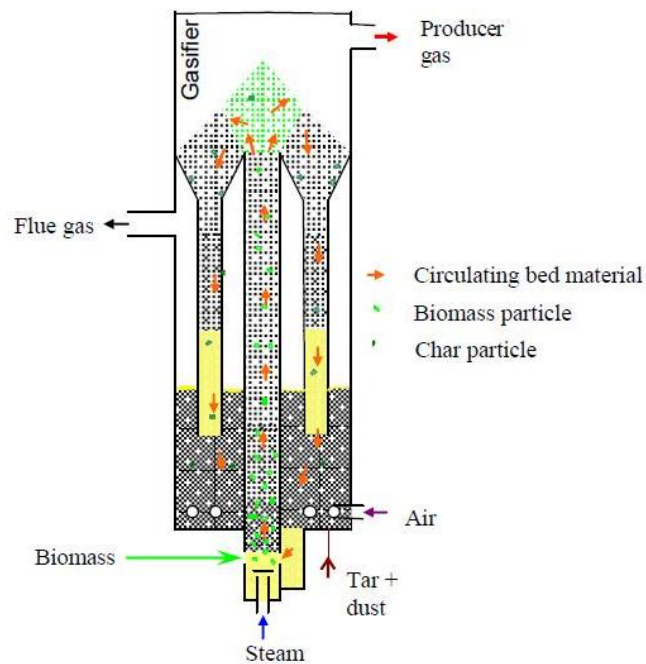


Figure 2.16: Simplified scheme of MILENA gasifier [40].

Finally, within the AER process (Absorption Enhanced Reforming), biomass steam gasification can continuously produce a raw gas with more than 75 Vol% hydrogen, suitable for downstream fuel synthesis or electricity production. The CO_2 produced during the steam gasification is separated from the reaction zone by a high temperature CO_2 absorbent, e.g. $CaO/CaCO_3$. The CO_2 absorption shifts the reaction equilibrium towards increased hydrogen concentration. As the reaction of carbon dioxide with the absorber is exothermic, it supplies in-situ the required heat for the reforming/gasification. A flue gas with increased CO_2 concentration is produced when the sorbent is regenerated in a subsequent process step [41].

In order to realise continuous operation, two fluidized-bed reactors are coupled. In the first reactor, the biomass gasification with steam takes place with absorbent as the bed material while the second one operates in the combustion mode to regenerate the sorbent. The technical concept of the AER process can be seen in the following figure 2.17.

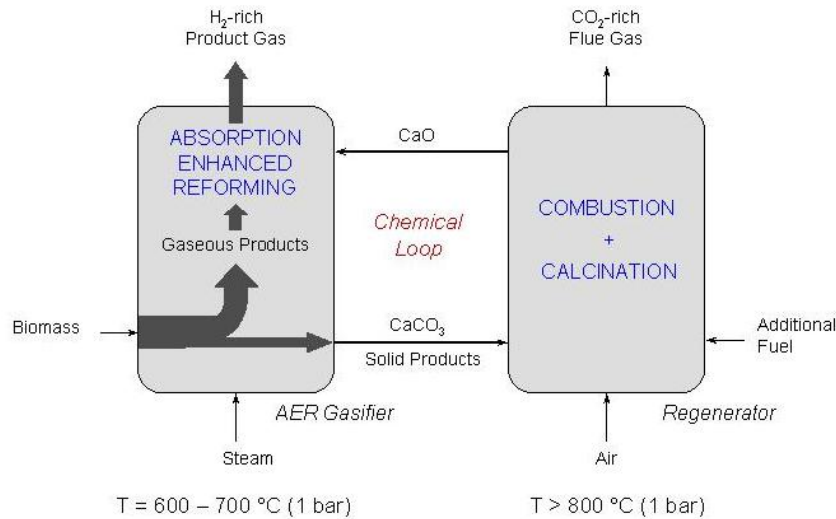


Figure 2.17: Technical concept of the AER process [42].

2.4 Biomass gasification producer gas

2.4.1 Quality of the producer gas

The composition of the producer gas obtained from the gasification of biomass depends on various parameters, which affect not only the producer gas quality but also the efficiency of the whole process [43]. The most important of these parameters are the following:

- Fuel characteristics
- Reactor type
- Gasification medium
- Gasification temperature
- Operating pressure
- Steam to biomass ratio (in case of steam gasification)
- Equivalence ratio (in case of oxygen or air gasification)
- Use of catalysts and absorbents
- Bed material type

The characteristics of each fuel are determined through physical properties, proximate and ultimate analyses. Physical properties contain the particulate size as well as the absolute and the bulk density. Proximate analysis includes the volatile matter, moisture content, fixed carbon, ash content and higher heating value (HHV) while the ultimate analysis comprises the carbon, hydrogen, oxygen, nitrogen and sulfur elements of the dry biomass on a weight percentage basis. The moisture of the fuel effects the amount of combustible gases and can increase the amount of hydrogen gas and other hydrocarbon

components. If high moisture fuel is used in the gasifier, the efficiency of the gasifier decreases [44].

The quality of the producer gas depends mainly on the reactor type. Table 2.5 provides an overview of typical producer gas compositions from different gasifiers for the gasification of wood with air. The concentrations are based on dry gas volume (n.d.: not determined) and the LHV is calculated from the values for H_2 , CO and CH_4 .

Table 2.5: Gas compositions of different wood gasification systems [45].

Gas composition (vol %, dry basis)	Fixed bed		Fluidized bed	
	co-current	counter-current	bubbling	circulating
H_2	14	21	9,3	14,8
CO	20	22,5	15,8	15,4
CO_2	10	11,5	16,7	15
CH_4	2,5	1,5	3,8	4,2
C_nH_m	n.d.	n.d.	1,6	2
N_2	n.d.	n.d.	52,8	39,6
LHV (MJ/Nm^3)	4,9	5,6	4,4	5

Biomass can be gasified using steam or air as gasification medium. Air gasification is an exothermic process, which produces a low heating-value gas (LHV 5–6 MJ/Nm^3) rich in CO but having not so big amounts of H_2 and higher hydrocarbons. Steam gasification on the other hand is an endothermic process, which produces a medium heating value gas (LHV 12–13 MJ/Nm^3) rich in H_2 and CO [46]. The influence of different gasification mediums on the composition of the product gas can be seen in the following table 2.6.

Table 2.6: Composition of biomass gasification producer gas for different gasification mediums [47].

Gas composition (vol %, dry basis)	Air	Steam	Steam- O_2 mixtures
H_2	5,0-16,3	38-56	13,8-31,7
CO	9,9-22,4	17-32	42,5-52,0
CO_2	9,0-19,4	13-17	14,4-36,3
CH_4	2,2-6,2	7-12	6,0-7,5
C_2H_n	0,2-3,3	2,1-2,3	2,5-3,6
N_2	41,6-61,6	0	0
LHV (MJ/Nm^3)	3,7-8,4	12,2-13,8	10,3-13,5

Furthermore, the gasification temperature not only affects the product yield but also governs the process energy input. A high gasification temperature, particularly between 800 and 850 °C, produces a gas mixture rich in H_2 and CO with small amounts of CH_4 and higher hydrocarbons [46].

In addition, as the pressure of the gasification process increases, the equilibrium H_2 and CO yields reduce due to the Reforming reaction, which shifts its chemical equilibrium to the production of more H_2O and CH_4 and to the reduction of H_2 and CO . Simulations carried out to study the effect of reducing the pressure below 101,325 kPa on equilibrium product yield showed that increase in H_2 yield is negligible ($< 0,2\%$) even for pressures as low as 10,13 kPa [48].

Regarding steam gasification, the Steam to Biomass Ratio (SBR) refers to moles of steam fed per mole of biomass. SBR has a strong influence on both product gas composition and energy input. At low values of SBR, solid carbon and methane are formed. As more steam is supplied, both of these species are reformed to CO and H_2 . For SBR values higher than one, $C(s)$ and CH_4 content reduce to very small values and H_2 and CO_2 yields increase while CO reduces [46], [49].

In case of using air as gasification medium, the Equivalence Ratio (ER) refers to the amount of external oxygen (or air) supplied to the gasifier. ER is obtained by dividing the actual oxygen (or air) to biomass molar ratio by the stoichiometric oxygen (or air) to biomass molar ratio. Using air instead of oxygen, though economical, has the negative effect of diluting the product gas due to the presence of nitrogen. The optimum ER would supply enough air for the biomass to be partially oxidized without significant dilution of the product gas [46], [49].

Finally, the use of catalysts (tar cracking catalysts) and sorbents (CaO sorbent for CO_2 capture) as well as the type of bed material have a strong influence on the yield and composition of gas produced from the gasification process and constitute a promising pathway for hydrogen production. The effect of three different bed materials on the producer gas quality during gasification in a BFB at 650 °C is presented in table 2.7.

Table 2.7: Composition of biomass gasification producer gas for different bed materials [50].

Gas composition (vol %, dry basis)	Silica sand	Calcined limestone	Calcined waste concrete
H_2	21,84	63,56	46,94
CO	45,00	4,85	14,18
CO_2	14,99	24,75	30,55
CH_4	13,61	5,75	6,81
C_2H_4	3,34	0,66	1,05
C_2H_6	1,22	0,43	0,46
LHV (MJ/kg)	6,49	10,98	7,66

2.4.2 Tar content in the producer gas

The tar content in biomass gasification process depends generally on the same parameters as the ones which affect the composition of the producer gas and are mentioned in the previous subsection.

The amount of tar from a given gasifier is a function of the temperature/time history of the particles and gas, the point of introduction of feed in fluidized beds, the thoroughness of circulation (fluidized beds), the degree of channeling (fixed beds), the feed particle size distribution, the gaseous atmosphere (O_2 , steam), the geometry of the bed, the bed material and the method of tar extraction and analysis [1].

In view of this fact, it does not seem worthwhile trying to rationalize the amounts of tar except in the broadest terms. An effort to classify the influence of different parameters on the tar content is made in the following paragraphs.

Influence of reactor type on the tar content

Each type of gasifier has different reaction conditions and, consequently, different tar compositions and product yields. Table 2.8 presents the particle and tar content of raw producer gas from different gasifier systems.

Table 2.8: Ranges of particle and tar contents of raw producer gas from different gasifier systems [51].

	Fixed bed		Fluidized bed	
	co-current	counter-current	bubbling	circulating ^a
Particle content [g/Nm^3]	0,02-8	0,1-3	1-100	8-100
Tar content [g/Nm^3]	0,01-6	10-150	1-23	1-30

^avalues are determined after cyclone

The counter-current fixed bed gasifier generates a high yield of tar (typically 100-150 g/Nm^3), which is a mixture of the original low-temperature-pyrolysis products and more thermally processed products from the lower parts of the pyrolysis zone. On the other hand, co-current and fluidized bed gasifiers usually generate low amounts of tar (less than 20 g/Nm^3), due to the higher tar formation temperature. These tars are mainly in the gas phase at the gasifier's outlet temperatures. In a correctly operating co-current gasifier, the pyrolysis products pass through a hot char containing combustion zone, in which the tars are oxidised and thermally cracked. In theory, the organic vapours from co-current gasifiers should be decomposed totally, while in practice the amount of tars is mainly a function of the temperature, the efficiency of the combustion zone and the channeling of the bed. The fluidized bed gasifiers operate almost isothermally. The high

temperature and the good gas-solid contact result in partial cracking of the tarry pyrolysis products [52].

Influence of gasification medium on the tar content

Generally, the use of different gasification mediums has a severe effect on the tar reaction mechanism and consequently on the whole gasification process. The influence of the three different types of gasifying agents (pure steam, steam-oxygen mixtures, air or pure oxygen) on the tar content in an atmospheric bubbling fluidized bed has been studied by Gil et al. [47], who presented that using pure steam as gasification medium results in a higher tar content than using oxygen or steam-oxygen mixtures (table 2.9). On the other hand, nitrogen dilutes the gas mixture if air is used as gasification agent, which results in a lower heating value producer gas.

Table 2.9: Tar content and LHV for different gasification mediums in a BFB reactor [47].

	Air	Steam- O_2 mixtures	Steam
Tar content (g/Nm^3)	2-20	4-30	30-80
LHV (MJ/Nm^3 , dry basis)	4,5-6,5	12,5-13	12,7-13,3

Influence of gasification parameters on the tar content

The gasifier's operating conditions play a very important role in tar formation and tar reduction process. The most important influencing parameters include temperature, pressure, equivalence ratio (ER) in case of air gasification, steam to biomass ratio (S/B) in case of steam gasification and residence time.

Gasification temperature affects not only the amount but also the conversion rate and composition of tar by influencing the chemical reactions involved in the whole gasification network. Kinoshita et al. [53] observed during sawdust gasification in a fixed bed gasifier that the total number of detectable tar species decreased with increasing temperature. They also confirmed that higher temperatures favour the formation of fewer aromatic tar species without substituent groups such as benzene, naphthalene, phenanthrene, etc. Destruction of these aromatic hydrocarbons occurs only at temperatures above 850 °C.

Yu et al. [54] performed pyrolysis experiments of birch wood in a free-fall reactor to observe the temperature effect on the process and found that an increasing temperature promotes the formation of gaseous products at the expense of total tar. More than 40% reduction in tar yield was reported when the temperature was raised from 700 to 900 °C.

Furthermore, Narváez et al. [55] found out that by changing the bed temperature of the bubbling fluidized bed from 700 to 850 °C, a drastic decrease took place in the tar

content (about 74% less). The tar amounts decreased from 19 g/Nm^3 at $700 \text{ }^\circ\text{C}$ to 5 g/Nm^3 at $800 \text{ }^\circ\text{C}$.

Van Paasen et al. [56] studied the effect of temperature not only in the overall tar content but also in the amount of each tar class (described in the next chapter). Increasing the gasification temperature from 750 to $900 \text{ }^\circ\text{C}$ at constant ER appeared to have a large impact on tar formation, in particular on the tar composition. The class 2 tars were decomposed almost completely at $850 \text{ }^\circ\text{C}$ and higher. On the other hand, the 2-3 ring (class 4) and 4-7 ring Polycyclic Aromatic Hydrocarbon (PAH) compounds (class 5) concentration continuously increased with increasing temperature. These compounds are probably the products from the thermal cracking of even heavier hydrocarbons (class 1). The class 3 light aromatic compounds went through a maximum at $780 - 800 \text{ }^\circ\text{C}$, just as the total tar concentration.

Evans and Milne [1] studied also the effect of temperature on different groups of tars which are called primary, secondary and tertiary tars (classification is described in the next chapter) as it is illustrated in figure 2.18. Primary tars decrease with increasing temperature while secondary and tertiary-alkyl tars reach a maximum at 750 and $900 \text{ }^\circ\text{C}$ respectively and then start to decrease. On the other hand, tertiary-PNA tars show an increase with increasing temperature.

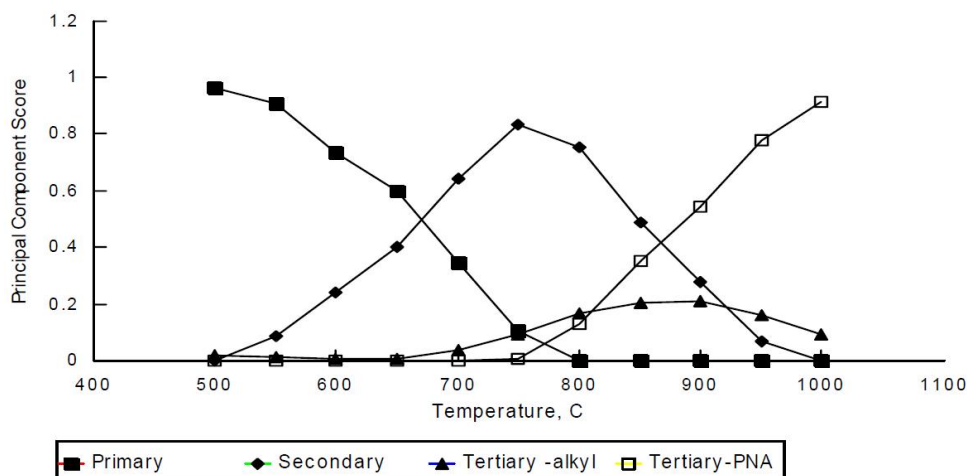


Figure 2.18: The distribution of the four tar component classes as a function of temperature at 0,3s gas-phase residence time [1].

Except for temperature, several researchers have investigated the effect of system pressure on biomass gasification. Knight et al. [57] presented that when pressure was increased to 21,4 bar, almost complete elimination of phenols was observed for wisconsin whole tree chips. Although the amount of total tar decreased, the fraction of PAH increased with increasing pressure.

Wang et al. [58] observed a decrease in the amount of light hydrocarbons (LHC, lower than naphthalene) as well as that of tar in the fuel gas with an increasing ER for pressurized gasification with 100% carbon conversion.

Concerning the equivalence ratio (ER), different publications have shown that it strongly influences the type of gasification products. According to Kinoshita et al. [53], tar yield as well as tar concentration decrease as the ER increases, because of the greater availability of oxygen to react with volatiles in the flaming pyrolysis zone. This effect of ER is more significant at higher temperatures. Narváez et al. [55] reported a similar trend with increasing ER for gasification of pine sawdust at 800 °C. A tar content of about 2,7 g/Nm^3 was reported when the ER was increased up to 0,45. They also gave a comparison of various experiments with varying ER from other researchers.

In case of steam gasification, Herguido et al. [59] reported the effect of steam to biomass ratio (S/B) on the gasification producer gas and especially on its tar content. A sharp reduction of the amount of tars was observed when the S/B ratio was increased from 0,5 to 2,5. The effect of steam as reagent on the tar reforming reaction was studied by Wang et al. [60], who presented that the tar residual rate (defined as the ratio of the tar amount in the reformed gas to the tar amount in the pyrolysis gas) in both reformed gases produced from pyrolysis gases of wood chips and polyethylene decreased with the increase of the steam ratio from 0 to 1,0.

Finally, the effect of residence time on the amount of tars was investigated by Van Paasen et al. [56], where it was found that increasing the gas residence time in the free-board of a bubbling fluidized bed gasifier has a similar, but much smaller, effect than increasing the gasification temperature.

According to Kinoshita et al. [53], residence time has little influence on the tar yield, but it significantly influences the tar composition. The reported residence time was based on the superficial velocity of the wet product gases in the gasifier. Amounts of O_2 -containing compounds tend to decrease with increasing residence time. Yields of 1- and 2-ring compounds (except benzene and naphthalene) decrease whereas that of 3- and 4-ring compounds increase in the total tar fraction.

Corella et al. [61] observed a decrease in the total tar content when the space time (kg calcined dolomite/kg biomass_{daf}h⁻¹) was increased for biomass gasification with in-bed use of dolomite. The tar amount decreased from 6 g/Nm^3 at a space time of 0,1 to 2 g/Nm^3 at space time 1,0.

Influence of bed additives and catalysts on the tar content

Catalytic tar destruction has been extensively reported in the literature over the last years. These catalysts include Ni-based catalysts, calcined dolomites and magnesites, zeolites, olivine and iron catalysts. Among all these only few have been tried as active bed additive inside the gasifier during gasification. There is a great potential for in-bed additives in terms of tar reduction and thus avoiding complex downstream tar removal methods. These bed additives act as in-situ catalysts promoting several chemical reactions inside the gasifier [62].

Several authors have studied the effect of different catalysts in reducing tars obtained by biomass gasification. Among all the active materials used as in-bed additives, dolomite is the most popular and mostly studied. Dolomite is a calcium magnesium ore with the general chemical formula $CaMg(CO_3)_2$ that contains 20% MgO , 30% CaO , and 45% CO_2 on a weight basis, with other minor mineral impurities. Dolomites, in their naturally occurring form, are not nearly as active for tar conversion until they are calcined. Calcination of dolomite involves decomposition of the carbonate mineral, eliminating CO_2 to form $MgO-CaO$. Complete dolomite calcination occurs at fairly high temperatures and is usually performed at 800 – 900 °C [63].

A lot of research has been done using this catalyst with regard to tar cracking both in-bed and downstream in a secondary reactor. Corella et al. [61] reported that in presence of dolomite and with suitable experimental conditions, it was possible to achieve tars reductions of about 80%. Orío et al. [64] compared the action of several dolomites with different origins and compositions in the reduction of tars produced by biomass gasification. These authors reported that dolomites with higher Fe_2O_3 contents were more effective in tar reduction. The catalytic action of dolomite was compared to those of olivine by Corella et al. [65], who stated that dolomite was 1,4 times more effective in tar reduction than olivine, but dolomite had the disadvantage of suffering more attrition, than olivine, thus producing 4 to 6 times more fine particulates, which by being entrained with the gasification gas demand extensive gas cleaning [66].

Rapagná et al. [67] investigated the catalytic activity of olivine and observed that it has a good performance in terms of tar reduction while its activity is comparable to calcined dolomite. They reported more than 90% reduction in the average tar content-the tar amount was 2,4 g/Nm^3 compared to 43 g/Nm^3 when using only sand.

Several authors have reported that, though dolomite and olivine could lead to the reduction of the amount of tars to a certain extent, if further decrease should be needed, other catalysts should be used, such as nickel and magnesium oxides [66]. Garcia et al. [68] synthesized different nickel and magnesium oxides supported on alumina and compared their performance in decreasing tar contents during biomass gasification. $NiMgAl_2O_5$ was the most effective catalyst in tar reduction as well as the most stable and the one with the highest initial activity, being followed by $NiMgAl_4O_8$.

Commercial nickel reforming catalysts have been applied in a number of model compound and novel feedstock studies for the purpose of producing a hydrogen-rich product gas, not necessarily for tar reforming, although typical tar compounds are often included in the feed. Simell et al. [69] have also investigated commercial nickel steam reforming catalysts for tar conversion. They used toluene as a model tar compound in several studies to investigate the effectiveness of Ni/Al_2O_3 catalysts at elevated pressures. Corella et al. [70] tested seven different commercial nickel-based catalysts for steam reforming of light and heavier hydrocarbons for tar removal in a producer gas from an atmospheric fluidized bed biomass gasifier, using air as the gasifying agent.

Regarding the use of Ni-based catalysts, the major problem is the fast deactivation due to carbon deposition on the catalyst and poisoning due to the presence of H_2S . In view of the experience of the Pacific Northwest Laboratory (PNL), in bed use of nickel catalyst is not an attractive option. Baker et al. [71] and Mudge et al. [72] reported that the lifetime of the nickel catalysts could be extended by placing it in a secondary bed instead of using it inside the gasifier. Placing the $NiCuMo$ on $Si-Al_2O_3$ and Ni on α -alumina catalysts in a secondary fluidized-bed reactor downstream to the gasifier, they observed no deactivation for 30–40 h tests.

Finally, another inexpensive material which could be applied as tar cracking catalyst is char, which has also been widely reported in the literature in the past. Char is not only a cheap and available material, but is also indigenously produced inside the gasifier itself. Char has been reported to be used in secondary tar cracking reactors [73]. Chembukulam et al. [74] presented that cracking over a char bed at a temperature of 950 °C resulted in almost complete decomposition of tar and pyrolygneceous liquor into gases of low calorific value. It should be noted that char itself gets converted during the gasification process, and hence there may be need of external continuous supply of char into the gasifier.

3 Biomass gasification tars

3.1 Definition of tars and their specific features

One of the main issues associated with biomass gasification is how tars are defined. Tar is a generic term describing a complex range of oxygenated organic constituents that are produced by the partial reaction of the biomass feedstock. Such materials reside in the hot gas stream as vaporized material or as persistent aerosols, but typically condense at cooler temperatures. These tars include a variety of oxygenated aromatics formed in the pyrolysis step of the gasification process. The definition of the term “tars” has been actively discussed over the past few years without conclusive resolution [75].

Several definitions of biomass tars have been given by many institutions working on biomass gasification like [76]:

- the mixture of chemical compounds which condense on metal surfaces at room temperature
- the sum of components with boiling point higher than 150 °C
- all organic contaminants with a molecular weight larger than benzene

However, one general (uniform) definition does not exist. Apart from the general definition of tars, definitions have been given for “heavy tars”, “gravimetric tars” and “light tars”.

In a review of biomass gasifier tars, Milne et al. [1] defined them as the organics produced under thermal or partial-oxidation regimes (gasification) of any organic material and reported that they are generally assumed to be largely aromatic.

In the context of gasification, all aromatic and polyaromatic hydrocarbons present in the producer gas are summarized with the definition of tars. In addition, due to the fact that tar is often given an operational definition based on organics from gasification that condensed under operating conditions of boilers, pipes and internal combustion engine (ICE) inlet devices, the diversity in the operational definitions of tars usually comes from the variable producer gas compositions required for a particular end-use application and how the tars are collected and analyzed [1].

3.2 Mechanism of tar formation and conversion in the gasification process

Biomass gasification is a complex combination of pyrolysis and oxidation reactions in the condensed and vapor phases, which results in the formation of tars in a series of complex reactions. The identification of the reaction regimes and the characterization of the gaseous constituents present as well as the nature of the major vapor- and solid-phase reactions were made by Evans and Milne [77] and are illustrated in figure 3.1. The product distribution in each regime is a function of process variables, such as oxygen level, steam-to-biomass ratio, pressure, and the time and temperature history of the solid and gaseous materials.

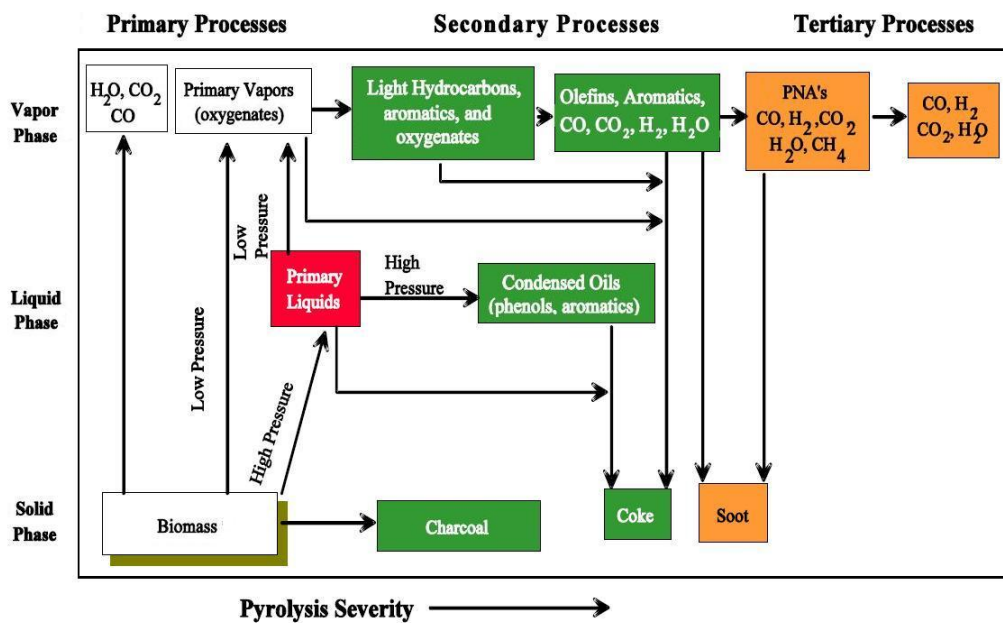


Figure 3.1: Pyrolysis pathways [77].

A *primary pyrolysis* regime is distinguished at temperatures from 400 to 700 °C that yields the production of primary vapors (oxygenates). The authors characterized the primary vapors as low molecular mass products, representing monomers and fragments of monomers of the biopolymers of biomass. The secondary *hydrocarbon* regime from 700 to 850 °C mainly produces phenolics and olefins. Tertiary products appear in the temperature range of 850 – 1000 °C and are characterized by the presence of aromatics.

The solid products can be distinguished by their origins: charcoal retaining the morphology of the original lignocellulosic, coke arising from the thermolysis after the deposition of liquids and organic vapors, and soot from the homogeneous nucleation of high-temperature products of hydrocarbons from the vapor phase. As mentioned by Evans and Milne [77], only the upper, vapor-phase pathway in figure 3.1 is experimentally verified. The condensed-phase transitions could not be tracked by their experimental setup.

A general correlation between temperature and tar composition is presented in figure 3.2 with temperature rising from about 400 °C on the left to about 900 °C on the right. This tar formation scheme is proposed by Elliott et al. [78], who reviewed the composition of biomass pyrolysis products and gasifier tars from various processes.

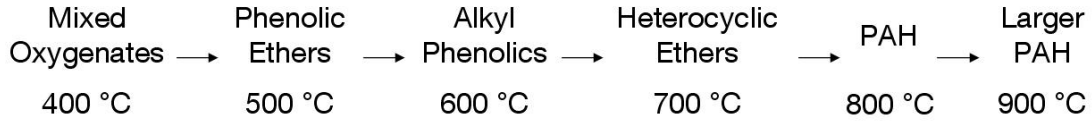


Figure 3.2: Tar formation pathway [78].

Figure 3.2 shows the transition as a function of process temperature from primary products to phenolic compounds and aromatic hydrocarbons. The formation of tar is highly dependent on the reaction conditions. Due to increased reaction temperature, secondary reactions occur in the gas phase converting oxygenated tar compounds into light hydrocarbons, aromatics, oxygenates and olefins, which subsequently form higher hydrocarbons and larger PAH in tertiary processes [1].

3.3 Tar cleaning systems

Removal of tar is among the greatest technical challenges to the wide application of gasification systems. Tar is undesirable because of various problems associated with condensation, formation of tar aerosols and polymerization to form more complex structures, which cause problems in the process equipment as well as the engines and turbines used in the downstream application of the producer gas. The various gas cleaning strategies and available technologies are presented schematically in figure 3.3.

Considerable efforts have been directed towards the removal of tar from the fuel gas of biomass gasification. Tar removal technologies can be broadly divided into two categories based on the method (physical or chemical) through which the tars are removed from the gasification process. Chemical methods lead to the destruction or thermal decomposition of tars while physical methods only remove tars downstream to the gasifier. A more detailed description of the tar removal technologies is given in the next subsections.

Another classification of the tar removal methods, which has been reported in the literature and is summarized by Devi et al. [62] proposes two approaches: treatments inside the gasifier, which are called primary methods and hot gas cleaning after the gasifier, which are called secondary methods. In both primary and secondary methods, tar removal is performed either by chemical treatment or physical separation.

However, the minimum allowable limit for tar is highly dependent on the kind of process and the end-use application. Specifications for contaminant levels that can be tolerated in these end-use applications are given by Milne et al. [1], who tabulated the tar tolerance limit for several end use devices, suggested by different researchers.

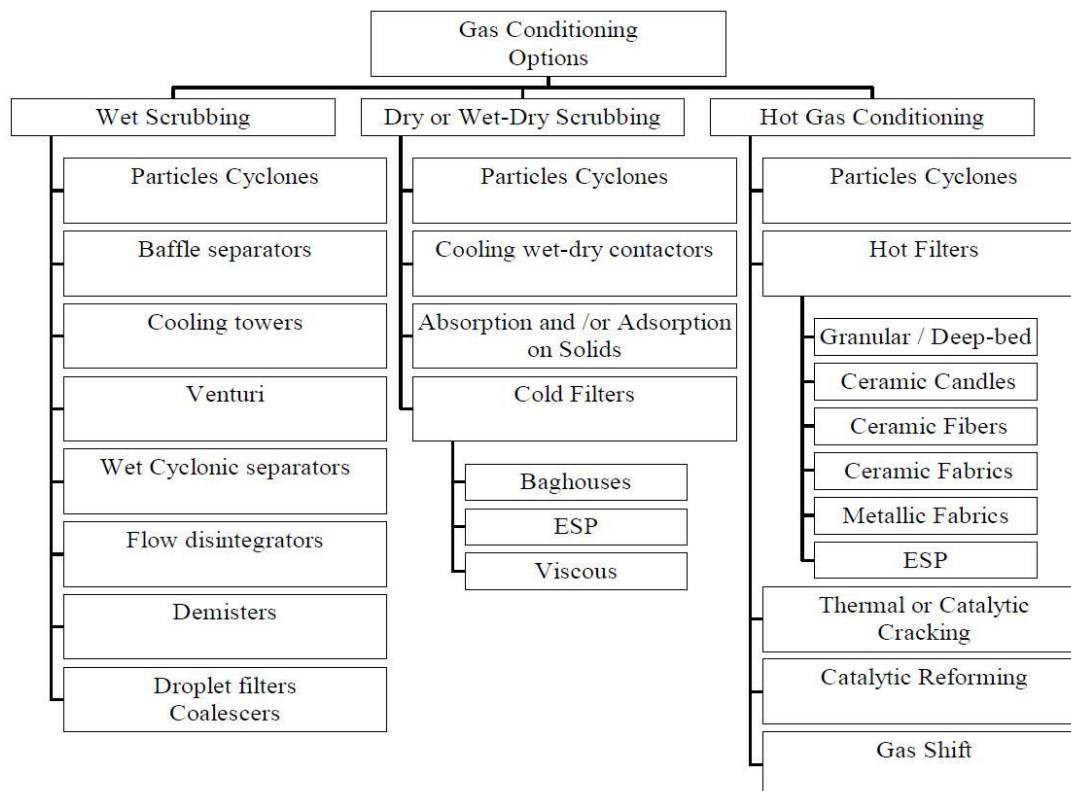


Figure 3.3: Gas cleaning technologies [1].

3.3.1 Physical removal of tar

Physical processes constitute the basic route for removing most raw gasifier contaminants, including tar. The most commonly used types for tar removal through physical methods are the following:

- Wet scrubbers
- Wet electrostatic precipitators
- Filters (baffle, fabric, ceramic, granular beds)
- Demisters

Tar is removed mainly through wet or wet-dry scrubbing. If water is used as the scrubbing medium, the tar separation efficiency is limited and multi-stage cleaning may be required. In order to be able to separate tars in a wet scrubber, the tars have to be condensed so that the aerosols and droplets collide with the water and increase their particle size. For this reason the product gas has to be cooled and saturated with water before the cleaning step.

By using lipophilic liquids as a scrubbing medium, gas phase tars can also be removed. An example of such a scrubbing technology, in which the removal of tars is accomplished by scrubbing the tar-loaded product gas with a specially developed liquid oil in an absorption column, has been developed by ECN and is called the OLGA tar removal technology [79].

Wet scrubbers (or separators) can be basically classified into four groups: packed column scrubbers, jet scrubbers, dip scrubbers and venturi scrubbers.

Packed column scrubbers are characterized by filling with packing materials, that are sprinkled by the washing medium. The scrubber vessels are equipped with jets that spray in the washing emulsion for the wetting of the packing. In the **jet scrubber**, the washing emulsion is sprayed into the scrubber vessel with overpressure, which results in an enlargement of the mass transfer surface area between the gas to be cleaned and the washing medium. In the **dip scrubber** the contaminated gas stream flows through a liquid bath, where the gas stream is mixed up with the scrubbing media providing good transfer of mass because of the high turbulence of the streaming gas-liquid phases. Finally, the manner of operation of the **venturi scrubber** is based on the increase of the speed of the gas stream through narrowing the cross-section and simultaneous spray injection of a washing liquid. The resulting high shearing forces between the gas and the liquid lead to an extra fine distribution of liquid drops, which agglomerate with the solid particles. On account of their mass moment of inertia the agglomerates are precipitated out of the gas stream through impact separation in the downstream droplet separator (demister) [80].

These processes are only effective for tar removal when the producer gas has been cooled to less than 100 °C, which is thermodynamically inefficient for power systems. The main problem arising from tar scrubbing is that the condensed tar components are merely transferred into another phase (water or solids such as scrubbing lime), which then has to be disposed of in an environmentally acceptable manner. The costs of water treatment may prohibit the use of these methods [1].

Wet electrostatic precipitators (ESP) can be also used to remove tars from biomass gasifier gas, because tar condensation on dry ESPs precipitation electrode would progressively inhibit particle removal. This apparatus offers advantages regarding aerosol separation (condensing tarry compounds, dust particles, etc.). The agglomerates (dust and tar load) on the collecting electrodes can be removed with the washer fluid. Attention must be paid to the accumulating pollutant mixture of particles and condensable load, etc., the processing of which requires additional expense [1], [80].

Filters can be used for cold as well as for hot gas filtration. Inorganic beds, usually consisting of silica or alumina sand, are used as impact or surface filtration media. When hot filtration is used, the filter operates usually at temperatures higher than 500 °C so that only particulates are removed while tars remain at the gas phase. On the other hand, when cold filtration is used, particulates and condensing tar droplets are removed [1].

Finally, demisters are centrifugal flow units designed to coalesce mist droplets from their gas flow. They resemble cyclones and hydro-cyclones and are usually used as a secondary stage in conjunction with classical wet scrubbing units. Their design depends on mist liquid phase properties and gas flow load [1].

3.3.2 Chemical removal of tar

Concerning the removal of tars through chemical methods, the three different existing techniques can be summarized in the following categories. The first two methods can be applied either in-situ or downstream to a gasification unit while the third one is used as a cleaning device after the gasifier.

- Thermal conversion (cracking)
- Catalytic destruction
- Plasma reactors (Corona, Pyroarc, Gliding arc)

Thermal conversion, also called cracking, is the application of extremely high temperatures to decompose complex organic compounds into more benign forms. This method is conventionally used as treatment to the hot producer gas from the gasifier. After such a process, the chemical energy of the tars can be used to increase the heating value of the producer gas.

Thermal cracking has been tested for tar disposal from the pyrolysis or gasification of various organic wastes. The minimum required temperature for efficient destruction is not well characterized and depends on the types of tars formed in the gasifier. Thus, thermal destruction of the oxygenated tars from updraft gasifiers might be treated at 900 °C while the refractory ones from high temperature reactors may require 1200 °C or more. The difficulties of attaining complete thermal cracking along with operational and economic considerations make thermal cracking less attractive in current large-scale gasifiers using cleaner biomass feedstocks [27].

Thermal conversion of tars is most of the times achieved by passing the producer gas through a second, high-temperature reactor where tars decompose or reform to carbon monoxide, hydrogen gas, and other light gases. Primary tar products readily decompose, with *CO* yields reaching 50 wt%, while condensed tertiary products are more difficult to crack [81].

Milne et al. [1] reported that in order to destroy aromatic tars without the use of a catalyst, temperatures higher than 1100 °C and reasonable residence times are necessary. On the other hand, these temperature values cause materials problems, requiring expensive alloys. Furthermore, soot is produced due to the high-temperature reaction conditions, which may be even more problematic than tars.

In case of catalytic destruction of tars, a great variety of approaches have been applied by using catalysts either as bed material inside the gasifier or in a separate reactor downstream to the gasifier. In this process, the gasifier is followed by a tar cracker (fixed bed or fluidized bed reactor) filled with catalytically active material. Catalytic tar treatment is based on the principle of tar cracking through thermochemical reactions supported by catalysts. The cracking process leads to the decomposition of tarry compounds, which results in the successive formation of permanent gas phases and lighter tar compounds [80].

Several catalyst materials have been applied in biomass gasification systems, such as alkali metals, non-metallic oxides, supported metallic oxides, commercial nickel reforming catalysts and optimized research catalyst formulations, which use the combination of the aforementioned materials.

Calcined dolomites are the most widely used non-metallic catalysts for tar conversion in biomass gasification processes. They are relatively inexpensive and are considered disposable. However, they are not very robust and quickly undergo attrition in fluidized bed reactors. Consequently, dolomites find most use in fixed bed catalytic reactors [63].

Commercial Ni catalysts are designed for use as secondary catalysts in separate fixed bed reactors operated independently to optimize performance and not as primary, in-bed catalysts. They have high tar destruction activity with the added advantages of complete reforming of methane and water-gas shift activity that allows the $H_2:CO$ ratio of the product gas to be adjusted. A limitation of nickel catalysts use for hot gas conditioning of biomass gasification product gases is the rapid deactivation either due to sulfur, chlorine, and alkali metals present in the producer gas or coke formation on the catalyst surface, which leads to limited catalyst lifetimes. The literature contains numerous studies detailing the use of commercial Ni-based catalysts for tar reforming. These studies are summarized by Dayton et al. [63] elsewhere.

Using fixed dolomite guard beds to lower the input tar concentration can extend nickel catalyst lifetimes. Several novel, Ni-based catalyst formulations have been developed that show excellent tar reforming activity, improved mechanical properties for fluidized bed applications, and enhanced lifetimes. In general, de-dusting has to be carried out prior to catalytic conversion in order to be able to provide a dust-free gas at a high temperature level for catalytic tar treatment [63].

A short review of the influence of bed additives and catalysts on the tar content is given in subsection 2.4.2. Detailed reports, which review the different methods and materials for catalytic biomass tar destruction are available in the literature [63], [1], [27], [62].

Finally, electric arc plasmas have been also used for the chemical removal of tar compounds. Plasmas are created by heating gases in the discharge arc between two electrodes. The electrical charge and the increased temperature in the arc cause ionization of part of the gases and subsequent reaction. Several plasma arc reactors have been built and tested for applications with biomass tars and are reviewed elsewhere [75], [82].

3.4 Classification of tar compounds

The amount and composition of tar compounds that are produced from the gasification of biomass are strongly dependent on the type and properties of each fuel (biomass), on the type of the reactor (gasifier) and on the gasification parameters. Generally, the term "**tar**" describes a lump involving thousands of single substances.

The most common and widely known classification of tar compounds reports two groups, into which these components are divided: gravimetric tar and individual organic compounds. **Gravimetric tar** is defined as the evaporation residue of a part of a bulk solution at standard conditions given in the Guideline [83], while **individual organic compounds** form a group of compounds, which appear in biomass gasification producer gases and are usually determined by means of Gas Chromatography [84].

Gravimetric tar represents a lump, which includes a large number of individual tar compounds, but it is not equal to the total mass of tar, due to the fact that lighter tar compounds will disappear during the evaporation procedure for the determination of the gravimetric tar. Figure 3.4 presents the range of tar compounds in the 1 kg/h bubbling fluidized bed biomass gasifier at ECN. The applied techniques were the SPA and the Guideline method (both described in the next section) for measuring tar compounds ranging from benzene up to coronene and the amount of gravimetric tar, respectively [56].

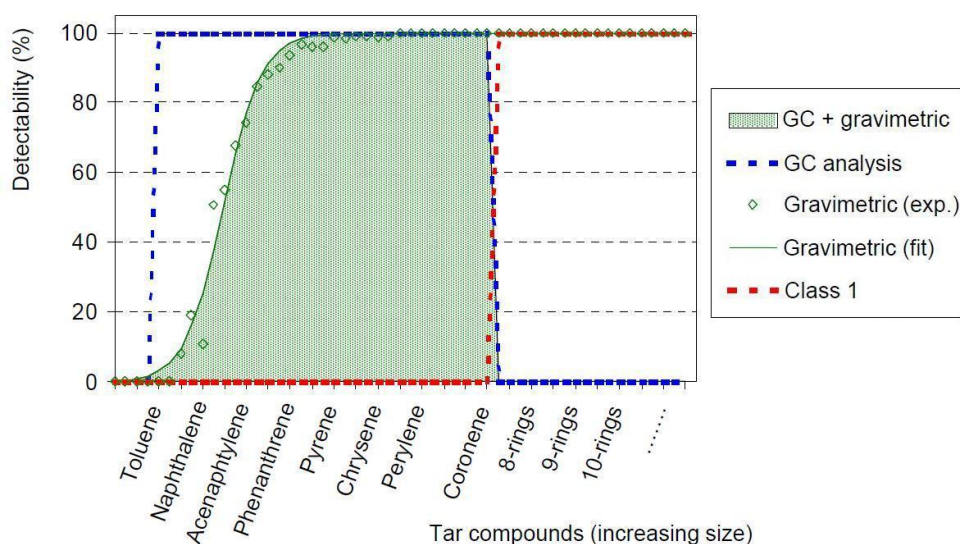


Figure 3.4: Range of tar compounds measured by SPA and Guideline method [56].

Figure 3.4 shows that standard GC analysis is not generally able to detect organic compounds larger than coronene (approximately 7 rings). On the other hand, compounds larger than 3 rings are included in the gravimetric tar determination (the upper limit on gravimetric tars is specified by molecular sizes). The gravimetric tars include GC-detectable as well as GC-undetectable tar compounds. Therefore, for some operating conditions, the gravimetric tars partly overlap with the GC-detectable tars [84].

Another classification based on a different tar analysis method reports five groups of tar compounds: particles, heavy tars, PAH, phenols and water soluble organic residue [85]. This sampling method applies a modified approach based on the tar protocol by using anisole as a solvent and evaporation under vacuum conditions. Moreover, Corella et al. [86] reported six tar classes (lumps), which were used to model the kinetics of catalytic

tar abatement downstream from a biomass gasifier. The sampling and characterization of tar were performed according to the SPA method.

The most commonly used classifications are the classification into primary, secondary and tertiary tars, presented by Milne et al. [1] and the classification system (five different classes of individual tar compounds) proposed by van Paasen et al. [56]. In the present work, the adopted classification system is based on the definition of five classes of tar compounds.

3.4.1 Primary, secondary and tertiary tars

In order to understand better the mechanism of tar cracking and formation inside the gasifier, the tar compounds can be divided into three groups: primary, secondary and tertiary tars. An example of the above tar formation and classification is illustrated in the following figure 3.5.

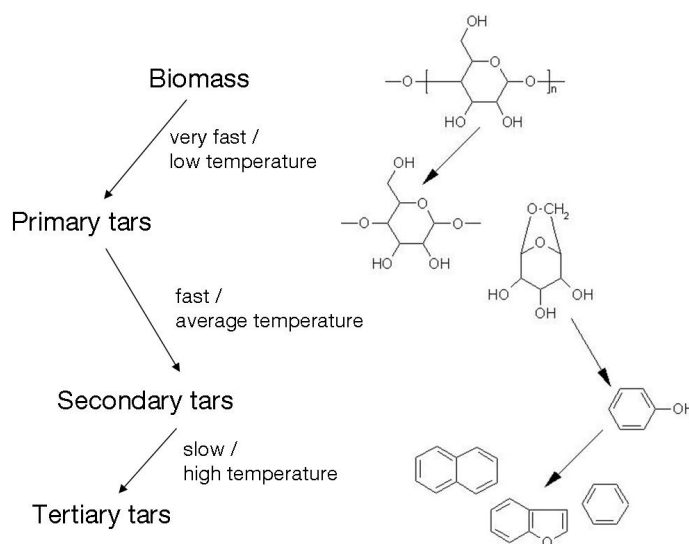


Figure 3.5: Formation of biomass tars and examples of compounds formed [76].

Milne et al. [1] used molecular beam mass spectrometry to suggest that a systematic approach to classify pyrolysis products as primary, secondary, and tertiary can be used to compare products from the various reactors that are used for pyrolysis and gasification. Three major product classes were identified as a result of thermal gas-phase tar cracking reactions.

The **primary products** are characterized by cellulose-derived products such as levoglucosan, hydroxyacetaldehyde and furfurals; analogous hemicellulose-derived products; and lignin-derived methoxyphenols. The **secondary products** include phenolics and olefins while the **tertiary products** are characterised by aromatics. This class is further subdivided into *alkyl tertiary products*, which are mainly methyl derivatives of aromatic compounds (e.g. methyl acenaphthylene, methylnaphthalene, toluene, and indene) and *condensed tertiary products*, which are PAH without substituent groups (e.g. benzene,

naphthalene, acenaphthylene, anthracene, phenanthrene, pyrene). A list of the important single tar compounds according to this classification study is given by Milne et al. [1] elsewhere.

3.4.2 Five tar classes system

The classification system proposed by van Paasen et al. [56] refers to five different classes of individual tar compounds by taking into account the behaviour of tars in downstream processes. This classification is mainly based on the solubility and condensability of different tar compounds, rather than the reactivity of these compounds.

The first group (Class 1) includes the heaviest tars that condense at high temperature even at very low concentrations. These tar compounds which have a molecular weight larger than coronene (i.e., approximately 7 rings)) cannot be detected with a GC and are determined by subtracting the GC-detectable tar fraction from the total gravimetric tar. Only HPLC analysis of the gravimetric tars allows the quantification of individual heavy hydrocarbons with a molecular weight larger than coronene. The second group (Class 2) consists of aromatic compounds with hetero atoms (e.g. phenol) that generally exhibit high water solubility due to their polarity. The third group (Class 3) are light compounds with one aromatic ring that are not important in condensation and water solubility issues. The last two categories consist of light polycyclic aromatic hydrocarbons (PAH) with 2 or 3 aromatic rings (Class 4), which condense at relatively high concentrations and intermediate temperatures and heavy PAH with 4 up to 7 aromatic rings (Class 5), which condense at relatively high temperature at low concentrations.

The following table 3.1 presents a detailed classification of the tar compounds of each group.

Table 3.1: Example of tar compounds in each tar class in the classification system [56].

Tar class	Name	Tar compounds
Class 1	GC-undetectable	Determined by subtracting the GC-detectable tar fraction from the total gravimetric tar concentration
Class 2	heterocyclic aromatics	pyridine, phenol, cresol, quinoline
Class 3	aromatics (1 ring)	xylene, styrene, toluene
Class 4	light PAH compounds (2-3 rings)	naphthalene, methyl-naphthalene, biphenyl, ethylnaphthalene, acenaphthylene, acenaphthene, indene, fluorene, phenanthrene, anthracene
Class 5	heavy PAH compounds (4-7 rings)	fluoranthene, pyrene, benzo-anthracene, chrysene, benzo-fluoranthene, benzo-pyrene, perylene, indeno-pyrene, dibenzo-anthracene, benzo-peryrene

3.5 Tar dewpoint

An important thermodynamic property for the condensation of tar compounds is the tar dewpoint. The tar dewpoint is the temperature at which the real total partial pressure of tar equals the saturation pressure of tar. Once the actual process temperature exceeds the thermodynamic tar dewpoint, tar can condense out. However, it does not mean that condensation will always happen, therefore kinetics might be slow.

In practice, it is very important to know when tar will condense in order to prevent damage of the downstream applications. ECN developed a dewpoint model for the calculation of a tar dewpoint from a measured tar composition. The model includes vapor/liquid equilibrium data for the tar compounds in the producer gas from a downdraft or fluidized bed gasifier. The calculation is based on ideal gas behaviour. Raoult's law is applied for the calculation of a mixture of hydrocarbons, using the vapor pressure data of individual compounds [87].

The tar dewpoint is calculated from the tar composition measured with the SPA or the Tar protocol (both described in the next section), i.e. tars with molecular size between toluene and coronene. Heavier tars are not considered but they may be expected to have a relatively high dewpoint at low concentration. Therefore, the calculated tar dewpoint should be considered as an underestimate while the actual dewpoint is probably higher [56].

An example of a dewpoint calculation is illustrated in figure 3.6 where the dewpoint for the tar classes 2 up to 5 is given at several concentrations.

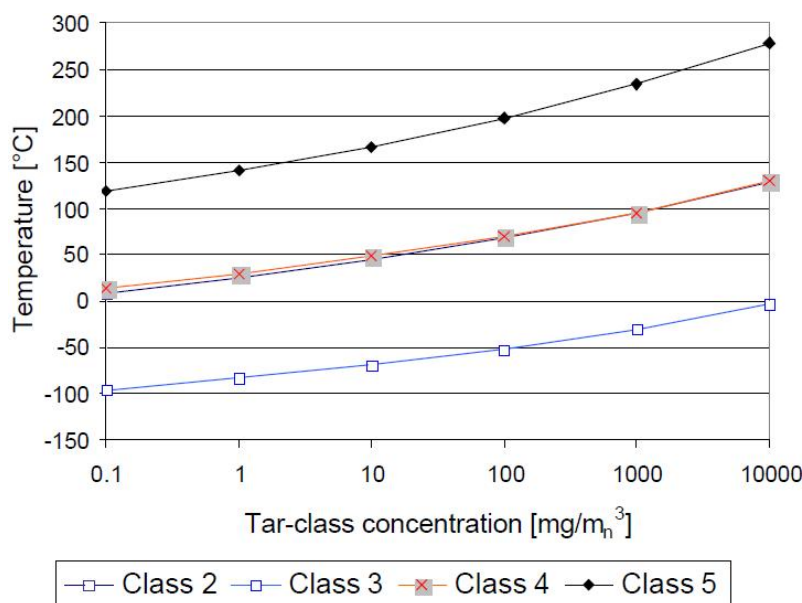


Figure 3.6: Tar dewpoint at atmospheric pressure versus tar concentration of different tar classes [56].

3.6 Tar measurement methods

Tar measurement and characterization in biomass gasification producer gases is one of the most challenging tasks due to the complexity of the tar mixtures produced in the gasification process. The further use of the producer gas in downstream applications requires the analysis of the tar content, whose qualification and quantification is therefore of high importance in research and development.

During the last years, several institutes and researchers have developed methods, which have been reported in the literature, for the sampling and analysis of tars. A short overview of these methods will be given in the following paragraphs of this section.

3.6.1 Conventional Cold Solvent Trapping (CST)-Tar protocol

Conventional methods for tar sampling are mainly based on cold trapping using condensers and cooling traps combined with solvent absorption in impinger bottles. The tar protocol proposes the concept of a modular sampling train, which consists of four main modules and respective submodules. The main modules are: **gas preconditioning**, **particle collection**, **tar collection** and **volume measurement**, which are described in detail elsewhere [83]. The experimental setup of the tar protocol is illustrated in the following figure 3.7.

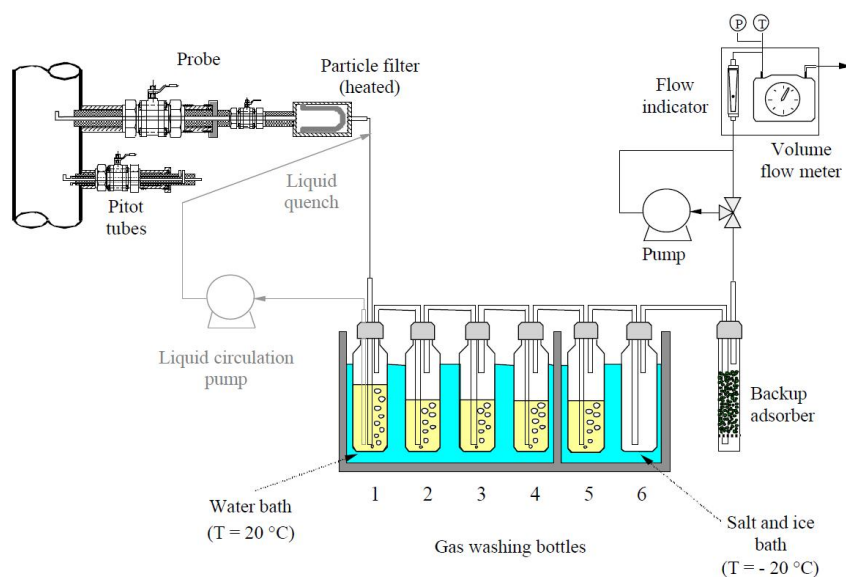


Figure 3.7: Experimental setup of the Tar Protocol [88].

The measurement principle is based on the discontinuous sampling of a gas stream containing particles and organic compounds (tars) under isokinetic or non-isokinetic conditions. Isokinetic sampling means that the velocity entering the sample probe (nozzle) must equal the free stream velocity of the gas being sampled. According to the guideline [83], non-isokinetic sampling is sufficient for measuring tar. It allows more freedom

for the design of the alignment of the probe in relation to the gas flow and for the construction of the shape of the probe nozzle to prevent it from blocking.

The tar and particle sampling system consists of a heated probe, a heated particle filter, a condenser (standard impinger bottle or it can optionally be equipped with an internal liquid quench system using isopropanol as the circulating liquid), a series of impinger bottles containing a solvent for tar absorption and equipment for pressure and flow rate adjustment and measurement. The impinger bottles are placed in a temperature controlled bath so that cooling of the sampled gas takes place. The gas is sampled for a specified time period while the flow rate is maintained with the aid of either process pressure or a pump. The sampling lines including the filter are heated to prevent tar condensation.

In the series of impinger bottles, the first one acts as moisture collector, in which water and tar from the process gas are condensed by absorption in isopropanol, which was found to be the most suitable solvent. After the moisture collector, the gas is passed through a series of four impingers with solvent and one final impinger bottle which is empty (drop collector). Volume, temperature, pressure and gas flow rate through the equipment are measured and finally the gases are vented safely to the atmosphere. After the sampling, the equipment is cleaned by washing with appropriate solvents (isopropanol).

The tar protocol determines the total amount of gravimetric tar but it cannot give any information about individual tar compounds. The concentration of the individual tar compounds can be measured by means of gas chromatography after re-evaporation of the condensed tars.

3.6.2 Petersen column

A different type of a sampling collector, the Petersen column, which is an alternative equipment to the six impinger bottles of the third module of the sampling train, has been developed by the Danish Technological Institute (DTI).

The Petersen column (see figure 3.8) consists of two washing stages filled with isopropanol. Stage 1 is a traditional washing stage with an impinger while the bottom of stage 2 consists of a G3 glass frit with two functions: 1) it retains tar droplets (aerosols) and 2) it generates a large number of very small gas bubbles in washing stage 2, which results in an improved washing efficiency. The Petersen column is jacket cooled so that the cooling fluid and cooling temperature can be selected as required (e.g. in relation to the gas temperature). Generally, the column is constructed in such a way that it is easy to replace the glass frit if it is polluted by particles that cannot be immediately rinsed out with solvent. Furthermore, since the Petersen column consists of a single unit, it is easier to handle than the Guideline train [89].

Tests have shown that the Petersen column has a high sampling efficiency. During measurements in heavily polluted producer gases, less than 1% of the light-GC detectable tar is found in a backup system.

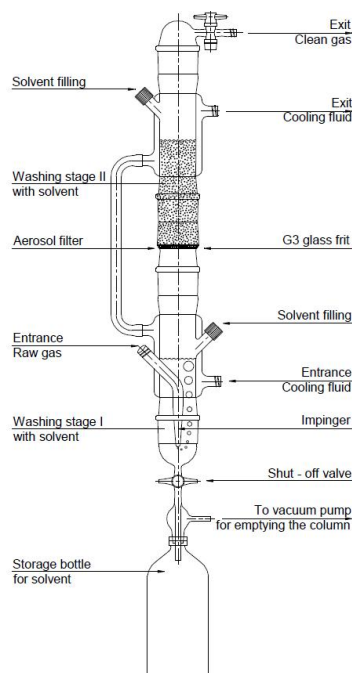


Figure 3.8: Experimental setup of the Petersen column [89].

3.6.3 Gas chromatography

Gas chromatography is one of the most commonly applied analytical tools for measuring concentrations of gas mixtures. The gas chromatograph can analyze individual components in a mixture by using a flow-through narrow tube (column) with a specific column filling (stationary phase), through which different gas samples pass in a gas stream (mobile phase) with the help of a carrier gas in order to be analyzed. The function of the stationary phase in the column is to separate different components, causing each one to exit the column at a different time (retention time), which is characteristic of each species. After having been calibrated for different concentrations of each compound, the GC provides both qualitative and quantitative analysis even of very complex mixtures.

Gas chromatography has been widely used for the analysis and measurement of aromatic and polycyclic aromatic hydrocarbon mixtures such as tars. The combination of a GC either with a Flame Ionization Detector (FID) or directly coupled to a Mass Spectrometer (MS) can give information about the concentration of each tar compound in a tar mixture [90], [91].

Gas Chromatograph-Flame Ionization Detector (GC-FID)

GC-FID system can be used for the separation and detection of non-polar organic compounds. Semi-volatiles such as PAHs are among the analytes that can be readily resolved and detected using such a system. Attention should be nevertheless paid to the use of the appropriate GC technique/column for the analysis of different types of organic compounds (polar/apolar).

The FID works by directing the gas phase output from the column into a hydrogen flame. A voltage of 100 – 200V is applied between the flame and an electrode located away from the flame and the increased current due to electrons emitted by burning carbon particles is then measured. Except for a very few low molecular weight organic compounds (e.g. carbon monoxide, etc.), the FID detects all carbon containing compounds and is therefore applied for qualifying and quantifying tar mixtures [92].

Gas Chromatograph-Mass Spectrometer (GC-MS)

A gas chromatograph can be also coupled to a mass spectrometer, which acts as the detector. MS can separate compounds that co-elute from the GC, providing interference-free detection and quantization of each individual compound in a complex sample. MS provides compound identification by retention time and mass spectrum and can determine the identity of a wide array of unknown compounds.

GC-MS technique has been applied by many researchers and has proven to be suitable for measuring primary as well as secondary and tertiary tar compounds [93], [84], [94]. However, due to the complexity of their operation and the interpretation of their output, GC-MS techniques tend to be more costly than other GC techniques.

3.6.4 High Performance Liquid Chromatography (HPLC)

High performance liquid chromatography is one of the most powerful tools in analytical chemistry and can be used for the analysis of heavy tar compounds. It has the ability to separate, identify, and quantitate the compounds that are present in any sample that can be dissolved in a liquid. Unlike GC systems, which require complete volatilization of the sample so that it can pass through the chromatograph, LC systems only require the sample to be dissolved in a solvent compatible with those used in the separation.

The advantage of HPLC systems compared to gas chromatography is that they can detect heavy PAH with large molecular weights. Van Paasen et al. [56] applied HPLC analysis (UV detector) of the gravimetric tar fraction to verify the occurrence and importance of Class 5 tar formation through the decomposition of Class 1 tars. This HPLC analysis allowed a qualitative analysis of PAH compounds with a molecular weight larger than coronene (i.e., tar compounds heavier than Class 5 tars). Zhang et al. [95] also made a systematic study on the identification and quantitative determination of PAHs in heavy products derived from coal and petroleum by means of high performance liquid chromatography.

3.6.5 Solid Phase Adsorption (SPA)

The SPA is a highly efficient method developed and tested at the Royal Institute of Technology (KTH) in Sweden and is based on solid-phase adsorption on amino phase. The method involves trapping of tar vapours on aminopropyl-bonded silica packed in

a small polypropene cartridge. Analytes are desorbed by using eluotropic elution (two different eluents) into aromatic and phenolic fractions, which are then analyzed by gas chromatography with flame ionization detection. The sampling step allows collection of one to three samples per minute while the method is applied for measuring light tar compounds that are enough volatile to undergo GC separation. A schematic diagram of the SPA analytical procedure is depicted in figure 3.9. A more detailed description is given elsewhere [96].

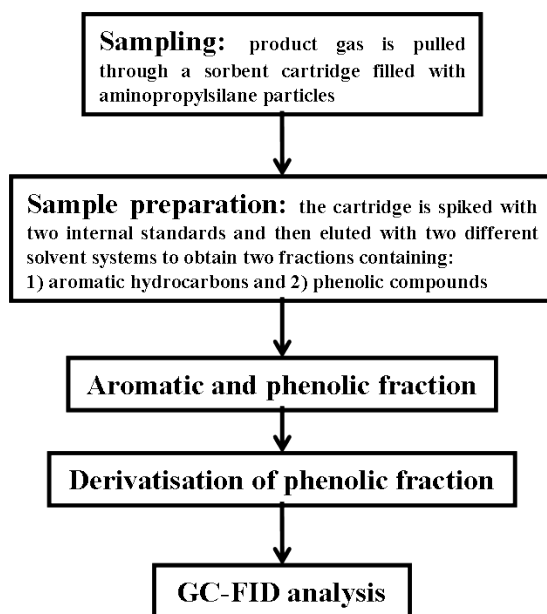


Figure 3.9: Schematic diagram of the SPA analytical procedure [96].

Recently, an extension of the SPA method is reported by Dufour et al. [97]. They presented a new application of multibed solid-phase adsorbent tubes followed by thermal desorption (SPA/TD), where the quantification of the tars is performed with a well reproducible GC-MS method with three internal deuterated standards.

3.6.6 Online tar analyzer

The online tar analyzer is a tar quantification method developed at the University of Stuttgart that allows quasi continuous on-line measurement of the content of condensable hydrocarbons (tars) in the producer gas from biomass gasification. The method is based on the comparison of the total hydrocarbon content of the hot biomass producer gas and that of the gas with all tars removed. The flow scheme of the online tar analyzer is shown in figure 3.10.

Main components of the system are two sample loops, high temperature switching valves, a flame ionization detector and a filter for tar condensation. The sample loops guarantee that the reference volume for both flows is identical and contains gas of exactly identical composition. The carrier gas provides the necessary pressure and gas flow rate

to the detector. The difference between the measurements from each loop (total tar content and non-condensable hydrocarbons respectively) yields the amount of condensable hydrocarbons or tars.

The online tar analyzer determines very low tar concentrations and it can be used in process control as a safeguarding tool for expensive process equipment. Sampling and analysis time are reduced to a minimum so that the effect of tar reduction measures can be directly verified. A detailed description about this method has been reported by Moersch et al. [98]. A further development of the method to the commercialized TA 120-3 online tar analyzer is reported elsewhere [99].

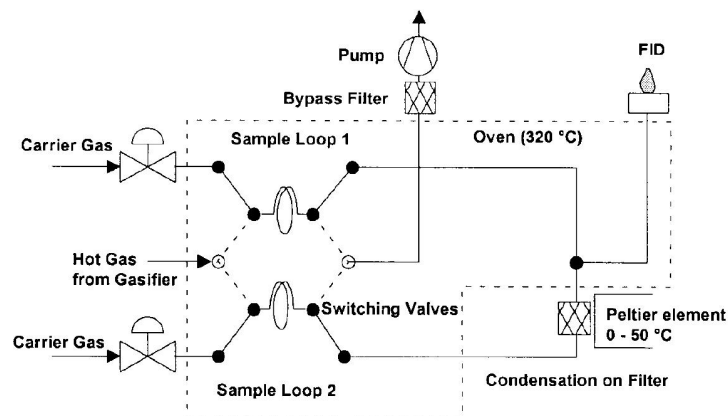


Figure 3.10: Flow scheme of the online tar analyzer [98].

3.6.7 Molecular Beam Mass Spectrometry (MBMS)

One of the most sophisticated techniques applied for the determination of tar compounds is Molecular Beam Mass Spectrometry (MBMS) [100]. The research group at the National Renewable Energy Laboratory (NREL), USA developed a Transportable Molecular-Beam Mass Spectrometer (TMBMS) to provide continuous, on-line chemical analysis of hot product vapors from indirect gasification. The TMBMS instrument has been successfully used on several occasions for similar projects and has proven to be a useful tool for monitoring high-temperature thermochemical processes.

The experimental setup of the TMBMS system is illustrated in figure 3.11. The design and operation of the TMBMS are described in detail by Ratcliff et al. [101], [102]. A complete description of the TCPDU, including a thorough analysis of the pyrolysis gas, can be found elsewhere [103].

The MBMS can be used to sample directly from harsh environments, including high-temperature, wet, and particulate-laden gas streams. Carpenter et al. [104] investigated the use of a molecular beam mass spectrometer as an alternative method for quantifying real-time tar concentrations in biomass gasifier derived syngas. The only drawback of this system is the complexity and size of the MBMS making it possibly the most expensive alternative for tar analysis thus limiting its use.

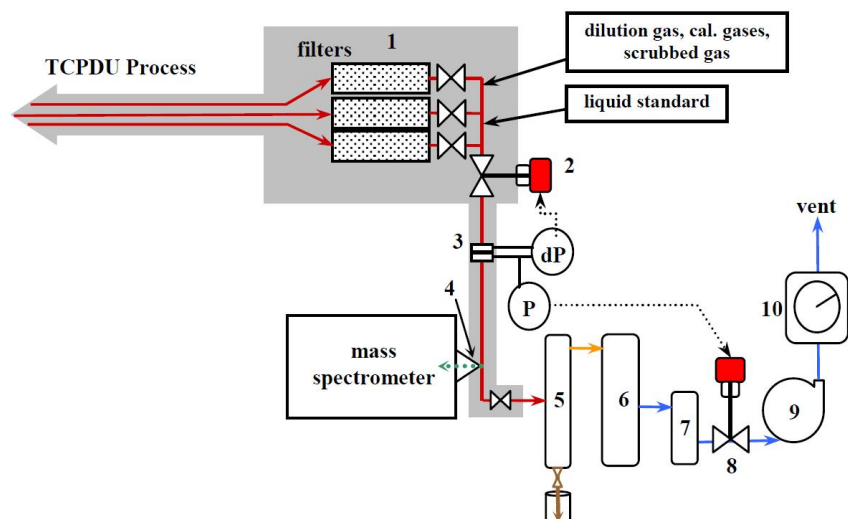


Figure 3.11: Schematic of the Transportable Molecular Beam Mass Spectrometer [105]. 1. sampling manifold; 2. flow-control valve; 3. orifice-plate flow meter; 4. sampling orifice; 5. condenser; 6. chilled impingers with cotton wool; 7. coalescing filter; 8. pressure control valve; 9. sample pump; 10. dry test meter. Shaded areas maintained at 450 °C.

3.6.8 Laser ionization system coupled to a gas chromatograph/ion trap mass spectrometer

Further research in the area of mass spectrometry uses the combination of a laser ionization system coupled to a gas chromatograph/ion trap mass-spectrometer (GC/MS), which enables fast analysis even in complex hydrocarbon matrices [106], [107]. An illustration of the experimental setup is depicted in the following figure 3.12.

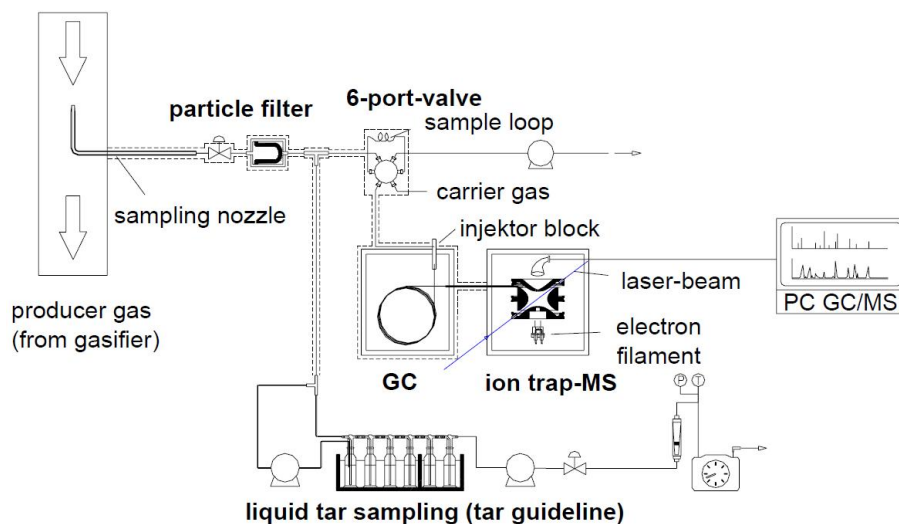


Figure 3.12: Experimental setup of the online tar analysis with GC/LAMS and liquid tar sampling according to the tar guideline [106].

A conventional benchtop gaschromatograph/ion-trap mass-spectrometer (GC/MS) system is equipped with an additional Laser Ionization (LI) system. Laser ionization results in lower detection limits for many tar compounds being analyzed. It further gives mass spectra with little or no fragmentation. The system offers the possibility of using Electron Impact (EI) as well as laser ionization in mass spectrometry, being able to perform hot gas online and liquid offline analyses with the option of gas chromatographic separation.

3.6.9 Photo Ionization Detector (PID)

An accurate, low-cost and fast online measuring method for tar analysis, based on PID (Photo Ionization Detector) detection is currently under investigation by the Biomass Technology Group (BTG) in co-operation with the Royal Institute of Technology (KTH). The PID is a commercial product used in laboratory instruments (combined to gas chromatography) and, nowadays, also separately as a portable vapor/gas detector. A PID analyzer is commonly used for volatile organic compound determination having the advantage of being selective to certain tar compounds and sensitive to aromatic compounds.

Knoef et al. [108] reported that components (such as tars) having an ionization potential lower than 8,4 eV will be detected by a Xenon PID lamp. BTG and KTH both work on the development of the online method testing two different UV lamps regarding criteria such as selectivity, accuracy, reproducibility, fouling and cleaning aspects. The long term objective is the development of an industrial PID analyzer of biomass gasification tars for monitoring, safeguarding and process control purposes.

3.6.10 Raman spectroscopy

An innovative approach in order to measure the tar content during the gasification process is to define it with the help of laser spectroscopy. Karellas et al. [109] developed an optical measurement system based on Raman spectroscopy, which can measure not only the basic components of the product gas (H_2 , CH_4 , CO , CO_2 , H_2O), but it can also give information concerning the tar content by correlating the background signal that is detected in the Raman profiles when measuring the hot producer gas from the gasification of biomass, with a standardized measurement technique like the tar protocol.

Further research to evaluate this background signal and to quantify and qualify tar compounds with the help of Raman spectroscopy has been made by Mitsakis et al. [110] and is reported elsewhere.

3.6.11 Overview of tar measurement methods

A summary of the main characteristics of each tar measurement method in terms of its development status and application, its measured tar concentration, its measurement way as well its cost is presented in table 3.2.

Table 3.2: Main characteristics of tar measurement methods.

Tar measurement method	Development status and application	Measured data	Measurement way	Cost
Tar protocol	CEN/TS pre-standard, laboratory use	gravimetric tar (Class 1-5)	offline	low cost
Petersen column	portable device, laboratory use	gravimetric tar (Class 1-5)	offline	low cost
GC-FID and GC-MS	not easy to transport, laboratory use	individual tar compounds (Class 2-5)	offline/online	expensive
HPLC	not easy to transport, laboratory use	individual tar compounds (Class 1-5)	offline/online	expensive
SPA	easy to use probes, laboratory use	individual tar compounds (Class 2-5)	offline	expensive
Online tar analyzer	portable device, industrial use	individual tar compounds (Class 2-5)	online	expensive
MBMS	transportable, industrial use	individual tar compounds (Class 2-5)	online	very expensive
GC/LAMS	transportable, laboratory use	individual tar compounds (Class 2-5)	online	very expensive
PID	under development	individual tar compounds (Class 2-5)	online	low cost
Raman spectroscopy	not transportable, laboratory use	gravimetric tar (Class 1-5)	online	very expensive

4 Laser Induced Fluorescence spectroscopy

Except for the conventional measurement techniques for sampling and analysis of tar compounds mentioned in the previous chapter, innovative optical measurements based on Laser Induced Fluorescence (LIF) spectroscopy can be successfully used for the analysis of the tar content in biomass gasification producer gases.

The use of laser techniques in various applications like the determination of temperature profiles in flames by means of Rayleigh spectroscopy [111], the detection of minority species with the help of LIF spectroscopy [112] and the online measurement of the composition of biogenous gases by detecting Raman signals of gas mixtures [113], have gained much attention during the last years. In addition, techniques such as Particle Image Velocimetry (PIV) for velocity measurements, Laser Doppler Velocimetry or Anemometry (LDV or LDA) for measuring the direction and speed of fluids and Phase Doppler Interferometry (PDI) for droplet detection approve the utility of optical systems for investigations in fluid mechanic processes.

Fluorescence spectroscopy is widely used in the fields of biochemistry and molecular biophysics and nowadays in environmental monitoring, clinical chemistry and genetic analysis. Furthermore, fluorescence can provide in situ and online information regarding the concentration of PAHs formed during combustion or pyrolysis processes.

In this chapter, the basic principles of Laser Induced Fluorescence (LIF) spectroscopy are presented together with previous attempts reported in the literature for detecting polycyclic aromatic hydrocarbons by means of LIF. Moreover, the motivation of the application of this measurement technique for the analysis of the tar content in an allothermal biomass gasification process is discussed as well.

4.1 Basic principles of Laser Induced Fluorescence (LIF) spectroscopy

Spectroscopy in general is an analytical technique arising from the interaction of species with electromagnetic radiation. When molecules absorb radiation of suitable wavelengths, they are excited to higher energy states. Since these excited states are unstable, molecules dissipate the absorbed energy and return to a stable level within the ground electronic state by emitting light.

Luminescence is the emission of light from any substance and occurs from electronically excited states. The two main categories of luminescence are *chemoluminescence*, where the excited species is formed in a chemical reaction and *photoluminescence*, where the excitation takes place through absorption of photons. Photoluminescence is formally

divided into two different forms, **fluorescence** and **phosphorescence**, depending on the nature of the excited state.

When a molecule is excited, the excited electrons fill molecular orbitals in pairs (the two electrons are said to be paired, $\uparrow\downarrow$) and their spins are in opposite direction (singlet state). In excited singlet states, the electron in the excited orbital is paired (of opposite spin) to the second electron in the ground state orbital. Consequently, return to the ground state is spin allowed and occurs rapidly by emission of a photon, which is called fluorescence. Molecules that are capable of absorbing and re-emitting light as fluorescence are called fluorophores. The emission rates of fluorescence are typically 10^8 s^{-1} , so that a typical fluorescence lifetime is near 10 ns [114].

Phosphorescence is the emission of light from triplet excited states, in which the electron in the excited orbital has the same spin orientation as the ground-state electron (unpaired electrons, $\uparrow\uparrow$). Transitions to the ground state are forbidden and the emission rates are slow (10^3 - 10^0 s^{-1}), so that phosphorescence lifetimes are typically milliseconds to seconds [114].

The energy E associated with the absorption bands of a molecule is given by the following equation:

$$E = E_{el} + E_{vib} + E_{rot} \quad (4.1)$$

where E_{el} describes the electronic energy of the molecule, E_{vib} the vibrational energy and E_{rot} the rotational energy. The number of rotational levels in a molecule is much larger than the number of vibrational states, which is in turn larger than the number of electronic levels. These facts are also related to the energy differences among different states (see eq. 4.2). For a given molecule, a number of electronic energy states exists while there is an even larger number of vibrational levels and also more rotational levels.

$$E_{el} > E_{vib} > E_{rot} \quad (4.2)$$

Figure 4.1 presents a typical Jablonsky energy level diagram, which illustrates the processes that occur between the absorption and emission of light. The singlet ground, first, and second electronic states are depicted as E_0, E_1, E_2 , respectively. At each of these electronic energy levels, the fluorophores exist in a number of vibrational energy levels (0, 1, 2, etc.). The rotational energy levels are located between the vibrational energy levels. The transitions between states are depicted as vertical lines to illustrate the instantaneous nature of light absorption. In this diagram, a number of interactions such as quenching, Resonance Energy Transfer (RET) and solvent interactions are excluded in order to be easier for the reader to understand the aforementioned transitions.

In Laser Induced Fluorescence (LIF) spectroscopy the molecule of interest absorbs one photon of the incident laser light. Having absorbed energy and reached one of the higher vibrational levels of an excited state, this molecule rapidly loses its excess of vibrational

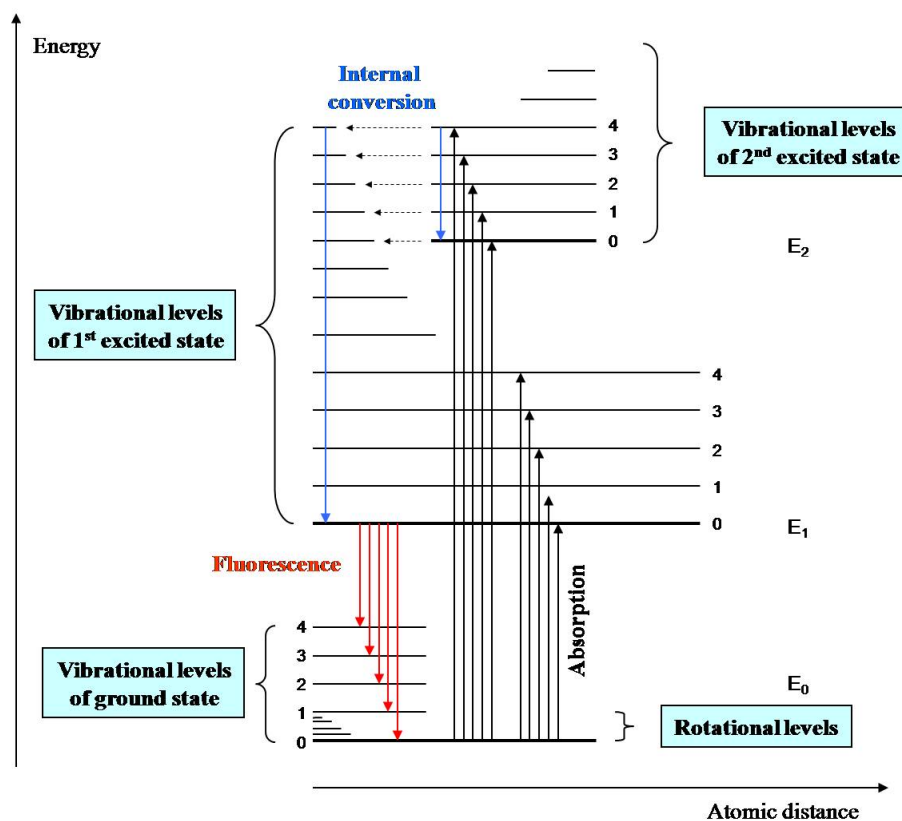


Figure 4.1: Energy diagram.

energy by collision and falls to the lowest vibrational level of the excited state. In addition, almost all molecules occupying an electronic state higher than the second undergo internal conversion and pass from the lowest vibrational level of the upper state to a higher vibrational level of a lower excited state, which has the same energy. From there the molecules again lose energy until the lowest vibrational level of the first excited state is reached. From this level the molecule can return to any of the vibrational levels of the ground state, emitting its energy in the form of fluorescence [115].

The 0–0 transition, that from the lowest vibrational level in the ground electronic state to the lowest vibrational level in the first excited state, is common to both the absorption and emission phenomena, whereas all other absorption transitions require more energy than any transition in the fluorescence emission (figure 4.2).

The entire fluorescence process is cyclical. Unless the fluorophore is irreversibly destroyed in the excited state (photobleaching), the same fluorophore can be repeatedly excited and detected. The fact that a single fluorophore can generate many thousands of detectable photons is fundamental to the high sensitivity of fluorescence detection techniques. The emitted radiation is characteristic for the concentration and temperature of the regarded species. Fluorescence spectral data are generally presented as emission spectra. A fluorescence emission spectrum is a plot of the fluorescence intensity versus wavelength (nm) or wavenumber (cm^{-1}).

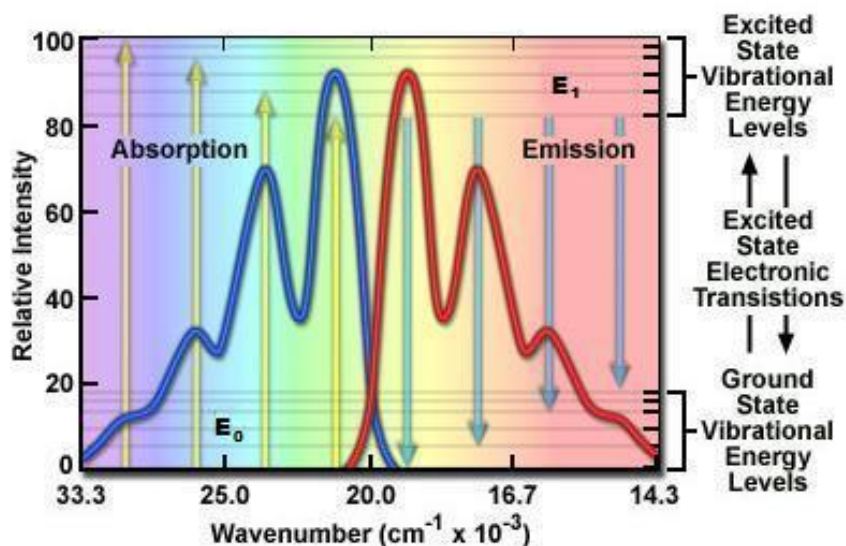


Figure 4.2: Absorption and emission bands [116].

4.2 Detection of polycyclic aromatic hydrocarbons by means of LIF spectroscopy

Laser-induced fluorescence spectroscopy is introduced as an optical technique that can serve as a rapid analytical method for the qualitative as well as for the quantitative analysis of Polycyclic Aromatic Hydrocarbons (PAHs). Several researchers have applied fluorescence spectroscopy for detecting polyaromatic hydrocarbon mixtures.

Niessner et al. [117] examined the optimum excitation and fluorescence wavelengths of 17 polycyclic aromatic hydrocarbon aerosols, while Karlitschek et al. [118] presented a mobile LIF system for the detection of aromatic pollutants in the environment by using UV laser induced fluorescence.

Further research has been done for the measurement and resolution of complex aqueous mixtures containing low concentrations of PAHs, as typical fluorescent pollutants in aquatic systems [119], as well as multicomponent determination of polyaromatic hydrocarbon mixtures by direct fluorescence measurements [120].

Regarding the detection of gas-phase polycyclic aromatic hydrocarbons, Zimmermann et al. [121] measured the lifetime of gas-phase toluene at elevated temperatures by means of laser induced fluorescence spectroscopy and Allain et al. [122] reported the real time analysis of high-temperature gas-phase PAH mixtures by collecting several fluorescence spectra of their vapors, demonstrating that LIF is a valuable tool for the rapid and in-situ monitoring of PAHs composition.

The above mentioned feedback has been the motivation to introduce this measurement technique for the determination of the tar content from biomass gasification process. The emitted light from every tar compound in the producer gas from biomass gasification is characteristic for each molecule while the emission spectrum provides information about

what kind of individual aromatic hydrocarbons are produced from the gasification of biomass as well as their concentration values. On the other hand, the fact that this kind of optical techniques give the possibility for online or in-situ measurements with only optical intervention in the measurement volume makes this technique very attractive for analyzing the tar content from biomass gasification process.

5 Experimental setup of the laser measurement technique

5.1 Optical facility for the investigation of tars

5.1.1 Motivation and background

The Institute of Energy Systems in the Technische Universität München (TUM) is applying optical measurement techniques for the determination of the concentration of biomass gasification producer gas in its basic compounds.

Previous experiments in the Biomass Heatpipe Reformer showed the possibility of defining the tar content by correlating the background signal that is detected in the Raman profiles when measuring the hot producer gas from the gasification of biomass, with a standardized measurement technique like the Tar Protocol. As long as this correlation is taken into account, the tar content can be measured online and the amount of the gravimetric tar can be also defined [109].

The motivation of this research is to evaluate this background signal and receive information not only about the overall quantity but also about the composition of each tar compound, which is included in biomass gasification producer gases.

5.1.2 Design and development of the optical facility

In an effort to improve the already existing tar measurement methods, this scientific work deals with a new online and non-intrusive quantitative and qualitative measurement technique for the analysis of tar compounds. For this purpose an optical measurement system based on laser spectroscopy has been designed and developed in order to enable not only the qualification but also the quantification of gas phase tar compounds and to define the concentration of single tar compounds in their mixtures.

The measurement setup which is used for the online analysis of individual tar compounds and enables the qualification and quantification of these components in the producer gas from biomass gasification is illustrated in figure 5.1. This setup is coupled downstream to a gasification test rig by means of a heating tube, which connects the exit (bypass) of the gasification facility and the input of the optical setup.

The main part of the optical setup is a specially designed measurement cell, which allows the optical analysis of biomass gasification producer gas in its tar compounds. The measurement cell consists of four optical ports (quartz windows) which are placed in each side of the measurement cell. The two optical windows allow the laser beam from the

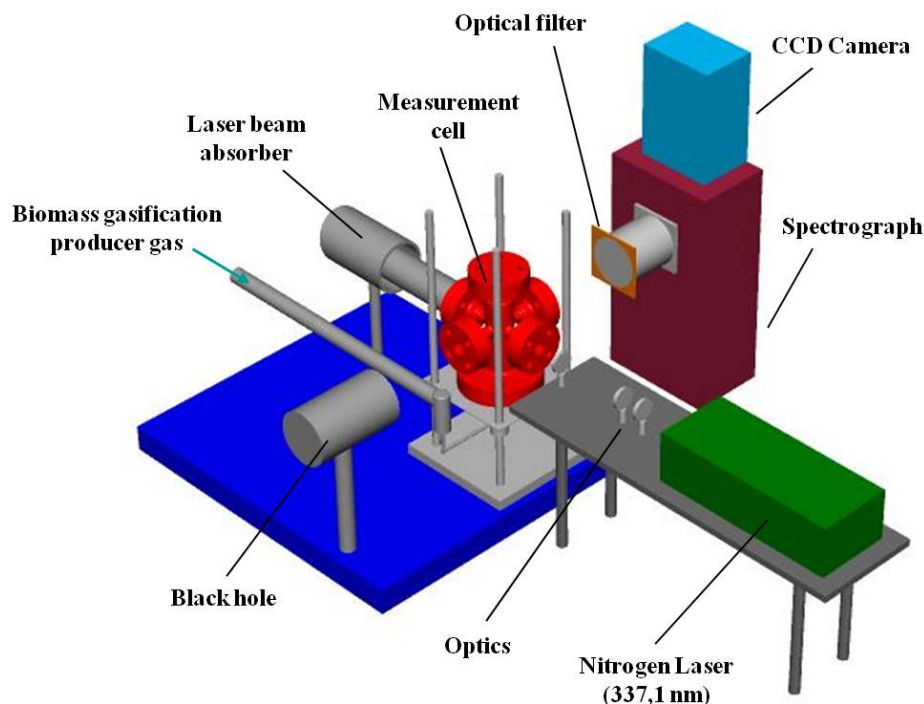


Figure 5.1: Experimental setup of the optical measurement technique.

excitation source to pass through the measurement cell while the other two allow the optical access of the camera view to the whole length of the measurement cell. The device is electrically heated by means of heating cords and it is controlled up to 450 °C, so that condensation of tar compounds is avoided. The laser that is used as an excitation source is a Nitrogen laser from Lasertechnik Berlin GmbH. This laser emits light at 337,1 nm, sends pulses of 3ns width with a repetition rate of up to 60 Hz and maximum average power of 10 mW [123]. The laser beam passes through an iris diaphragm and is focused on the centre of the measurement cell with the help of a focus lens.

The emission spectra are detected perpendicular to excitation (90°) through an intensified CCD camera (FlameStar 2F) of the company LaVision [124], which is attached to a spectrograph. The spectrograph (Chromex 250is) has a grating of 100 grooves/mm blazed at 450 nm. In front of the objective of the spectrograph, a long-pass filter (Bright-Line HC 341/LP) is used to block off the scattered light from the laser line and allow the fluorescence signal to enter the CCD camera. When measuring with such a system, a black background for the image taken with the CCD camera has to be assured. For this reason the so-called ‘black hole’ is placed opposite to the camera device.

The optical signals are gathered with the help of specific software by a computer, which enables the collection of pictures and profiles of the measured compounds in eligible time intervals. The data acquisition and evaluation of the experimental results take place in an online way in a second computer through specially constructed macro commands.

5.1.3 Design and construction of the transportable optical setup

Regarding the fact that the optical setup should be available to measure tar compounds from different gasification facilities, it is designed and repositioned in order to constitute a transportable box (see figure 5.2).

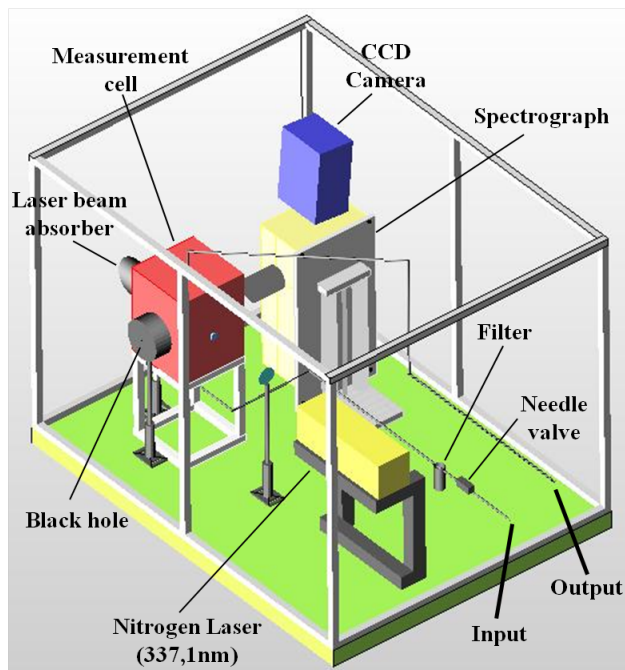


Figure 5.2: Transportable optical setup.

The main parts of the optical setup (measurement cell, laser, ICCD Camera and Spectrograph) are placed on an optical breadboard ($1,2m \times 0,9m$) together with the laser beam absorber, the black hole and the necessary lenses. All these parts are fixed on the breadboard to prevent vibrations, which would cause measurement errors. The control panel as well as the cooling of the camera, the controllers for the heating cords and the function generator, which is used for triggering the camera device and the laser, are placed outside the optical box. The producer gas from biomass gasification is driven by means of an electrical heated tube to the input of the setup and after its way through the measurement cell, it exits the optical box and goes to the chimney.

A high temperature filter (Headline Filters GmbH, Germany) is adjusted between the input of the setup and the measurement cell to clean the producer gas from particles (dust and chars) larger than 0,1 microns. The filter has 316L stainless steel housing (with high temperature gasket) and contains borosilicate glass microfibre elements (Type 25-64-50S with Silica Inorganic Binder). It is of high importance that the producer gas is as clean as possible before entering the measurement cell for optical analysis, due to reflections and Mie scattering that is caused by large diameter char and dust particles. A needle valve is put before the filter to enable the change of the filter element without disconnecting the heated tube containing producer gas coming from the gasifier.

All the pipes and the filter are electrically heated up to 350 °C so that condensation of tars on the way to the cell is avoided. The whole box is covered with PVC sheets to prevent light from entering the setup. The front, back and top side of the box are closed with fixed sheets while the left and right side's sheets can be attached to the box with the help of magnetic locks to allow access inside. In addition, two small ventilators are placed on the top to refresh the air inside the setup and contribute to the cooling of the laser. A picture of the transportable box is presented in figure 5.3.



Figure 5.3: Transportable box.

5.1.4 Advantages of the optical setup-Drawbacks of former existing methods

The application of optical measurement techniques for analyzing the producer gas from biomass gasification gives the possibility to investigate mixtures of tars according to their specific fluorescence spectra. By exploiting the different spectroscopic behavior of each tar compound, it is possible to qualify and quantify tar mixtures and execute tar concentrations in eligible time intervals.

The optical setup can be used for online and real-time monitoring of gasifier tars downstream from a gasification test rig and can provide both qualitative and quantitative measurement of the tar content in biomass gasification producer gases.

In addition, the fact that these kinds of methods are non-intrusive, provides the advantage to use them for insitu and online measurements with only optical intervention in the measured volume. Therefore, drawbacks of former techniques such as long sampling times (e.g. tar protocol), condensation and re-evaporation of the measured volumes and additional time for laboratory analysis of the obtained samples (e.g. SPA, GC) can be avoided.

5.2 Tar mixing station

5.2.1 Design and construction of the tar mixing station

The tar mixing station that is constructed and coupled to the laser measurement setup is presented in the following figure 5.4.

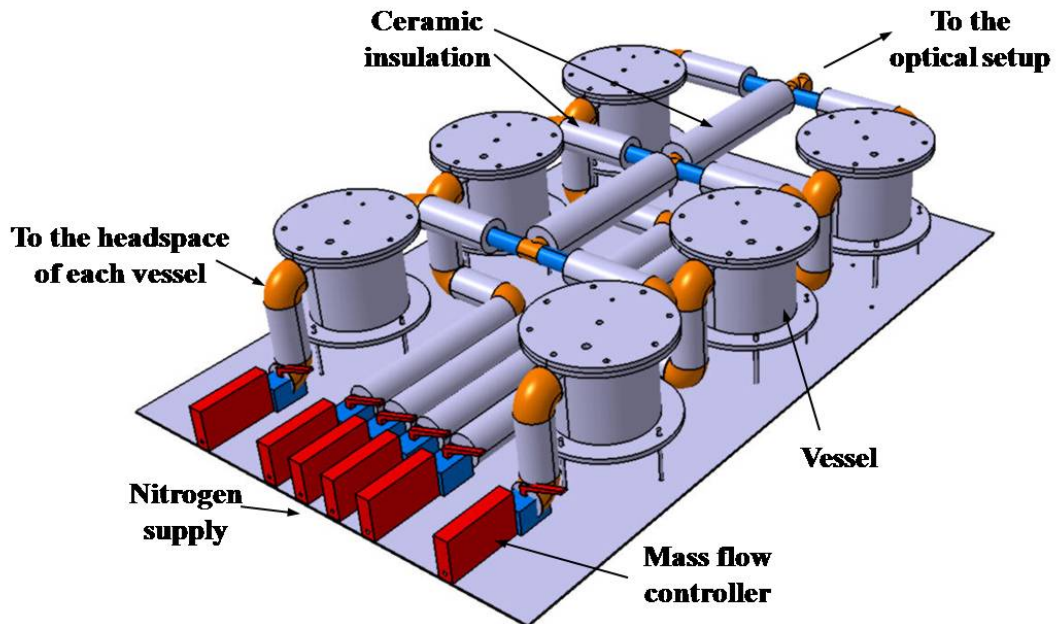


Figure 5.4: Tar mixing station.

It consists of six different vessels, which are placed in two series of three and contain the individual tar compounds of interest, which are either in the liquid or in the solid phase at room temperature. Each vessel can be electrically heated up to 450 °C while nitrogen is applied to the headspace of each vessel as carrier gas in order to provide an inert atmosphere and carry the vapors to the vessel vent and through heated pipes (condensation of tars is avoided) directly to the input and consequently into the measurement cell of the optical setup. A positive pressure of nitrogen also helps to prevent moisture from entering the vessel and having an adverse impact on the process chemistry. Evaporation of the tar compounds takes place within the vessel and continues at a steady rate as long as the flow of fresh purge gas is maintained and the solid or liquid content exists.

An illustration of each vessel is shown in figure 5.5. The electrical heating (heating cords) is placed around the walls of the vessel and is surrounded with ceramic insulation. The flow of the carrier gas is measured with mass flow controllers in the input of each vessel and pressure valves control the excess pressure inside. Thermocouples are also placed in the freeboard to control the heating temperature, while electrical heating is provided along the pipes from the output of each vessel up to the end of the main pipeline of the tar mixing station.

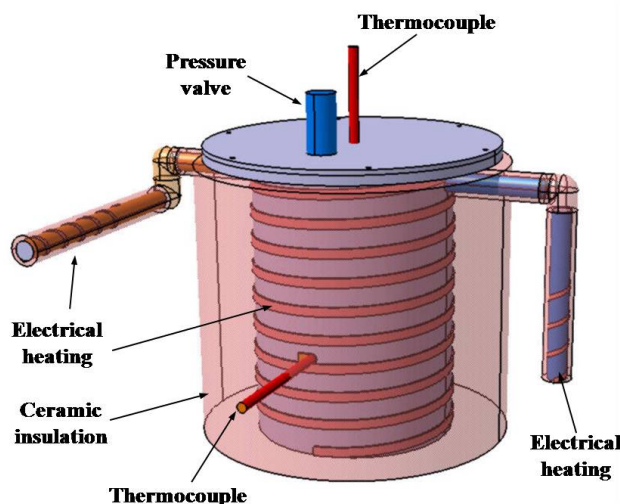


Figure 5.5: Illustration of each vessel of the tar mixing station.

The tar mixing station allows the generation of different tar concentrations in the gas phase and is used for the calibration of the experimental setup of the optical measurement technique.

5.2.2 Theoretical assessment of the concentration of gas phase tar compounds

The model that predicts the values of the concentration for each individual tar compound of interest is based on an algorithm described in detail by Hatfield et al. [125], who presents a general gas sweep model for estimating the emissions from a broad range of purge or gas sweep process operations.

The mechanism for the vaporization of a fluid (liquid or solid) in a vessel consists of the initial volatilization at the liquid-gas or solid-gas interface and the movement of vapors away from this interface into the vessel headspace. The movement of vapors throughout the headspace is accomplished by way of gas phase diffusion and convection eddy currents [126]. The basic driving force behind evaporation is for the fluid to achieve equilibrium between the component in the liquid or solid as well as in the vapor phase. Evaporation of the fluid will continue at a steady rate as long as the flow of fresh purge gas is maintained and the presence of the fluid exists.

The theoretical model takes into account the mass transfer process in the headspace of each vessel between the tar compounds and the carrier gas (nitrogen), the vapor pressure equations for each hydrocarbon as well as their saturation level and finally the nitrogen purging model equations, which calculate the emission rate and consequently the concentration of each tar compound in nitrogen. The whole theoretical model is divided into the aforementioned three phases, which are described in more detail in the following subsections. A thorough analysis of the model is given elsewhere [127].

Mass transfer model

Mass transfer is defined as the transport of one or more components of a fluid mixture within one phase or over phase boundaries. Mass transfer between two fluids and especially convective mass transfer depends on the material properties of the fluid and the type of flow. When the flow is externally injected (e.g. by pumps), the convection is no longer free, but forced.

Mass transfer is being caused by concentration, pressure and temperature gradients. The components of a mixture tend to move from higher to lower concentration regions and from higher to lower pressure regions. As soon as the gradients of different extents are balanced, equilibrium prevails regarding material transfer between the mixture components.

In order to be able to calculate diffusion or mass-transfer coefficients, a model must be selected, through which the existing process is best described by the appropriate experimentally determined equations. The three most widely used mass transfer theories are the boundary-layer theory, the film theory and the penetration model theory, which are described in detail elsewhere [128].

The theory that can be better applied to the process of mass transfer between each tar compound and nitrogen (carrier gas) is chosen to be the boundary-layer theory by taking into account the assumption that mass transfer takes place in a thin layer (plate) close to the tar surface (see figure 5.6). Changes of concentration can not only happen in direction from surface to gas (y) but also within the boundary layer (x and z). In fact, the concentration gradient in y -direction is more dominant than the other effects and therefore it is sufficient to take only the diffusion processes in this direction into account.

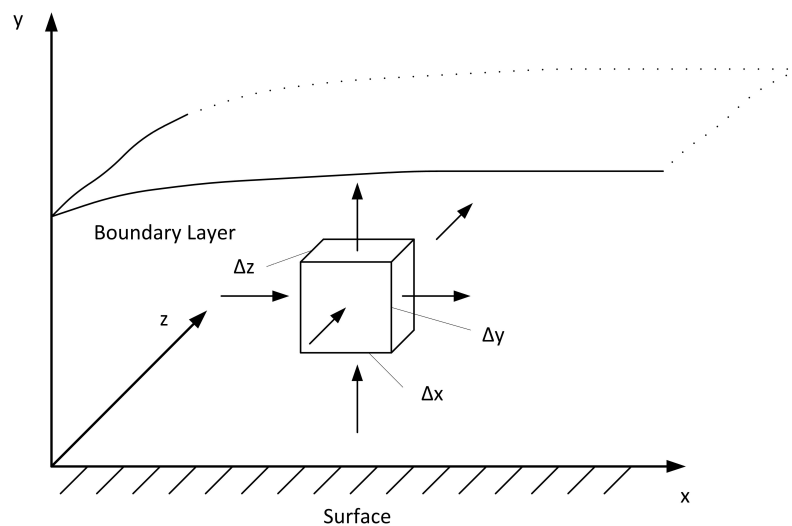


Figure 5.6: Boundary layer theory.

The surface of each tar compound filled into the vessels represents the so-called plate while the flow of the carrier gas into the containers and onto the surface of each tar is

laminar. The mass transfer process takes places in the boundary layer over the tar's surface.

The mass transfer coefficient K depends on the Sherwood-number Sh , the diffusion coefficient D and the length of the plate L due to the following equation (5.1). The length of the plate represents the diameter of the vessels filled with tar compounds.

$$K = \frac{Sh \cdot D}{L} \quad (5.1)$$

The diffusion coefficients for non-polar compounds like most of the tars and for polar compounds such as phenol and o,m-cresol are defined by the Fuller-Schettler-Giddings equation (5.2) and Brokaw equation (5.3) respectively [129], [130] while the Sherwood number is calculated by the equation 5.4.

$$D = \frac{0,001 \cdot T^{1,75} \cdot M_{AB}^{1/2}}{P \cdot \left[(\sum \nu)_A^{1/3} + (\sum \nu)_B^{1/3} \right]^2} \quad (5.2)$$

$$D = \frac{0,002628 \cdot T^{3/2} \cdot M_{AB}^{1/2}}{P \cdot \sigma_{AB}^2 \cdot \Omega_D} \quad (5.3)$$

$$\begin{aligned} \Omega_D &= \Omega'_D + 0,19\delta_{AB}^2/T^o & \Omega'_D &= (44,54T^{o-4,909} + 1,911T^{o-1,575})^{0,10} \\ M_{AB} &= 1/M_A + 1/M_B & T^o &= kT/\varepsilon_{AB} \\ \sigma_{AB} &= (\sigma_A\sigma_B)^{1/2} & \sigma_i &= [1,585V_{bi}/(1 + 1,3\delta_i^2)]^{1/3} \\ \delta_{AB} &= (\delta_A\delta_B)^{1/2} & \delta_i &= 1,94 \times 10^3 \mu_i^2/V_{bi}T_{bi} \\ \varepsilon_{AB} &= (\varepsilon_A\varepsilon_B)^{1/2} & \varepsilon_i/k &= 1,18(1 + 1,3\delta_i^2)T_{bi} \end{aligned}$$

In the above equations, T is the temperature of the tar compound, M_{AB} the molecular weight of the mixture of each tar compound and nitrogen, P the pressure inside the vessel (in bar), ν_A and ν_B the atomic diffusion volumes (see table A.1) for estimating D (in cm^2/s), σ_{AB} the binary pair characteristic length of the mixture of each tar compound and nitrogen, Ω_D the diffusion collision integral, k the film mass transfer coefficient, ε_{AB} the characteristic Lennard-Jones energy, δ_{AB} the effective thickness of stagnant-film layer, T^o the temperature for the calculation of Ω_D , μ_i the dipole momentum, T_{bi} and V_{bi} the temperature and volume at normal boiling point, respectively (see table A.2).

The Sherwood number, also called the mass transfer Nusselt number, is a dimensionless number that represents the ratio of convective to diffusive mass transport. Regarding the assumption of laminar flow in plates over the surface of each tar compound, the correlation that best describes the Sherwood number is given by the Pohlhausen equation (5.4) [131].

$$Sh = 0,664 \cdot Re^{1/2} \cdot Sc^{1/3} \quad (5.4)$$

The Reynolds and Schmidt numbers are calculated by the following equations:

$$Re = \frac{\rho \cdot w \cdot L}{\mu} \quad (5.5)$$

$$Sc = \frac{\mu}{\rho \cdot D} \quad (5.6)$$

where ρ the density of nitrogen, μ the dynamic viscosity of nitrogen, D the diffusion coefficient, L the length of the plate (vessel's diameter) and w the velocity of nitrogen, which is defined as the nitrogen flow divided by the cross sectional area of the pipe which drives nitrogen into the vessel's headspace.

Partial vapor pressure equations

The saturated vapor pressure for each tar compound is calculated using Wagner and Antoine vapor pressure equations (5.7 and 5.8a, 5.8b), where T the evaporation temperature of each hydrocarbon inside the tar mixing station's vessels.

$$\ln\left(\frac{P^{Sat}}{P_c}\right) = \frac{aT + bT^{1,5} + cT^{2,5} + dT^5}{1 - \tau} \quad (5.7)$$

where $\tau = 1 - \frac{T}{T_c}$ and P_c , T_c the critical pressure and temperature, respectively.

$$\log P^{Sat} = a - \frac{b}{T + c} \quad (5.8a)$$

$$\ln P^{Sat} = a - \frac{b}{T + c} \quad (5.8b)$$

The coefficients a, b, c and d, the critical pressure and temperature for Wagner correlation as well as the corresponding vapor pressure equation and its applicable temperature range for each tar compound are presented in the following table 5.1.

Table 5.1: Coefficients and units for each tar compound vapor pressure equation.

Tar compound	Vapor pressure equation	a	b	c	d	Ref	T range [K]	$P_c \cdot 10^5$ [Pa]	T_c [K]
phenol	5.8a	4,27	1523,42	175,4	-	[132]	353-481	-	-
o-cresol	5.8a	4,1834	1534,54	176,3	-	[132]	357-492,11	-	-
m-cresol	5.8a	4,215	1556,83	167,6	-	[132]	368,8-503,3	-	-
toluene	5.7	-7,316	1,594	-1,932	-3,722	[132]	-	41,06	591,8
styrene	5.8a	6,3318	1597,003	-49,03	-	[133]	285-418	-	-
o-xylene	5.7	-7,605	1,754	-2,275	-3,738	[132]	-	37,35	630,33
biphenyl	5.8b	21,572	4599,5	-75,42	-	[134]	342-544	-	-
naphthalene	5.7	-7,614	1,916	2,508	-3,23	[132]	-	40,5	748,4
indene	5.8a	6,3441	1749,215	-52,375	-	[133]	297-457	-	-
fluorene	5.8a	6,9967	3245,362	-18,374	-	[133]	424-572	-	-
anthracene	5.8a	4,799	2819,63	247,02	-	[132]	460-653	-	-
fluoranthene	5.8a	2,5121	1017,476	-253,87	-	[135]	470-657	-	-

Nitrogen purging model

If the condition in which the gas in the headspace of the vessel exists as a perfectly mixed gas phase is considered, then the steady-state evaporation or emission rate for a given component would become a function of only a few factors as shown in equation 5.9 [136].

$$Q_m = \frac{M_i K_i A}{RT} (P_i^{sat} - P_i) \quad (5.9)$$

where: Q_m the mass evaporation rate, M_i the molecular weight of compound i, K_i the mass transfer coefficient, A the surface area of the fluid, R the universal gas constant, T the fluid temperature, P_i^{sat} the saturated vapor pressure for compound i, P_i the actual vapor pressure of compound i in the vessel headspace and $P_i^{sat} - P_i$ the driving force for evaporation.

For a vessel undergoing a purge at a steady flow rate, the solvent vapor emission rate at the process discharge vent must be equal to the evaporation rate of the fluid in the vessel as shown in the following equation.

$$Q_m = Q_\nu \quad (5.10)$$

The emission rate Q_ν from the vessel vent is:

$$Q_\nu = \frac{F P_{sys}}{RT} \frac{P_i}{P_{sys}} M_i = \frac{M_i F P_i}{RT} \quad (5.11)$$

where F the exit gas volume flow rate at the system temperature and pressure, P_{sys} the overall system pressure, R the ideal gas constant, T the fluid temperature, P_i the actual vapor pressure of compound i and M_i the molecular weight of compound i.

Equation 5.10 can be simplified to equation 5.12 by defining the vapor pressure saturation level for a component as P_i/P_i^{sat} . S_i is dimensionless and represents the level of saturation as a decimal fraction between 0 and 1.0 under all purge rate conditions.

$$S_i = \frac{P_i}{P_i^{sat}} = \frac{K_i A}{F + K_i A} \quad (5.12)$$

Regarding the fact that for most industrial processes the exit vent flow rate F is not a measured variable, but only the inlet purge rate F_{nc} of nitrogen can be controlled by means of a flow meter, equation 5.12 can be further modified so that the degree of saturation S_i is calculated directly from the inlet gas purge rate F_{nc} .

The exit vent gas stream can be divided into the partial volume stream for nitrogen and tar compound, where F_i^{sat} is the theoretical partial volume stream for compound i at saturated vapor pressure.

$$F = F_{nc} + F_i = F_{nc} + S_i F_i^{sat} \quad (5.13)$$

By substituting equation 5.13 into equation 5.12 the resulting vapor pressure saturation level is given by the following expression:

$$S_i = \frac{-(K_i A + F_{nc}) + \sqrt{(K_i A + F_{nc})^2 + 4F_i^{sat} K_i A}}{2F_i^{sat}} \quad (5.14)$$

By measuring the volume flow of nitrogen in the inlet of each vessel, the mass flow of each tar compound is calculated by the following equation.

$$Q_i = \frac{M_i P_{sys} F_{nc}}{RT} \frac{S_i P_i^{sat}}{(P_{sys} - S_i P_i^{sat})} \quad (5.15)$$

Consequently, the concentration of each tar compound is given by equation 5.16, where Q_i is the mass flow of tar in g/min and F_{nc} the volume flow of nitrogen in ml/min, after having been normalized in g/Nm^3 .

$$C_i = \frac{Q_i}{F_{nc}} \quad (5.16)$$

The whole calculation model consists of the three aforementioned steps. After checking that the nitrogen flow is laminar ($Re < 2300$), the diffusion coefficient, the Sc and Sh number as well as the mass transfer coefficient for each tar compound are calculated. The saturation level and consequently the concentration of tar compounds is computed through equations 5.14-5.16 by taking into account the saturated vapor pressure of each hydrocarbon at the tar heating temperature.

When the eligible concentration range (especially low values of tar concentration in mg/Nm^3) cannot be generated by the provided flow of nitrogen from the mass flow controllers, further dilution is necessary. For this reason, a pipe is coupled to the exit of the main line of the tar mixing station in order to enable the dilution of the gas mixture with nitrogen. In that case, the final concentration is calculated by equation 5.17, where F_{ext} the externally applied nitrogen flow.

$$C_i = \frac{Q_i}{F_{nc} + F_{ext}} \quad (5.17)$$

The results of the concentration values of each tar compound in relation to the temperature to which tars are heated and to the flow of the carrier gas into the vessels as well as the main line of the tar mixing station are depicted in the following figures 5.7-5.8. Table 5.2 presents the data values that are used for the calculation regarding the nitrogen flow, the pressure and the design characteristics of the tar mixing station.

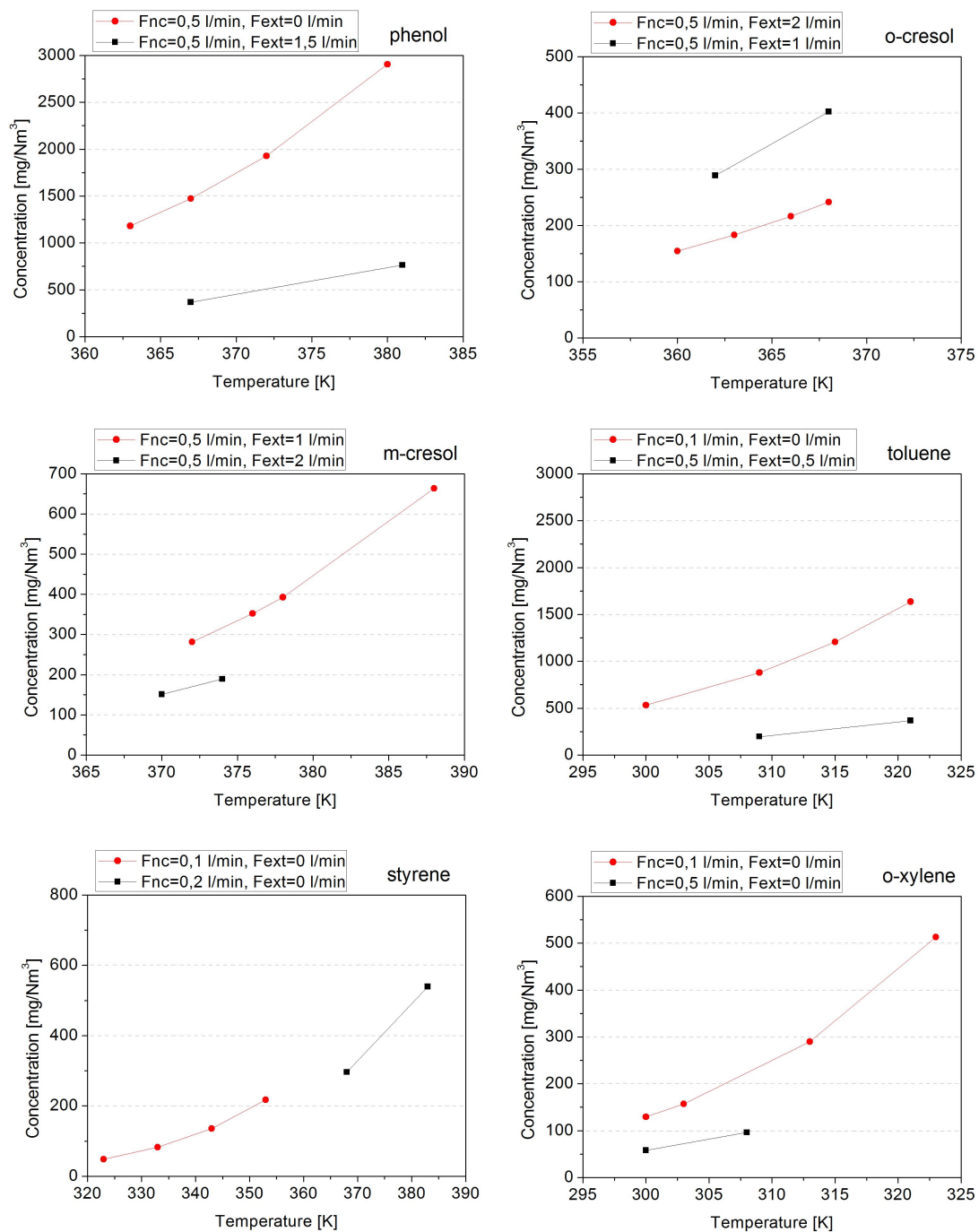


Figure 5.7: Calculated concentration values of individual tar compounds.

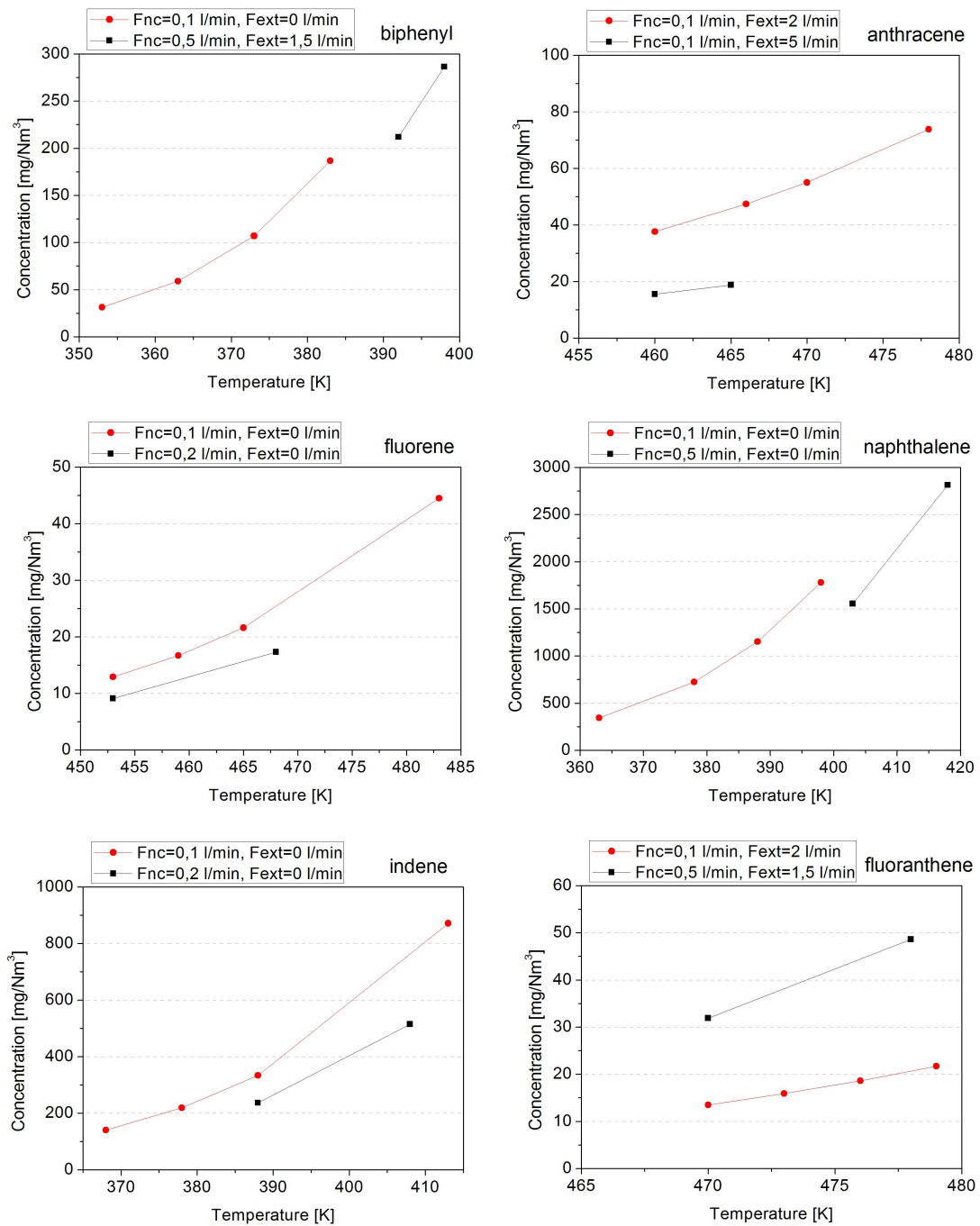


Figure 5.8: Calculated concentration values of individual tar compounds.

Table 5.2: Data values for the nitrogen purging model.

Nitrogen flow (F_{nc})	0 – 500 ml/min
System pressure of the tar mixing station (P_{sys})	1 bar
Characteristic length L (Vessel diameter)	0,15 m
Surface area of each tar compound (A)	0,01766 m^2
Internal diameter of pipes carrying nitrogen into the vessels's headspace	0,008 m
Cross sectional area of pipes carrying nitrogen into the vessel's headspace	$5,026 \cdot 10^{-5} m^2$

5.2.3 Validation of the tar concentration from the tar mixing station

The theoretical assessment of the concentration of each tar compound was validated by applying a sampling train (tar protocol) after the exit of the tar mixing station, where condensation of the tars occurs. The sampling train consists of four impinger bottles containing iso-propanol, which are placed into an ice bath, an eductor as well as a volume flow meter, which measures the total flow of the mixture coming from the tar mixing station for a specified time period. Since the gas phase tar compounds are collected in iso-propanol, they are analysed gravimetrically in a rotary evaporator after evaporation of the solvent.

Figures 5.9-5.10 present the measured concentration of each tar compound by means of the tar protocol (blue symbol), which is compared to the theoretically calculated concentration by the nitrogen purging model (red symbol). The observed data show a very good correlation to each other, which means that the purging model simulates the real tar concentration coming out from the tar mixing station with a very low relative error.

Regarding pyrene and perylene, a similar tar mixing station was used, which is based on the same nitrogen purging principle but has smaller vessels than the aforementioned one. The reason for using a different setup was the extremely high cost of these two pure compounds when filling the vessels of the main tar mixing station.

The similar tar mixing station consists of four 0,05m internal diameter vessels, which are placed in a series and contain the individual hydrocarbons. The small tar mixing station was calibrated by applying a sampling train (tar protocol) directly after the main line, where the gas phase tar compounds exit the setup. The concentration of pyrene and perylene in relation to the evaporation temperature are presented in figure 5.11.

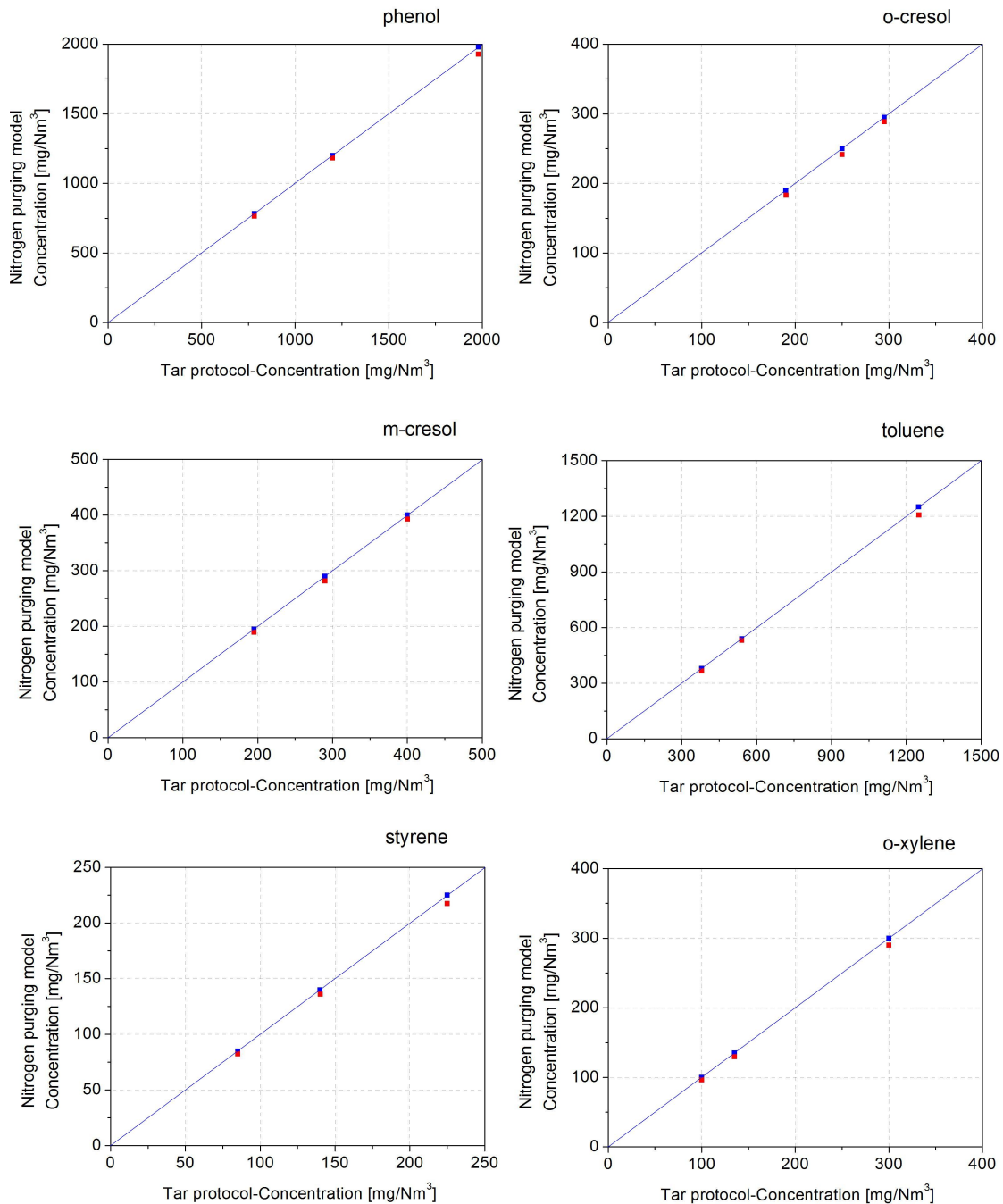


Figure 5.9: Comparison between concentration values from the nitrogen purging model and the tar protocol for each individual tar compound.

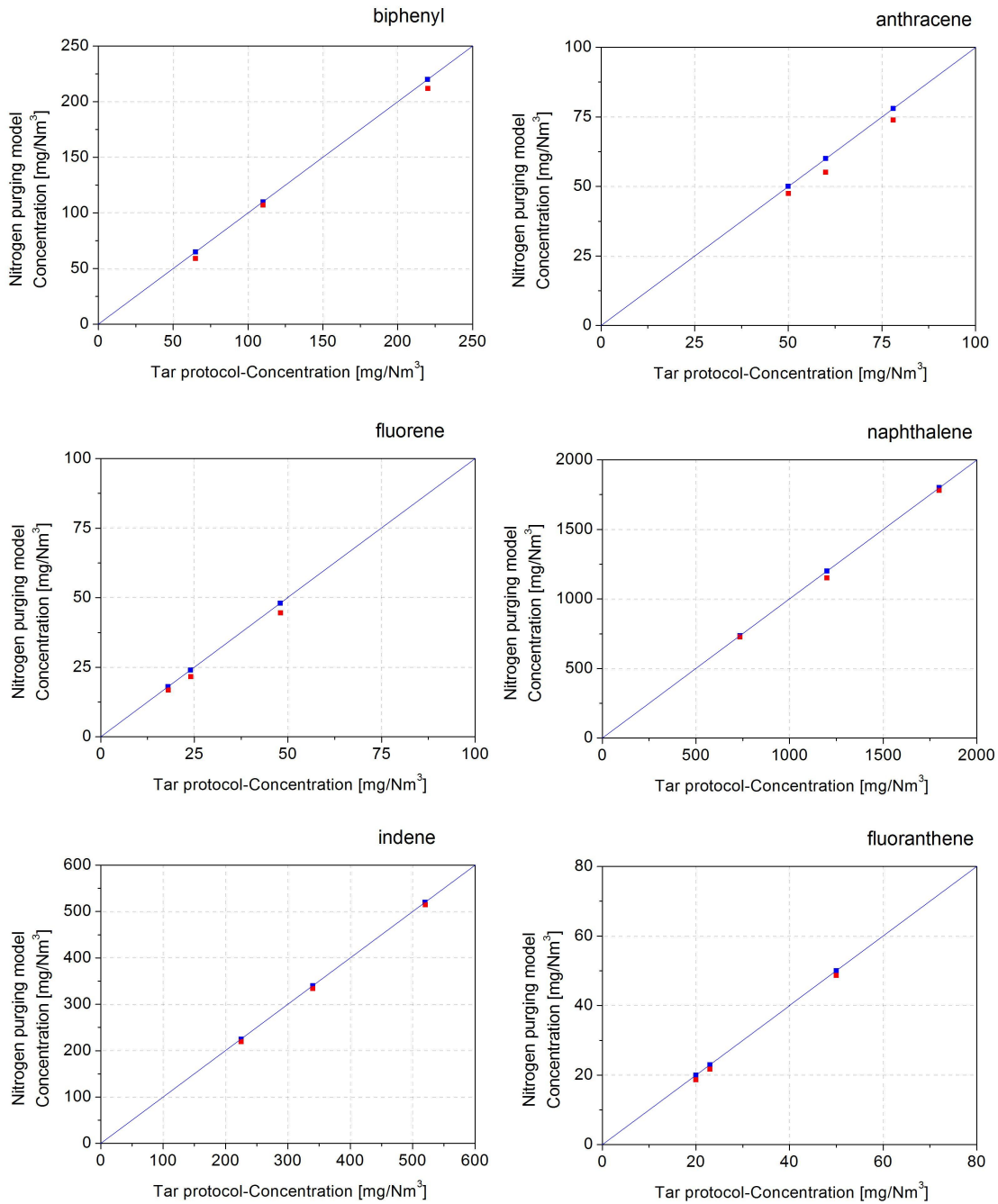


Figure 5.10: Comparison between concentration values from the nitrogen purging model and the tar protocol for each individual tar compound.

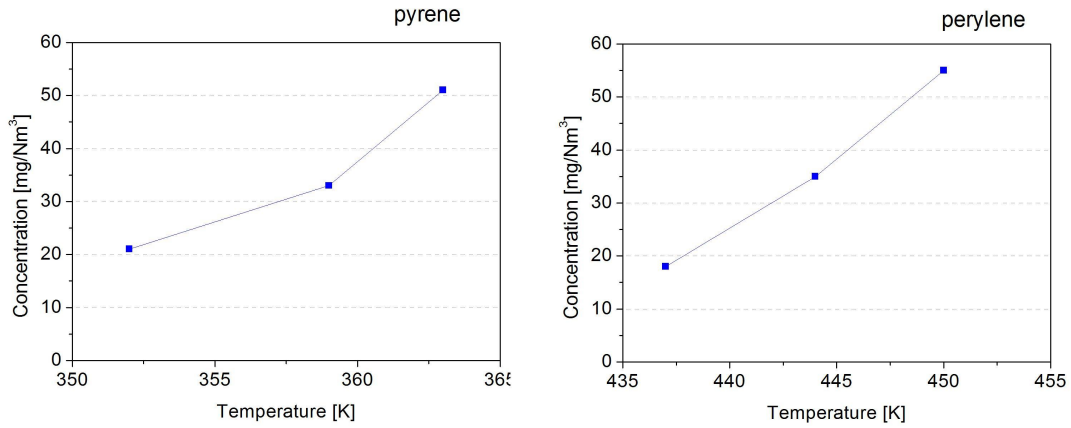


Figure 5.11: Concentration values of pyrene and perylene in relation to the heating temperature.

5.3 Analysis of the optical signals

5.3.1 Calibration of the laser system

In principle, the calibration of a measurement system is the most important step for observing correct and accurate results. Therefore, careful attention should be paid when calibrating the optical setup with model tar compounds.

The fourteen aromatic hydrocarbons that are used as model compounds for the experiments and have been chosen as representatives of each class of tar compounds, according to the classification proposed by van Paasen et al. [56], are presented in the following table 5.3.

Table 5.3: Model tar compounds.

Tar class	Tar compounds
Class 2	phenol, o-cresol, m-cresol
Class 3	toluene, styrene, o-xylene
Class 4	biphenyl, naphthalene, indene, fluorene, anthracene
Class 5	fluoranthene, pyrene, perylene

The calibration of the optical measurement technique implies the detection of the fluorescence signal that is emitted by the model tar compounds of interest. The optical setup is coupled directly to the tar mixing station by means of a heating tube in order to avoid condensation of the gas phase hydrocarbons. The calibration process includes experiments with different concentrations of each model tar compound as well as with

mixtures of them. The temperature of the vapors in the measurement cell is 300 °C while the parameters of the optical setup (gain, width and delay of the ICCD Camera, data acquisition timing) are kept unaltered during the calibration process and during the experiments in the gasification test rigs. The gain is set to maximum while the width of the camera is set to 200 ns to detect the fluorescence signal of compounds with long decay times such as pyrene (decay time of 122 ns [118]).

The influence of the temperature on the profiles of each hydrocarbons is of significant importance for the whole calibration and measurement process. The emitted fluorescence signal is characteristic not only for the concentration but also for the temperature of the regarded species. As indicated by Byrne et al. [137], the line width broadening of large molecules at higher temperatures are mainly attributed to thermal vibrational sequence congestion. Doppler linewidth broadening as well as pressure linewidth broadening also contribute to the additional diffuseness illustrated by the spectra [138]; however their magnitude is much smaller compared to sequence congestion. Therefore, they are not taken into account within this study.

Figure 5.12 shows the fluorescence spectra of vapor-phase pyrene and anthracene, which have been plotted on the same intensity scale to demonstrate the change in band structure associated with the temperature. Based on the increased signal to noise levels in the higher temperature spectra, it can be seen that pyrene's fluorescence intensity increases at temperatures higher than 250 °C while the fluorescence bands begin to redshift resulting in a broader bandwidth. This increase in fluorescence intensity with the increasing temperature is due to an absorption increase by pyrene at the fixed excitation wavelength as temperature increases [139]. The same phenomenon appears to anthracene, where the band positions are gradually redshifted with increasing temperature.

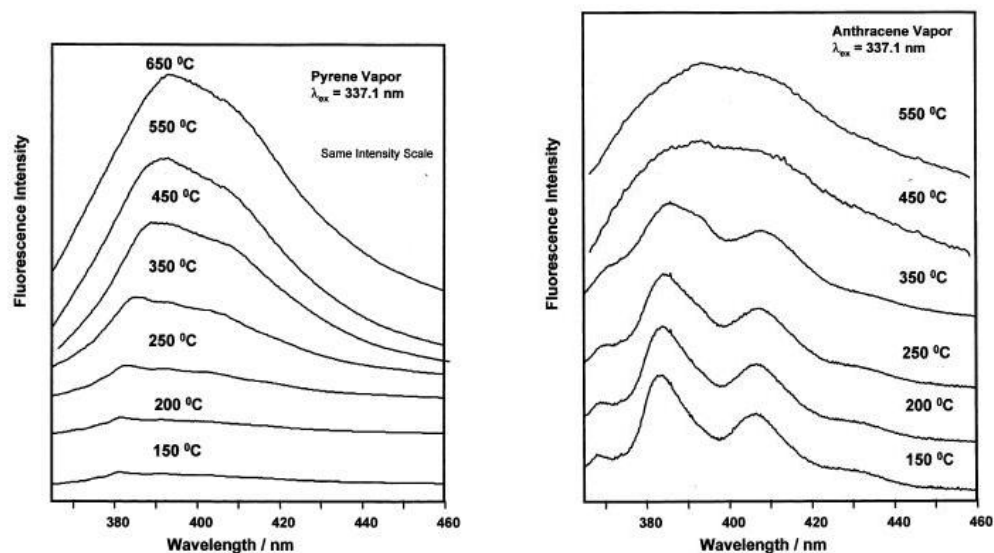


Figure 5.12: Fluorescence spectra of pyrene and anthracene vapor at 150, 200, 250, 350, 450, 550 and 650 °C [140].

Since the producer gas temperature, which is measured with a thermocouple placed inside the measurement cell of the optical setup, during the gasification experiments is kept at 300 °C, the calibration is also carried out at the same temperature. Figures 5.13-5.16 present the profiles of each tar compound at different concentration values at 300 °C while in figure 5.17 the fluorescence intensity is plotted as a function of concentration for each hydrocarbon, where a linear relation is observed.

Finally, a series of experiments with predefined mixtures of tar compounds is carried out to verify the success of the calibration process in determining the concentration of individual hydrocarbons in their mixtures.

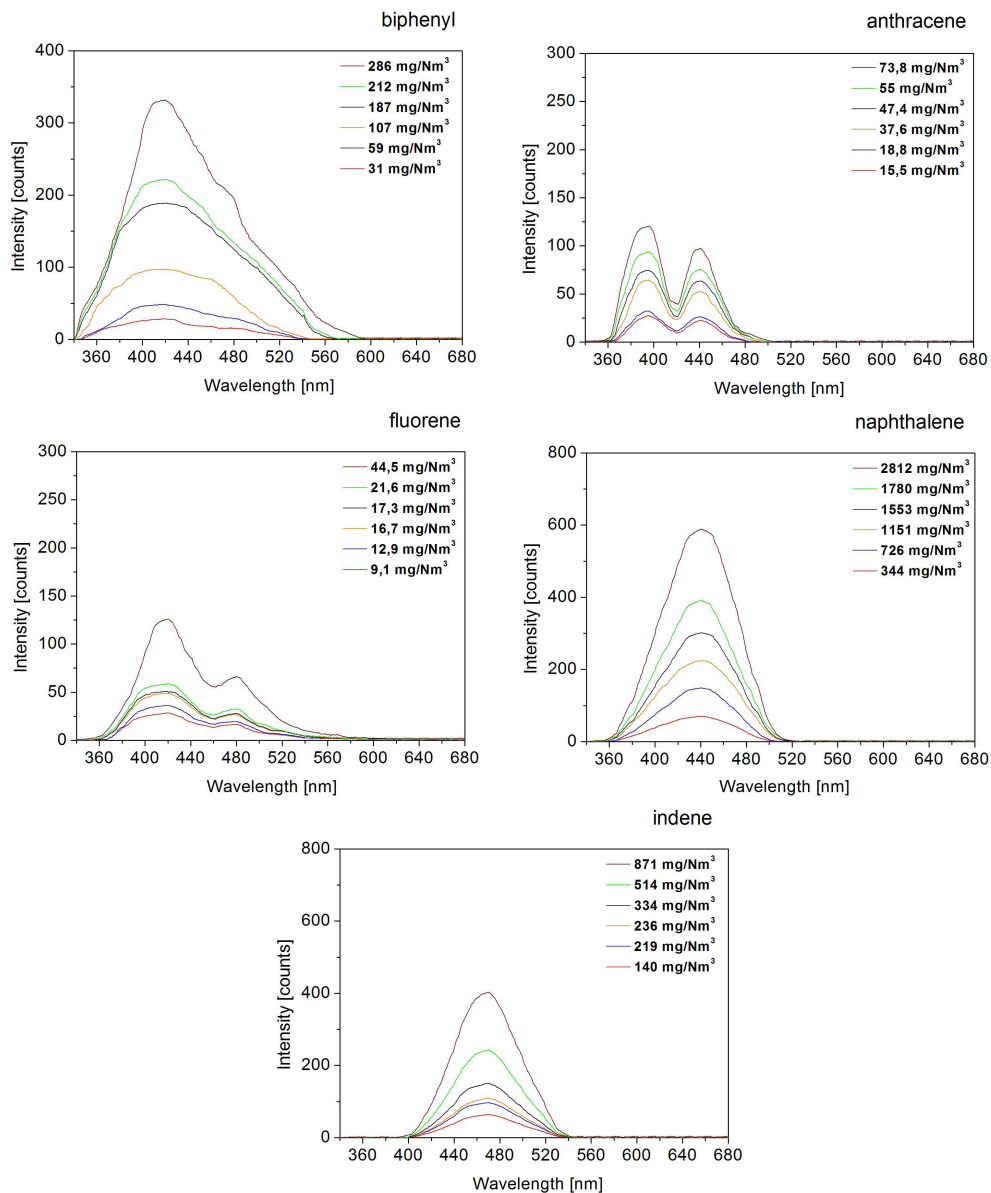


Figure 5.13: Fluorescence spectra of Class 4 tar compounds.

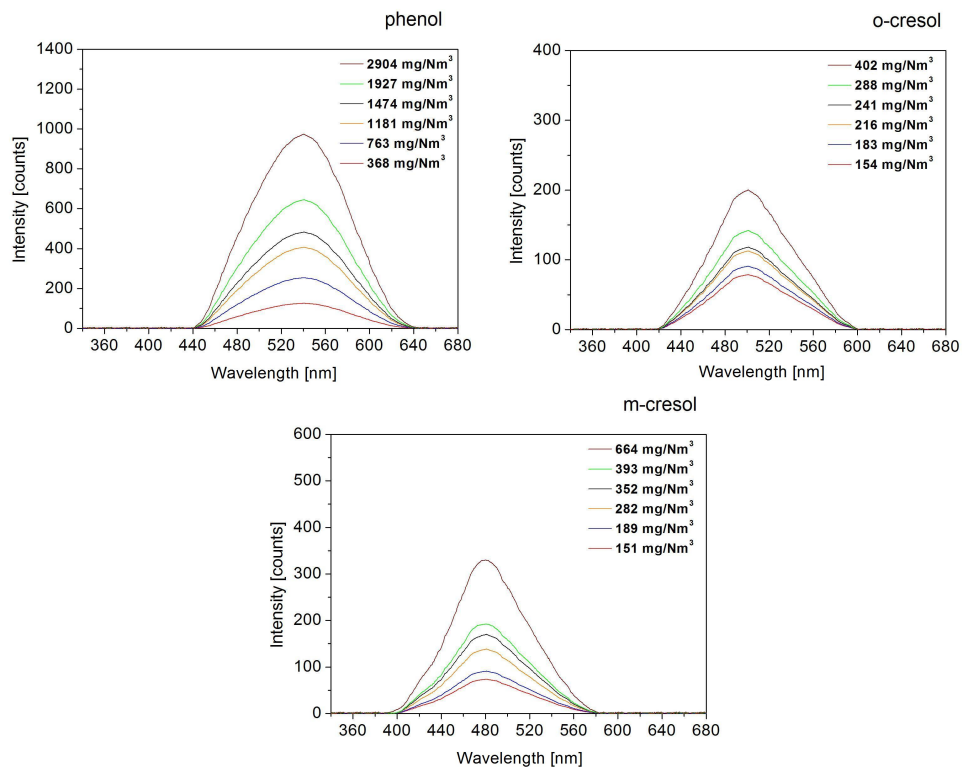


Figure 5.14: Fluorescence spectra of Class 2 tar compounds.

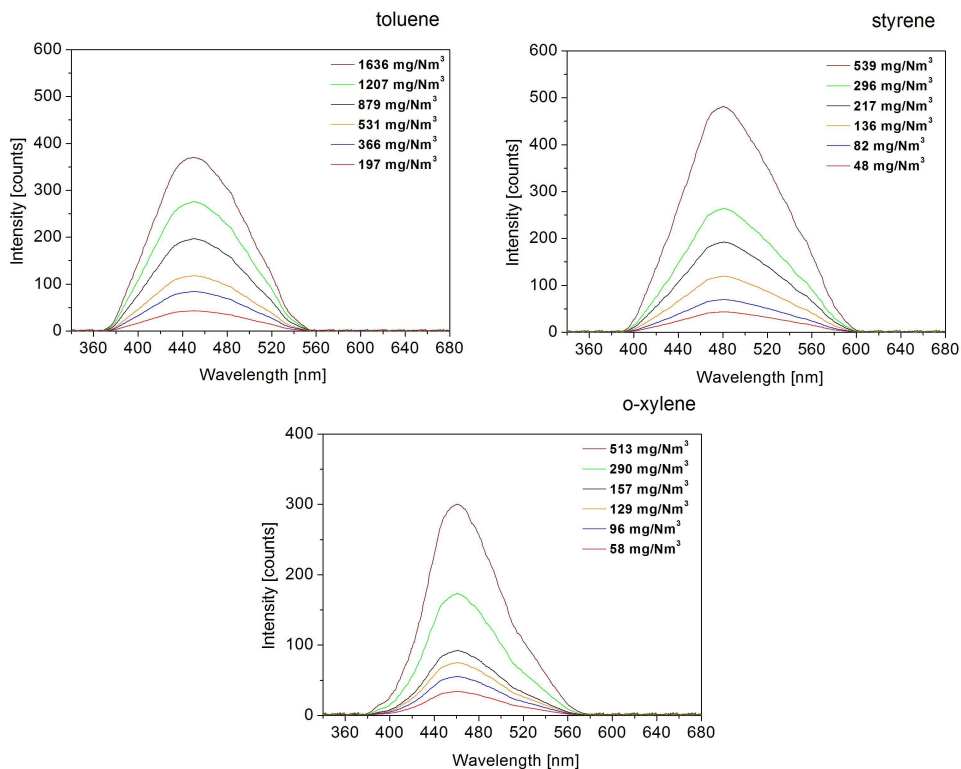


Figure 5.15: Fluorescence spectra of Class 3 tar compounds.

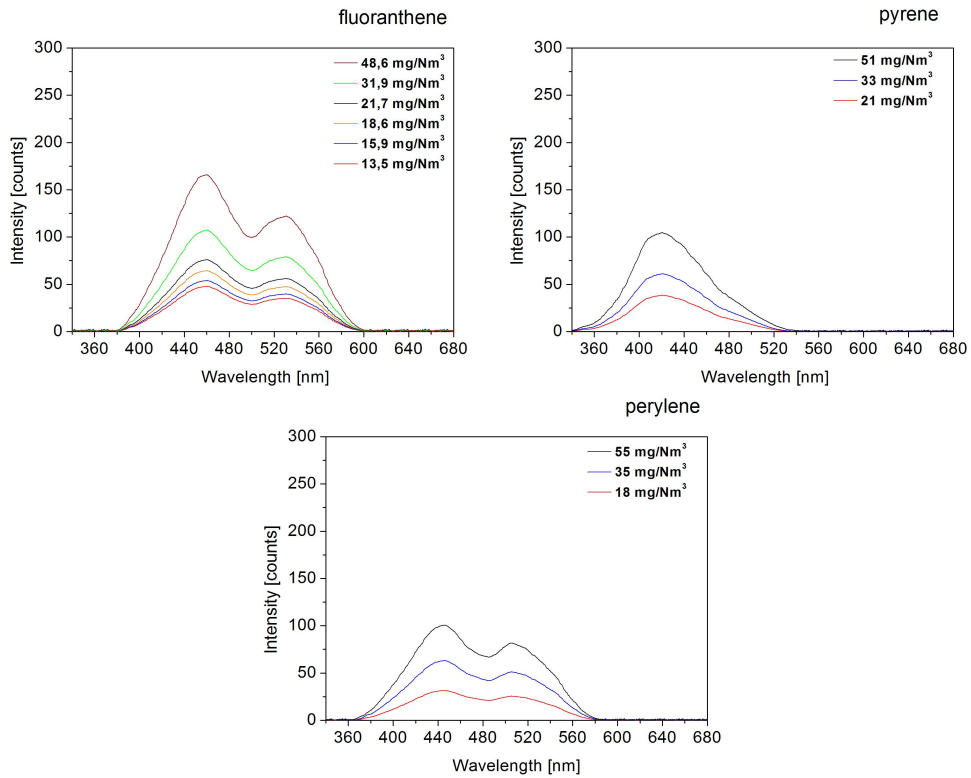


Figure 5.16: Fluorescence spectra of Class 5 tar compounds.

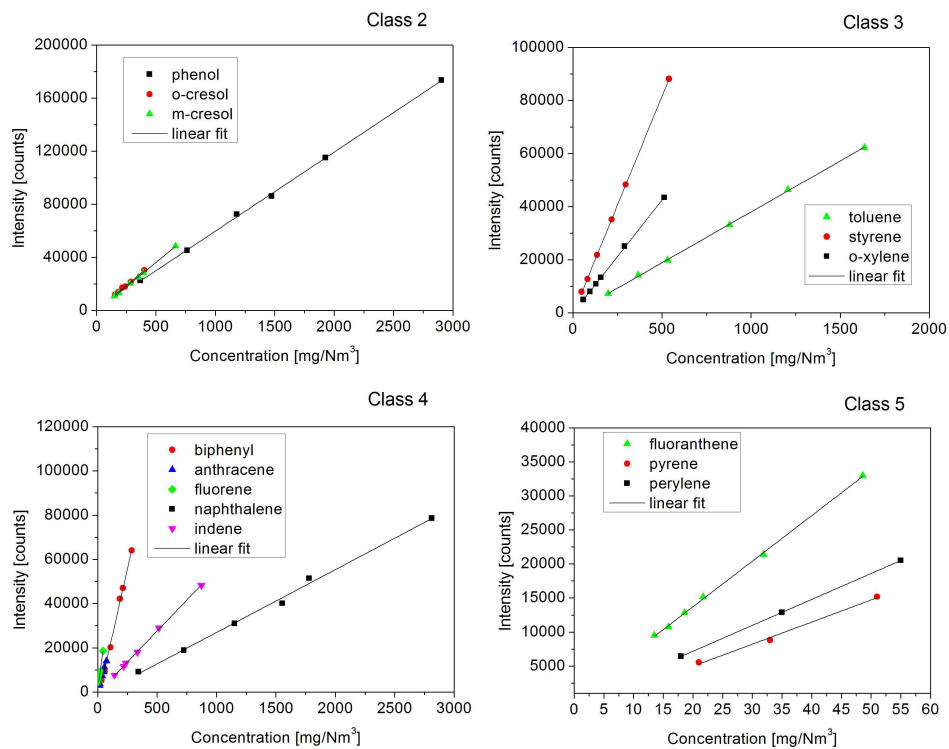


Figure 5.17: Fluorescence intensity as a function of concentration.

5.3.2 Numerical evaluation of the spectra

The signal intensity I_i of the compound i corresponds to the area underneath the profile of this tar compound, where λ_2 - λ_1 the wavelength range of the fluorescence signal.

$$I_i = \int_{\lambda_1}^{\lambda_2} I(\lambda) d\lambda \quad (5.18)$$

The fluorescence intensity I_F can be described by the following general equation, which is derived from the Lambert-Beer law [141]:

$$I_F = \text{const.} \cdot I_0 \Phi_F (1 - \exp(-\varepsilon b C)) \quad (5.19)$$

where the term *const.* includes constant apparatus and experimental parameters such as detection geometry, detection sensitivity etc., I_0 is the power of the excitation source, Φ_F is the fluorescence quantum efficiency, i.e. the ratio between the number of molecules that fluoresce and the total number of excited molecules, ε the molar absorptivity, b the cell pathlength and C the analyte concentration.

If the term $\varepsilon b C < 0,05$, then equation 5.19 is simplified to equation 5.21 where:

$$K = \text{const.} \cdot I_0 \Phi_F \varepsilon b : \quad (5.20)$$

$$I_F = \text{const.} \cdot I_0 \Phi_F \varepsilon b C = K \cdot C \quad (5.21)$$

For one given analyte, with the excitation conditions kept constant, equation 5.21 expresses the linear relation between the LIF signal intensity and analyte concentration.

As it can be seen in figure 5.18 there is a strong overlapping between the individual signals of every tar compound in a tar mixture. The overlapping of these signals makes it necessary to create an algorithm that can separate the profiles of each tar compound and therefore to determine the influence of these signals on the tar mixture.

Since the aromatic compounds studied have a linear fluorimetric response in relation to different concentrations, a linear mathematical model based on the partial least squares regression method is adopted in order to evaluate the signal from the mixtures of different tar compounds and provide further information not only about the quality of the mixture, but also about the quantity of each compound in it.

The measured fluorescence signal from the CCD camera is described by a profile F_{meas} . This profile is approximated with a profile (F_{approx}), which consists of the sum of the profiles of the fourteen individual tar compounds multiplied with respective factors (a_1 till a_{14}), and a background profile multiplied with a factor a_{15} . Each basic profile for the individual tar compounds is chosen from the set of the calibration profiles while the background profile describes the fluorescence signal from the unidentified hydrocarbons, for which the optical setup has not been calibrated. The basic background profile is

calculated from the measured profile by subtracting the area where no fluorescence signal from the fourteen basic profiles appears.

$$\begin{aligned}
 F_{approx} = & a_1 \cdot F_{phenol} + a_2 \cdot F_{o-cresol} + a_3 \cdot F_{m-cresol} + a_4 \cdot F_{toluene} \\
 & + a_5 \cdot F_{styrene} + a_6 \cdot F_{o-xylene} + a_7 \cdot F_{biphenyl} + a_8 \cdot F_{naphthalene} \\
 & + a_9 \cdot F_{indene} + a_{10} \cdot F_{fluorene} + a_{11} \cdot F_{anthracene} + a_{12} \cdot F_{fluoranthene} \\
 & + a_{13} \cdot F_{pyrene} + a_{14} \cdot F_{perylene} + a_{15} \cdot F_{background}
 \end{aligned} \tag{5.22}$$

By applying the least squares fit method, the difference between F_{meas} and F_{approx} is minimised for the whole length n of the profile:

$$G = \min_{\mathbf{a} \in \mathbb{R}} \left(\sum_{i=1}^n \left(F_i^{meas} - \sum_{l=1}^{15} a_l F_i^l \right)^2 \right) \tag{5.23}$$

where i each profile point representing the pixels of the CCD chip, F_i^{meas} the intensity of the measured profile at point i and $\sum_{l=1}^{15} a_l F_i^l = F_i^{approx}$ the intensity of the approximated profile at the same point i .

After the calculation of the factors \mathbf{a} , the intensity I of each individual tar compound is determined by multiplying these factors with the basic tar profiles. Therefore, knowing the linear relation between intensity and concentration (see figure 5.17), the concentration C of each tar compound is calculated through the appropriate linear equations.

5.3.3 Measurement of model compounds and their mixtures

Except for the measurement of different concentrations of model tar compounds, a series of experiments is carried out with predefined mixtures of hydrocarbons generated by the tar mixing station. The numerical approximation algorithm is applied to mixtures with already known concentrations of the individual tar compounds in order to examine and validate the algorithm and to optimize the calibration method as well.

An example of the Partial Least Squares (PLS) fit in a mixture containing six model tar compounds is presented in figure 5.18. The dotted line displays the spectrum obtained by the least squares fit to the experimental profile of the mixture (solid line). Table 5.4 gives information about the predicted concentrations for each tar compound versus the actual ones.

The results obtained through the numerical algorithm using the PLS regression method show very good correlation between the actual and the predicted individual PAH concentrations in the tar mixture spectrum. The approximation profile is almost identical to the measured spectrum leading to the conclusion that the least squares fit was successful. Even though there is a strong overlapping between the fluorescence signals of the individual tar compounds, the obtained results for the six aromatic hydrocarbons are satisfactory. This can be also verified after taking into account the low relative error of the measurement, which does not exceed the value of 4%.

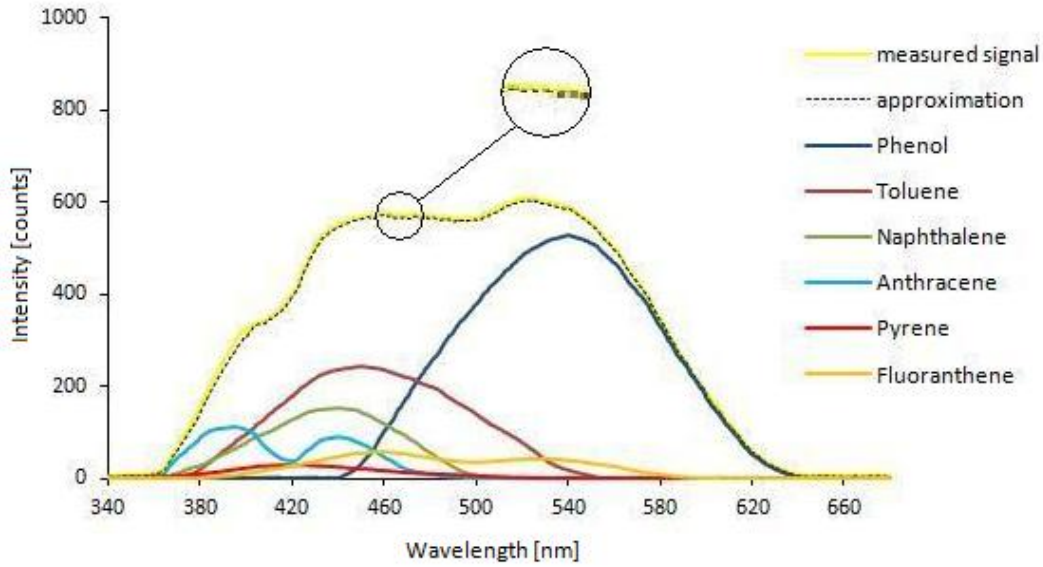


Figure 5.18: Fluorescence signal of a mixture with six model tar compounds.

Table 5.4: Results from the measurement of a tar mixture.

Tar compound	Actual value (g/Nm^3)	Predicted value (g/Nm^3)	Relative error (%)
Phenol	1,55	1,53	1,3
Toluene	1,10	1,07	2,7
Naphthalene	0,75	0,73	2,7
Anthracene	0,065	0,063	3,1
Pyrene	0,0155	0,0150	3,2
Fluoranthene	0,0165	0,0162	1,8

Therefore, since the calibration procedure has been successfully achieved, the algorithm shows the potential of identifying single compounds in complex mixtures, demonstrating that it can be applied to the analysis of LIF spectra for qualifying and quantifying gasifier tars.

5.3.4 Qualitative and quantitative measurement of biomass gasification tars

As it can be seen in the previous subsections, every tar compound gives a characteristic fluorescence emission in a specific wavelength range, which denotes the signature of every individual hydrocarbon. This wavelength range allows the qualification of each tar compound in the producer gas from biomass gasification. The area underneath each profile corresponds to a specific concentration value of every component and allows the quantification of biomass gasification tar compounds.

The above described characteristics have been the motivation to apply this optical technique for the determination of the tar content from the biomass gasification process. The online measurement of the composition of individual tar compounds gives information about the extent of the tar cracking reactions, which occur inside the gasifier, and validates the effect of different gasification parameters on the tar production.

Since the approximation algorithm has been programmed through specially constructed macro commands in Davis CL programming language of the company Lavision [142], the evaluation of the results takes place in an online way with the help of a computer system, consisting of two computers which are connected via an ethernet crossover cable.

The ICCD camera takes a picture, which represents the LIF signal of the tars. The first computer, which controls the whole camera system, saves an average picture in a specific buffer in eligible time intervals. The second computer evaluates the average picture and displays not only the spectrum but also the profile of the tar mixture. By applying equations 5.18 till 5.23, the approximation profile is calculated and is displayed as well. Consequently, the intensity of each individual tar compound is determined using the basic tar profiles multiplied with the calculated factors from the partial least squares regression method. The composition of the tar mixture is then defined through the linear relations between intensity and concentration for each tar compound and is finally presented in a table. At the same time, all the data are saved in the respective folders. A screenshot of the online evaluation process is illustrated in figure 5.19.

In that screenshot, the CCD image of the emission signal, the measured (red solid line) and the approximated (black dotted line) profile of the average picture (fluorescence signal) as well as the table including the concentration of each tar compound are displayed. The x-axis of the profiles is displayed in pixels. These pixels refer to the ones of the CCD camera and correspond to the wavelength of the emission signal. On the other hand, the pixels in the y-axis correspond to intensity counts. Furthermore, the control panel of the nitrogen laser and the digital thermometer showing the temperature inside the measurement cell of the optical setup can be also viewed in order to be easier for the user to monitor and control the whole process from the same computer device.

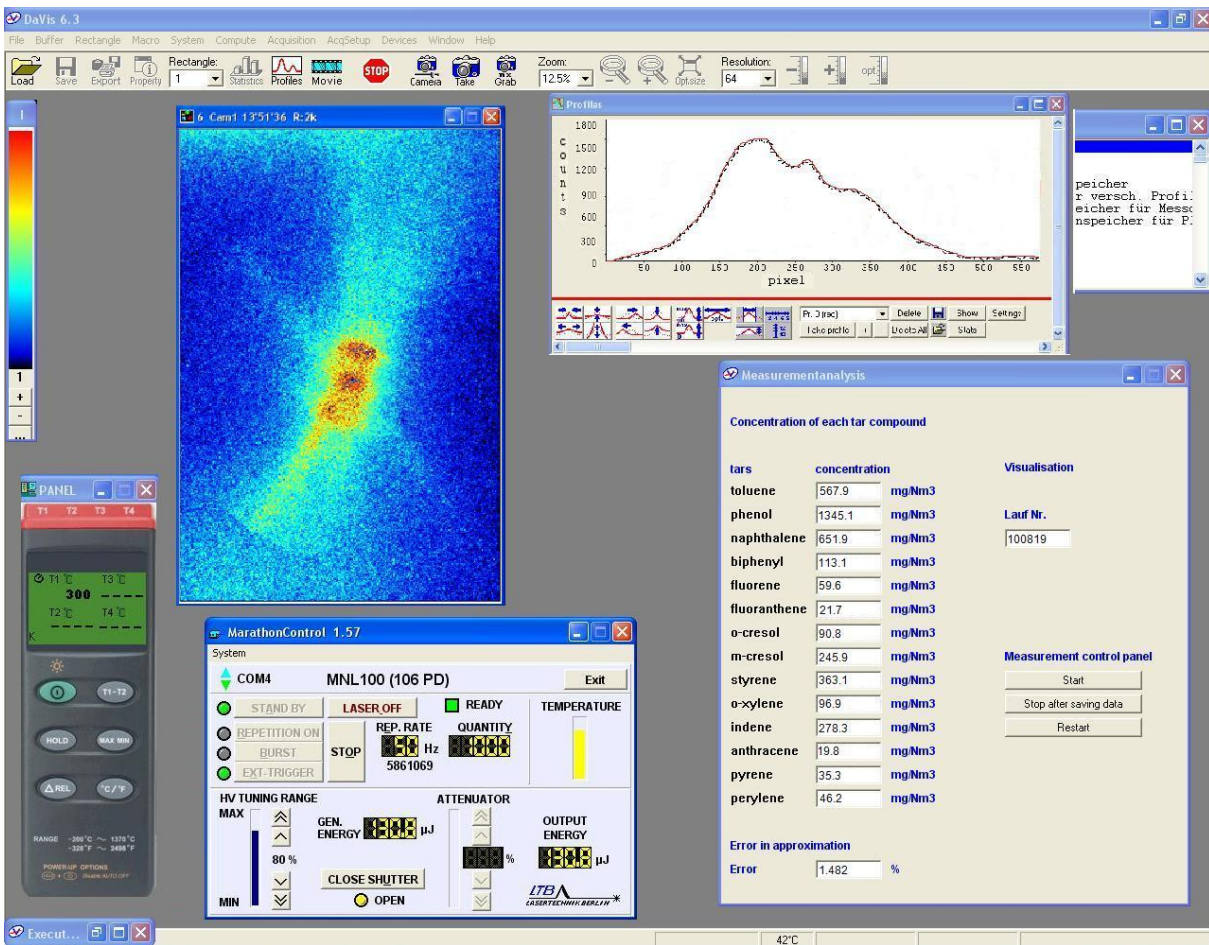


Figure 5.19: Online monitoring of the tar content of the producer gas.

5.4 Accuracy of the measurement procedure

Except for the advantages of the transportable optical setup such as the online way and the non-intrusive character of the measurement, the online determination of the sum of measured tars as well as the measurement of the concentration of individual hydrocarbons depends on many parameters, which can result in an error during the measurement procedure. The most important parameters that can cause a measurement error are discussed in detail in the following sections.

5.4.1 Measurement error due to numerical approximation

One of the most important errors that occur during the determination of the concentration of the individual tar compounds is the error due to the numerical approximation of the signals. The fact that the transportable setup analyses optical signals necessitates the creation of an algorithm, which approximates the signal of the tar mixture with a signal consisting of the sum of the optical signals of each individual tar compound plus a background signal (see section 5.3.2).

The error in the approximation curve is mainly caused by the calculation of the background profile as well as by the fitting of the approximated profile to the measured one. The strong overlapping between the profiles of individual tar compounds is the main reason for the error during the partial least squares (PLS) fitting. An example of the fitting of the approximation profile to the measured profile is illustrated in figure 5.18. The error between the approximation and the measured curve is defined by the area between the two curves.

The approximation error for every measurement of the tar composition is most of the times positive leading to the conclusion that the approximation curves are lower than the measured ones. This tendency is observed for all hydrocarbons measured with the transportable setup. The mean error for the sum of measured tars during the experiments in both TUM and TUD gasification facilities varies from 1% to 6%, which means that the difference between the measured profile and the approximated one is very low.

5.4.2 Measurement error due to chemical reactions

Another error that can occur in the measurement procedure is the error due to chemical reactions. Various chemical reactions can take place inside the heated lines, through which the producer gas from the biomass gasification process is driven to the measurement cell of the optical setup. On the one hand, the amount of steam that is included in the producer gas can favor the tar cracking reactions while on the other hand, the amount of Nickel which is added in the stainless steel sampling lines in order to stabilize the austenite structure of iron can act as a catalyst for the tar destruction.

However, due to the low temperature of the producer gas inside the sampling line (approx. 300 °C), the chemical reactions between the individual hydrocarbons and steam are not favored to such an extent that will cause considerable change in the tar composition. Regarding the structure of the stainless steel heated tubes, the amount of nickel is very low to cause a significant catalytic destruction of the tar compounds and therefore a significant change in the tar composition.

Furthermore, due to the relatively high volume flow of the producer gas and the fact that the internal diameter of the heated sampling line is only 4mm, the velocity of the producer gas is high. Therefore, the residence time is very low, which prevents the completion of the tar cracking reactions or the catalytic tar destruction.

5.4.3 Measurement error due to the parameters of the optical setup

Finally, measurement errors can occur due to the change of the parameters of the optical setup. First of all, small vibrations of the optical facility during the measurement can influence the optical signal and produce measurement error by changing the position of the camera as well as the focus of the laser beam on the centre of the measurement cell.

In addition, small fluctuations in the flow of the producer gas can cause fluctuation in the producer gas' temperature inside the measurement cell. Considering the fact that the calibration of the optical facility is carried out at the same constant temperature, a slight change results in an error during the measurement.

Furthermore, the output energy per pulse of the Nitrogen laser is not always constant but has some slight fluctuations of approx. 1-2 μJ . Changes in the excitation energy influence the intensity of the signal obtained by the CCD camera and can cause error in the determination of the tar composition considering that the calibration signals are detected with a different excitation energy.

Due to the fact that the parameters of the optical setup are kept as constant as possible, the aforementioned errors do not appear often during the measurement procedure. Therefore, they are considered as negligible and they are not analyzed further in this study.

6 Experimental results

6.1 Experimental facility for biomass gasification

6.1.1 The Biomass Heatpipe Reformer-BioHPR (TUM)

The Biomass Heatpipe Reformer (BioHPR) is an innovative gasification concept which uses the technology of high temperature heatpipes in order to transfer the high heat flux needed for the gasification reactions from a combustion chamber into the gasifier.

Heatpipes are heat exchangers which are based on enclosed two-phase systems. The heatpipe components are a hermetic sealed container, a wick structure and a small amount of working fluid (acetone, ethanol, water, sodium, mercury, etc...), which is in equilibrium with its own vapour. A high temperature heatpipe is divided into three zones: the evaporation zone, where heat is provided to the heatpipe, the condensation zone, where heat from the heatpipe is transferred to its environment and the middle section, which is called adiabatic zone [143]. Figure 6.1 presents the operational principle of a heatpipe with the installed capillary flow.

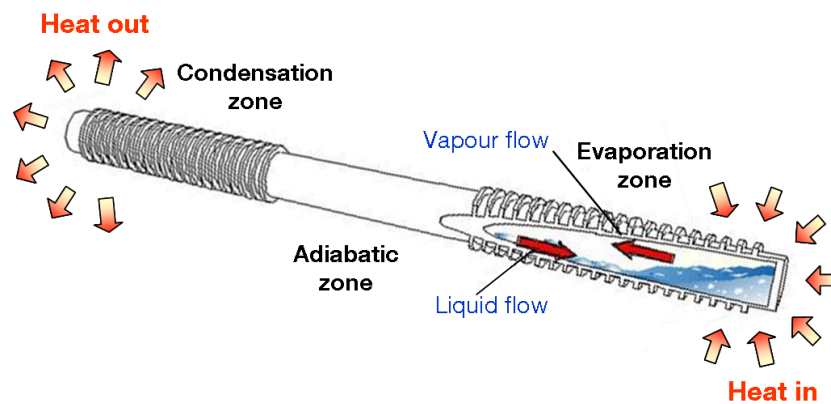


Figure 6.1: Operational principle of a heatpipe.

Heatpipes utilise the phase change of a working fluid operating in a completely evacuated and sealed enclosure. The fluid exists within the pipe as a wet saturated vapour. When heat is applied to the evaporation zone, the working fluid is evaporated and then condenses again at the condensation zone by giving the applied heat back to its environment. This process is continuously ongoing as long as there is a sufficient capillary pressure to drive the condensate back to the evaporation zone [143]. The latent heat of vaporization during the phase change process is utilized to realize a very efficient heat transfer.

The gasifier is designed as an allothermal bubbling fluidized bed, where the required heat for the endothermic gasification reactions is provided through heatpipes. There are two different configurations of the facility, one in laboratory scale (the heatpipes are heated electrically) and one pilot scale (the heat is transferred through heatpipes from an external combustion chamber). Regarding this experimental research the heatpipes are electrically heated. The gasifier is illustrated in the following figure 6.2.

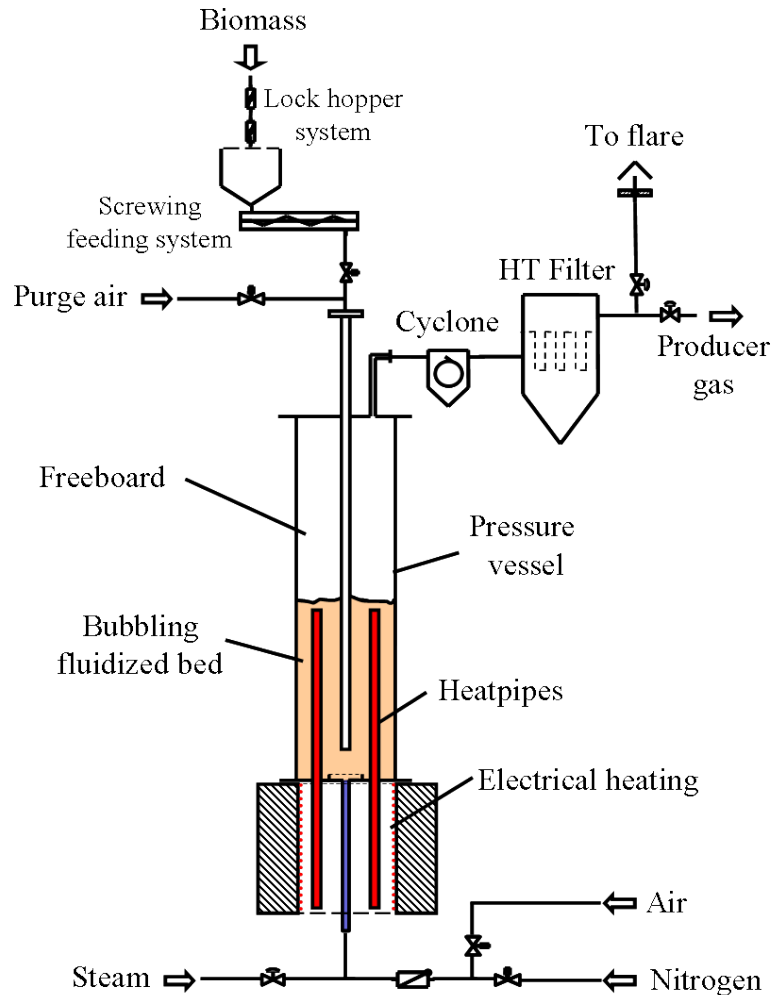


Figure 6.2: TUM gasification test rig.

The main design data and specifications of the gasification unit are presented in table 6.1. The experimental facility consists of the following parts:

- pressure vessel-gasifier
- high temperature heatpipes
- electrical heating
- screwing feeding system and lock hopper system
- cyclone
- high temperature ceramic candle filter

Table 6.1: Design data and specifications of the BioHPR.

Fluidized bed reactor	
Reactor inner diameter (<i>mm</i>)	154
Reactor height (<i>m</i>)	1,5
Bed height (<i>m</i>)	0,7
Freeboard height (<i>m</i>)	0,8
Steam injection cross	
Length of each tube (<i>mm</i>)	58
Diameter of each tube (<i>mm</i>)	12
Number of holes per tube	5
Hole diameter (<i>mm</i>)	6
Heatpipes	
Heatpipe length (<i>m</i>)	1,3
Heatpipe diameter (<i>mm</i>)	19

The biomass is fed through a screwing feeding system directly into the bubbling fluidized bed reactor. The maximum fuel input is 50 kW_{th} based on woody biomass. The reactor (gasifier) consists of a cylindrical stainless steel vessel (AISI314, DIN X15 CrNiSi 25 20, 1.4841), which can be pressurized up to 5 bar. The screwing feeding system is an orthogonal vessel (20l volume) with a screw, which can be pressurized (up to 10 bar) as well. A lock hopper system is coupled to the screwing feeding system to achieve the continuous filling of the orthogonal vessel with pelletized biomass and avoid feeding discontinuance when the reactor is operated under pressure.

The bed is fluidized with steam, which is used as gasification medium while olivine is used as bed material. Oversaturated steam is produced by a steam generator and after being heated to a temperature of 600 °C with the help of a superheater, is injected into the reactor through an injection cross. Bed and freeboard temperature are controlled by type K thermocouples located all over the entire length of the gasifier with the help of a vertical probe, which contains the above mentioned thermocouples and is placed inside the reactor. Pressure loss is measured by differential pressure sensors placed at the bottom and top of the reactor vessel respectively.

The producer gas exits the reactor and after its way through a cyclone, it is driven to a high temperature ceramic candle filter (Pall-Schumacher, Germany) for further purification. The remaining chars are removed from the gasifier together with the producer gas and are separated in the cyclone. A small amount of nitrogen is used to flush the biomass feeding system to avoid producer gas and steam to exit the reactor over the screwing feeding system. The whole gasification test rig (gasifier and gas purification unit) can

be pressurized up to 5 bar by means of a pressure control valve placed after the high temperature ceramic filter.

The heat is transferred via four high temperature heatpipes, which work nearly isothermal over their entire length, into the gasification zone. The evaporation zone of the heatpipes is placed in the radiation heater, which is electrically heated, while the condensation zone is placed into the gasifier. The working fluid (sodium) is evaporated by heat input, flows to the gasification zone, where it condenses by heat emission providing the required heat for the endothermic gasification reactions.

6.1.2 Atmospheric circulating fluidized bed (TUD)

The gasification test rig at the Process & Energy Laboratory of TUD that is used to conduct the gasification experiments is an atmospheric 100 kW_{th} steam-oxygen blown circulating fluidized bed gasifier. A schematic drawing of the working principle of the CFBG is presented in Figure 6.3, while a Piping and Instrumentation Diagram (PID) of the whole test rig is presented in Figure 6.4.

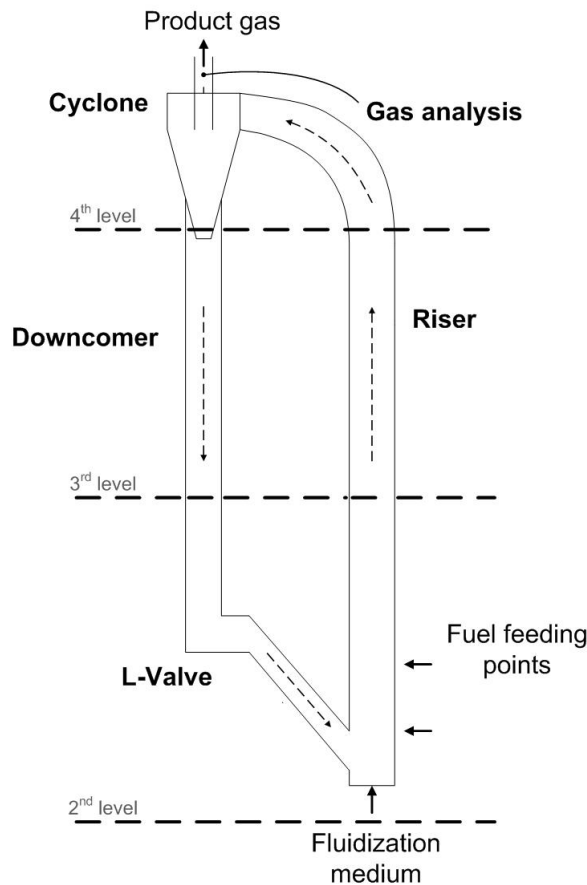


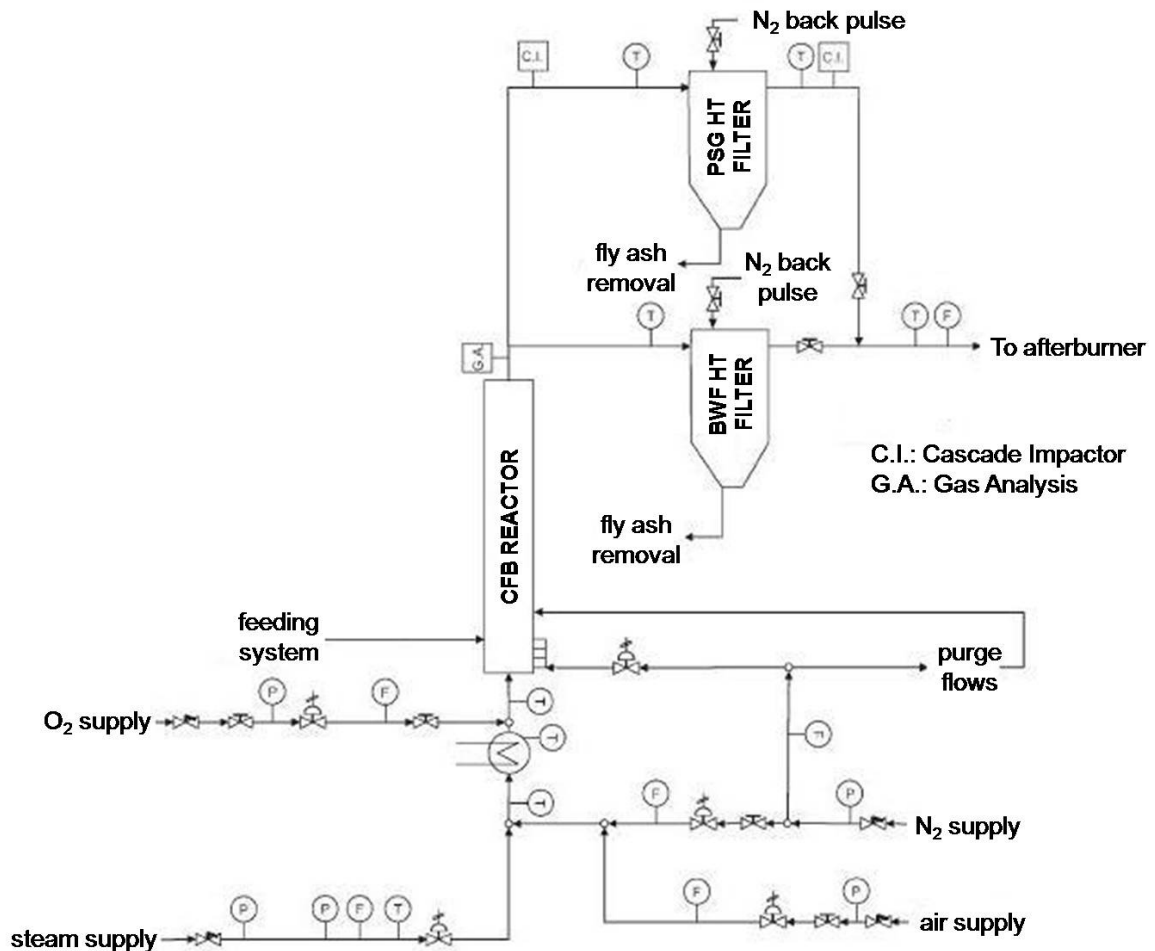
Figure 6.3: Schematic drawing of the CFB gasifier at TUD [144].

The main characteristics of the gasification rig are listed in the following table 6.2.

Table 6.2: Design data and specifications of the atmospheric CFB.

Reactor height (<i>m</i>)	5,5
Riser inner diameter (<i>mm</i>)	83
Downcomer inner diameter (<i>mm</i>)	54
Maximum biomass feed rate (<i>kg/h</i>)	20

The riser and the downcomer are cylindrical stainless-steel (AISI310, DIN 1.4845) vessels, which together with the feeding system and the high temperature filters are the main parts of the whole gasification facility. The two filters that are used for the gas purification are a high-temperature ceramic tissue candle filter unit (BWF, Germany) operating at 450 °C and a high temperature Si-SiC ceramic candle filter (Pall-Schumacher, Germany) operating at 800 °C. The whole rig is electrically heated (22 kW; $T_{max} = 1200$ °C; $T_{nom} = 850$ °C) by means of modular ceramic fiber heaters (ZMC Zamac, Poland).

**Figure 6.4:** PID of the TUD gasification test rig, with CFBG and high-temperature ceramic filters [144].

The feeding system (main screw feeder) is located 900 *mm* above the gas distribution plate. It has a maximum feed rate of ca. 20 *kg/h* of biomass plus the possibility of independent co-feeding of two other kinds of solids (e.g., additives). The gas distribution plate consists of nine tuyeres with two holes each. Regarding the fluidization medium (mixture of steam and oxygen), it reaches the reactor after having been heated by an electrical preheater (6 *kW*; $T_{max} = 400$ °C; $T_{nom} = 360$ °C; Watlow, St. Louis, MO).

The measurement equipment consists of mass flow meters and controllers for all primary input streams, a differential pressure flowmeter for measuring the flow of the producer gas, type K thermocouples, which are located in the riser and the downcomer, differential pressure meters, weighing devices, and differential pressure cells measuring the pressure drop over different parts of the installation. A more detailed description of the whole gasification facility together with the measurement equipment is reported by Siedlecki et al. [144] elsewhere.

6.2 Test program at the TUM and TUD gasifiers

The test program of the experiments consists of the gasification of three different biomass fuels in the pressurized bubbling fluidized bed reactor at TUM and in the atmospheric circulating fluidized bed gasifier at TUD. The biomass feedstocks are tested under different gasification parameters to examine their influence on the tar content of the producer gas. The three different biomass fuels which are tested during the experiments are the following:

- AGROL wood pellets
- Short Rotation Coppice-Willow pellets
- Distilled Dried Grains with Solubles (DDGS)

One of the advantages of pelletized biomass fuels is the high volumetric energy density, which makes them more flexible and cheaper than non-pelletized fuels regarding transport and investment costs for fuel storage and process feeding, respectively. AGROL wood pellets are made from pure sawdust and shavings from sawmills, using 100% virgin timber from sustainably managed plantation forestry. Willow pellets are originally made from harvested willow coppice while DDGS is the coproduct of the ethanol production process. When ethanol plants produce ethanol, they use starch from corn and grain sorghum. The remaining nutrients (protein, fiber and oil) are the by-products used to create livestock feed called distilled dried grains with solubles. The pelletized DDGS used in this study is the coproduct of the ethanol production process from corn. All different kinds of biomass fuels are delivered by the Lantmännen Group, Sweden within the framework of the European GreenSyngas project (FP7-ENERGY-2007-GreenSyngas-213628).

Prior to gasification, the three biomass fuels as well as their ashes are analyzed. The proximate analysis of the fuels is performed by an IR-60 moisture analyzer (Denver Instrument) and a Heraeus muffle furnace (Thermo scientific). The heating value is measured by a Parr 1351 bomb calorimeter while Carbon, Hydrogen, Nitrogen and Sulphur elements are analyzed by CHNS-analyzer (System LECO). Inorganic main components of the three biomasses are analysed by Inductively Coupled Plasma Optical Emission Spectroscopy (ICP-OES) (Model: TJA IRIS Advantage with Echelle-Optic and CID-semiconductor detector). Chlorine in biomasses is analysed by Cl-Ion Chromatography (IC) after Wickbold combustion while chlorine in biomass-ashes is analysed after soda extraction. The main ash mineral phases are analysed by X-Ray Diffraction (XRD) using a Siemens D500 X-Ray diffractometer with a Cu-K α monochromated radiation source.

The proximate analysis of the fuels as well as their heating value determination is performed at TUM while the other measurements are carried out at Forschungszentrum Jülich. The results are presented in the following tables 6.3 and 6.4.

Table 6.3: Chemical composition of the three biomass fuels.

	AGROL	Willow	DDGS
<i>Proximate analysis, %wt (db)</i>			
moisture	4,84	8,46	6,91
ash	0,12	3,2	4,75
volatiles	85,58	78,35	79,86
fixed carbon	14,30	18,45	15,39
<i>Heating value</i>			
HHV (MJ/kg)	20,6	18,4	19,4
<i>Ultimate analysis, %wt (db)</i>			
C	51,0	50,3	48,2
H	6,26	6,17	6,54
N	0,15	0,69	5,52
S	-	-	1,8852
Cl	0,005	0,007	0,210
P	-	0,1787	2,0622
O	42,309	40,9668	32,2139
Al	-	0,0699	-
Ba	0,0011	0,0011	-
Ca	0,1091	0,6576	0,1399
Fe	0,0057	0,0486	0,0171
K	0,053	0,3012	2,1201
Mg	0,0282	0,0812	0,4974
Mn	0,0155	0,009	0,009
Na	0,0108	0,0283	0,4718
Si	0,0192	0,4706	0,1134
Ti	0,0334	0,02	-

Table 6.4: Chemical composition of 550 °C-ashes of the three biomass fuels (%wt).

	AGROL	Willow	DDGS
Al_2O_3	2,6830	4,2324	0,0510
BaO	0,4131	0,0625	0,0145
CaO	33,3011	26,3051	2,8683
Fe_2O_3	1,3154	1,5441	0,2574
K_2O	16,5031	13,1302	38,0655
MgO	7,7939	2,8854	8,8718
MnO	3,9641	0,2970	0,1549
Na_2O	0,9975	1,6715	10,0424
SiO_2	6,4608	33,8015	1,8612
TiO_2	0,0601	0,1835	-
P_2O_5	3,2537	6,37	38,7241
Cl	0,0670	0,1100	0,0180
SO_3	2,4570	2,2722	10,0376

The measurement campaign took place in April 2010 at TUD and in June 2010 at TUM, where the influence of different gasification parameters on the tar content was investigated. The test program of the whole measurement campaign can be summarized in table 6.5 where the ranges for the different gasification parameters are presented in relation to the reactor type and the biomass feedstock used.

A more detailed overview of the operational parameters for each experimental day is given in the following subsections.

Table 6.5: Test program of the measurement campaign.

	BFB (TUM)			CFB (TUD)		
Biomass feedstock	AGROL	Willow	DDGS	AGROL	Willow	DDGS
Temperature [°C]	750-850	750-850	700-800	715-820	725-800	690-750
Pressure [bar]	1-2,5	1-2,5	1	1	1	1
Steam to biomass ratio	0,85-1,2	0,85-1,2	0,9-1,2	0,95-1,5	0,85-1,2	0,95-1,1
Bed material	Olivine	Olivine	Olivine	treated & untreated Austrian olivine	treated & untreated Austrian olivine	treated & untreated Austrian olivine

6.2.1 Operational parameters of the pressurized bubbling fluidized bed (BioHPR)

The influence of temperature, pressure and steam to biomass ratio (S/B) on the tar content is investigated during the experiments at the pressurized bubbling fluidized bed of the Technische Universität München (TUM). The main operational parameters of the gasifier during each experimental day are depicted in the following figures 6.5-6.8.

Olivine is used as bed material in the gasifier during the whole series of experiments. Olivine (chemical formula: $(Mg, Fe)_2SiO_4$) is a naturally occurring silicate mineral containing oxides of magnesium, iron and silicon. The chemical composition of the used olivine as well as its particle size, bulk density and porosity are given in table 6.6.

Table 6.6: Bed material properties of TUM gasifier.

Particle size [mm]	0, 1-0, 3
Bulk density [kg/l]	1, 45
Porosity	0, 52
Chemical composition (%wt)	Olivine
<i>SiO₂</i>	42
<i>Fe₂O₃</i>	9, 75
<i>MgO</i>	47, 6
<i>CaO</i>	0, 13
<i>MnO</i>	0, 126
<i>Al₂O₃</i>	0, 4

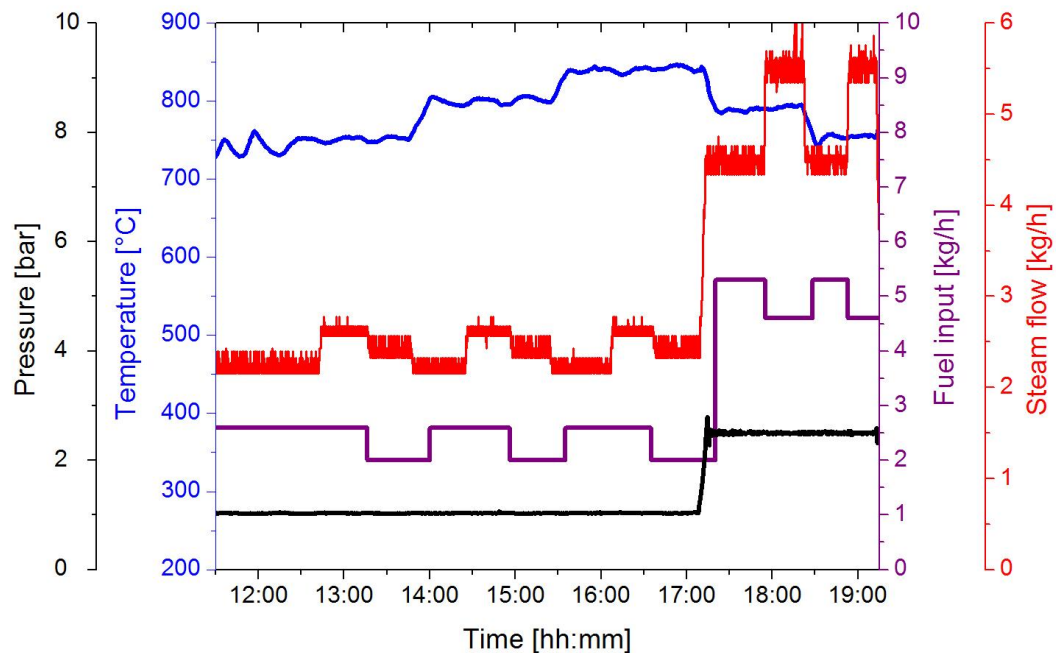


Figure 6.5: Operational parameters during AGROL gasification-07.06.2010.

Figure 6.5 depicts the operational parameters of the BioHPR during atmospheric and pressurized gasification of AGROL pellets. Figures 6.6 and 6.7 present the gasification parameters for atmospheric and pressurized conditions using Willow pellets as biomass feedstock.

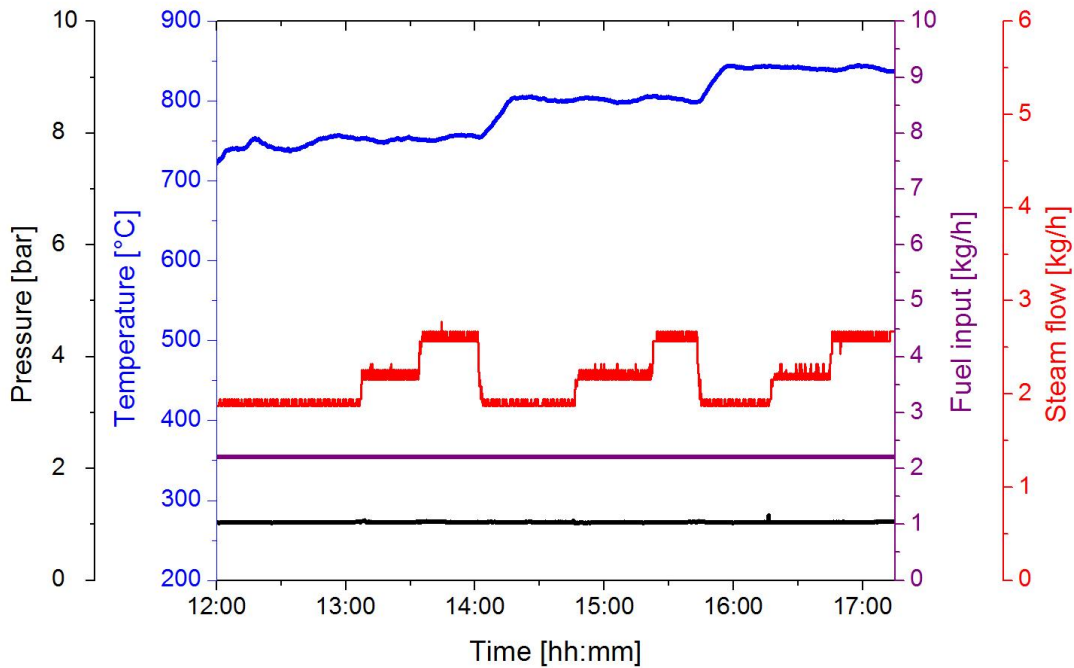


Figure 6.6: Operational parameters during atmospheric Willow gasification-08.06.2010.

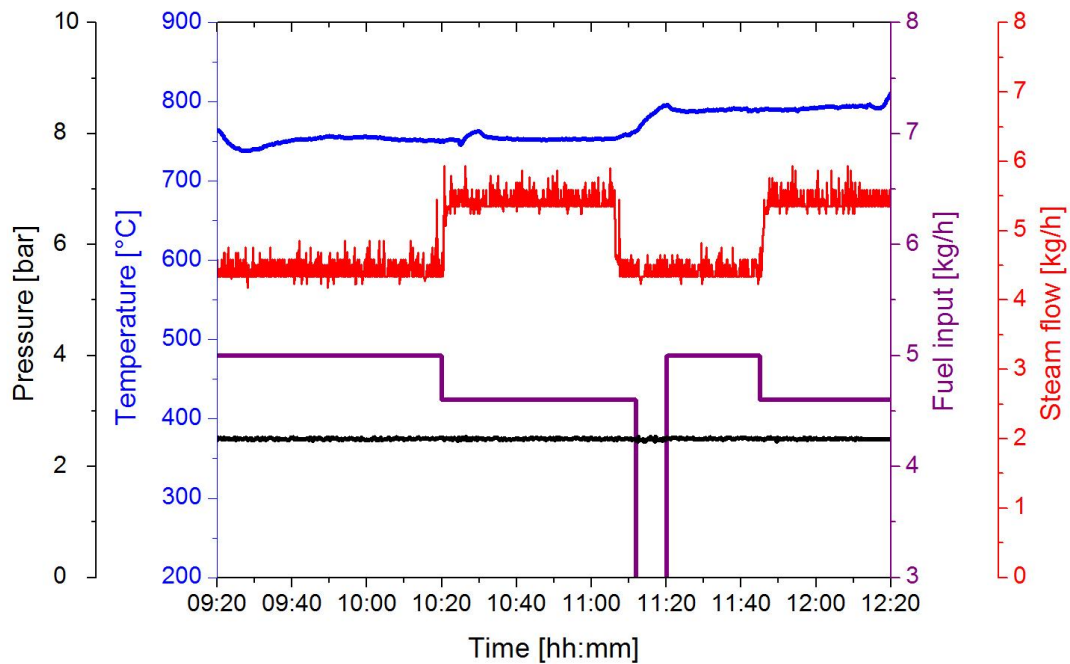


Figure 6.7: Operational parameters during pressurized Willow gasification-09.06.2010.

Regarding atmospheric gasification of AGROL and Willow pellets, three different S/B values (0.85, 1, 1.2) are tested for each of the three gasification temperatures (750, 800, 840 °C), respectively. Furthermore, two different S/B values (0.85, 1.2 for AGROL and 0.9, 1.2 for Willow) are tested for two temperatures (750, 790 °C) during pressurized gasification of the aforementioned two fuels.

Figure 6.8 illustrates the operational parameters of the BioHPR during atmospheric gasification of DDGS pellets, where two different S/B values (0.9, 1.2) are tested in 700, 750 and 800 °C, respectively. The operating temperature is chosen to be lower than in case of AGROL and Willow gasification to prevent slagging and deposition problems due to the high ash content of this fuel and the low melting point of the produced residual ash. Regarding this feedstock, no gasification experiments are carried out under pressurized conditions.

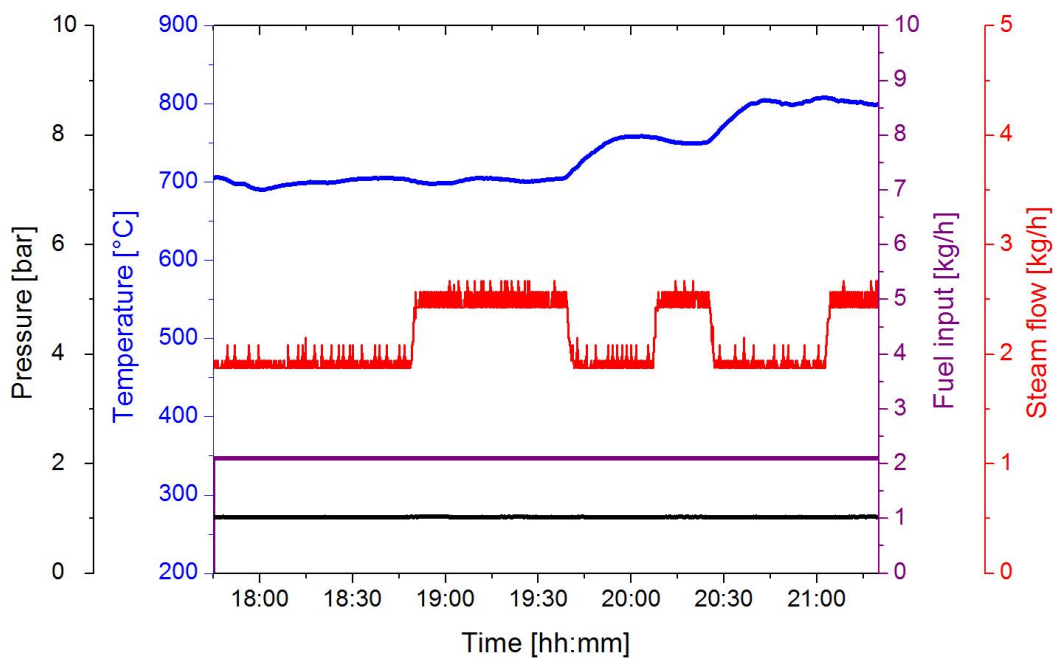


Figure 6.8: Operational parameters during DDGS gasification-09.06.2010.

6.2.2 Operational parameters of the atmospheric circulating fluidized bed

The operational parameters of the atmospheric steam-oxygen blown circulating fluidized bed gasifier of the Delft University of Technology (TUD) during the experimental campaign are presented in figures 6.9-6.13. The influence of temperature, steam to biomass (S/B) ratio and bed material type on the concentration of tar compounds is investigated.

Two different bed materials (treated and untreated Austrian olivine) and one additive (Kaolin) are used during the gasification experiments. The properties of the untreated (fresh) Austrian olivine as well as the additive characteristics are presented in table 6.7.

The treated olivine properties are relatively the same as the untreated ones except for some calcium integrated into the treated olivine.

Table 6.7: Bed material and additive properties of TUD gasifier.

Bed material and additive	Particle size [mm]	Porosity
untreated Austria olivine	0,315 – 0,63	0,14
Kaolin	0,063 – 0,2	-
Chemical composition (%wt)	untreated Austria olivine	Kaolin
<i>SiO₂</i>	39 – 42	57,7
<i>Fe₂O₃</i>	8 – 10,5	0,9
<i>MgO</i>	48 – 50	0,4
<i>CaO</i>	0,4	0,1
<i>Al₂O₃</i>	0,8	37,5
<i>Mn₃O₃</i>	0,8	-
<i>Cr₂O₃</i>	0,8	-
<i>K₂O</i>	-	3,1
<i>TiO₂</i>	-	0,2
<i>Na₂O</i>	-	0,1

Figure 6.9 and 6.10 illustrate the operational parameters of the atmospheric steam-oxygen blown circulating fluidized bed reactor during gasification of AGROL pellets. During the first day, two different S/B values (1.5, 1.4) are tested for the low temperature of 715 °C, while the same value (S/B:1.35) is kept constant for the next two temperature values (770, 820 °C) to investigate the influence of gasification temperature on the tar content. During the second day, three different S/B values are tested for each of the two temperatures (750, 800 °C) to check the influence of steam input on the tar cracking.

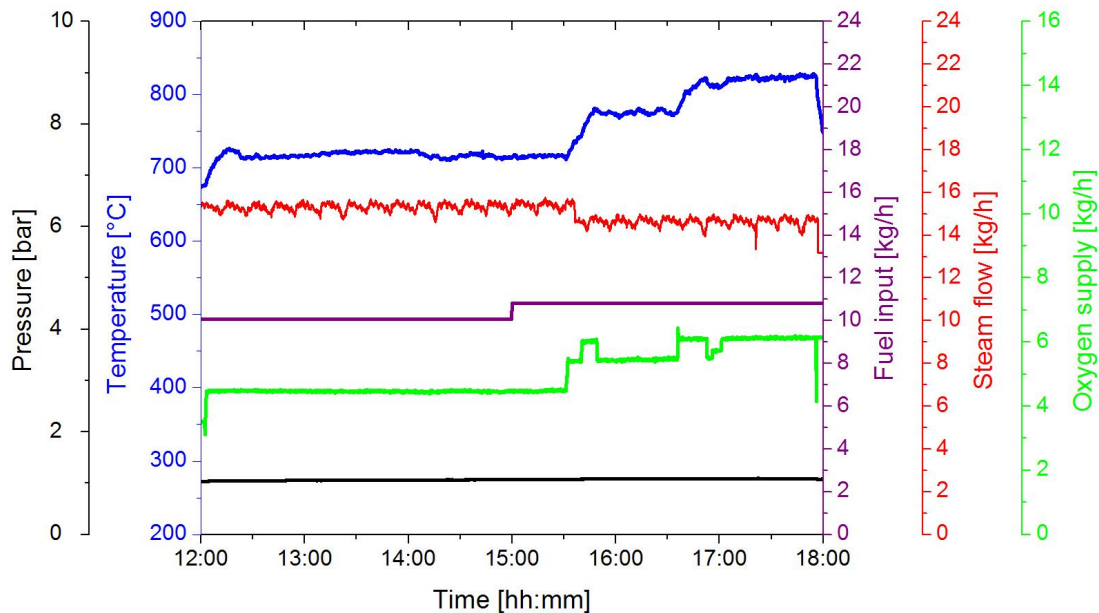


Figure 6.9: Operational parameters during AGROL gasification-13.04.2010.

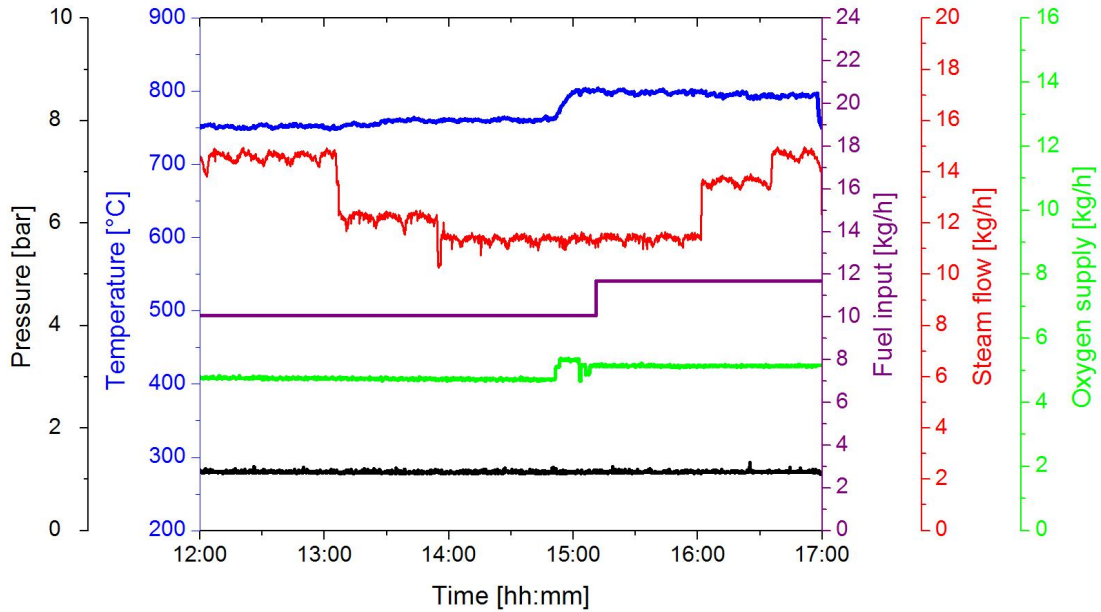


Figure 6.10: Operational parameters during AGROL gasification-15.04.2010.

Figure 6.11 depicts the operational parameters of the circulating fluidized bed reactor during Willow gasification, where three different S/B ratio values are applied to each of the three gasification temperatures (725, 755 and 800 °C). In the next figure 6.12, DDGS is gasified in the temperature range from 690 to 750 °C. Due to the blockage of the L-valve of the CFB reactor (possible formation of agglomerates), gasification is stopped after three hours and therefore only few gasification parameters are tested.

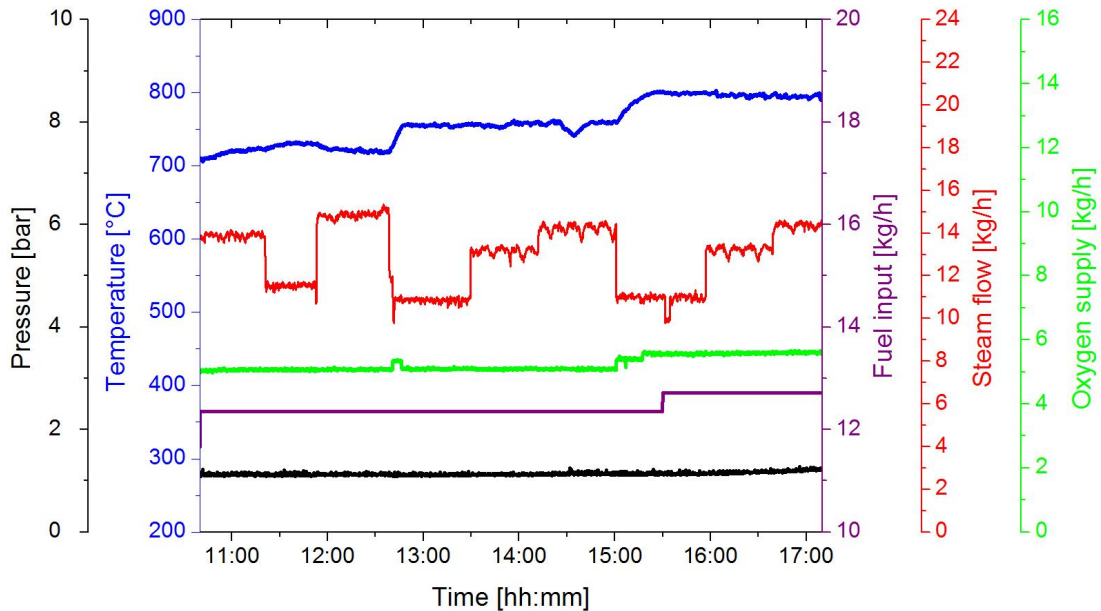


Figure 6.11: Operational parameters during Willow gasification-19.04.2010.

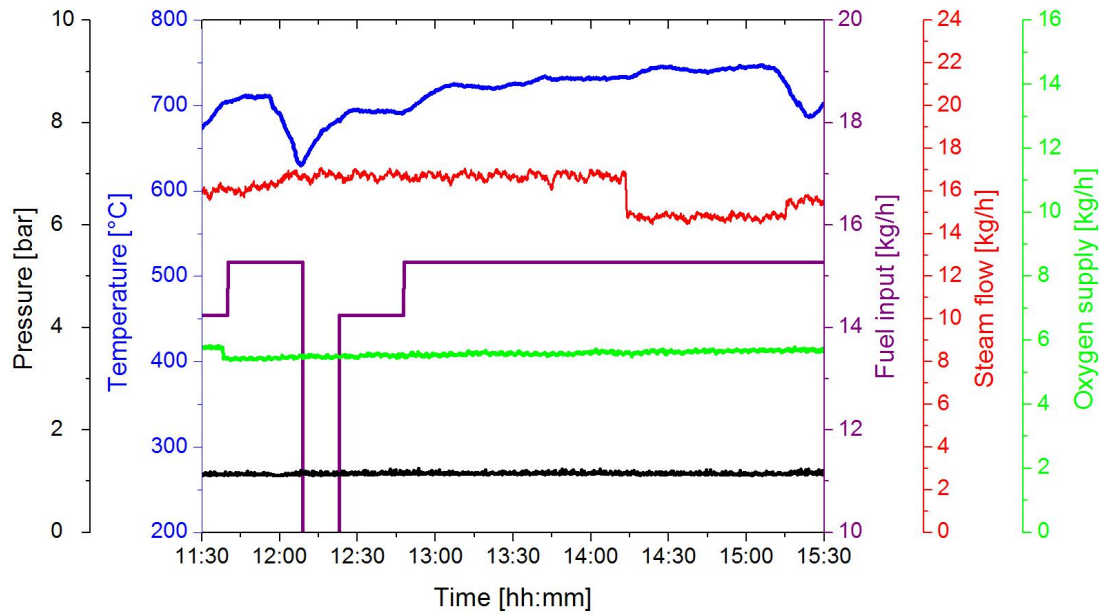


Figure 6.12: Operational parameters during DDGS gasification-21.04.2010.

Finally, figure 6.13 presents the main parameters during gasification of all the three biomass feedstocks using untreated olivine as bed material. The purpose of the experiment is to investigate the influence of the bed material type on the concentration of tar compounds.

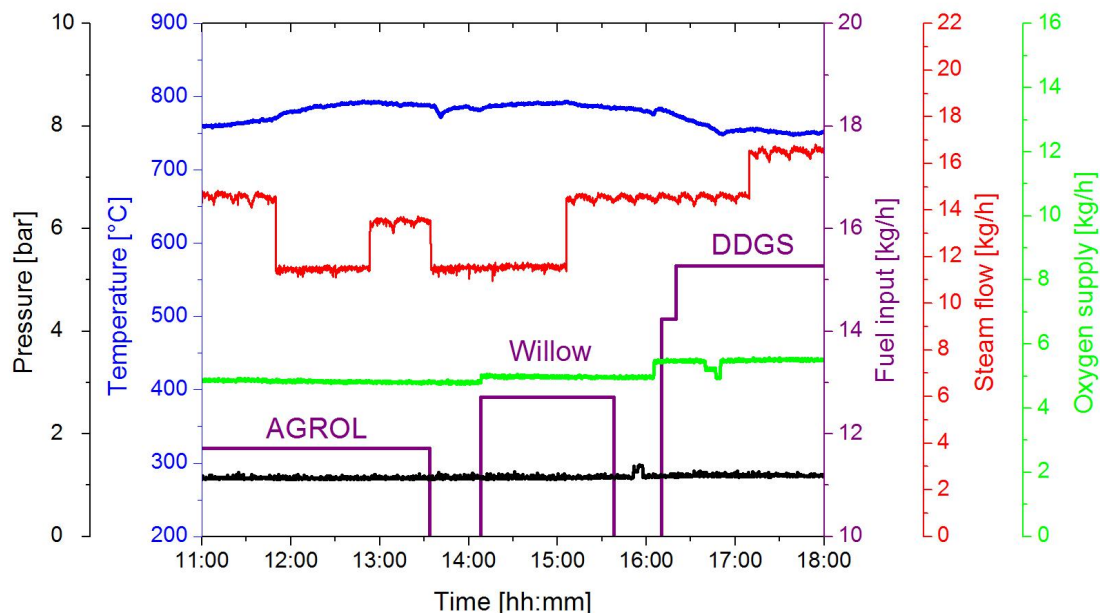


Figure 6.13: Operational parameters during gasification using untreated olivine as bed material-23.04.2010.

6.3 Online measurement of the tar content with the optical setup

The transportable optical setup gives the opportunity to qualify and quantify the tar compounds in the producer gas from biomass gasification process. The facility offers the possibility of measuring and monitoring the concentration of tar compounds online while at the same time provides information about the influence of different gasification parameters on the thermal and chemical tar cracking. The results from the two gasification test rigs are presented in the following subsections.

6.3.1 Results from TUM gasifier

An overview of the concentration of the fourteen individual tar compounds as well as the sum of measured tars for each experimental day is displayed in figures 6.14-6.17. The first four blocks of each diagram illustrate the concentration of the individual tar compounds which are representative of each tar class while the sum of measured tars is depicted in the bottom block. The term *sum of measured tars* is used in this study to represent the concentration sum of the fourteen individual tar compounds and not the overall tar content of the gasification process.

The sum of measured tars by the online optical setup is an underestimation of the overall tar content considering the fact that the optical setup is not calibrated for all of the tars but only for those which represent in a better way the tar content from the biomass gasification process. The lack of information regarding the background signal (see section 5.3), which is emitted by the tars for which the setup is not calibrated, as well as their influence and intensity percentage on this signal makes its further quantification impossible. Moreover, the influence of the heaviest, GC-undetectable tars (Class 1) on the optical emission and on the detected measurement signal does not provide the measurement of the overall tar content due to the fact that there is no information about the chemical formulas of these compounds and they are not available in the market in case of calibration of the experimental facility.

However, the optical setup can qualify and quantify the most important biomass gasification tars and can quantify in a very good way the overall tar content. An attempt to correlate the undefined background signal with another tar measurement technique (e.g. Tar protocol, SPA method, online tar analyzer, etc.) can give more details about the quantity of tars that is represented by this signal as well as a more precise value of the overall tar content.

Figure 6.14 presents the concentration of the individual tar compounds of each tar class during atmospheric and pressurized gasification of AGROL pellets as well as the sum of measured tars. Regarding Class 2, phenol has the highest concentration value while toluene and styrene contribute more to the Class 3 tar content. Naphthalene is the tar compound with the highest concentration concerning the fourth class while on the other

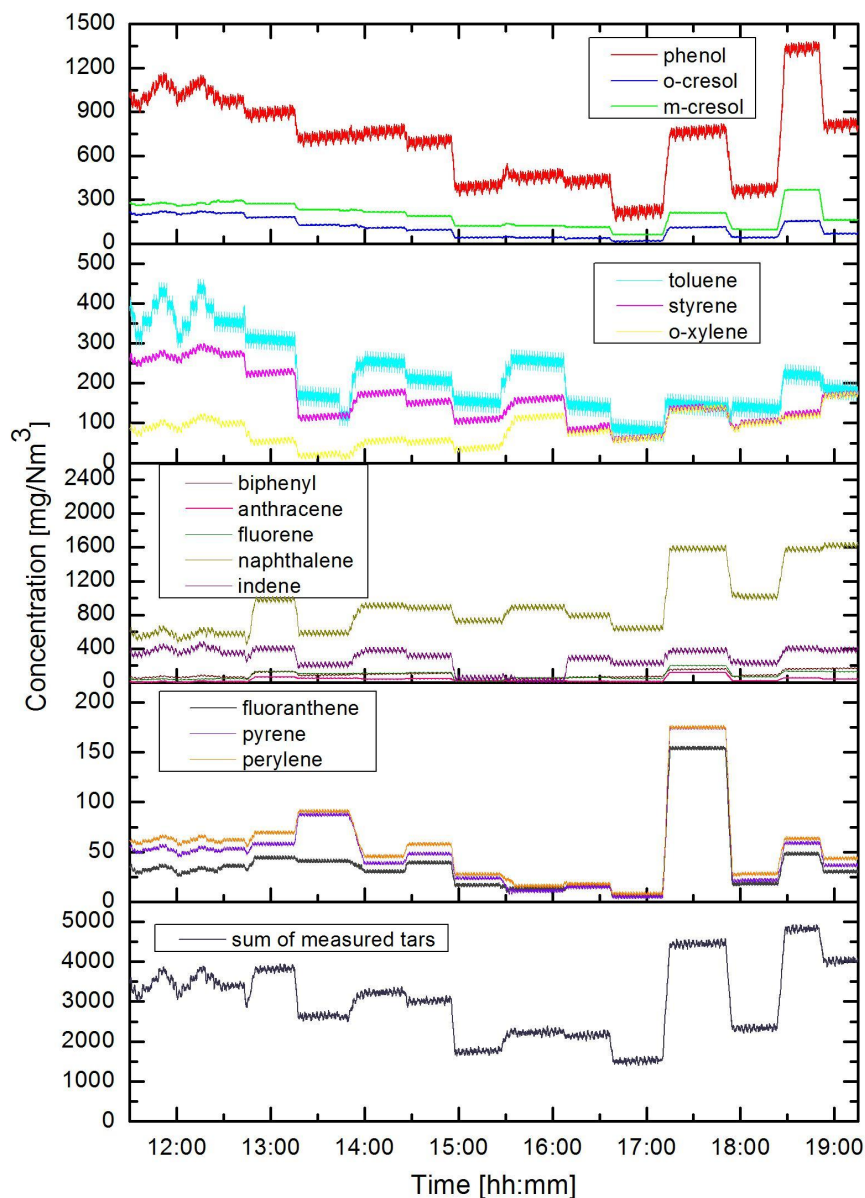


Figure 6.14: Tar composition during AGROL gasification-07.06.2010.

hand biphenyl, anthracene and fluorene have considerably low values. The concentration of Class 5 compounds is the lowest compared to the other tar classes and the one that reaches the smallest value (from 16:40 till 17:10) during the whole gasification period. The sum of measured tars ranges from $3,9 \text{ g/Nm}^3$ to $1,4 \text{ g/Nm}^3$ during atmospheric gasification while the values are higher under pressurized conditions.

Figure 6.15 illustrates the tar composition during atmospheric gasification of Willow pellets. The same aforementioned characteristics apply to the concentration values with the exception of indene, which contributes more to the Class 3 tar content than during gasification of AGROL pellets. In addition, the sum of measured tars is slightly higher than in case of atmospheric AGROL gasification.

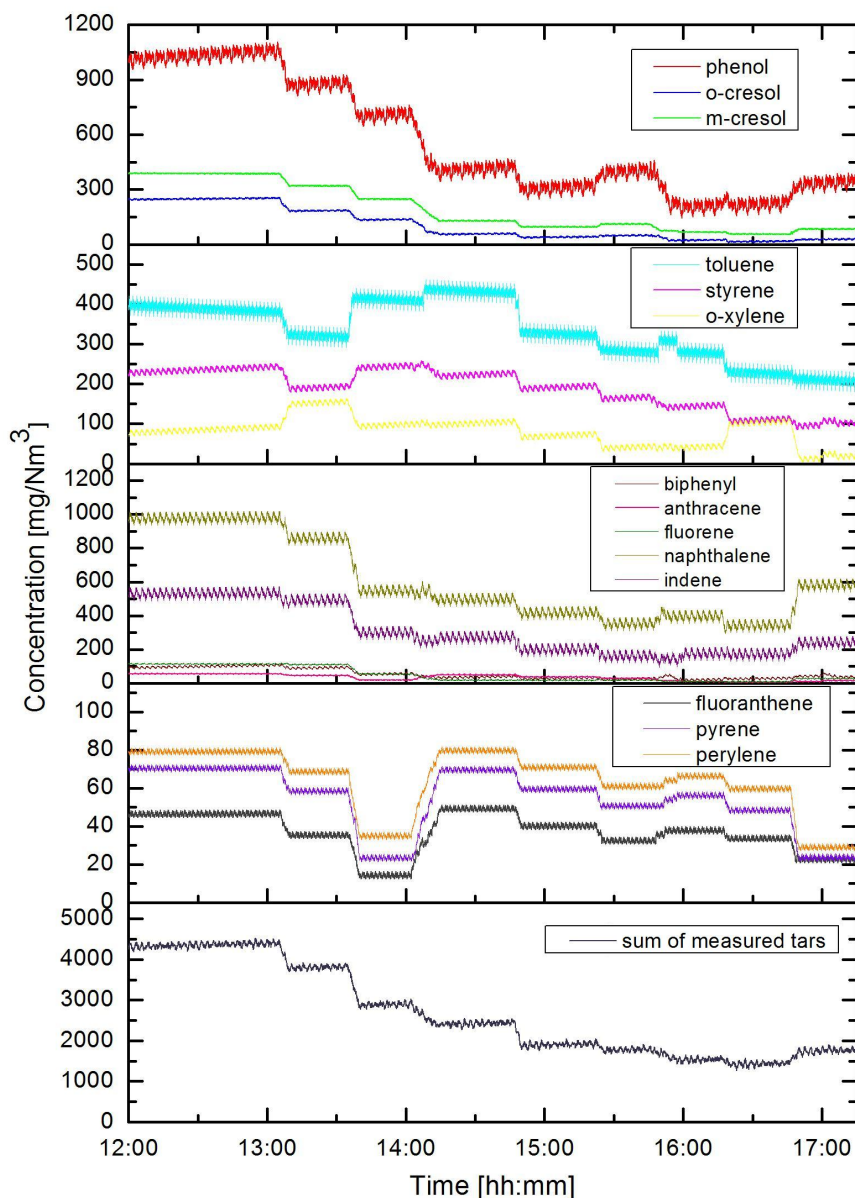


Figure 6.15: Tar composition during atmospheric Willow gasification-08.06.2010.

The concentration of the individual tar compounds of each tar class as well as the sum of measured tars during pressurized gasification using Willow as biomass feedstock are presented in figure 6.16. The vertical black lines show the time period that no fuel is filled into the reactor due to the unexpected rising of the temperature reaching the safety limit. During this time period, only gasification of the char particles takes place inside the reactor and therefore the tar concentration is chosen to be omitted as the values do not correspond to the gasification of the fuel.

The sum of measured tars is lower than in case of atmospheric gasification of Willow pellets while Class 3 and Class 4 concentration values have the greatest contribution to the reduction of this measured sum of tars.

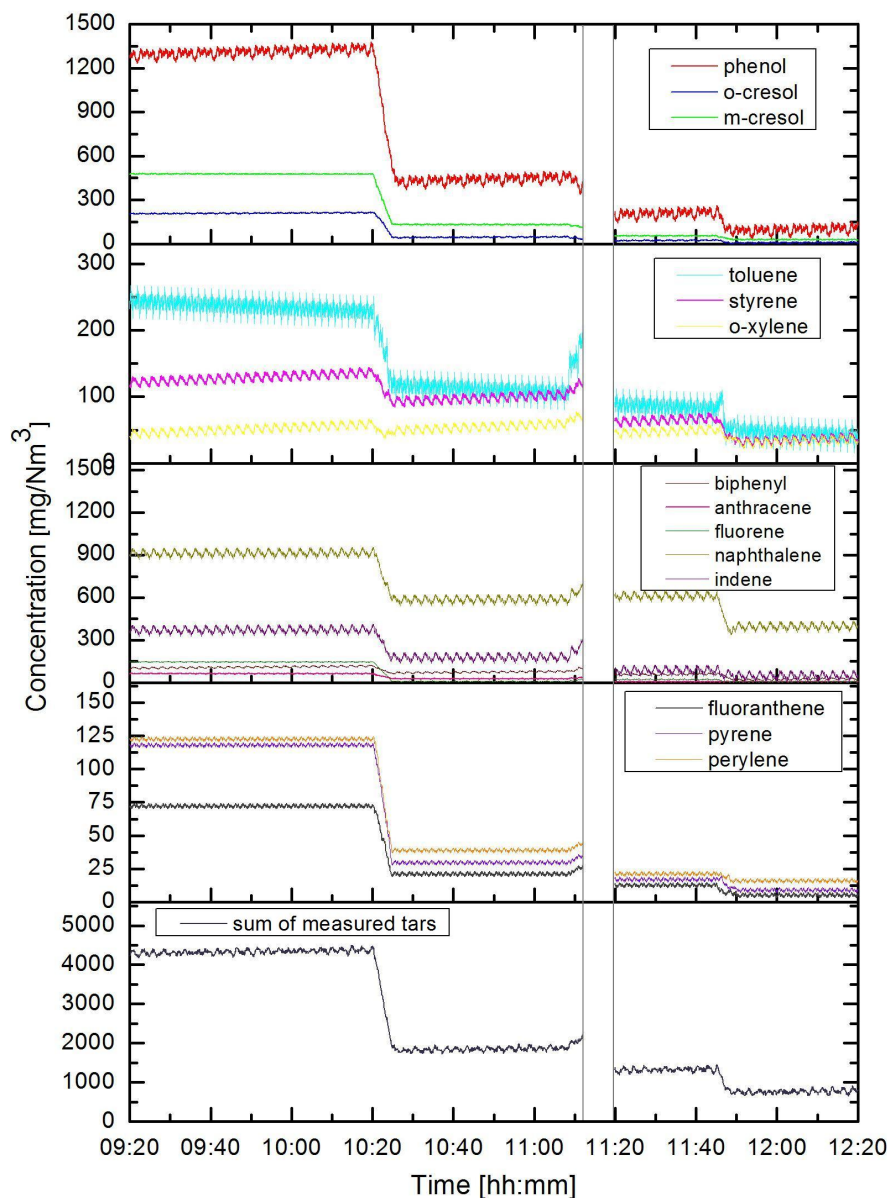


Figure 6.16: Tar composition during pressurized Willow gasification-09.06.2010.

Figure 6.17 presents the results from the atmospheric gasification of DDGS pellets. Class 2 and Class 4 tar compounds have the highest concentration values and therefore contribute more to the tar content than the other tar classes. The sum of measured tars reaches the highest values in the lower temperature range of 700 °C while it reduces as the temperature increases.

Although the sum of measured tars is not always higher than the ones from the gasification of the other two biomass feedstocks, DDGS results in the highest intensity regarding the detected emission as well as background signal of the producer gas. Therefore, the overall tar content is assumed to be the highest, despite the fact that DDGS gasification does not result in the highest sum of measured tars compared to the other two fuels.

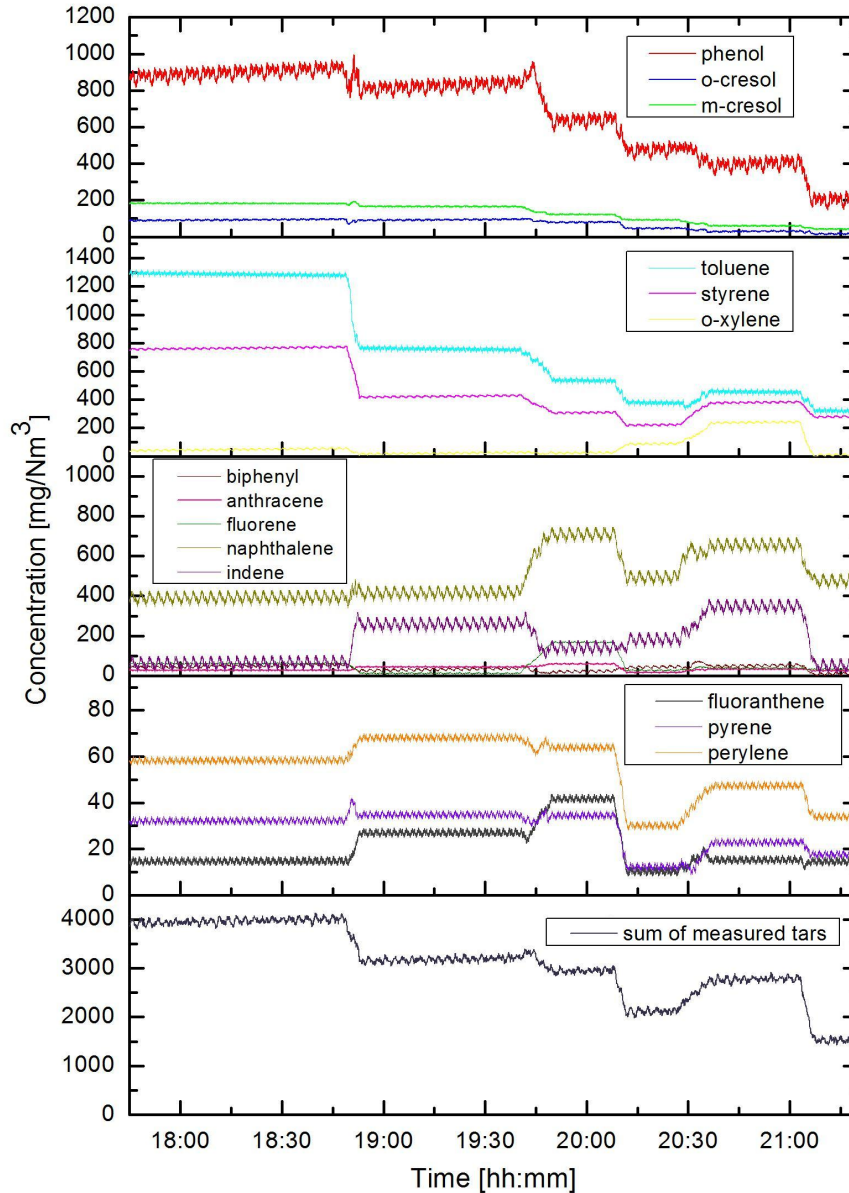


Figure 6.17: Tar composition during DDGS gasification-09.06.2010.

6.3.2 Results from TUD gasifier

An overview of the concentration of tar compounds for the five experimental days is displayed in the following figures 6.18-6.22. As in the results from the TUM gasification test rig, each diagram illustrates the concentration of the individual tar compounds in the first four blocks while the bottom block presents the sum of measured tars.

Figure 6.18 presents the results during the first day of AGROL gasification (13.04.2010). Phenol concentration is considerably higher than o-cresol and m-cresol, regarding the Class 2 tar compounds while o-xylene has the lowest concentration value among the tar compounds of the third class, which is controlled by the values of toluene and styrene. Naphthalene and indene contribute more to the concentration of the fourth class than

the other three compounds (fluorene, anthracene and biphenyl) while the Class 5 tar compounds reach the highest values (perylene reaches approximately 290 mg/Nm^3) for the temperature of $770 \text{ }^\circ\text{C}$ than in all other experimental days.

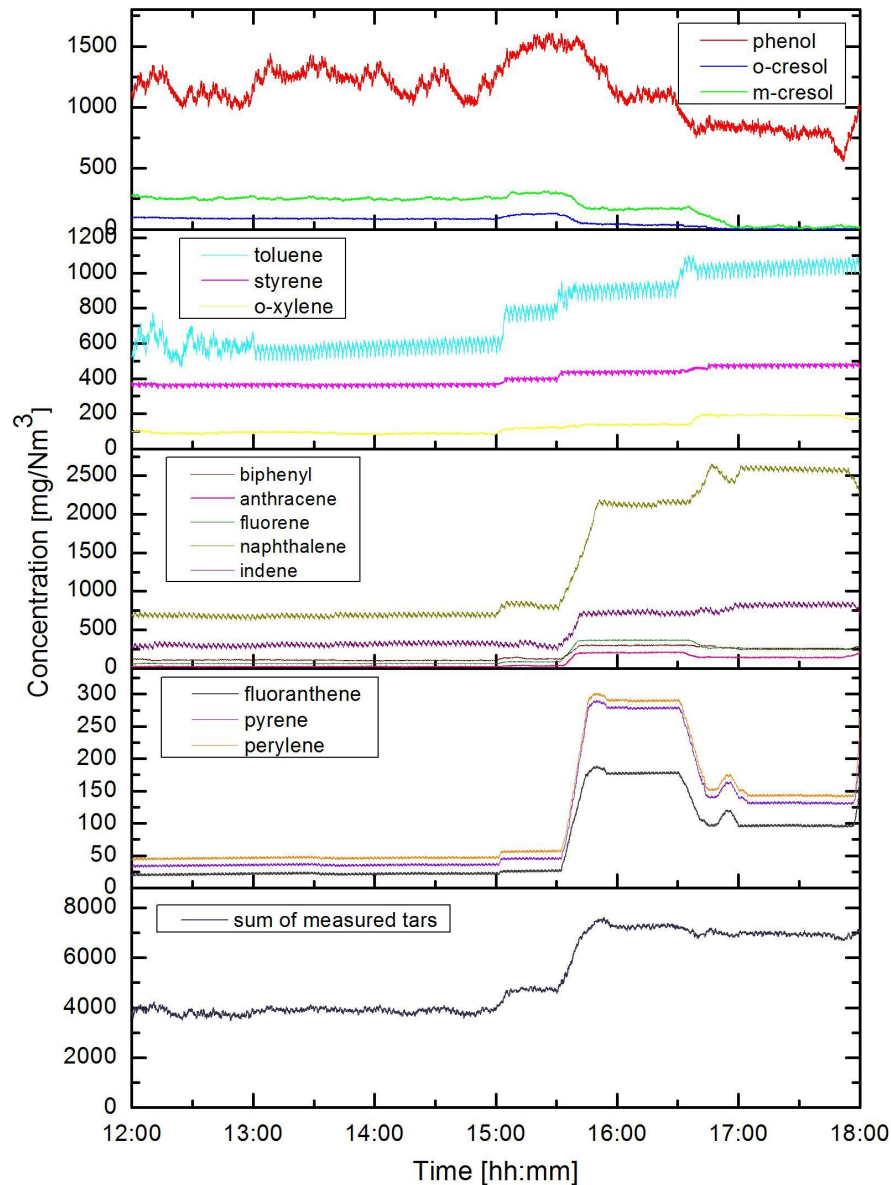


Figure 6.18: Tar composition during AGROL gasification-13.04.2010.

The same characteristics apply to the results from the second day of AGROL gasification (15.04.2010), which are depicted in figure 6.19. Styrene contributes more to the concentration of the second class of tar compounds than during the first AGROL gasification day while the compounds of the fourth class do not reach such high values as in the first experimental day. Regarding the sum of measured tars, the concentration values are almost at the same level (considering the same temperature range) during both days where AGROL is used as biomass feedstock.

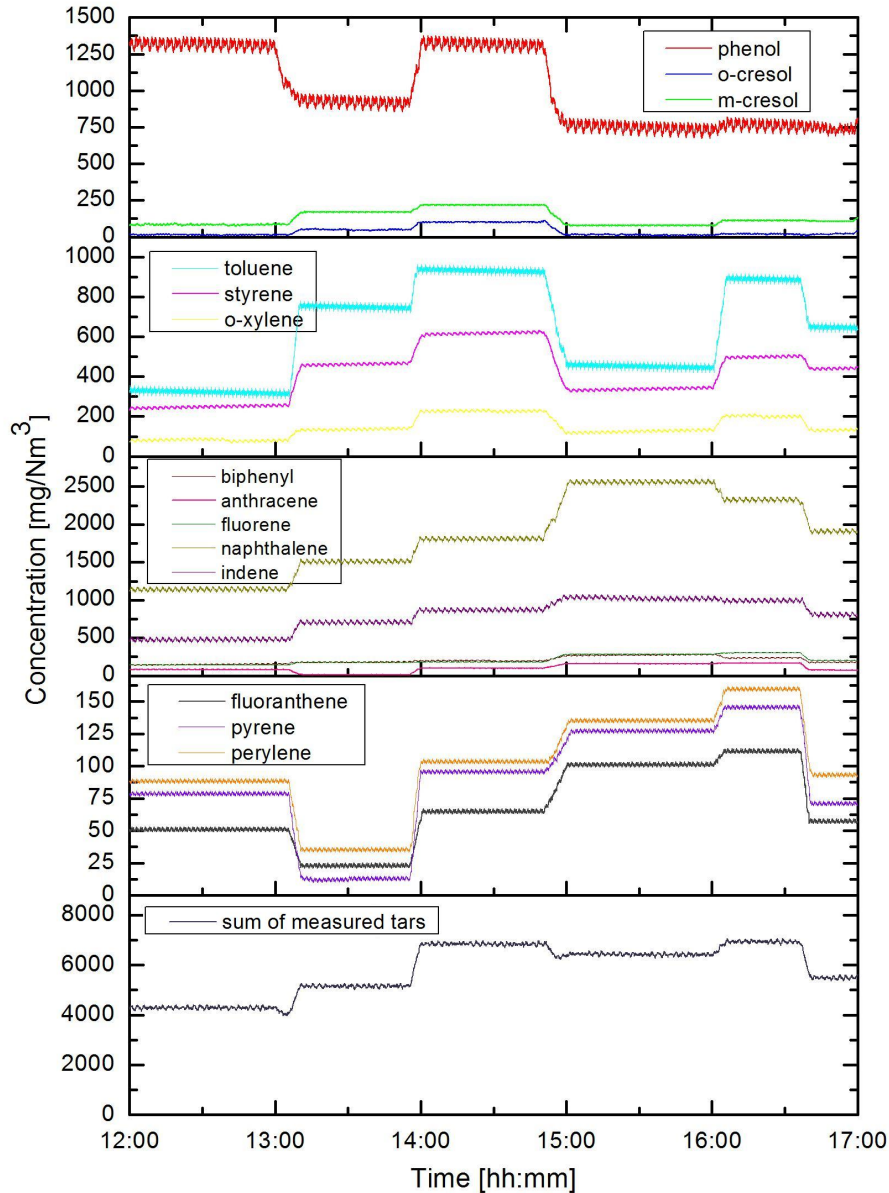


Figure 6.19: Tar composition during AGROL gasification-15.04.2010.

Figure 6.20 illustrates the results for the tar composition during Willow gasification. Phenol contributes more than the other two compounds to the concentration of the second class in the low temperature ranges while in higher temperatures, its contribution becomes less. Regarding the Class 3 tar compounds, styrene appears to have almost the same contribution to the concentration values of the third class for some temperature ranges while in some cases, for the time period when high steam to biomass ratios are tested (see figure 6.11), its contribution becomes greater than this of toluene. This tendency is not detected in all of the previous experimental results. Regarding the compounds of the fourth and fifth tar class, the comments made in the previous diagrams can be applied here as well.

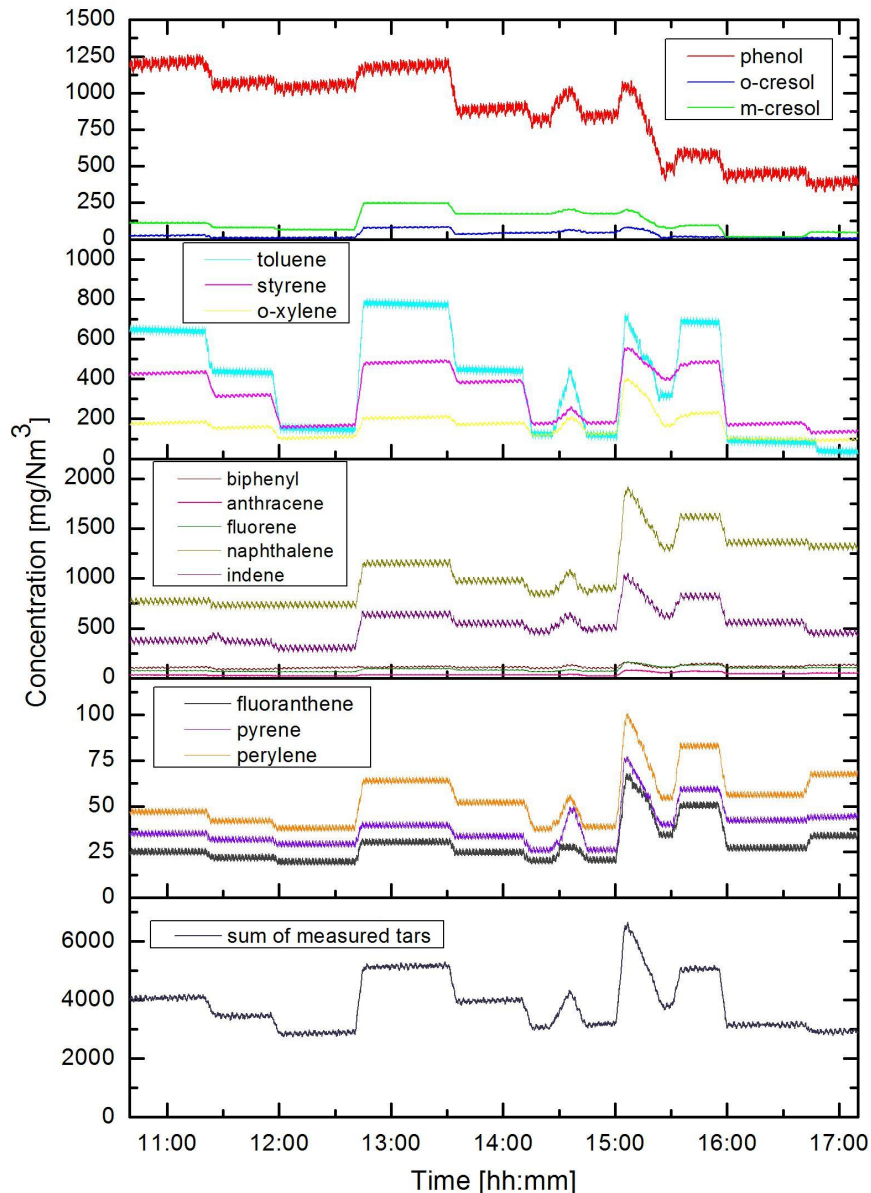


Figure 6.20: Tar composition during Willow gasification-19.04.2010.

The following figure 6.21 presents the tar composition during gasification of DDGS pellets. The contribution of o-cresol and m-cresol to the tar content of the second class is considerably lower compared to phenol during the whole experiment. Regarding the third and fourth class tar compounds, the same tendencies can be observed as in the previous experimental results. The tendency that is different from all the previous diagrams concerns the Class 5 tar compounds. Perylene has the greatest contribution to the tar content of the fifth class while the concentration value of perylene is twice as high compared to the other two compounds (pyrene and fluoranthene).

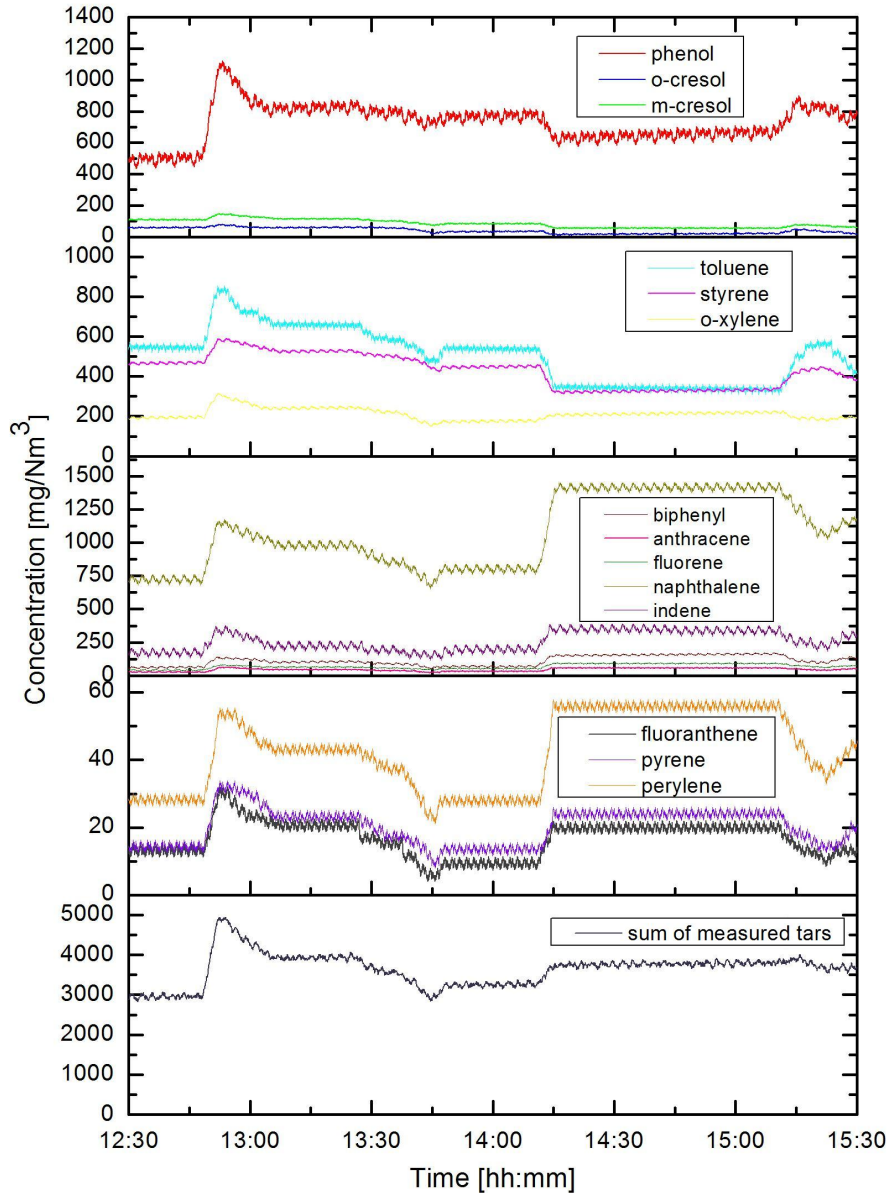


Figure 6.21: Tar composition during DDGS gasification-21.04.2010.

Finally, figure 6.22 depicts the concentration of individual tar compounds as well as the value of the sum of measured tars during gasification of all the three biomass feedstocks using untreated olivine as bed material. The two blank areas (13:35-14:10 and 15:35-16:10) which are denoted by the vertical black lines show the time period applied for the switching to the next fuel. During this period, a mixture of the previous and the next used fuel is fed into the reactor till the fuel is gradually replaced by the next one to be used. Therefore the tar concentration is chosen to be omitted as the values do not correspond to the gasification of a unique biomass feedstock.

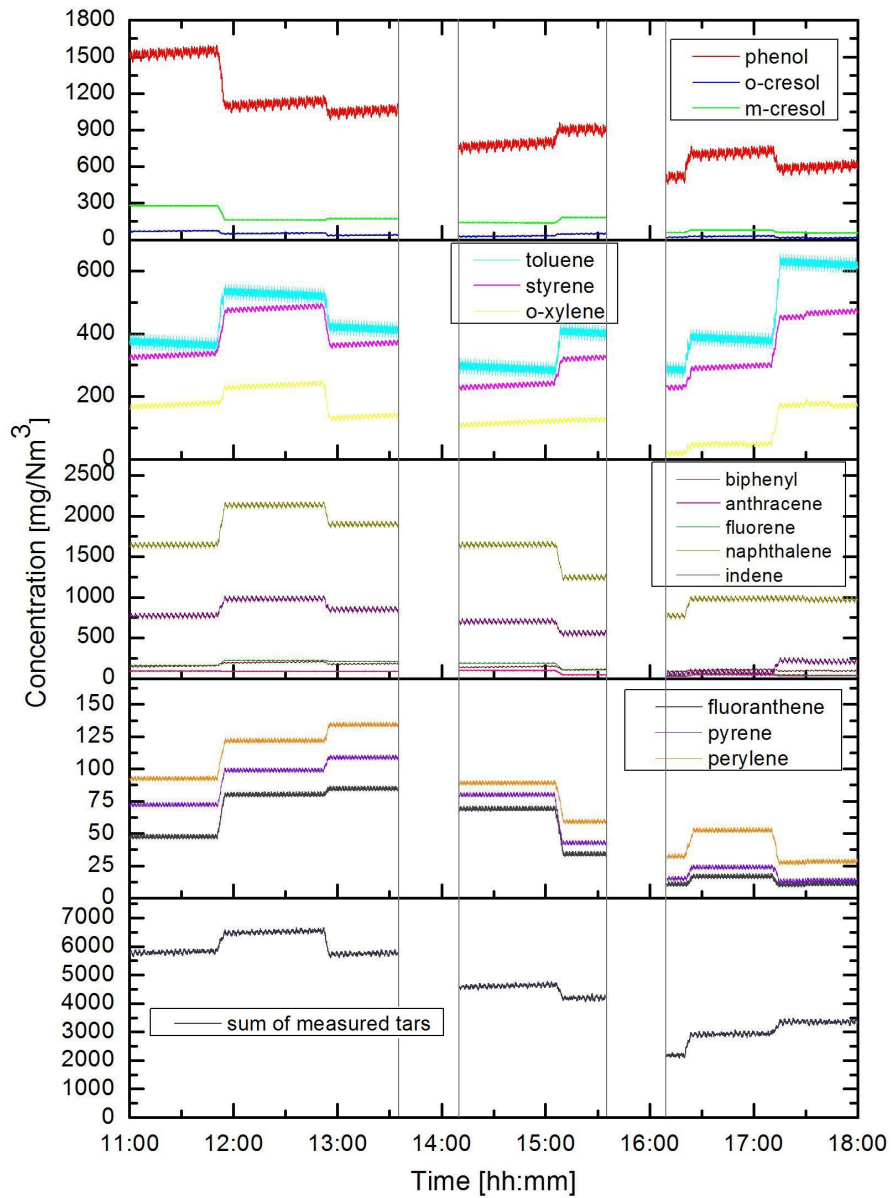


Figure 6.22: Tar composition during gasification using untreated olivine as bed material-23.04.2010.

7 Evaluation of the experimental results

7.1 Evaluation of the optical results

Except for the online measurement of the concentration of tar compounds with the help of the transportable optical setup, parallel measurement techniques are applied as well. The online tar analyzer TA 120-3 from the company Ratfisch Analysensysteme GmbH is used to monitor the overall tar content in the gasification process while samples are also taken with a syringe coupled to an SPE amino (NH_2) disposable extraction column and are analyzed by means of gas chromatography after elution of the sample (SPA method).

The results from the above two measurement techniques are presented in the following subsections. In addition, a comparison between the results from the optical and the other two applied measurement techniques is given in order to validate the optical method and test its accuracy.

7.1.1 Results from parallel measurement techniques

Solid Phase Adsorption (SPA)

The results from the SPA method during the experimental campaign at the atmospheric steam-oxygen blown circulating fluidized bed gasifier of the Delft University of Technology (TUD) are presented in figures 7.1-7.5.

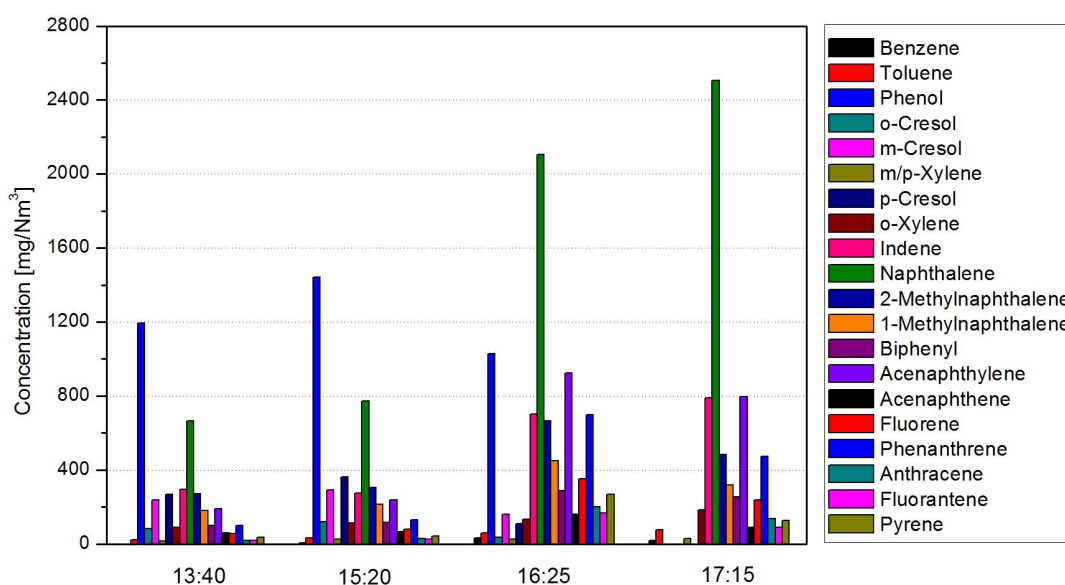


Figure 7.1: SPA analysis during AGROL gasification-13.04.2010.

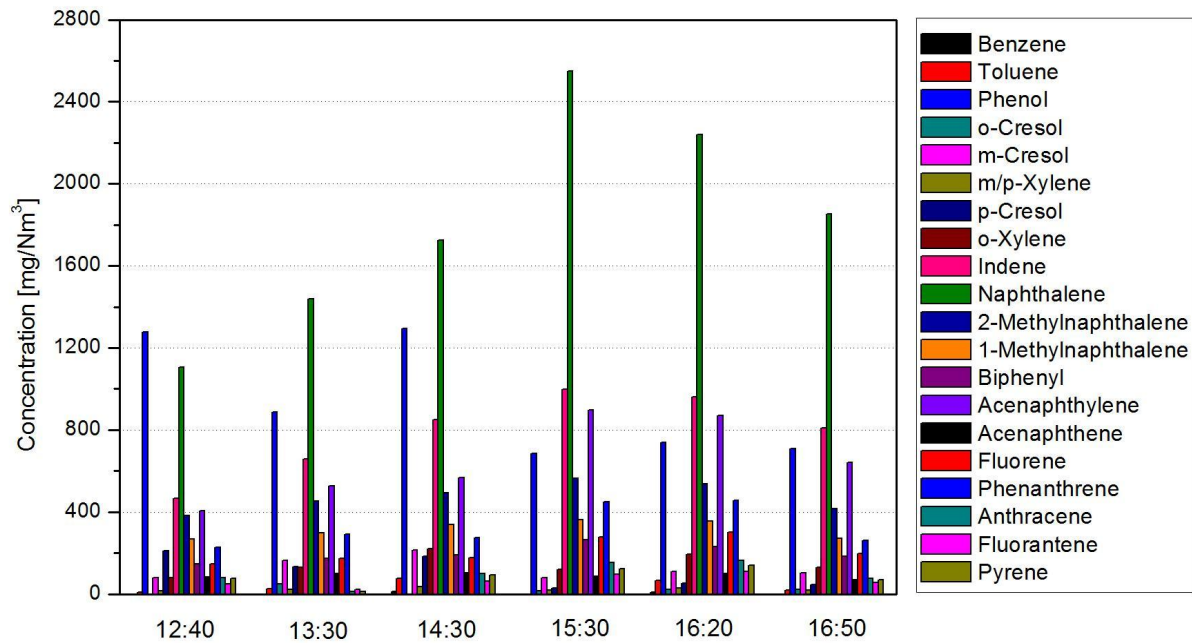


Figure 7.2: SPA analysis during AGROL gasification-15.04.2010.

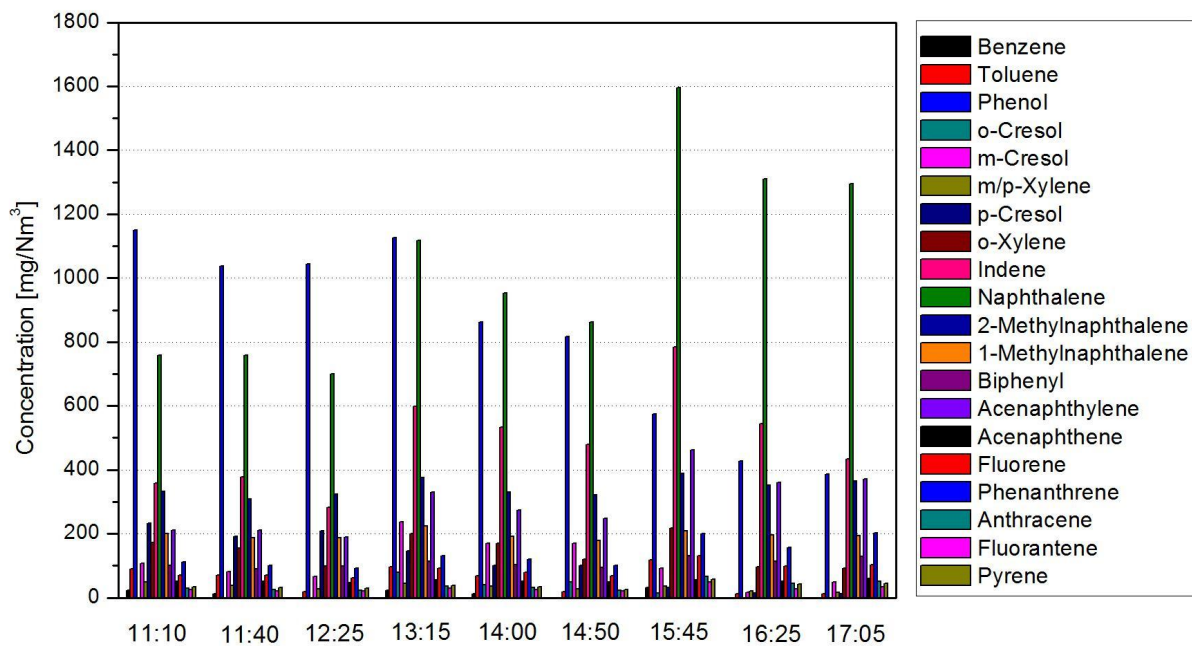


Figure 7.3: SPA analysis during Willow gasification-19.04.2010.

As it can be seen, the tar concentration is measured in large time intervals due to the fact that the samples are taken when the producer gas composition reaches steady values, after the gasification parameters are changed. Regarding AGROL and Willow gasification, four, six and nine different sampling time-points are chosen during each experimental day respectively in relation to the changes in the gasification parameters.

Due to the agglomeration problems during DDGS gasification, only few parameters are tested (two sampling time-points) while during gasification using untreated olivine as bed material, seven SPA samples are taken.

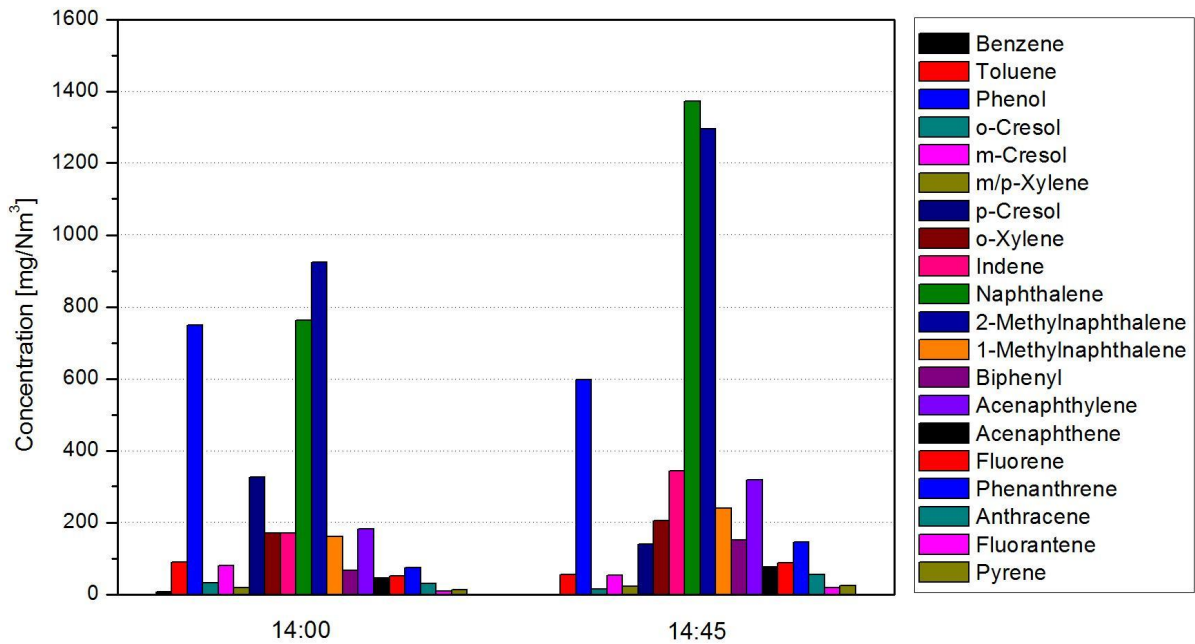


Figure 7.4: SPA analysis during DDGS gasification-21.04.2010.

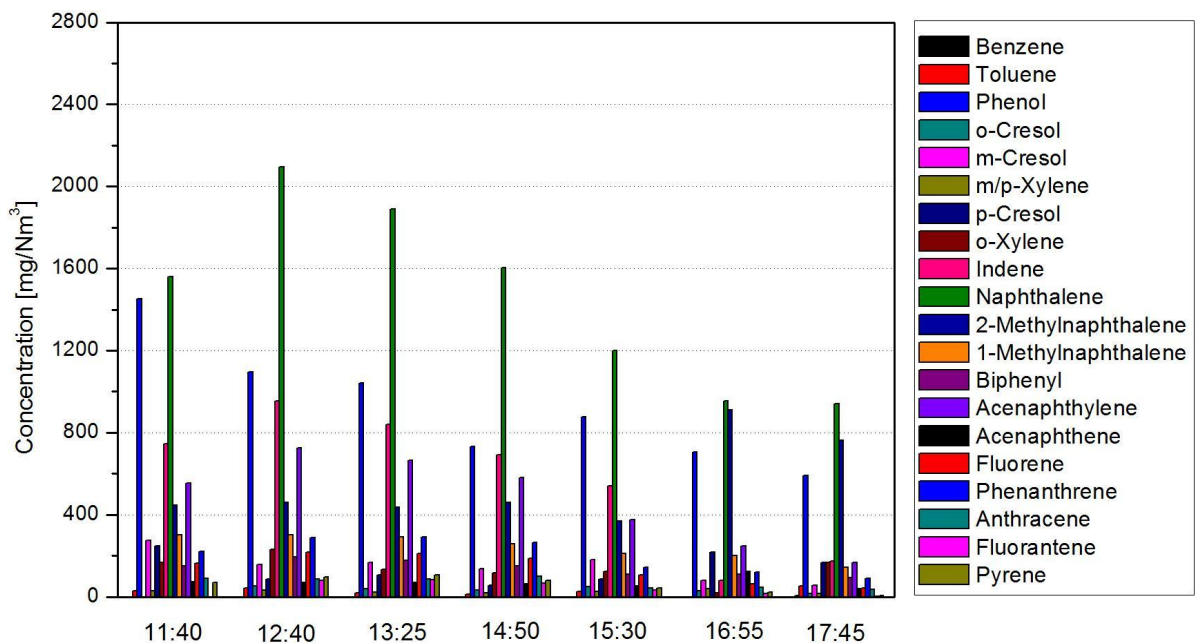


Figure 7.5: SPA analysis during gasification using untreated olivine as bed material-23.04.2010.

The results from the SPA method during the experimental campaign in BioHPR are presented in figures 7.6-7.10. Regarding atmospheric gasification of AGROL and Willow pellets (see figure 7.6 and 7.8), nine different sampling time-points are chosen for each gasification parameter tested.

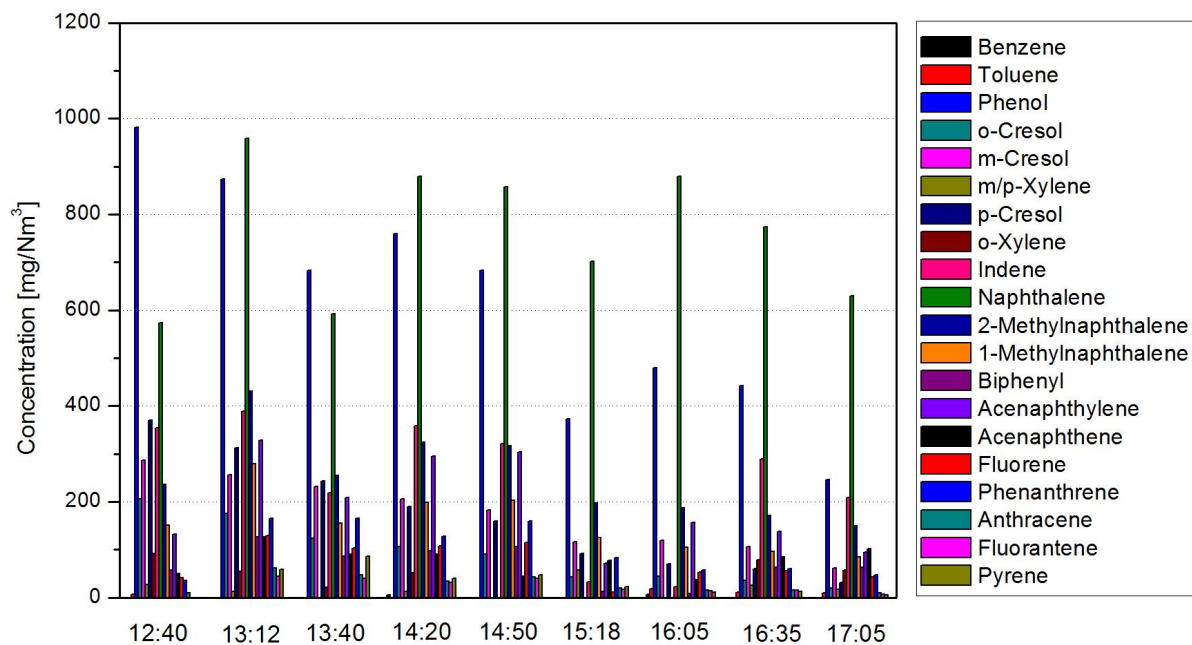


Figure 7.6: SPA analysis during atmospheric AGROL gasification-07.06.2010.

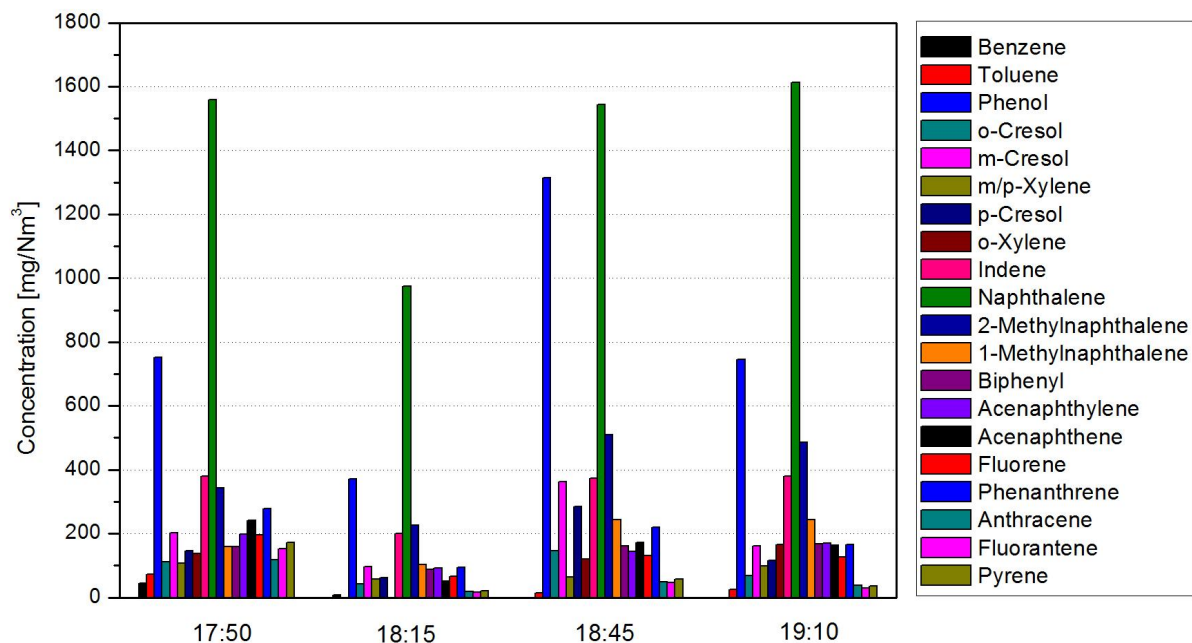


Figure 7.7: SPA analysis during pressurized AGROL gasification-07.06.2010.

In case of pressurized gasification of the two aforementioned fuels (see figure 7.7 and 7.9), four different sampling time-points are chosen due to the fact that fewer parameters are tested under pressurized conditions. Finally, during DDGS gasification six SPA samples are taken.

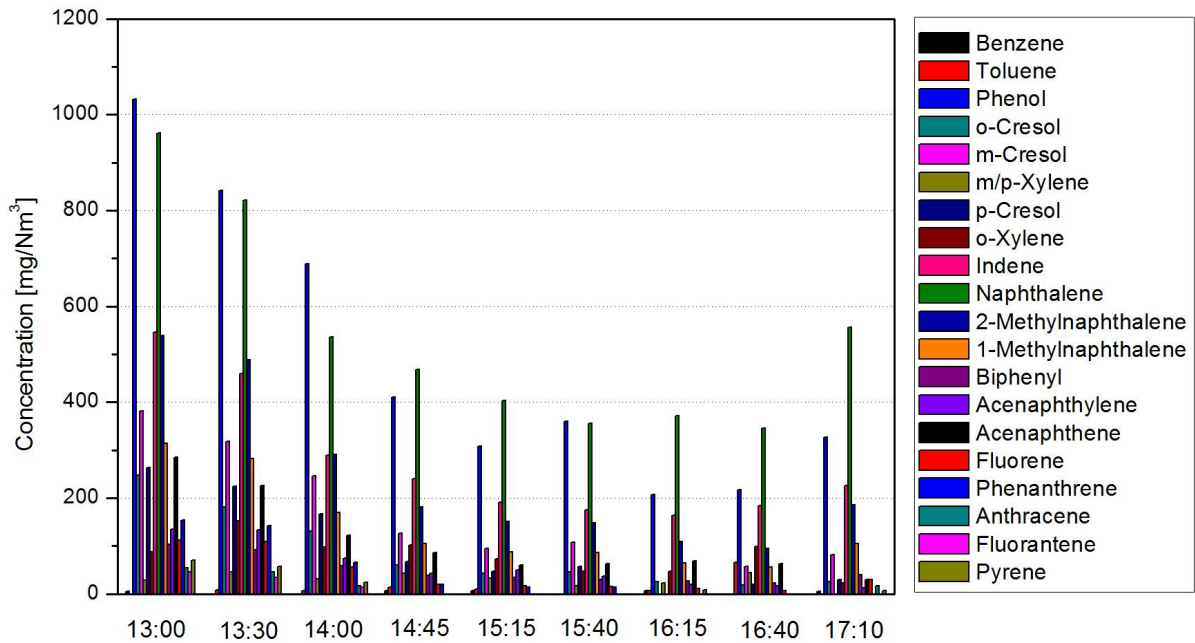


Figure 7.8: SPA analysis during atmospheric Willow gasification-08.06.2010.

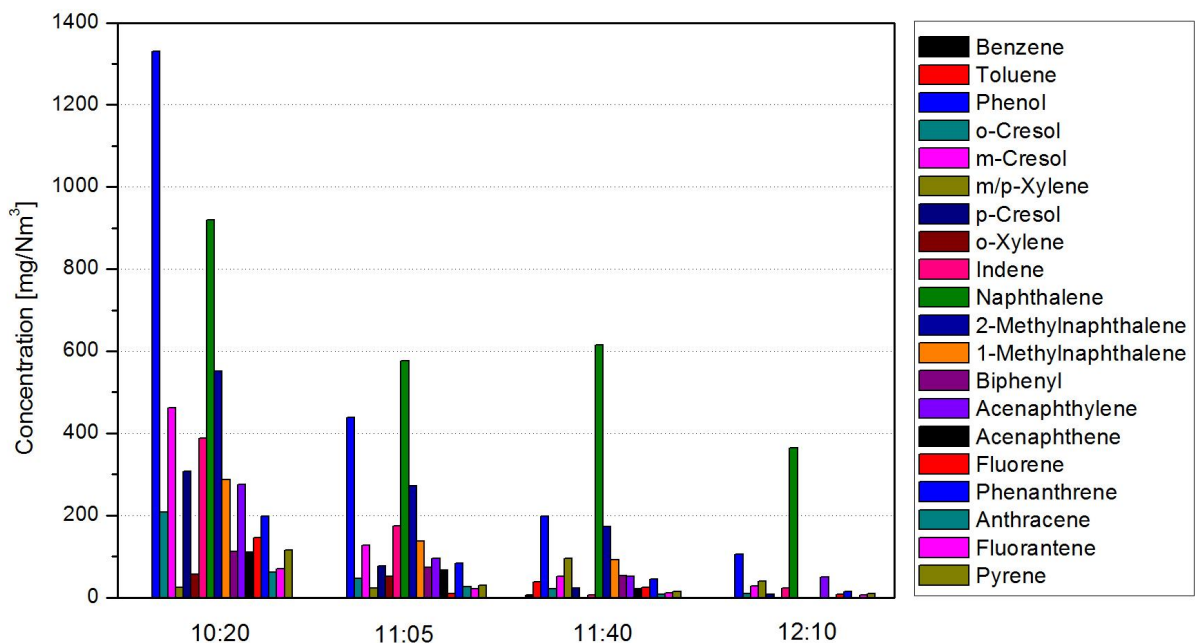


Figure 7.9: SPA analysis during pressurized Willow gasification-09.06.2010.

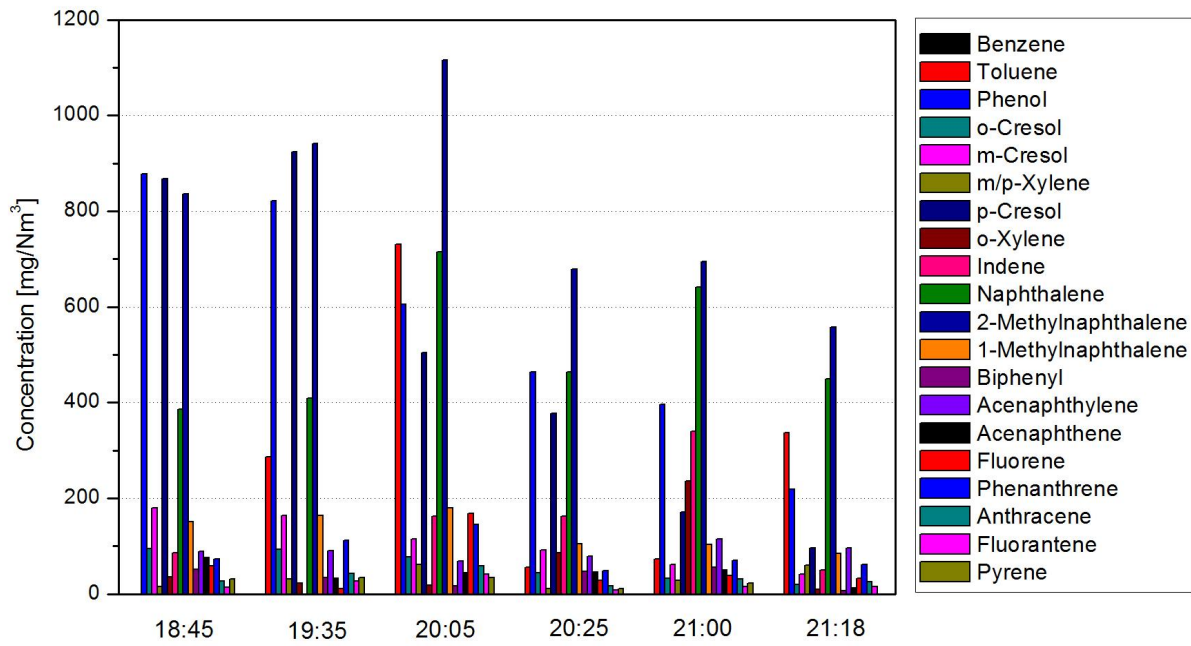


Figure 7.10: SPA analysis during DDGS gasification-09.06.2010.

Online tar analyzer

The online tar analyzer is used to monitor the overall tar content from the two gasifiers. Figures 7.11-7.14 present the overall tar content for each biomass fuel from the experiments at BioHPR.

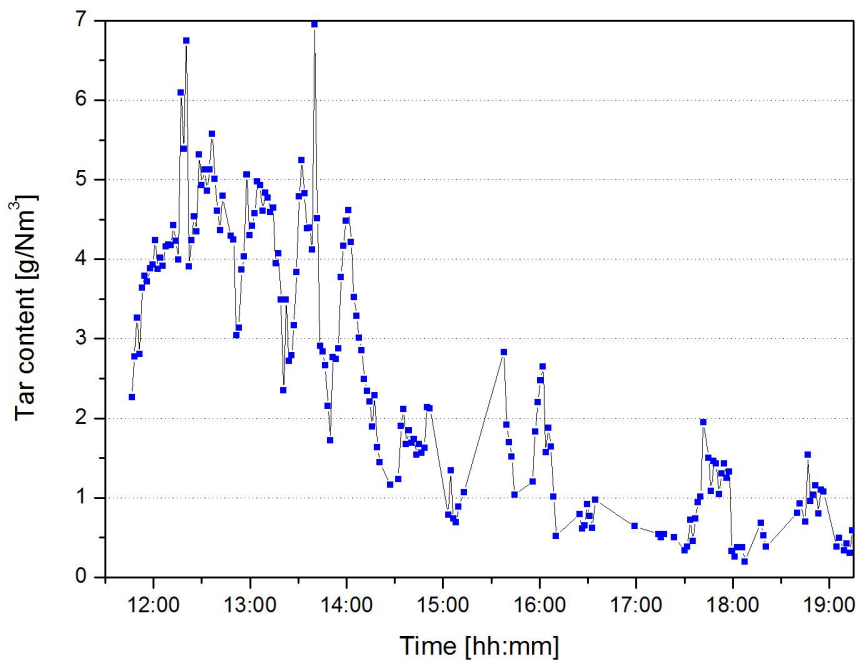


Figure 7.11: Online tar analyzer results during AGROL gasification-07.06.2010.

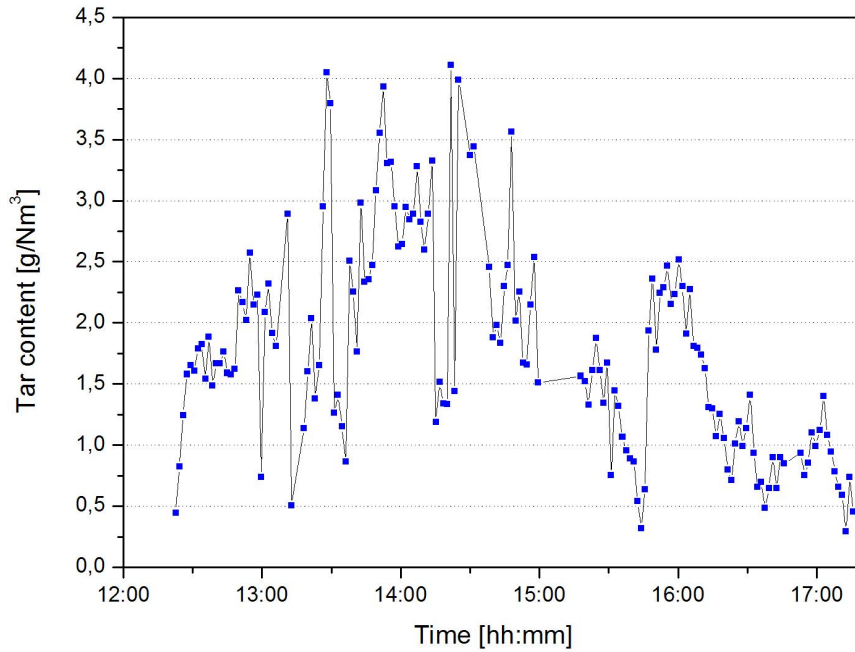


Figure 7.12: Online tar analyzer results during atmospheric Willow gasification-08.06.2010.

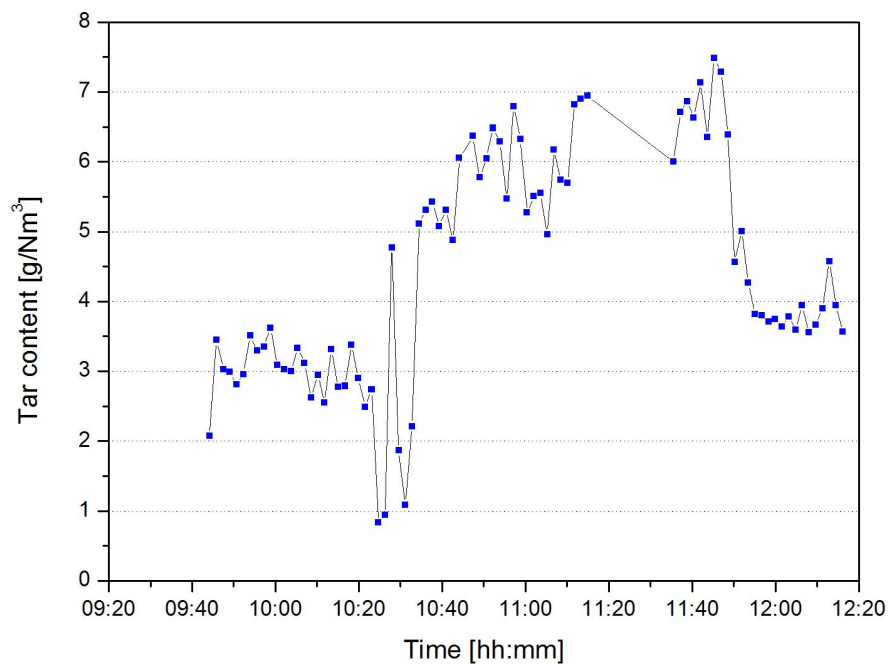


Figure 7.13: Online tar analyzer results during pressurized Willow gasification-09.06.2010.

Compared to the SPA method, the online tar analyzer measures the tar concentration approximately every 3 minutes. Therefore, due to its online way, it is considered to be a better measurement technique for validating the sum of measured tars measured with the optical setup.

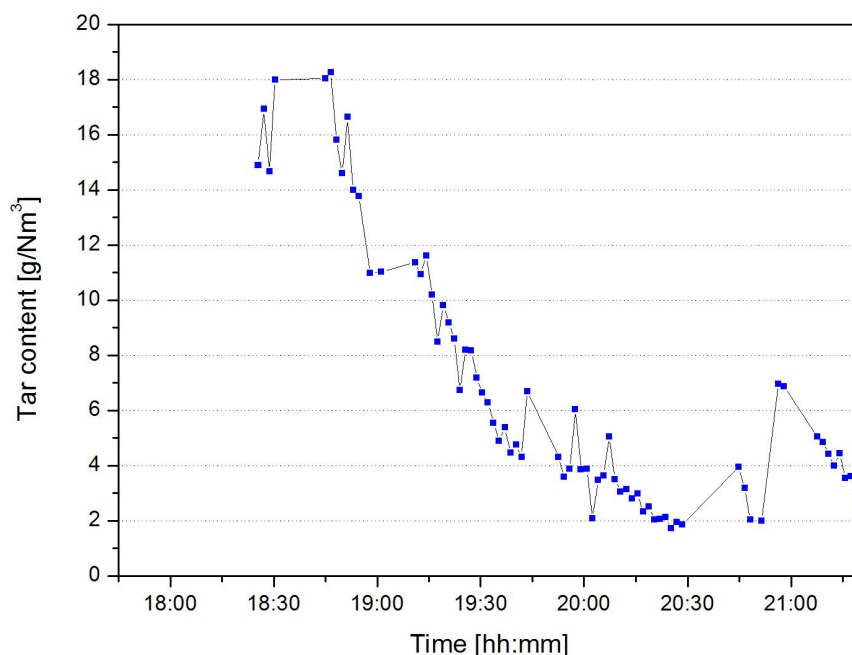


Figure 7.14: Online tar analyzer results during DDGS gasification-09.06.2010.

Due to some problems with the calibration of the device, after the first two gasification hours during the measurements in the CFB facility of the TUD, the online tar analyzer could not define the tar content in a correct way and therefore it was not used for the further analysis of the tar concentration. Regarding the measurements in the pressurized bubbling fluidized bed reactor at TUM, the device is recalibrated and is successfully applied for determining the tar content during the whole series of experiments.

7.1.2 Comparison between optical and parallel measurement techniques

A comparison between the results obtained from the optical setup and the two parallel measurement techniques can be seen in figures 7.15-7.20. Figures 7.15 and 7.16 illustrate the results from the optical setup versus the SPA measurements during the experiments at the TUD gasification test rig while figures 7.17 and 7.18 depict the difference between the optical and the SPA results at the TUM gasifier. Except for styrene and perylene, which are not measured by the SPA method, the optical results for each tar compound are compared with the SPA measurements.

Regarding the results from the experiments at the TUD gasification facility, the tendency of the optical setup is to measure always higher concentrations than the actual ones as it can be observed from all the results. As it can be seen from the error tabs, which are depicted in both figures 7.15 and 7.16, the difference between the concentration of each hydrocarbon from the two measurement techniques does not extend the value of 10%.

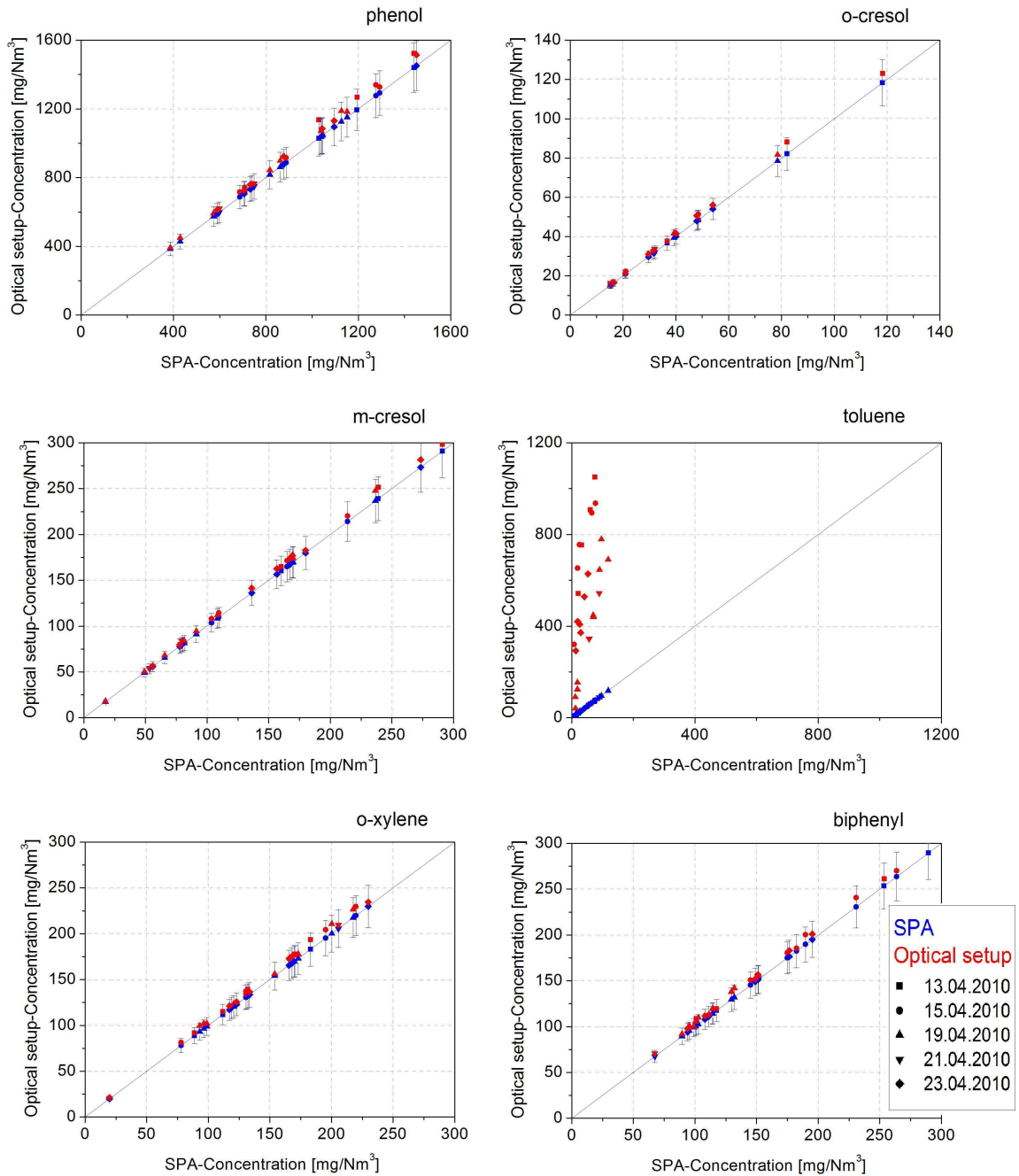


Figure 7.15: Comparison between optical measurements and SPA results from the TUD gasification test rig.

Except for toluene, all the concentration values for the other hydrocarbons show a good match with an average relative error range of 3-7 %. The reason for the large difference between the results of toluene is probably the fact that the SPA samples are not analyzed directly after the sampling but after a period of more than two weeks. Due to the low boiling point of toluene, the aforementioned delay has led to the evaporation of the largest part of this tar compound, which has resulted in inaccurate measurement values.

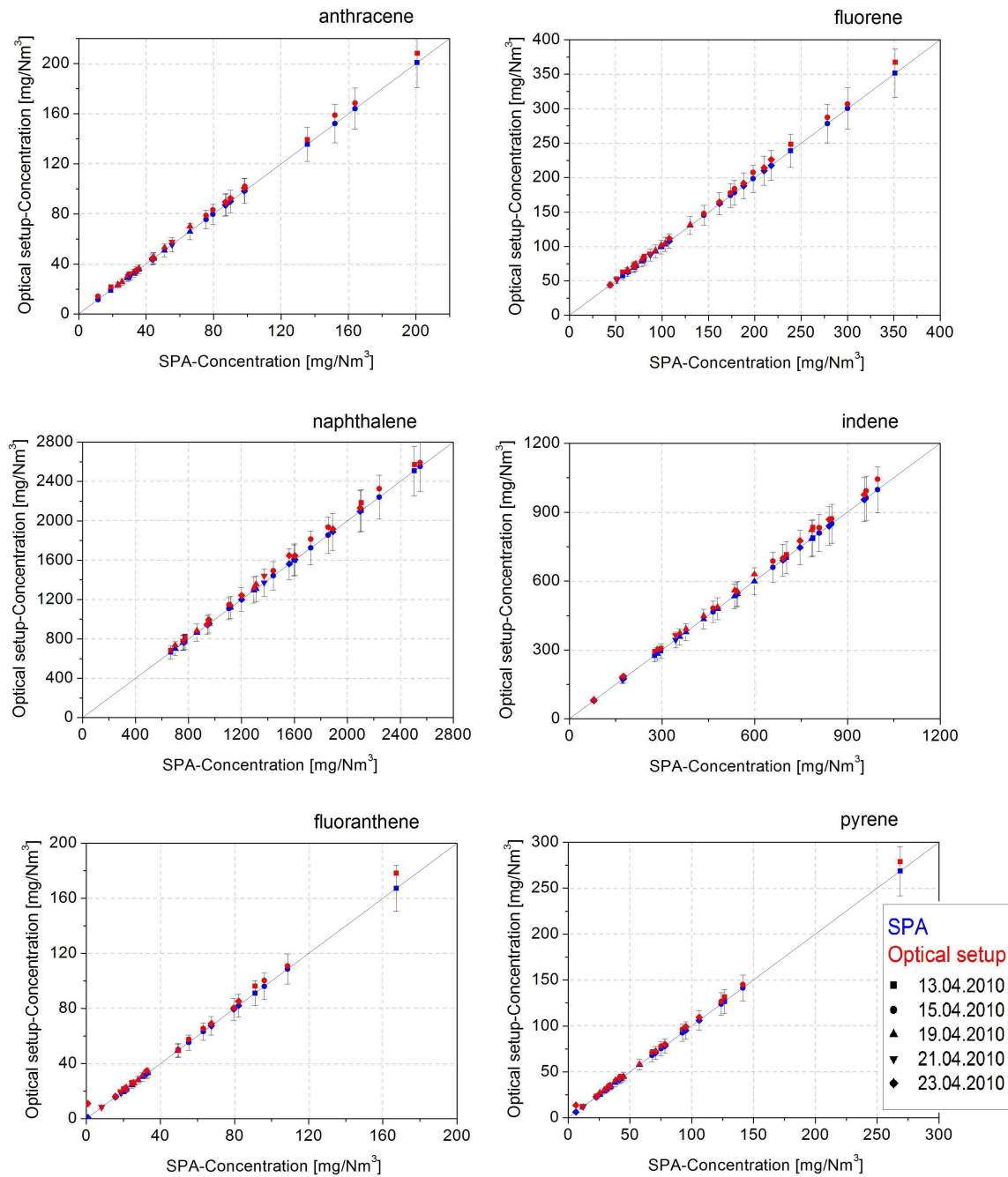


Figure 7.16: Comparison between optical measurements and SPA results from the TUD gasification test rig.

The same tendency as in the case of the TUD gasification facility appears to the results from the TUM gasifier. The optical setup measures always higher concentrations than the ones measured with the SPA method. Only in one time period during DDGS gasification (09.06.2010), toluene's concentration is lower than the SPA value. In general, the concentration values for all hydrocarbons except for toluene show a good match with an average relative error range of 3-8 %.

In a few cases, like for example the concentration values of Class 3 and Class 4 tar compounds and especially of *o*-xylene and biphenyl respectively, the relative error is higher than 10%, but generally it is always lower. The same fact appears during the measurements at the TUD gasification test rig. In two cases where extremely low concentrations need to be measured, such as in the case of fluoranthene and pyrene (see figure 7.16), the error exceeds the value of 10%.

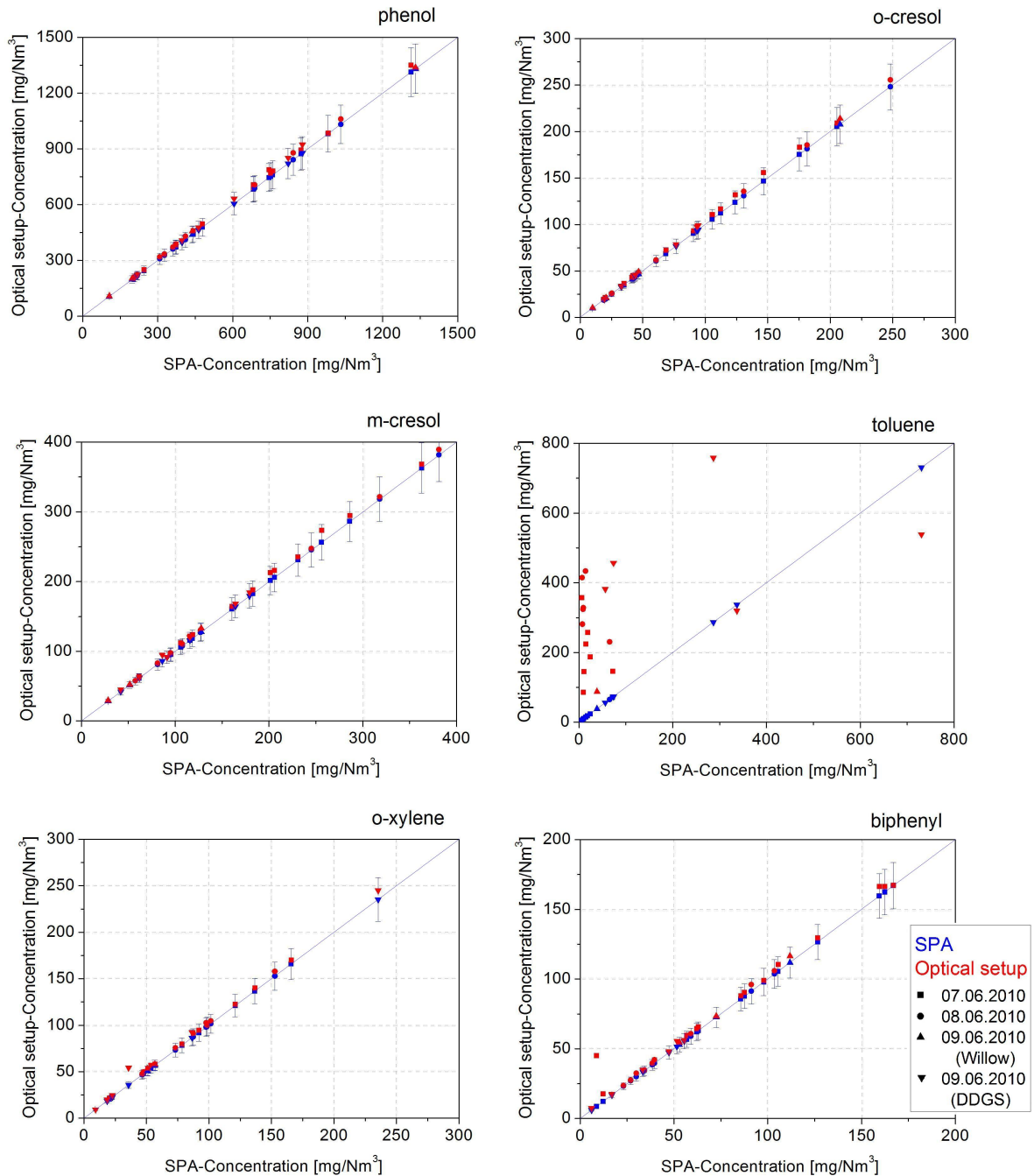


Figure 7.17: Comparison between optical measurements and SPA results from the TUM gasification test rig.

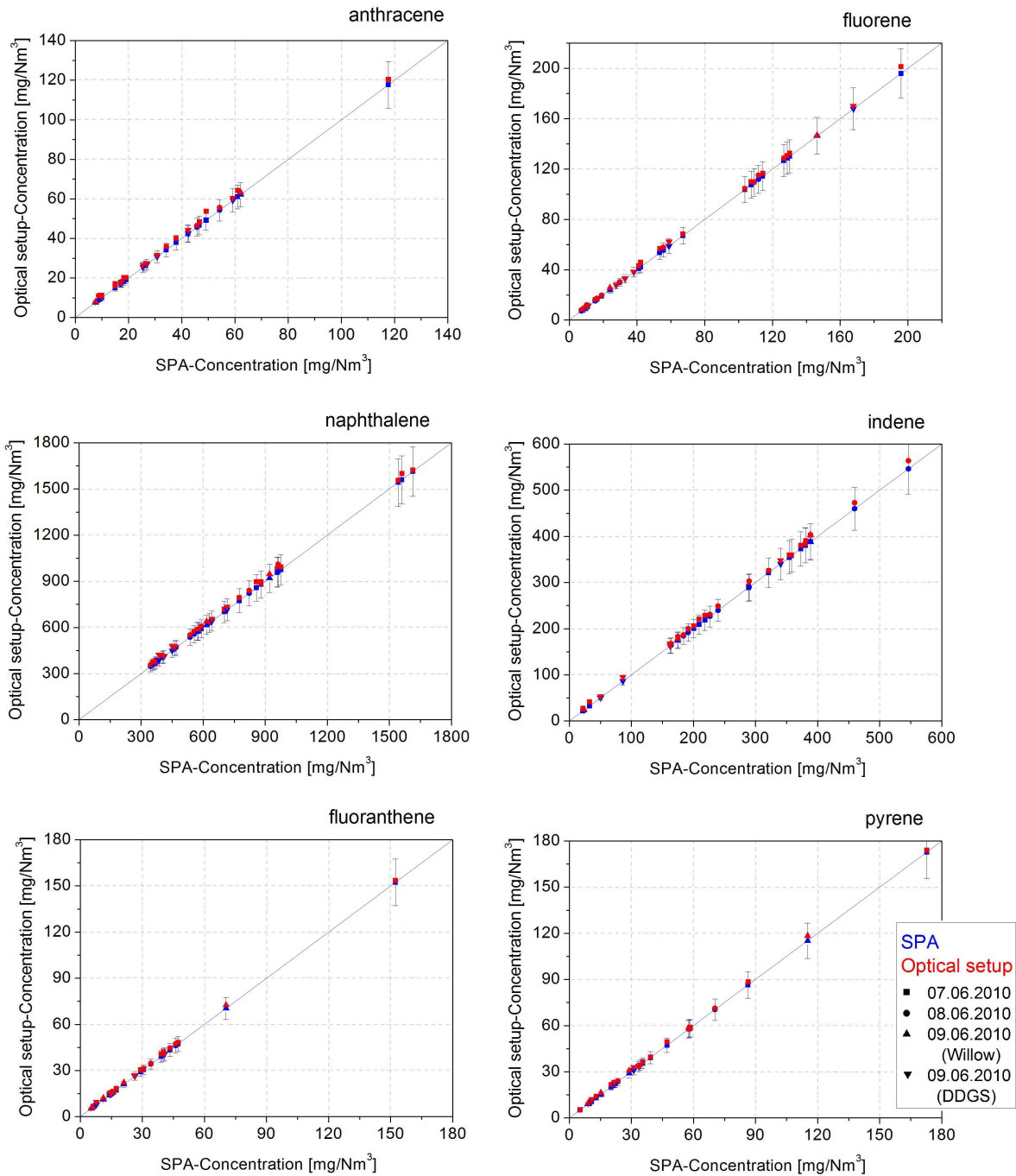


Figure 7.18: Comparison between optical measurements and SPA results from the TUM gasification test rig.

Figure 7.19 illustrates the difference between the results in the concentration sum from the optical setup and the SPA measurements during the experiments at both gasification facilities. Figures 7.19a depict the difference between the concentration sum of 12 tar compounds (except for styrene and perylene), which are measured by both optical setup and SPA method while figures 7.19b present the concentration difference between the sum

of all compounds measured by the optical setup (14 tar compounds) and SPA method (20 tar compounds).

In case of the sum of 12 tar compounds, the optical setup measures always higher concentrations than the SPA method. This is also depicted in the comparison for each individual tar compound. The error exceeds the value of 10% due to the large difference in toluene's concentration. In case of all measured tars, the optical setup gives always lower concentration values due to the fact that the optical setup can measure fourteen compounds while the SPA method twenty. In some cases (08.06.2010), the concentration sum from the optical setup is higher than the one from the SPA method due to the fact that toluene's concentration is higher than the concentration of the eight compounds that are not measured by the optical setup, resulting in a higher concentration sum.

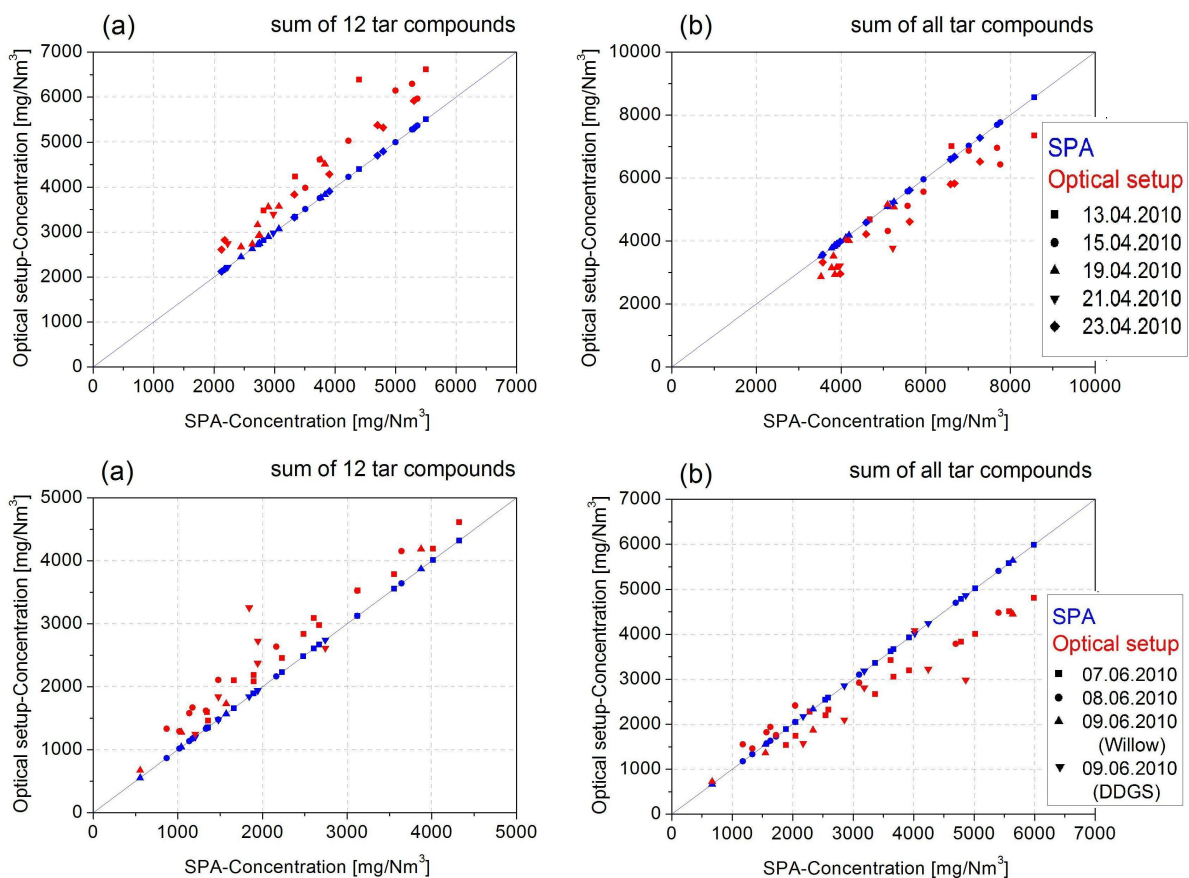


Figure 7.19: Comparison between the concentration sum of optical measurements and SPA results at TUM and TUD gasification test rigs.

Figure 7.20 presents the comparison between the sum of tars measured by the optical setup and the overall tar content measured by the online tar analyzer during the experiments in the TUM gasification facility. Regarding the fact that the sum of tars measured by the optical facility is the sum of fourteen hydrocarbons while the online tar analyzer measures all the tar compounds detected by the flame ionization detector, a direct comparison between the results is not possible.

As it can be seen in the following figures, in some cases such as during atmospheric AGROL (07.06.10) and DDGS gasification (09.06.10) as well as in a long period of pressurized Willow gasification (09.06.10), the sum of tars measured by the optical setup is lower than the tar content measured by the online tar analyzer. On the other hand, during pressurized AGROL gasification (07.06.10), atmospheric Willow gasification (08.06.10) and a short period of pressurized Willow gasification (09.06.10), the optical setup measures higher concentration sum of tars. Due to the aforementioned behaviour and the calibration problems of the device, the results from the online tar analyzer do not seem to be accurate for all experimental periods. Therefore, a general conclusion cannot be made.

However, in most of the cases, the tendency of the optical setup is to measure lower tar content than the actual one due to the fact that it is not calibrated for all tars. Tar compounds especially from Class 4 (e.g. 1-methylnaphthalene and 2-methylnaphthalene), whose concentration values are high as it can be seen from the SPA measurements, cannot be measured with the optical setup and are detected as background signal. Therefore, they are not included in the sum of measured tars while on the other hand, they are measured by the online tar analyzer and contribute to the overall tar content.

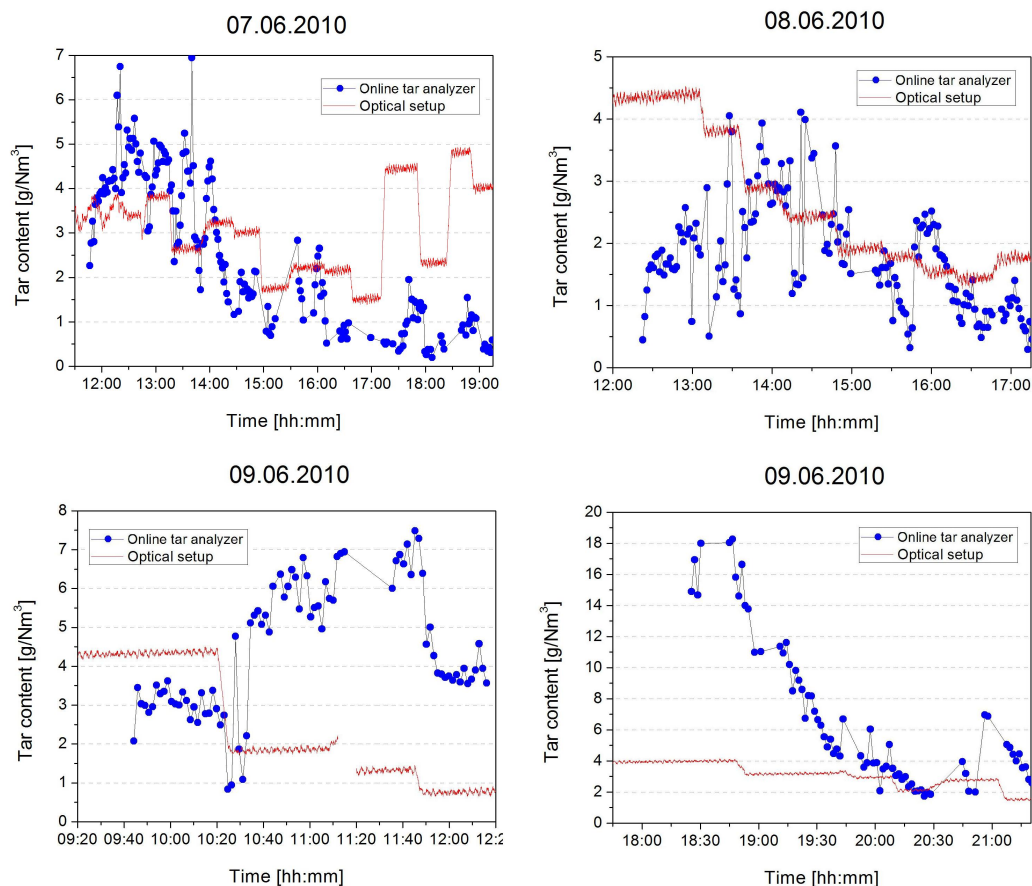


Figure 7.20: Comparison between optical measurements and online tar analyzer's results from the TUM gasification test rig.

7.2 Influence of gasification parameters on the tar content

The producer gas has been continuously measured and monitored with the help of the innovative transportable optical setup. Figures 6.14-6.22 present the online determination of the concentration of individual tar compounds in both biomass gasification reactors. However, several parameters such as the reactor type, the biomass feedstock, the gasification temperature and pressure, the steam to biomass ratio and the type of bed material have influenced the tar content of the producer gas from the two gasification test rigs. The influence of these gasification parameters on the tar concentration is presented and discussed in details in the following sections.

7.2.1 Reactor type

The reactor type is one of the parameters that influences the tar composition due to the different behavior of the fluids regarding their flow inside the reactor. The two different gasification reactors that are used in this study are the bubbling fluidized bed reactor at TUM and the circulating fluidized bed reactor at TUD, respectively. The following figures 7.21-7.23 present the tar composition in relation to the reactor type during gasification of each of the three biomass feedstocks.

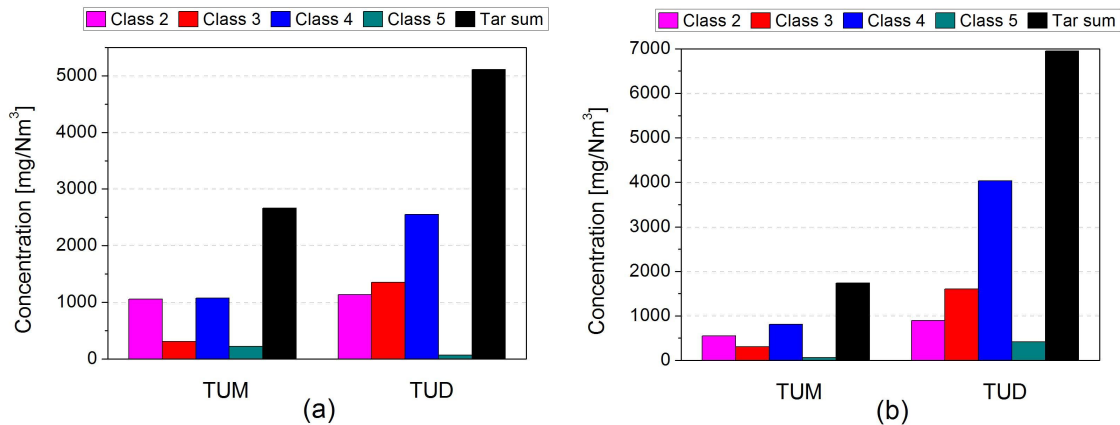


Figure 7.21: Tar composition during AGROL gasification for TUM and TUD reactors at (a) 750 °C, S/B:1,2 and (b) 800 °C, S/B:1,2.

Figure 7.21 illustrates the difference between the concentration of tar compounds during gasification of AGROL pellets for two experimental cases. As it can be seen, each tar class concentration (except for Class 5, see figure 7.21a) and consequently the sum of measured tars is higher when the gasification takes place inside the circulating fluidized bed reactor. The same results are observed for the other two fuels as well, which means that the CFB reactor produces a higher tar content gas than the bubbling fluidized bed facility.

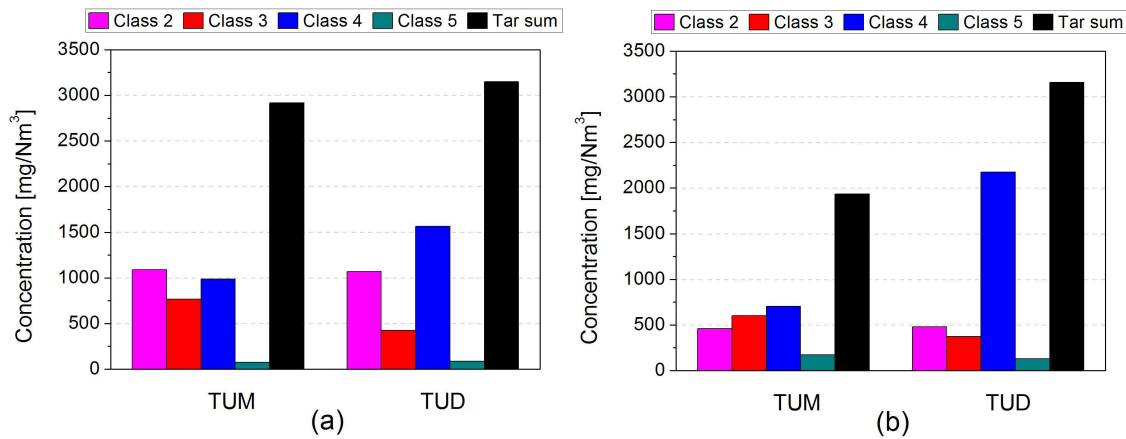


Figure 7.22: Tar composition during Willow gasification for TUM and TUD reactors at (a) 750 °C, S/B:1,2 and (b) 800 °C, S/B:1.

Regarding Willow gasification, a slight decrease in the Class 3 and Class 5 tar concentration of the TUD test rig can be realized in case of 800 °C (see figure 7.22b), which is dominated by the increase in the other two tar classes and consequently in the sum of measured tars. A similar tendency appears during gasification of DDGS pellets (see figure 7.23), where a decrease in the second as well as in the fifth tar class is observed, without affecting the increase in the concentration sum in case of the TUD reactor.

The aforementioned conclusions verify the fact that not only the excellent gas-solid contact but also the further thermal cracking of the tar compounds in the freeboard region of the bubbling fluidized bed reactor, results in a producer gas with considerably lower tar content than the CFB facility.

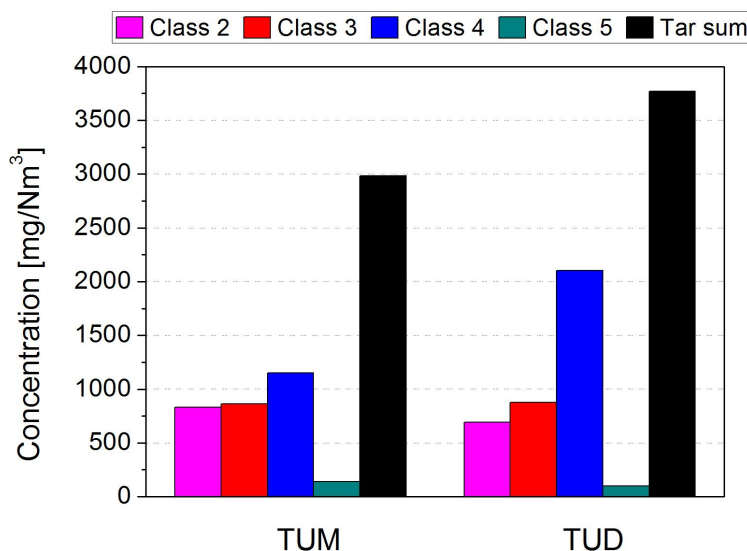


Figure 7.23: Tar composition during DDGS gasification for TUM and TUD reactors at 750 °C, S/B:0,9.

7.2.2 Biomass feedstock

Another important parameter which affects the tar content in the biomass gasification process is the type of feedstock which is used in the gasifier. A comparison between the tar composition for the three different biomass feedstocks in both gasification test rigs is displayed in figures 7.24-7.27.

Figure 7.24 presents the concentration of each tar class as well as the sum of measured tars for each biomass feedstock during gasification at the bubbling fluidized bed reactor of TUM. As it can be seen, the tar content is higher when Willow is used as biomass feedstock at both temperatures. Furthermore, DDGS results in the lowest tar content at the temperature of 750 °C and 800 °C (the steam to biomass ratio value is kept the same), respectively.

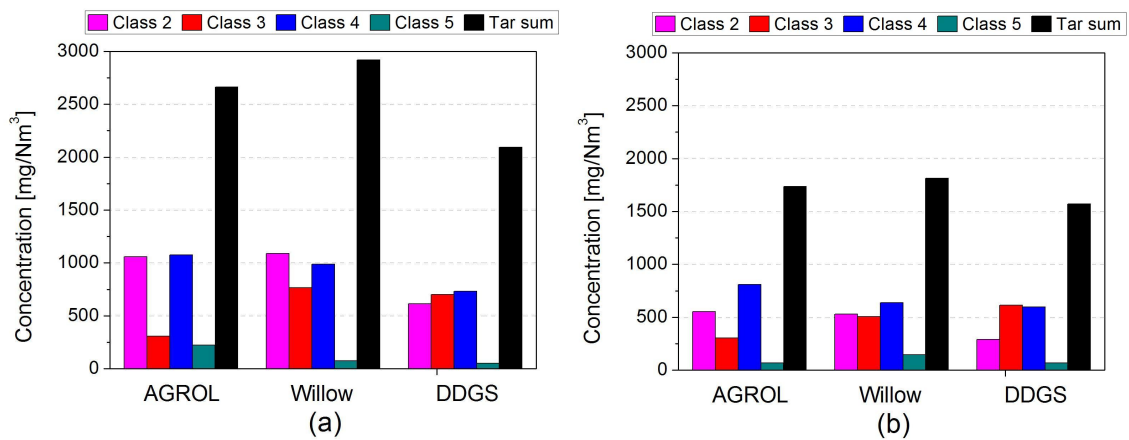


Figure 7.24: Tar composition in TUM reactor for different biomass feedstocks at (a) 750 °C, S/B:1,2 and (b) 800 °C, S/B:1,2.

Figure 7.25 illustrates the difference between the tar content of AGROL and Willow fuels for the temperature range of 800 °C-840 °C and low steam to biomass ratios (1 and 0,85, respectively). In both cases, AGROL pellets result in a producer gas with a higher tar content than using Willow as biomass feedstock. The same tendency applies also to the concentration of Class 2 and Class 4 tars, which is always higher when the reactor is fed with AGROL pellets and dominates the concentration of Class 3 and Class 5 tar compounds resulting in a higher value of the sum of measured tars.

The above results cannot facilitate a general tendency for the amount of tars produced at the TUM gasification facility regarding each biomass feedstock. When low temperatures (750 °C-800 °C) and high steam to biomass ratios (S/B:1,2) are applied, the sum of measured tars is higher in case of Willow feedstock while when high temperatures in the range of 800 °C-850 °C and low S/B (0,85-1) are applied, AGROL has the highest sum of measured tars. Therefore the influence of other gasification parameters such as the temperature and the steam to biomass ratio on the tar content should always be taken into consideration when evaluating the results for each biomass feedstock used.

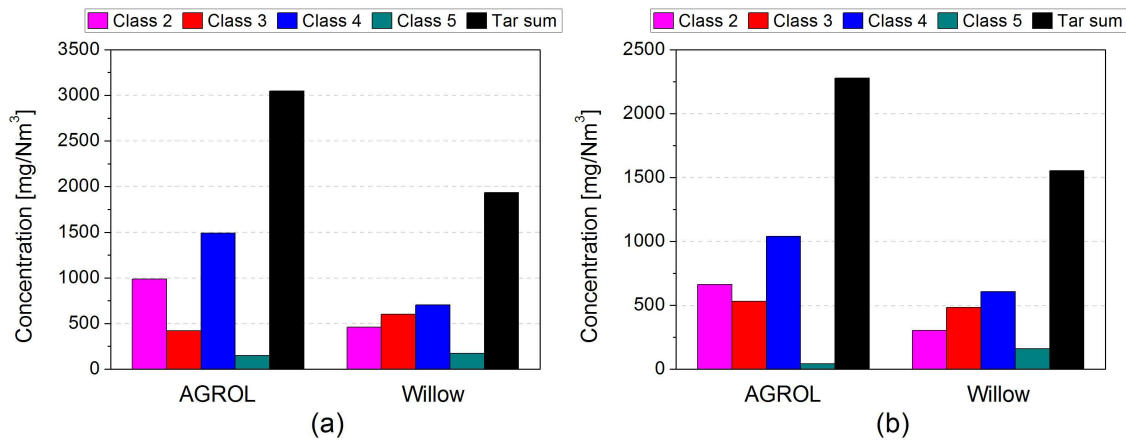


Figure 7.25: Tar composition in TUM reactor for different biomass feedstocks at (a) 800 °C, S/B:1 and (b) 840 °C, S/B:0,85.

Regarding gasification at the circulating fluidized bed of TUD, figure 7.26 displays the comparison between the tar content of the three biomass fuels at the temperature of 750 °C and S/B:1,08. As it can be seen, AGROL has the highest tar content while DDGS the lowest. Regarding the concentration of each tar class, the highest concentration values are observed for AGROL feedstock while the lowest are observed for DDGS. The increase of the DDGS Class 3 tars compared to the Class 3 concentration value for Willow is dominated by the decrease in all the other tar classes, which consequently decreases the sum of measured tars between these two fuels.

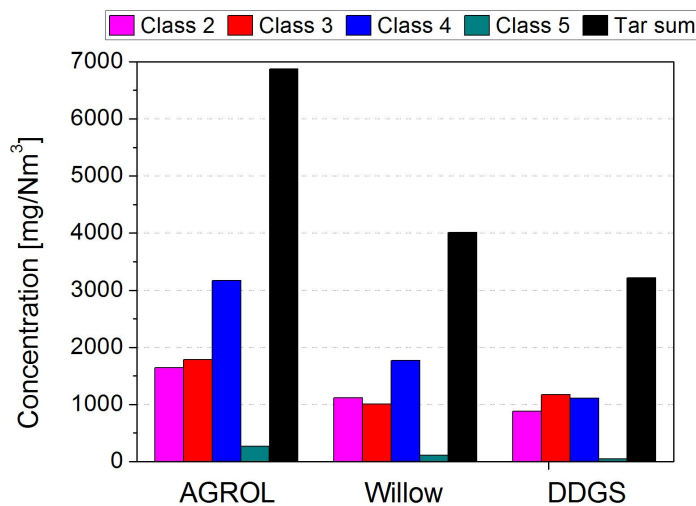


Figure 7.26: Tar composition in TUD reactor for different biomass feedstocks at 750 °C, S/B:1,08.

Figure 7.27 depicts the difference between the tar content of AGROL and Willow fuels for two experimental cases. In both cases, AGROL produces a gas with a higher tar

content than Willow. Due to the fact that few parameters are tested during DDGS gasification at the TUD facility, a general conclusion for the tar concentration regarding all the three biomass feedstocks is not feasible.

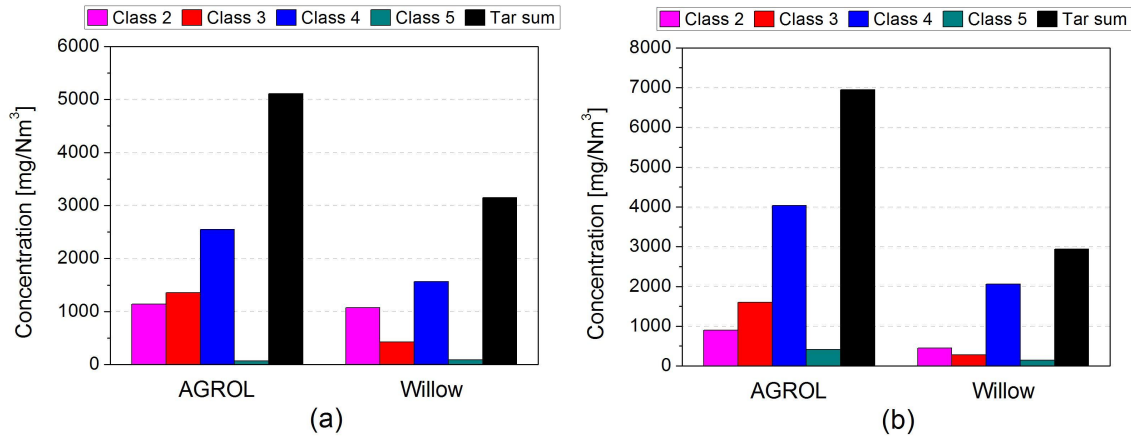


Figure 7.27: Tar composition in TUD reactor for different biomass feedstocks at (a) 750 °C, S/B:1,2 and (b) 800 °C, S/B:1,1.

7.2.3 Reactor temperature

The most important parameter which contributes to the thermal tar cracking in the gasification process is the reactor temperature. The temperature plays a significant role in all chemical reactions by affecting not only the sum of measured tars but also the conversion rate and composition of individual tar compounds. The influence of the temperature on the concentration of each tar class as well as on the sum of measured tars during gasification of all the three biomass feedstocks in both TUM and TUD reactors is presented in figures 7.28-7.33.

To determine the influence of the gasification temperature on the tar formation during the experiments at the TUM gasification facility, the temperature is increased from 750 °C to 840 °C for AGROL and Willow gasification and from 700 °C to 800 °C for DDGS gasification. The steam to biomass ratio (S/B) is kept constant.

Figure 7.28 displays the tar composition for AGROL gasification in relation to temperature variation for two different S/B values. When both low and high steam to biomass ratio values (S/B:0,85 and 1,2) are applied, the concentration of each tar class and consequently the concentration sum of measured tars decreases from 750 °C to 840 °C except for the Class 4 tar concentration, which appears to increase from 750 °C to 800 °C at low S/B (see figure 7.28a) as well as from 800 °C to 840 °C at high S/B (see figure 7.28b). The increase in the Class 4 tar concentration in high temperatures can be explained by the thermal tar cracking of the heavy Class 1 (GC-undetectable) and consequently of the Class 5 tar compounds, which decompose and produce lighter tar compounds. Furthermore, in case of low temperatures (from 750 °C to 800 °C), the low S/B does not promote the

further conversion of the tar compounds into main producer gas components, preventing their further decrease.

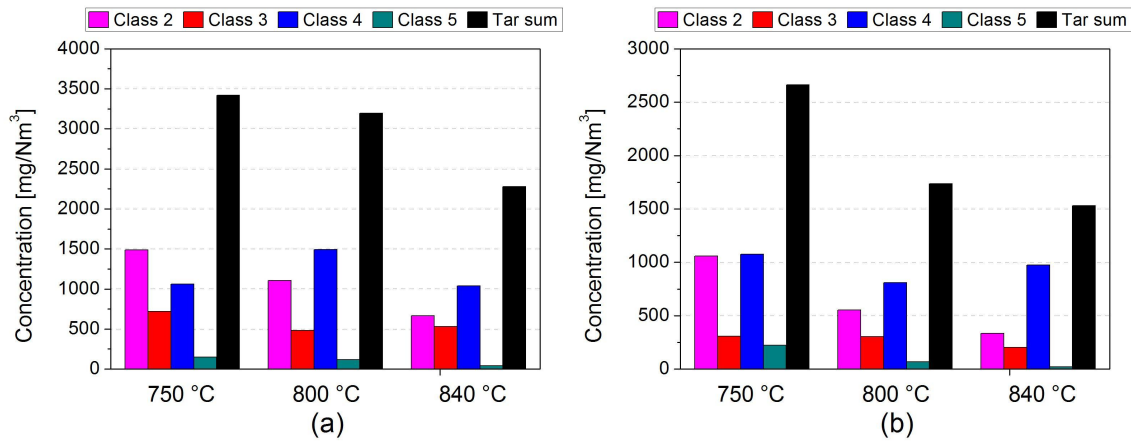


Figure 7.28: Tar composition during AGROL gasification in TUM reactor for different temperatures at (a) S/B:0,85 and (b) S/B:1,2.

Figure 7.29 illustrates the tar composition for gasification of Willow pellets as a function of process temperature for two different S/B values. Regarding the low steam to biomass ratio (S/B:0,85), the concentration of each tar class and consequently the concentration sum of measured tars decreases with increasing temperature. When a high steam to biomass ratio (S/B:1,2) is applied, a decrease in the tar concentration is realized in the temperature range of 750 °C-800 °C. A further temperature increase (from 800 °C to 840 °C) results in a very slight decrease of the tar content. Probably the extent of the thermal tar cracking due to the higher temperature is not high enough to decrease the tar content. Moreover, the high steam to biomass ratio promotes the cracking of heavy (GC-undetected) tar compounds (Class 4 tar content increases, see figure 7.29b) preventing the further decrease of the tar concentration.

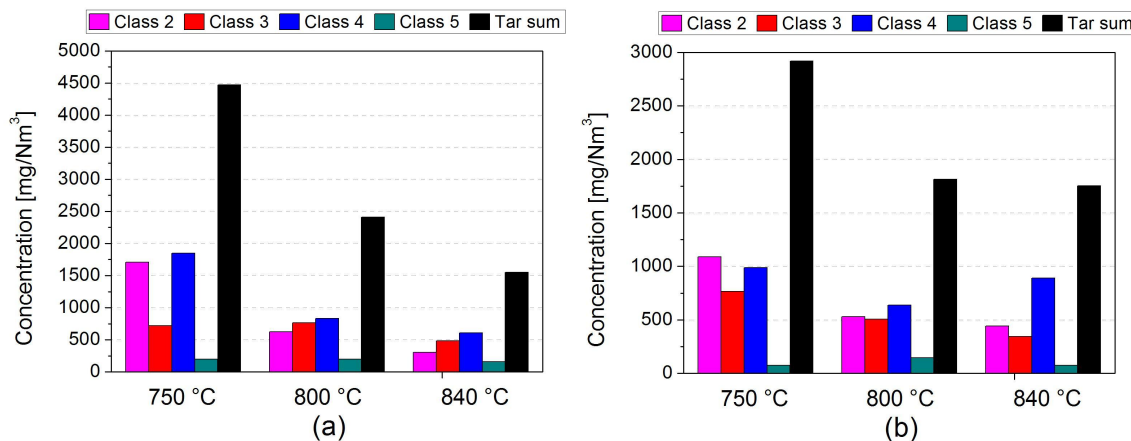


Figure 7.29: Tar composition during Willow gasification in TUM reactor for different temperatures at (a) S/B:0,85 and (b) S/B:1,2.

In case of DDGS gasification, the tar composition in relation to temperature variation is depicted in figure 7.30. For the high S/B value (S/B:1,2), the concentration of each tar class and consequently the sum of measured tars decreases with increasing temperature. When a low S/B is applied (see figure 7.30a) Class 4 and Class 5 tar concentration increases from 700 °C to 750 °C due to the decomposition of heavy Class 1 tar compounds and then decreases from 750 °C to 800 °C due to the thermal cracking into lighter tar compounds. On the other hand, Class 3 tar concentration balances the aforementioned behaviour by showing a decrease from 700 °C to 750 °C and then an increase from 750 °C to 800 °C due to the cracking of heavier tar compounds from Class 4 and Class 5. Regarding the sum of measured tars, it decreases with increasing temperature.

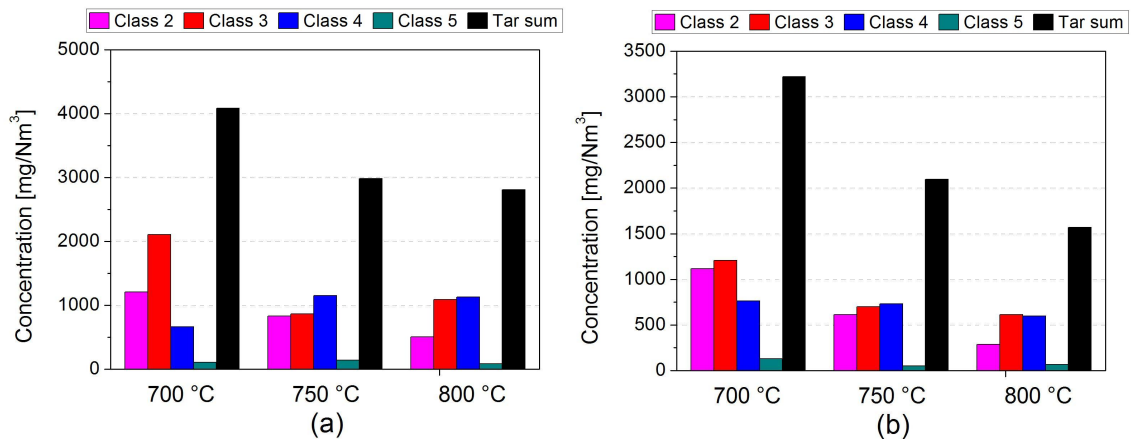


Figure 7.30: Tar composition during DDGS gasification in TUM reactor for different temperatures at (a) S/B:0,9 and (b) S/B:1,2.

During the experiments at the circulating fluidized bed gasifier of TUD, the temperature is increased from 715 °C to 800 °C for AGROL and Willow gasification and from 690 °C to 750 °C for DDGS gasification. The steam to biomass ratio (S/B) is kept constant during the temperature variation. Figure 7.31 illustrates the tar composition for gasification of AGROL pellets as a function of process temperature for two different S/B values.

In the first case, where the temperature varies from 715 °C to 750 °C, the sum of measured tars decreases, while in the second case, where the temperature varies from 750 °C to 800 °C, the sum of measured tars increases. As it can be seen in both cases, there is a decrease in the concentration of Class 2 and Class 3 tar compounds when the temperature increases while on the other hand, the concentration of Class 4 and Class 5 tars increases with increasing temperature. This fact can be explained by the mechanism of formation of heavier hydrocarbons, which describes that Class 4 and Class 5 tars can be the products from even lighter hydrocarbons due to the PAH growth reactions occurring in the gasification process.

Regarding Willow gasification, when the steam to biomass ratio ranges from 1,05 to 1,1, the sum of measured tars remains approximately the same up to the temperature of 755 °C. The same tendency as in the TUM gasification facility is observed in the temper-

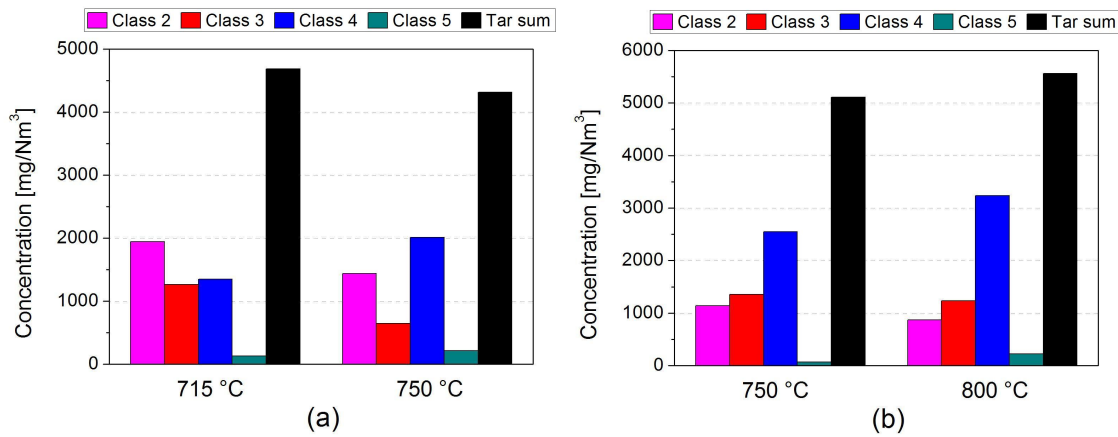


Figure 7.31: Tar composition during AGROL gasification in TUD reactor for different temperatures at (a) S/B:1,45 and (b) S/B:1,25.

ature range from 755 °C to 800 °C, where the sum decreases with a further temperature increase (see figure 7.32a). Although there is an increase in the concentration values of Class 4 and Class 5 tar compounds, the decrease in the other two tar classes dominates and results in the decrease of the sum of measured tars. When low steam to biomass ratio is applied (see figure 7.32b), the temperature increase (from 725 °C to 755 °C) results in the increase of the tar content not only due to the cracking of heavier hydrocarbons but also due to the low amount of steam supply in relation to biomass feeding.

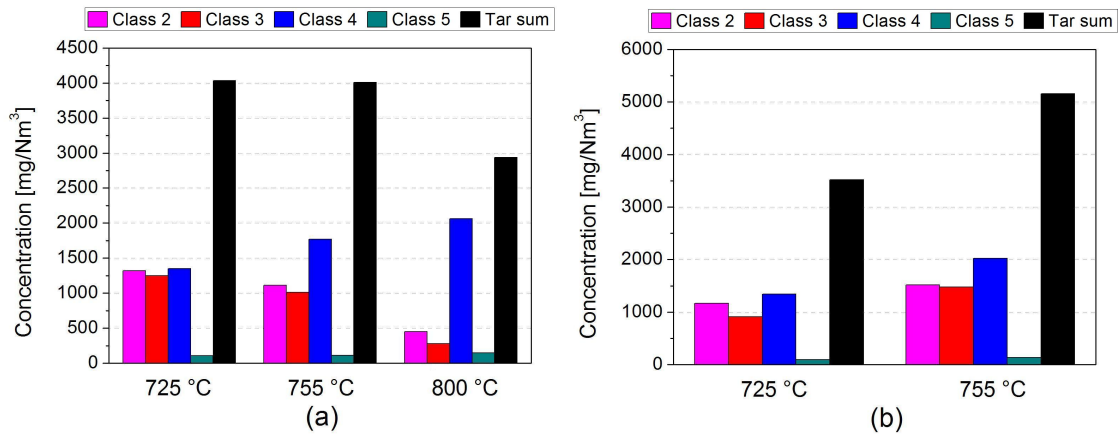


Figure 7.32: Tar composition during Willow gasification in TUD reactor for different temperatures at (a) S/B:1,05-1,1 and (b) S/B:0,9.

In case of DDGS gasification, the tar composition as a function of temperature variation is displayed in figure 7.33. As it can be seen, there is an increase in the sum of measured tars with increasing temperature, which denotes that the low temperature range from 690 °C to 740 °C does not favour the tar cracking, which results in the slight increase of the tar content. Moreover, despite the slight decrease in the Class 3 tars, the increase in all the other classes has a greater influence on the sum of measured tars.

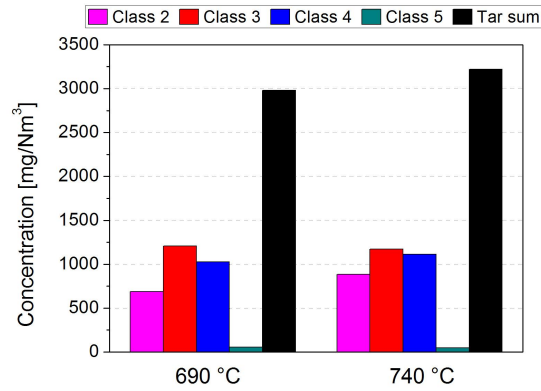


Figure 7.33: Tar composition during DDGS gasification in TUD reactor for different temperatures at S/B:1,08.

7.2.4 Reactor pressure

Figures 7.34-7.37 present the influence of pressure on AGROL and Willow gasification at the pressurized bubbling fluidized bed facility of TUM. The pressure which is tested in all experiments is 2,5 bar.

The difference between the tar composition during atmospheric and pressurized gasification of AGROL pellets at the temperature of 800 °C is presented in the following figure 7.34.

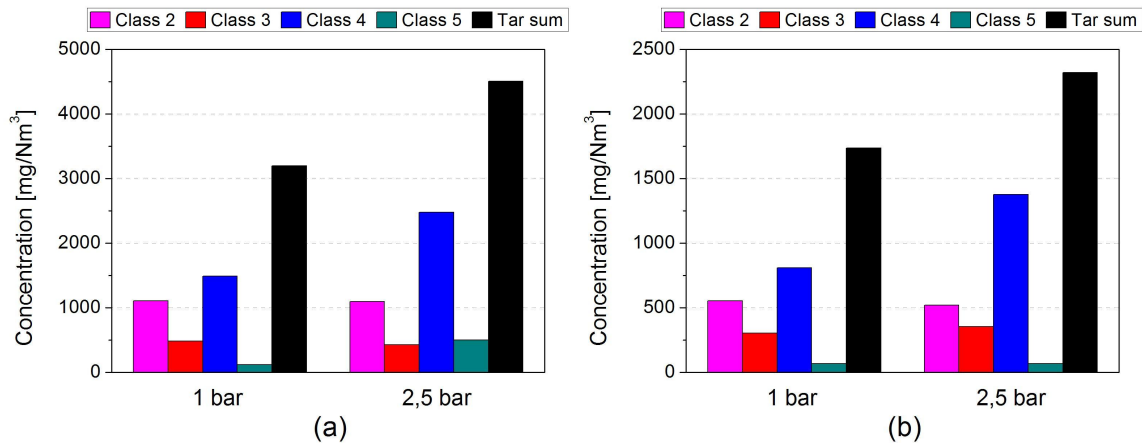


Figure 7.34: Tar composition during AGROL gasification in TUM reactor for different pressures at (a) 800 °C, S/B:0,85 and (b) 800 °C, S/B:1,2.

As it can be observed from the results, the sum of measured tars is increasing with increasing pressure for both S/B tested. When pressure increases, the velocity of the gas phase compounds decreases due to the density influence of pressure. For this reason, the steam flow rate has to be increased to keep bed fluidization at the same level as in atmospheric gasification. Therefore, the biomass supply to the gasifier is also increased to reach the desired S/B value as in atmospheric gasification. The increase in the sum of

measured tars with increasing pressure in case of AGROL gasification can be explained by the fact that the biomass feedstock used contains a high amount of volatiles, which favors the production of tar compounds and a low amount of alkalis, which is not sufficient for catalytic tar destruction. Hence, the increase in the fuel amount has a large influence on the tar formation and results in the increase of the tar content when the reactor works under pressurized conditions. The same tendency is also observed at the temperature of 750 °C for the same low and high S/B values as before (see figure 7.35).

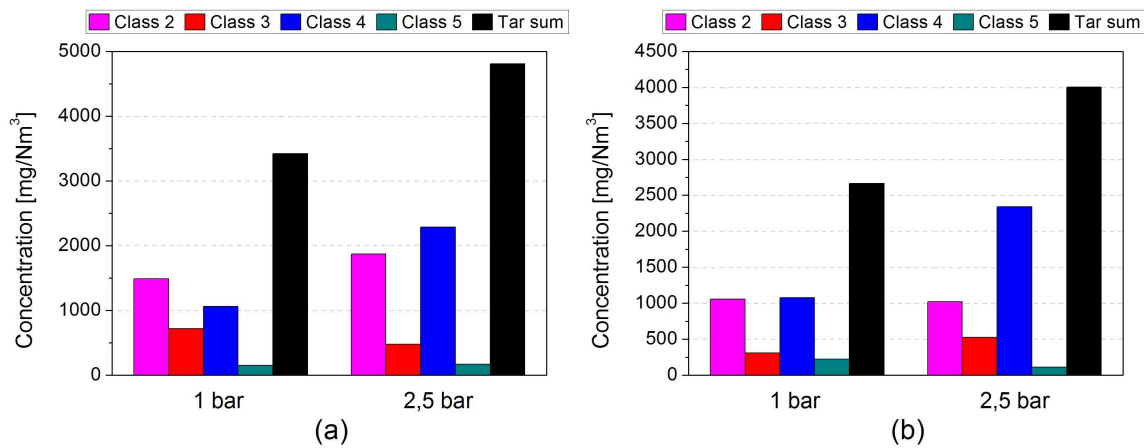


Figure 7.35: Tar composition during AGROL gasification in TUM reactor for different pressures at (a) 750 °C, S/B:0,85 and (b) 750 °C, S/B:1,2.

Regarding pressurized gasification of Willow pellets, figure 7.36 displays the difference between the tar composition during atmospheric and pressurized conditions at the temperature of 800 °C. As it can be seen, the tar concentration is decreasing with increasing pressure for both low and high S/B values.

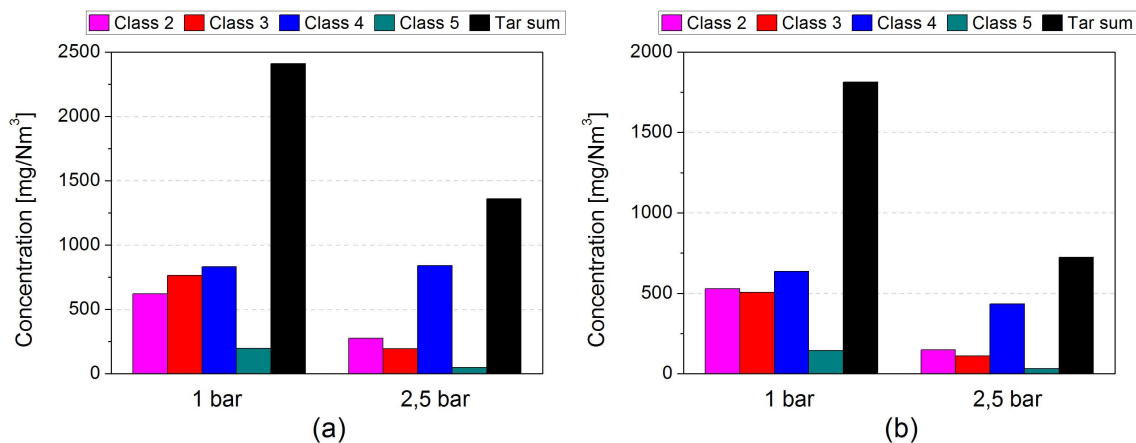


Figure 7.36: Tar composition during Willow gasification in TUM reactor for different pressures at (a) 800 °C, S/B:0,85 and (b) 800 °C, S/B:1,2.

The aforementioned result is totally different compared to the pressurized gasification of AGROL pellets. Willow pellets contain a lower amount of volatiles and a higher

amount of alkali compounds than in case of AGROL. Therefore, they produce a lower tar content than gasifying AGROL pellets despite the increase in the fuel amount. This happens not only due to the lower amount of volatiles but also due to the higher amount of alkalis, which promotes catalytic tar destruction. The same tendency of decreasing tar concentration when pressure increases can be also realized at the temperature of 750 °C for the same steam to biomass ratio values (see figure 7.37).

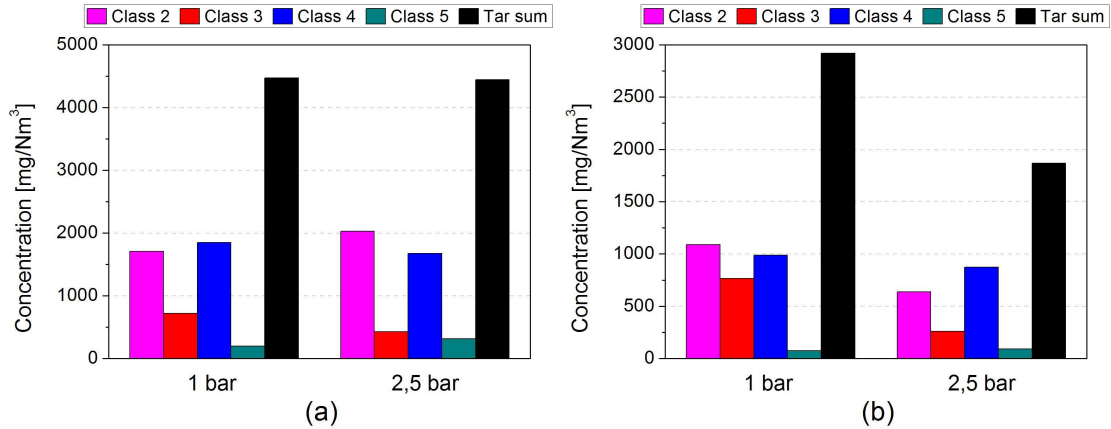


Figure 7.37: Tar composition during Willow gasification in TUM reactor for different pressures at (a) 750 °C, S/B:0,85 and (b) 750 °C, S/B:1,2.

7.2.5 Steam to biomass ratio

One of the most important parameters affecting the amount of tars produced in the gasification process is the steam to biomass ratio (S/B), which represents the amount of steam supply divided by the amount of biomass feedstock fed into the reactor. Figures 7.38-7.43 present the tar composition in relation to different S/B values during gasification of the three different biomass feedstocks in both gasification test rigs of TUM and TUD.

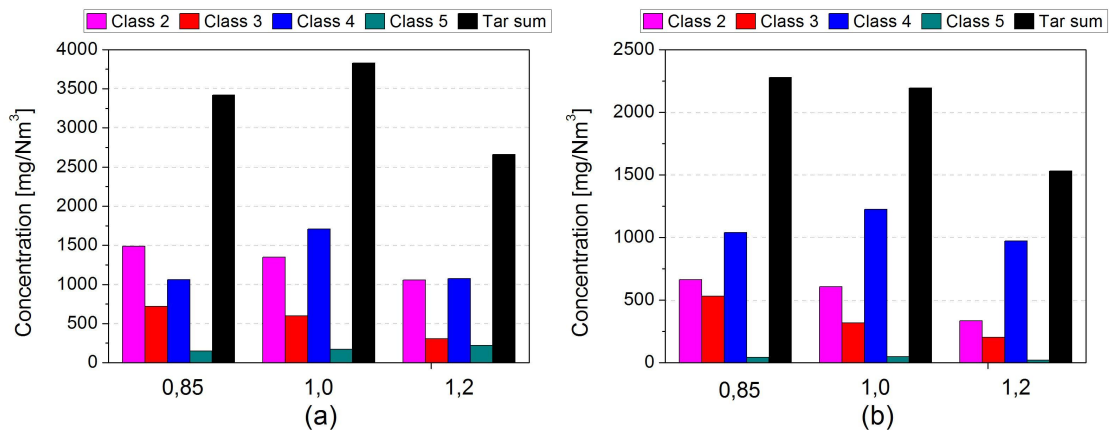
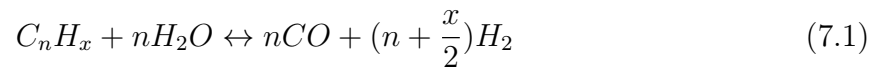


Figure 7.38: Tar composition during AGROL gasification in TUM reactor for different S/B values at (a) 750 °C and (b) 850 °C.

Regarding AGROL gasification in TUM reactor, the sum of measured tars is decreasing with increasing steam to biomass ratio at the temperature of 850 °C. Despite the increase in the concentration of Class 4 tar compounds from S/B:0,85 to S/B:1, the concentration decrease of the other tar classes prevails, decreasing the sum of measured tars (see figure 7.38b). Steam plays a significant role in the reduction of tars as it reacts with the individual hydrocarbons producing main gas compounds such as hydrogen and carbon monoxide through the steam reforming reaction. Therefore, the higher amount of steam favors the steam reforming reaction resulting in a lower tar concentration.

The steam reforming chemical reaction of the tar compounds is illustrated by the following equation. The individual hydrocarbons are described by the generalized chemical formula C_nH_x .



When a low temperature of 750 °C is applied (see figure 7.38a), the increase in the concentration of Class 4 and Class 5 tar compounds from S/B:0,85 to S/B:1 dominates, resulting in the increase of the sum of measured tars. A further increase in the steam to biomass ratio (from S/B:1 to S/B:1,2) results in the decrease of the sum of measured tars.

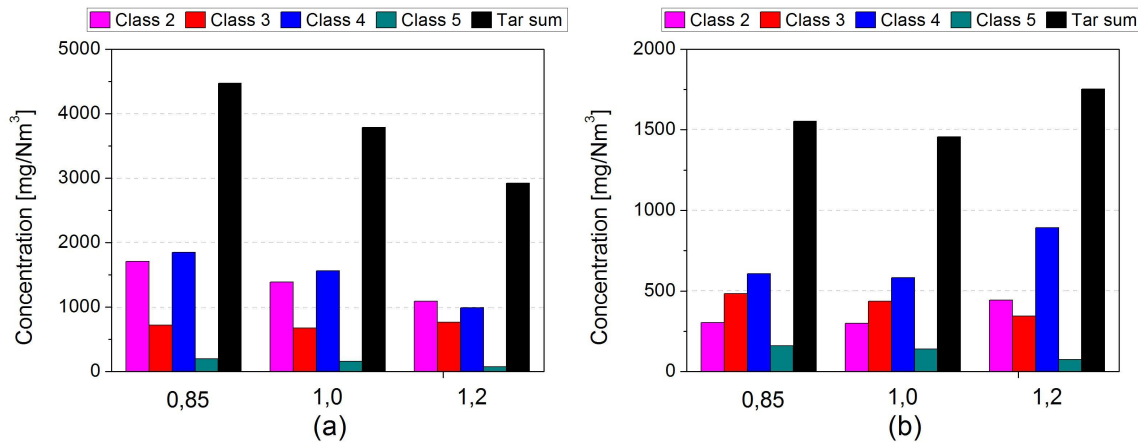


Figure 7.39: Tar composition during Willow gasification in TUM reactor for different S/B values at (a) 750 °C and (b) 850 °C.

Regarding Willow gasification, the sum of measured tars shows a decrease with increasing steam to biomass ratio at the temperature of 750 °C (see figure 7.39a). In case of high temperatures (850 °C), the sum of measured tars as well as the concentration of each tar class are decreasing from S/B:0,85 to S/B:1 while a further increase in the S/B results in the increase of the tar content (see figure 7.39b). This increase in the tar content denotes that in high temperatures, the amount of steam is high enough to promote the cracking of Class 1 hydrocarbons resulting in the production of GC-detectable tar compounds.

In case of DDGS gasification, figure 7.40 displays the tar composition for different S/B values at the lowest and highest experimental temperatures, where the same tendency of the decrease in tar content with increasing S/B is realized.

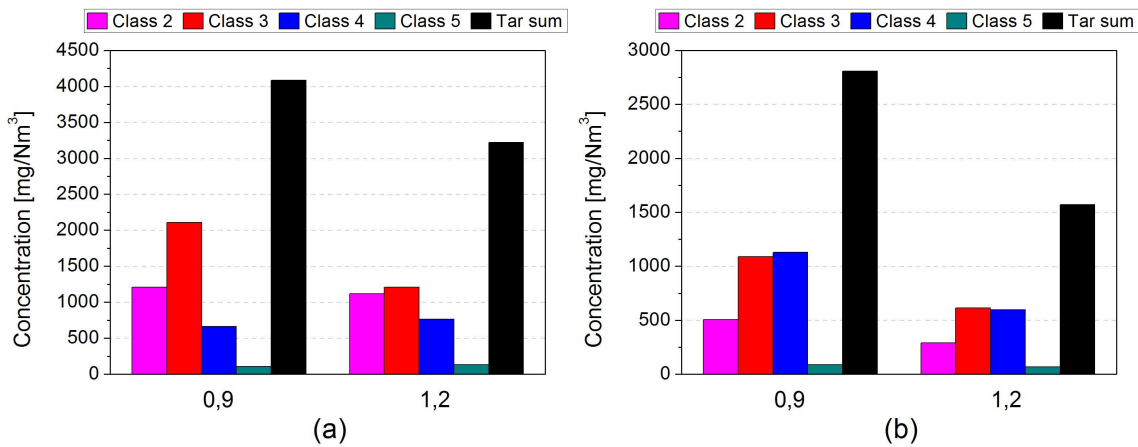


Figure 7.40: Tar composition during DDGS gasification in TUM reactor for different S/B values at (a) 700 °C and (b) 800 °C.

Regarding AGROL gasification in TUD test rig, figure 7.41 depicts the tar composition in two different temperatures (715 °C and 800 °C). In case of the low temperature, there is a decrease in the sum of measured tars as well as in the concentration of every tar class with increasing steam to biomass ratio. On the other hand, when high temperature is applied, the sum of measured tars increases from S/B:0,95 to S/B:1,15 while a further increase in the S/B results in the decrease of the tar content. The aforementioned behavior can be explained by the fact that the increase in the Class 2, 3 and 5 tars from S/B:0,95 to S/B:1,15 dominates the decrease in the concentration of Class 4 tar compounds resulting in the increase of the sum of measured tars. When a higher steam to biomass ratio is applied (S/B:1,25), the tar cracking is favored resulting in a lower tar concentration.

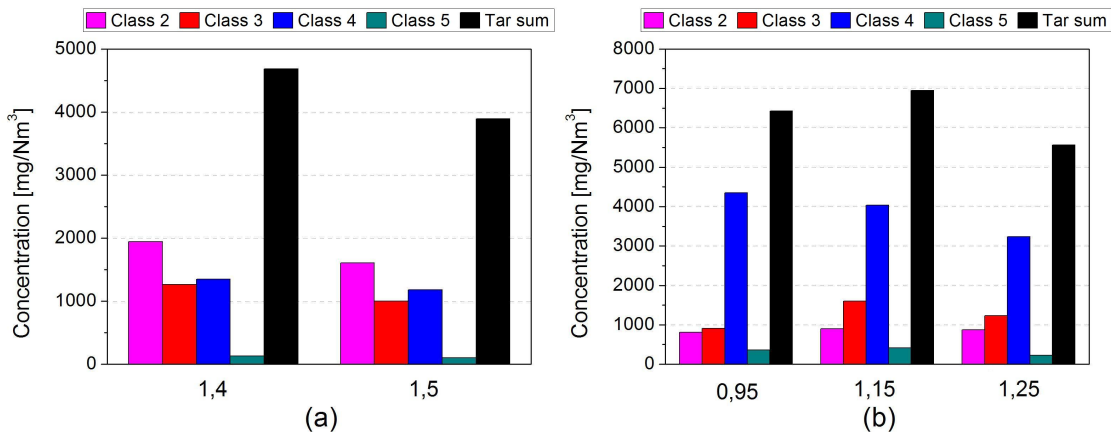


Figure 7.41: Tar composition during AGROL gasification in TUD reactor for different S/B values at (a) 715 °C and (b) 800 °C.

Figure 7.42 illustrates the tar composition for gasification of Willow pellets as a function of steam to biomass ratio for two different temperatures. In case of low temperature (700 °C), the concentration of each tar class as well as the sum of measured tars increases from S/B:0,9 to S/B:1,1 due to the tar cracking of the heavy GC-undetectable hydrocarbons (Class 1) with increasing S/B values. A further increase in the steam to biomass ratio value (S/B:1,2) results in the decrease of the tar content as the influence of the steam supply on the tar cracking reactions results in the production of less hydrocarbons. Regarding the temperature of 800 °C, as it can be seen in figure 7.42b, the concentration of each tar class as well as the sum of measured tars decreases with increasing S/B due to the the aforementioned influence of the steam on the tar reduction.

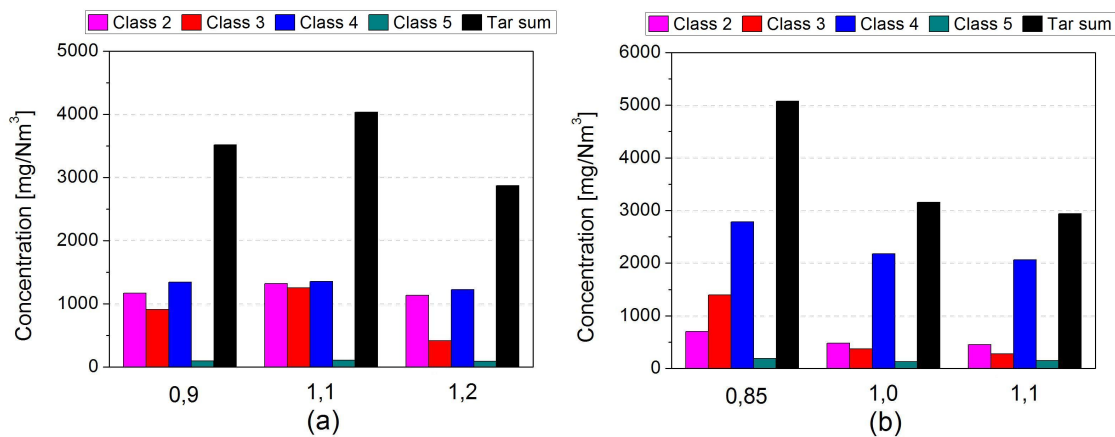


Figure 7.42: Tar composition during Willow gasification in TUD reactor for different S/B values at (a) 700 °C and (b) 800 °C.

Regarding gasification of DDGS pellets in the TUD test rig, figure 7.43 illustrates the tar composition for two different S/B values at the temperature of 750 °C. The same tendency as in most of the previous figures is realized, where a decrease in tar content appears with increasing steam to biomass ratio.

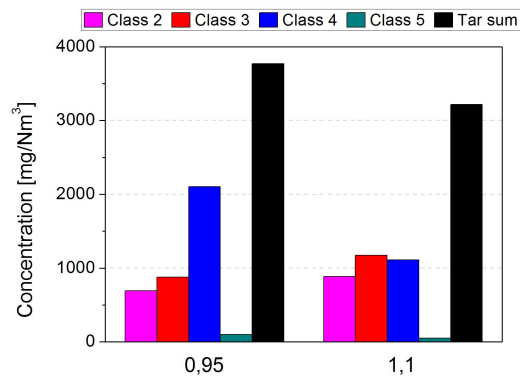


Figure 7.43: Tar composition during DDGS gasification in TUD reactor for different S/B values at 750 °C.

7.2.6 Bed material

The type of bed material used in the gasifier is one of the parameters that influences the tar composition while it plays a significant role in the tar destruction due to the catalytic influence on the tar cracking reactions. Figures 7.44-7.46 display the difference in the tar composition during gasification of each biomass feedstock in the TUD reactor using two different bed materials (treated and untreated Austrian olivine).

Figure 7.44 illustrates the tar composition during AGROL gasification for the two different bed materials at the same temperature of 755 °C and S/B ratios 1,1 and 1,2, respectively. When untreated olivine is used as bed material, there is a decrease in the sum of measured tars in case of low steam to biomass ratio (S/B:1,1). The decrease in the concentration of the Class 2 and Class 3 tar compounds dominates the increase in the concentration of the Class 4 and Class 5 tars, which results in a producer gas with a lower tar content. On the other hand, in case of higher steam to biomass ratio (S/B:1,2), the sum of measured tars increases when using untreated olivine as bed material. Regarding the concentration of each tar class, except for the third class tars, all the other tar classes have a higher tar concentration in case of untreated olivine, which denotes its catalytic influence on the destruction of Class 3 tar compounds.

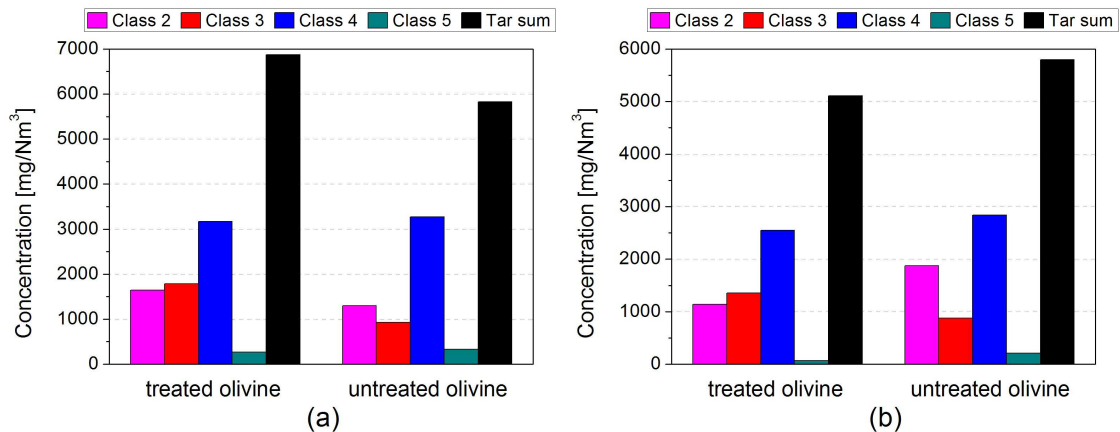


Figure 7.44: Tar composition during AGROL gasification in TUD reactor for different bed materials at (a) 755 °C, S/B:1,1 and (b) 755 °C, S/B:1,2.

In case of Willow gasification (see figure 7.45), the same behavior as in gasification of AGROL pellets is observed. When a low steam to biomass ratio (S/B:0,9) is applied, the decrease in the concentration of the Class 2 and Class 3 tar compounds due to the use of untreated olivine dominates the increase in the concentration of the Class 4 and Class 5 tars resulting in a lower sum of measured tars. Regarding the high steam to biomass ratio (S/B:1,1), the influence of untreated olivine on the destruction of Class 3 tar compounds can be also noted as well as the increase in the sum of measured tars.

Regarding DDGS gasification, when a low steam to biomass ratio (S/B:0,93) is applied, there is a decrease in the sum of measured tars by using untreated olivine as bed material

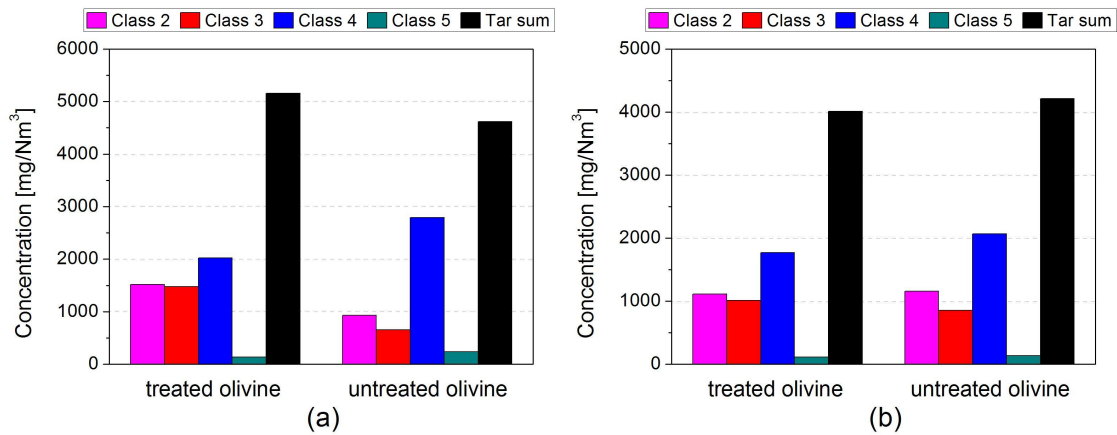


Figure 7.45: Tar composition during Willow gasification in TUD reactor for different bed materials at (a) 755 °C, S/B:0,9 and (b) 755 °C, S/B:1,1.

(see figure 7.46a). Moreover, the concentration of each tar class decreases except for the Class 2 tar compounds, which show a different behavior due to the little influence of the low S/B ratio on the reaction of the mixed oxygenates (Class 2 tar compounds) with steam. On the other hand, the sum of measured tars slightly increases when a higher steam to biomass ratio (S/B:1,06) is applied (see figure 7.46b). The same increasing behavior is detected in the concentration of each tar class apart from the Class 2 compounds probably due to the greater influence of the S/B ratio on their chemical reactions with steam.

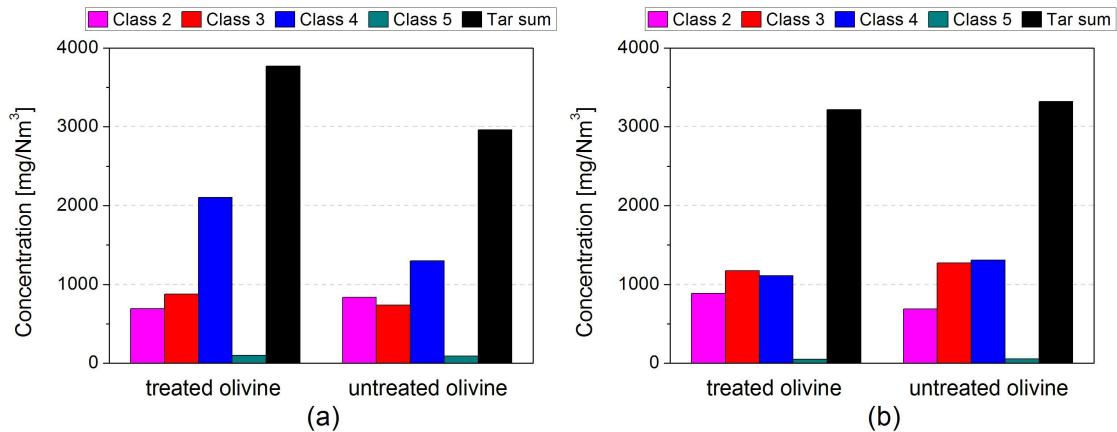


Figure 7.46: Tar composition during DDGS gasification in TUD reactor for different bed materials at (a) 755 °C, S/B:0,93 and (b) 755 °C, S/B:1,06.

The aforementioned experimental results cannot facilitate a general tendency concerning the influence of untreated olivine on the tar cracking as the use of this kind of bed material does not always result in a producer gas with a lower tar content. The influence of the S/B value on the tar composition has to be taken into account in conjunction with the applied bed material.

However, at the temperature of 755 °C, the influence of untreated olivine dominates when applying low S/B values during gasification of all the three biomass feedstocks, resulting in lower sum of measured tars. On the other hand, when high steam to biomass ratios are applied, the influence of the steam supply on the cracking of heavier hydrocarbons (Class 5 tars) is greater than the catalytic activity of untreated olivine. Therefore, this fact results in a producer gas with higher tar content regarding gasification of all the three biomass feedstocks.

7.2.7 Overview of the influence of different parameters on the tar content

A summary of the general tendencies regarding the influence of each gasification parameter on the tar content is presented in table 7.1. A detailed overview is discussed in the previous subsections.

Table 7.1: Influence of gasification parameters on the tar content.

Parameters	Tar content	
	High	Low
Reactor type	CFB	BFB
Biomass feedstock	no general tendency, S/B and Temperature influence must be taken into account	
	Willow at high S/B in BFB AGROL at high S/B in CFB	Willow at low S/B in BFB DDGS at high S/B in CFB
Reactor temperature	700 – 750 °C in BFB	800 – 840 °C in BFB
	no general tendency in CFB, S/B and biomass feedstock influence must be taken into account	
Reactor pressure	2,5 bar for AGROL	2,5 bar for Willow
	no general tendency, biomass feedstock influence must be taken into account	
Steam to biomass ratio	0,85-1	1-1,2
Bed material	no general tendency, S/B and Temperature influence must be taken into account	

8 Summary

The gasification process and especially the use of biomass feedstock as a renewable source of energy is a promising technology which can lead to the production of biofuels as well as to the generation of electricity and heat through CHP plants. The most important problem for biomass gasification is the production of undesirable hydrocarbons (tars) within the process, which can cause many problems to the further downstream application of the producer gas for the production of energy and fuels.

The determination of the tar content is of significant importance in order to verify the suitability of the producer gas for its further downstream use. Therefore, a transportable optical facility based on the principle of Laser Induced Fluorescence (LIF) spectroscopy is developed, which allows not only the quantification but also the qualification of biomass gasification tars downstream to a gasification facility.

The optical measurement system is an online and non intrusive tar analysis method which can quantify and qualify gas phase tar compounds with only optical intervention in the measured producer gas. By exploiting the different spectroscopic behavior of each individual tar compound, it is possible to investigate mixtures of tars according to their specific fluorescence spectra, which facilitates a multicomponent analysis. Furthermore, drawbacks of former measurement techniques such as long sampling times, condensation and re-evaporation of the measured volumes and additional time for laboratory analysis of the obtained samples are avoided.

The transportable facility enables the online determination of the concentration of fourteen tar compounds, which are considered as the most important and representative compounds in a tar mixture. With the help of a tar mixing station, which generates different concentrations of gas phase tar compounds, the optical facility is calibrated and then coupled to two different gasification test rigs, where the producer gas has been continuously measured and monitored.

The evaluation of the results provides the influence of different gasification parameters such as temperature, pressure, type of biomass feedstock used and steam to biomass ratio, on the tar composition. Moreover, the influence of the reactor configuration as well as the type of bed material on tar production is examined. The extent of the thermal tar cracking of heavy polyaromatic hydrocarbons is investigated while the influence of the chemical reactions which lead either to tar formation or tar decomposition is detected as well.

Finally, the accuracy of the measurement procedure is discussed, demonstrating that the online transportable setup can be used for the continuous monitoring of gasifier tars. The fact that the obtained results show a very good match to other measurement techniques,

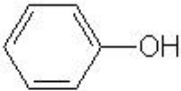
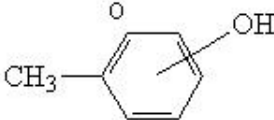
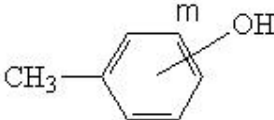
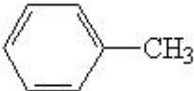
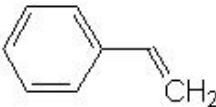
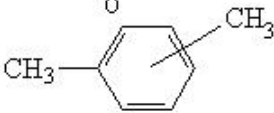
reveals the possibility of the optical technique for qualifying and quantifying tar mixtures directly downstream from a gasification unit.

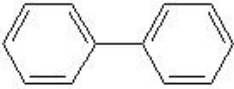
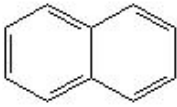
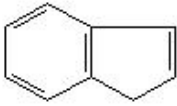
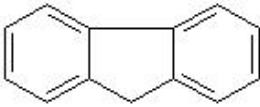
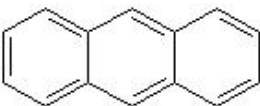
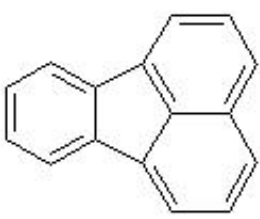
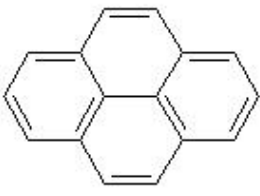
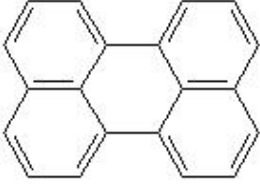
Further research should be also directed to increase the sensitivity of the method as well as to minimize the error of the measurement procedure. Moreover, different configurations of the facility should be considered and investigated in order to optimize the transportability of the setup, while the calibration of the facility can be extended for measuring as many individual tar compounds as possible.

A Appendix

A.1 Tar compounds and structures

The names, CAS registry numbers and boiling points of the individual organic compounds that are determined in biomass gasification producer gases are presented in the technical document of the European Committee of Standardization (CEN) [6]. A list of tar compounds together with their structures according to the five tar classes system is available at *www.thersites.nl*. The names and structures of the tar compounds used in this study are the following:

Name	Class	Structure	Chemical formula	Boiling point (°C)
phenol	2		C_6H_6O	182
o-cresol	2		C_7H_8O	191
m-cresol	2		C_7H_8O	202
toluene	3		C_7H_8	111
styrene	3		C_8H_8	145
o-xylene	3		C_8H_{10}	144

Name	Class	Structure	Chemical formula	Boiling point (°C)
biphenyl	4		$C_{12}H_{10}$	256
naphthalene	4		$C_{10}H_8$	218
indene	4		C_9H_8	183
fluorene	4		$C_{13}H_{10}$	293-295
anthracene	4		$C_{14}H_{10}$	340
fluoranthene	5		$C_{16}H_{10}$	375
pyrene	5		$C_{16}H_{10}$	393
perylene	5		$C_{20}H_{12}$	497

A.2 Parameters for the mass transfer model

The parameters used for the calculation of the diffusion coefficients for each tar compound are presented in tables A.1 and A.2.

Table A.1: Atomic Diffusion Volumes [129]

Atomic and Structural Diffusion Volume increments in cm^3/mol	
C	16.5
H	1.98
O	5.48
N_2	17.9
Aromatic ring	-20.2
Heterocyclic ring	-20.2

Table A.2: Properties for each compound.

Compound	M [g/mol]	T_b [K]	V_b [cm^3/mol]	ν [cm^3/mol]	μ [De]	References
nitrogen	28,01	77,34	6344,4	17,9	-	[135]
phenol	94,11	455,02	140,372	96,16	1,224	[134], [129], [132], [145]
o-cresol	108,14	464,19	167,64	116,62	1,45	[134], [129], [132], [145]
m-cresol	108,14	475,42	173,86	116,62	1,48	[134], [129], [132], [145]
toluene	92,14	-	-	111,14	-	[134], [129], [132]
styrene	104,15	-	-	127,64	-	[134], [129], [133]
o-xylene	106,17	-	-	131,6	-	[134], [129], [132]
biphenyl	154,21	-	-	177,4	-	[134], [129]
naphthalene	128,17	-	-	140,44	-	[134], [129], [132]
indene	116,16	-	-	123,94	-	[134], [129], [133]
fluorene	166,23	-	-	173,7	-	[134], [129], [133]
anthracene	178,24	-	-	190,2	-	[134], [129], [132]
fluoranthene	202,25	-	-	203	-	[134], [129], [135]

References

- [1] Milne T.A., Evans R.J., and Abatzoglou N. Biomass gasifier tars: their nature, formation and conversion. *NREL/TP-570-25357*, 1998.
- [2] IEA Bioenergy. Annual Report 2008, 2008.
- [3] IEA Bioenergy. Bioenergy – a sustainable and reliable energy source, A review of status and prospects, 2009.
- [4] IEA International Energy Agency. World energy outlook 2006, Paris, 2006.
- [5] IPCC Intergovernmental Panel on Climate Change-Mitigation of Climate Change. Working group *III*, Chapter 4 of the 4th assessment report, 2007.
- [6] Biomass gasification-Tar and particles in product gases-Sampling and analysis. *DIN Deutsches Institut für Normung e.V., German Version DIN CEN/TS 15439:2006 D*, 2006.
- [7] E4tech. Internal analysis, 2009.
- [8] Balat M., Balat M., KÝrtay E., and Balat H. Main routes for the thermo-conversion of biomass into fuels and chemicals. Part 2: Gasification systems. *Energy Conversion and Management*, 50:3158–3168, 2009.
- [9] Demirbas A. Gaseous products from biomass by pyrolysis and gasification: effects of catalyst on hydrogen yield. *Energy Conversion and Management*, 43:897–909, 2002.
- [10] Ganan J., Al-Kassir Abdulla A., Cuerda Correa E.M., and Macías-García A. Energetic exploitation of vine shoot by gasification processes: A preliminary study. *Fuel Processing Technology*, 87:891–897, 2006.
- [11] Demirbas A. New opportunities resulting from cogeneration systems based on biomass gasification. *Energy Source*, 27:941–948, 2005.
- [12] Demirbas A. Biomass-based combined heat and power systems. *Energy Source*, 3:245–253, 2006.
- [13] Rodrigues M., Faaij A.P.C., and Walter A. Techno-economic analysis of co-fired biomass integrated gasification/combined cycle systems with inclusion of economies of scale. *Energy*, 28:1229–1258, 2003.

- [14] Maniatis K. *Progress in thermochemical biomass conversion*. AV Bridgwater, Blackwell Science Ltd., 2001.
- [15] Maher K.D. and Bressler D.C. Pyrolysis of triglyceride materials for the production of renewable fuels and chemicals. *Bioresource Technology*, 98:2351–2368, 2007.
- [16] Vallios I., Tsoutsos Th., and Papadakis G. Design of biomass district heating systems. *Biomass and Bioenergy*, 33:659–678, 2009.
- [17] Fan Y., Li C., Lay J.J., Hou H., and Zhang G. Optimization of initial substrate and pH levels for germination of sporing hydrogenproducing anaerobes in cow dung compost. *Bioresource Technology*, 91:189–193, 2004.
- [18] Fang H.H.P. and Liu H. Effect of pH on hydrogen production from glucose by a mixed culture. *Bioresource Technology*, 82:87–93, 2002.
- [19] Guo L.J., Lu Y.J., Zhang X.M., Ji C.M., Guan Y., and Pei A.X. Hydrogen production by biomass gasification in supercritical water: A systematic experimental and analytical study. *Catalysis Today*, 129:275–286, 2007.
- [20] Florin N.H. and Harris A.T. Review-Enhanced hydrogen production from biomass with in situ carbon dioxide capture using calcium oxide sorbents. *Chemical Engineering Science*, 63:287–316, 2008.
- [21] Zhang W. Automotive fuels from biomass via gasification. *Fuel Processing Technology*, 91:866–876, 2010.
- [22] European Biofuels Research Advisory Council. Biofuels in the European Union—a vision for 2030 and beyond. page 13, 2006.
- [23] Wilmes B. and Behrendt F. Mathematical model of the gasification of wood particles. In *Sino-German Workshop on Energetic Utilisation of Biomass, Beijing, China, October 8-11*, 2003.
- [24] Bridgewater A.V., Beenackers A.A.C.M., and Sipila K. An assessment of the possibilities for transfer of european biomass gasification technology to China. *Executive summary*, 1999.
- [25] Prins M.J. *Thermodynamic analysis of biomass gasification and torrefaction*. PhD thesis, Eindhoven University of Technology, 2005.
- [26] Munzinger M. and Lovegrove K. Biomass gasification using solar thermal energy. In *Proceedings of ANZSES annual conference, Solar 2006, Canberra, September 13–15*, 2006.

-
- [27] Stevens D.J. Hot gas conditioning: Recent progress with larger-scale biomass gasification systems. *NREL Subcontractor Report, NREL/SR-510-29952, Golden, Colorado*, 2001.
- [28] Boerrigter H., van der Drift A., Hazewinkel J.H.O., and Küpers G. Biosyngas: multifunctional intermediary for the production of renewable power, gaseous energy carriers, transportation fuels, and chemicals from biomass. *Final report of the OTC Project, ECN-04-112, Energy research Centre of the Netherlands, Petten*, December 2004.
- [29] Warnecke R. Gasification of biomass: comparison of fixed bed and fluidized bed gasifier. *Biomass and Bioenergy*, 18:489–497, 2000.
- [30] Susta M., Luby P., and Mat S.B. Biomass energy utilization and environment protection—commercial reality and outlook. In *POWERGEN ASIA 2003, Ho Chi Minh City, Vietnam*, 23–25 September 2003.
- [31] McKeough P. and Kurkela E. Production and conversion of biomass-derived synthesis gas. In *Nordic Wood Biorefinery Conference, Stockholm, Sweden*, 2008.
- [32] VTT Technical Research Centre of Finland. Finland, Country Report Highlights. In *IEA Task 33 Meeting, Chicago*, October 2006.
- [33] Hofbauer H. and Knoef H. Success stories on biomass gasification. *Handbook Biomass Gasification, BTG*, pages 115–161, 2005.
- [34] Babu S. Biomass gasification for hydrogen production – Process description and research needs. *IEA Bioenergy, Task 33, Thermal Gasification of Biomass, Technology Report, Dublin, Ireland*, 12-13 October 2005.
- [35] Spliethoff H. Status of biomass gasification for power production. *IFRF Combustion Journal, Article No. 200109*, November 2006.
- [36] Schindler M., Claußen M., and Vodegel S. The CUTEC concept of biomass gasification. In *RENEW - 1st European summer school on Renewable Motor Fuels*, 29-31 August 2005.
- [37] Paisley M.A., Litt R.D., and Creamer K.S. Gasification of refuse derived fuel in a high throughput gasification system. *Technical paper, P012990, Battelle, Energy from Biomass and Waste XIV, USA*, 1990.
- [38] Mühlen H.J. and Schmid C. Der Blaue Turm-Wasserstoff aus Biomasse. *Ökologische Stoffverwertung, Berichte der Fördergemeinschaft, Wasserstoffreiches Vergasungsgas*, December 2003.
- [39] <http://www.blue-tower.de/index-a-195.html>.

- [40] van der Meijden C.M., Veringa H.J., van der Drift A., and Vreugdenhil B.J. The 800 kW_{th} allothermal biomass gasifier milena. In *Proceedings of the 16th European Biomass Conference and Exhibition, Valencia, Spain*, pages 711–715, 2008.
- [41] Zuberbühler U., Specht M., and Bandi A. Gasification of biomass-an overview on available technologies. In *RENEW - 1st European summer school on Renewable Motor Fuels*, 29-31 August 2005.
- [42] <http://www.aer-gas.de/>.
- [43] Kalinci Y., Hepbasli A., and Dincer I. Biomass-based hydrogen production: A review and analysis. *International Journal of Hydrogen Energy*, 34:8799–8817, 2009.
- [44] Midilli A., Dogru M., Howarth C.R., and Ayhan T. Hydrogen production from hazelnut shell by applying air-blown downdraft gasification technique. *International Journal of Hydrogen Energy*, 26:29–37, 2001.
- [45] Morf P.O. *Secondary reactions of tar during thermochemical biomass conversion*. PhD thesis, Swiss Federal Institute of Technology Zürich, 2001.
- [46] Mahishi M. *Theoretical and experimental investigation of hydrogen production by gasification of biomass*. PhD thesis, University of Florida, 2006.
- [47] Gil J., Corella J., Aznar M.P., and Caballero M.A. Biomass gasification in atmospheric and bubbling fluidized bed: Effect of the type of gasifying agent on the product distribution. *Biomass and Bioenergy*, 17:389–403, 1999.
- [48] Mahishi M.R. and Goswami D.Y. Thermodynamic optimization of biomass gasifier for hydrogen production. *International Journal of Hydrogen Energy*, 32:3831–3840, 2007.
- [49] Cateni B.G. *Effects of feed composition and gasification parameters on product gas from a pilot scale fluidized bed gasifier*. PhD thesis, Oklahoma State University, 2007.
- [50] Weerachanchai P., Horio M., and Tangsathitkulchai C. Effects of gasifying conditions and bed materials on fluidized bed steam gasification of wood biomass. *Bioresource Technology*, 100:1419–1427, 2009.
- [51] Graham R. and Bain R. Biomass gasification: Hot-gas clean-up. *Report submitted to the International Energy Agency (IEA) Biomass Gasification Working Group*, 1993.
- [52] Ståhlberg P., Lappi M., Kurkela E., Simell P., Oesch P., and Nieminen M. Sampling of contaminants from product gases of biomass gasifiers. *VTT Technical Research Centre of Finland. Espoo, Finland*, 1998.

-
- [53] Kinoshita C.M., Wang Y., and Zhou J. Tar formation under different biomass gasification conditions. *Journal of Analytical and Applied Pyrolysis*, 29:169–181, 1994.
- [54] Yu Q., Brage C., Chen G., and Sjöström K. Temperature impact on the formation of tar from biomass pyrolysis in a free-fall reactor. *Journal of Analytical and Applied Pyrolysis*, 40-41:481–489, 1997.
- [55] Narváez I., Orío A., Aznar M.P., and Corella J. Biomass gasification with air in an atmospheric bubbling fluidized bed. Effect of six operational variables on the quality of the produced raw gas. *Industrial and Engineering Chemistry Research*, 35:2110–2120, 1996.
- [56] van Paasen S.V.B. and Kiel J.H.A. Tar formation in a fluidized-bed gasifier, impact of fuel properties and operating conditions. *ECN report ECN-C-04-013*, Petten, The Netherlands, April 2004.
- [57] Knight R.A. Experience with raw gas analysis from pressurized gasification of biomass. *Biomass and Bioenergy*, 18:67–77, 2000.
- [58] Wang W.Y., Ye Z.C., Padban N., Olofsson G., and Bjerle I. Gasification of biomass/waste blends in a pressurized fluidized bed gasifier. In *Proceedings of the 1st World Conference on Biomass for Energy and Industry, Seville, Spain*, page 1698–1701, 2000.
- [59] Herguido J., Corella J., and González-Saiz J. Steam gasification of lignocellulosic residues in a fluidized bed at a small pilot scale. Effect of the type of feedstock. *Industrial and Engineering Chemistry Research*, 31:1274–1282, 1992.
- [60] Wang Y., Namioka T., and Yoshikawa K. Effects of the reforming reagents and fuel species on tar reforming reaction. *Bioresource Technology*, 100:6610–6614, 2009.
- [61] Corella J., Aznar M.P., Gil J., and Caballero M.A. Biomass gasification in fluidized bed: where to locate the dolomite to improve gasification? *Energy and Fuels*, 13:1122–1127, 1999.
- [62] Devi L., Ptasiński K.J., and Janssen F. A review of the primary measures for tar elimination in biomass gasification processes. *Biomass and Bioenergy*, 24:125–140, 2003.
- [63] Dayton D. A review of the literature on catalytic biomass tar destruction-Milestone completion report. *NREL/TP-510-32815*, <http://www.nrel.gov/publications>, 2002.
- [64] Orío A., Corella J., and Narváez I. Performance of different dolomites on hot raw gas cleaning from biomass gasification with air. *Industrial and Engineering Chemistry Research*, 36:3800–3808, 1997.

- [65] Corella J., Toledo J.M., and Padilla R. Olivine or dolomite as in-bed additive in biomass gasification with air in a fluidized bed: Which is better? *Energy and Fuels*, 18:713–720, 2004.
- [66] Pinto F., Lopes H., André R.N., Gulyurtlu I., and Cabrita I. Effect of catalysts in the quality of syngas and by-products obtained by co-gasification of coal and wastes. 1. Tars and nitrogen compounds abatement. *Fuel*, 86:2052–2063, 2007.
- [67] Rapagná S., Jand N., Kiennemann A., and Foscolo P.U. Steam-gasification of biomass in a fluidized-bed of olivine particles. *Biomass and Bioenergy*, 19:187–197, 2000.
- [68] Garcia L., Benedicto A., Romeo E., Salvador M.L., Arauzo J., and Bilbao R. Hydrogen production by steam gasification of biomass using Ni-Al coprecipitated catalysts promoted with magnesium. *Energy and Fuels*, 16:1222–1230, 2002.
- [69] Simell P.A., Hepola J.O., and Krause A.O.I. Effects of gasification gas components on tar and ammonia decomposition over hot gas cleanup catalysts. *Fuel*, 76:1117–1127, 1997.
- [70] Corella J., Orío A., and Toledo J.M. Biomass gasification with air in a fluidized bed: Exhaustive tar elimination with commercial steam reforming catalysts. *Energy and Fuels*, 13:702–709, 1999.
- [71] Baker E.G., Mudge L.K., and Brown M.D. Steam gasification of biomass with nickel secondary catalysts. *Industrial and Engineering Chemistry Research*, 26:1335–1339, 1987.
- [72] Mudge L.K., Baker E.G., Brown M.D., and Wilcox W.A. Catalysts for gasification of biomass. In *Symposium papers on Energy from Biomass and Wastes, IGT, Washington DC*, page 1639–1640, 1987.
- [73] Seshadri K.S. Effects of temperature, pressure, and carrier gas on the cracking of coal tar over a char–dolomite mixture and calcined dolomite in a fixed-bed reactor. *Industrial and Engineering Chemistry Research*, 37:3830–3837, 1998.
- [74] Chembukulam S.K., Dandge A.S., Kovilur N.L., Seshagiri R.K., and Valdyeswaran R. Smokeless fuel from carbonized sawdust. *Industrial Engineering Chemistry Product Research and Development*, 20:714–719, 1981.
- [75] Neeft J.P.A., Knoef H.A.M., and Onaji P. Behavior of tars in biomass gasification systems. *NOVEM EWAB Program Report 9919*, page 75, 1999.
- [76] <http://www.btgworld.com/technologies/tar-removal.html/>.

-
- [77] Evans R.J. and Milne T.A. Molecular characterization of the pyrolysis of biomass. 1. Fundamentals. *Energy and Fuels*, 1:123–138, 1987.
- [78] Elliott D.C. Relation of reaction time and temperature to chemical composition of pyrolysis oils. In *Proceedings of the ACS symposium series 376, pyrolysis oils from biomass*, 1988.
- [79] Boerrigter H. 'OLGA' tar removal technology. *The Energy research Centre of the Netherlands*, ECN-C-05-009, 2005.
- [80] Lettner F., Timmerer H., and Haselbacher P. Deliverable 8: Biomass gasification—State of the art description. *Project: Guideline for safe and eco-friendly biomass gasification, Intelligent Energy—Europe (IEE)*, December 2007.
- [81] Cummer K.R. and Brown R.C. Review-Ancillary equipment for biomass gasification. *Biomass and Bioenergy*, 23:113–128, 2002.
- [82] Nair S.A. *Corona plasma for tar removal*. PhD thesis, Technische Universiteit Eindhoven, 2004.
- [83] Neeft J.P.A., van Paasen S.V.B., Knoef H.A.M., Buffinga G.J., Zielke U., Sjöström K., Brage C., Hasler P., Simell P.A., Suomalainen M., Dorrington M.A., and Thomas L. Tar guideline - A standard method for measurement of tars and particles in biomass producer gases. In *Proceedings of the 12th European Conference and Technology Exhibition on Biomass for Energy, Industry and Climate Protection, Amsterdam, The Netherlands*, pages 469–572, 2002.
- [84] Coda B., Zielke U., Suomalainen M., Knoef H.A.M., Good J., Liliedahl T., Unger C., Ventress L., Neeft J.P.A., van de Hoek H., and Kiel J. Tar measurement standard: A joint effort for the standardisation of a method for measurement of tars and particulates in biomass producer gas. In *Proceedings of the 2nd World Biomass Conference - Biomass for Energy, Industry and Climate Protection, Rome, Italy*, pages 793–796, 2004.
- [85] Hasler P. and Nussbaumer T. Sampling and analysis of particles and tars from biomass gasifiers. *Biomass and Bioenergy*, 18:61–66, 2000.
- [86] Corella J., Caballero M.A., Aznar M.P., and Brage C. Two advanced models for the kinetics of the variation of the tar composition in its catalytic elimination in biomass gasification. *Industrial and Engineering Chemistry Research*, 42:3001–3011, 2003.
- [87] <http://www.thersites.nl/>.

- [88] van Paasen S.V.B., Kiel J.H.A, Neeft J.P.A., Knoef H.A.M., Buffinga G.J., Zielke U., Sjöström K., Brage C., Hasler P., Simell P.A., Suomalainen M., Dorrington M.A., and Thomas L. Guideline for sampling and analysis of tar and particles in biomass producer gases – Final report documenting the guideline, R&D work and dissemination. *Report ECN-C-02-090, Petten, The Netherlands, 2002.*
- [89] Good J., Ventress L., Knoef H., Zielke U., Lyck Hansen P., van de Kamp W., de Wild P., Coda B., van Passen S., Kiel J., Sjöström K., Liliedahl T., Unger Ch., Neeft J., and Suomalainen M. Sampling and analysis of tar and particles in biomass producer gases. *Technical report, CEN BT/TF 143, organic contaminants (tar) in producer gases, July 2005.*
- [90] van de Kamp W., de Wild P., Zielke U., Suomalainen M., Knoef H.A.M., Good J., Liliedahl T., Unger C., Whitehouse M., Neeft J.P.A., van de Hoek H., and Kiel J. Tar measurement standard for sampling and analysis of tars and particles in biomass gasification product gas. In *Proceedings of the 14th European Biomass Conference and Exhibition, Paris, France*, pages 791–794, 2005.
- [91] Kübel M., Gfereis C., Waizmann J., Michel M., and Hein K.R.G. Hydrogen rich syngas production from steam gasification of BCO in a FB reactor-Gas composition and tar formation at various conditions. In *Proceedings of the 2nd World Biomass Conference - Biomass for Energy, Industry and Climate Protection, Rome, Italy*, pages 763–766, 2004.
- [92] <http://www.chromatography-online.org/>.
- [93] Pakdel H. and Roy C. Hydrocarbon content of liquid products and tar from pyrolysis and gasification of wood. *Energy and Fuels*, 5:427–436, 1991.
- [94] de Sousa L.C. *Gasification of Wood, Urban Wastewood (Altholz) and other Wastes in a Fluidized Bed Reactor*. PhD thesis, Swiss Federal Institute of Technology Zürich, 2001.
- [95] Zhang C., Zhang X., Yang J., and Liu Z. Analysis of polynuclear aromatic hydrocarbons in heavy products derived from coal and petroleum by high performance liquid chromatography. *Journal of Chromatography A*, 1167:171–177, 2007.
- [96] Braage C., Yu Q., Chen G., and Sjöström K. Use of amino phase adsorbent for biomass tar sampling and separation. *Fuel*, 76:137–142, 1997.
- [97] Dufour A., Girods P., Masson E., Normand S., Rogaume Y., and Zoulalian A. Comparison of two methods of measuring wood pyrolysis tars. *Journal of Chromatography A*, 1164:240–247, 2007.

-
- [98] Moersch O., Spliethoff H., and Hein K.R.G. Tar quantification with a new online analyzing method. *Biomass and Bioenergy*, 18:79–86, 2000.
- [99] Staiger B. *Untersuchung stationärer und dynamischer Vorgänge bei der Teerentstehung in Biomassevergaseren und Gasreinigungen mit Hilfe der kontinuierlichen Teeranalyse*. PhD thesis, Universität Stuttgart, 2010.
- [100] Evans R.J. and Milne T.A. Chemistry of tar formation and maturation in the thermochemical conversion of biomass. *Developments in Thermochemical Biomass Conversion*, 2:803–816, 1997.
- [101] Ratcliff M.A. Design and construction of a transportable molecular beam mass spectrometer and its application to the analysis of diesel exhaust. Master's thesis, Colorado School of Mines, Golden, CO, 1994.
- [102] Ratcliff M.A., French R.J., Patrick J.A., Anselmo M., and Netter J. Development of a third generation transportable MBMS for more versatile and cost-effective field applications. *Final Report, NREL FIRST Program*, 1998.
- [103] Ratcliff M.A., Deutch S., Feik C., French R.J., Graham J., Meglen R., Overly C., Patrick J.A., Phillips S., and Prentice B. Biosyngas characterization test results. *Technical Report, NREL/TP-510-31224*.
- [104] Carpenter D.L., Deutch S.P., and French R.J. Quantitative measurements of biomass gasifier tars using a molecular-beam mass spectrometer: Comparison with traditional impinger sampling. *Energy and Fuels*, 21:3036–3043, 2007.
- [105] Hrdlicka J., Feik C., Carpenter D., and Pomeroy M. Parametric gasification of oak and pine feedstocks using the TCPDU and slipstream water-gas shift catalysis. *Technical Report, NREL/TP-510-44557*, December 2008.
- [106] Neubauer Y. and Behrendt F. Application of laser mass spectrometry for a fast and detailed online tar analysis. In *Proceedings of the 15th European Biomass Conference and Exhibition, Berlin, Germany*, pages 850–854, 2007.
- [107] Neubauer Y. *Online-Analyse von Teer aus der Biomassevergasung mit Laser-massenspektrometrie*. PhD thesis, Technische Universität Berlin, 2008.
- [108] Knoef H.A.M., van de Beld L., Ahmadi M., Sjöström K., Brage C., and Liliedahl T. Development of an on-line tar measuring method for quantitative analysis of biomass producer gas. In *Proceedings of the 17th European Biomass Conference and Exhibition, Hamburg, Germany*, pages 884–888, 2009.
- [109] Karellas S. and Karl J. Analysis of the product gas from biomass gasification by means of laser spectroscopy. *Optics and Lasers in Engineering*, 45:935–946, 2007.

- [110] Mitsakis P., Karellas S., and Spliethoff H. Application of laser spectroscopy for the quantitative analysis of biomass gasification tars. In *Proceedings of the 16th European Biomass Conference and Exhibition, Valencia, Spain*, pages 652–658, 2008.
- [111] Linow S. *Über das Potential spektroskopischer Methoden zur Messung von Temperatur und Konzentration in reagierenden technischen Strömungen*. PhD thesis, Technische Universität Darmstadt, 2001.
- [112] Stocker R. *Bestimmung Verbrennungsrelevanter Größen in Flammen mit laseroptischen Verfahren*. PhD thesis, Technische Universität München, 2004.
- [113] Karellas S. *Online analysis of the composition of biogenous gases and their effect on microturbine and fuel cell systems*. PhD thesis, Technische Universität München, 2005.
- [114] Lakowicz J.R. *Principles of Fluorescence Spectroscopy*. Kluwer Academic/Plenum Publishers, 2 edition, 1999.
- [115] PerkinElmer Ltd. An introduction to fluorescence spectroscopy. page 8, 2000.
- [116] <http://www.olympusfluoview.com/theory/fluoroexciteemit.html>.
- [117] Niessner R., Robers W., and Krupp A. Detection of particulate polycyclic aromatic hydrocarbons by laser-induced time-resolved fluorescence. *Fresenius' Journal of Analytical Chemistry*, 341:207–213, 1991.
- [118] Karlitschek P., Lewitzka F., Bünting U., Niederkrüger M., and Marowsky G. Detection of aromatic pollutants in the environment by using UV-laser-induced fluorescence. *Applied Physics B-Lasers and Optics*, 67:497–504, 1998.
- [119] Selli E., Zaccaria C., Sena F., Tomasi G., and Bidoglio G. Application of multi-way models to the time-resolved fluorescence of polycyclic aromatic hydrocarbons mixtures in water. *Water Research*, 38:2269–2276, 2004.
- [120] Giamarchi P., Stephan L., Salomon S., and Bihan A. Multicomponent determination of a polyaromatic hydrocarbon mixture by direct fluorescence measurements. *Journal of Fluorescence*, 100:393–402, 2000.
- [121] Zimmermann F., Koban W., Roth C., Herten D., and Schulz C. Fluorescence lifetime of gas-phase toluene at elevated temperatures. *Chemical Physics Letters*, 426:248–251, 2006.
- [122] Allain L., Stratis D., Cullum B., Mobley J., Hajaligol M., and Vo-Dihn T. Real-time detection of PAH mixtures in the vapor phase at high temperatures. *Journal of Analytical and Applied Pyrolysis*, 66:145–154, 2003.

-
- [123] LTB Lasertechnik Berlin GmbH. Nitrogen Laser, MNL 100 Manual. 2006.
- [124] LaVision GmbH. FlameStar 2F Operation Manual. *Göttingen*, 1998.
- [125] Hatfield J. A model for estimating process emissions from gas sweep operations in batch and continuous chemical operations. *Environmental Progress*, 23(1):45–51, 2004.
- [126] U.S. Environmental Protection Agency. Control of volatile organic compound emissions from batch processes-Alternative control techniques information documentation. *U.S. EPA, Office of Air Quality Planning and Standards, Research Triangle Park, NC, EPA-450/R-94-020, Appendix B*, 1994.
- [127] Braun M. *Online analysis of biomass gasification tars by means of laser spectroscopy*, Semester thesis, Supervisor: P. Mitsakis, Technische Universität München, 2010.
- [128] Baehr H.D. and Stephan K. *Wärme- und Stoffübertragung*. Springer Verlag, Berlin, 1996.
- [129] Perry R.H. *Perry's Chemical Engineers' Handbook*. McGraw-Hill, 7 edition, 1997.
- [130] Brokaw R.S. Predicting transport properties of dilute gases. *Industrial and Engineering Chemistry*, 8(2):241–253, 1969.
- [131] Reinicke H. Einheitliche Darstellung des Wärme- und Stoffüberganges bei überströmten Körpern und Kanälen Wärmeübergang bei zähen Flüssigkeiten. *Chemie Ingenieur Technik*, 42:364–370, 1970.
- [132] Poling B., Prausnitz J., and O'Connell J. *Properties of Gases and Liquids*. McGraw-Hill, 5 edition, 2001.
- [133] Dykyj J., Svoboda J., Wilhoit R.C., Frenkel M., and Hall K.R. Vapor Pressure and Antoine Constants for Hydrocarbons, and Sulphur, Selenium, Tellurium and Halogen Containing Compounds. *Landolt-Börnstein: Numerical Data and Functional Relationships in Science and Technology*, 20A, 1999.
- [134] Lide D.R. and Kehiaian H.V. *CRC Handbook of Thermophysical and Thermochemical Data*. CRC Press, 1994.
- [135] Knovel. *Knovel Critical Tables*. Knovel, Norwich, New York, 2 edition, 2008.
- [136] Crowl D.A. and Louvar J.F. *Chemical Process Safety, Fundamentals with Applications*. Prentice Hall, Upper Saddle River, NJ, 2 edition, 2001.
- [137] Byrne J.P. and Ross I.G. Diffuseness in electronic spectra. The vapor spectrum of anthracene. *Canadian Journal of Chemistry*, 43:3253–3257, 1965.

- [138] Demtröder W. *Laser spectroscopy, Basic Concepts and Instrumentation*. Springer Verlag, Berlin, 3 edition, 2003.
- [139] Thöny A. and Rossi M.J. Gas-phase UV spectroscopy of anthracene, xanthone, pyrene, 1-bromopyrene and 1,2,4-trichlorobenzene at elevated temperatures. *Journal of Photochemistry and Photobiology A: Chemistry*, 104:25–33, 1997.
- [140] Chi Z., Cullum B.M., Stokes D., Mobley J., Miller G.H., Hajaligol M.R., and Vo-Dihn T. Laser-induced fluorescence studies of polycyclic aromatic hydrocarbons (PAH) vapors at high temperatures. *Spectrochimica Acta Part A*, 57:1377–1384, 2001.
- [141] Jandris L.J. and Forcé R.K. Determination of polynuclear aromatic hydrocarbons in vapor phases by laser-induced molecular fluorescence. *Analytica Chimica Acta*, 151:19–27, 1983.
- [142] LaVision GmbH. Command language manual for DaVis 6.2. *Göttingen*, 2004.
- [143] Faghri A. *Heat pipe science and technology*. Taylor and Francis Press, Washington, D.C., 1995.
- [144] Siedlecki M., Nieuwstraten R., Simeone E., de Jong W., and Verkooijen A.H.M. Effect of magnesite as bed material in a 100 kW_{th} steam-oxygen blown circulating fluidized-bed biomass gasifier on gas composition and tar formation. *Energy and Fuels*, 23:5643–5654, 2009.
- [145] ESIS-European chemical Substances Information System. <http://ecb.jrc.ec.europa.eu/esis/>.